Characterisation and dynamic modelling of the behaviour of platinum group metals in high pressure sulphuric acid/oxygen leaching systems

by

Christie Dorfling

Dissertation presented for the degree

of

DOCTOR OF PHILOSOPHY
(Extractive Metallurgical Engineering)

in the Faculty of Engineering
at Stellenbosch University

Supervisors:
Prof. S.M. Bradshaw
Prof. G. Akdogan

DECEMBER 2012

DECLARATION

By submitting this dissertation electronically, I declare that the entirety of the work contained therein is my own, original work, that I am the sole author thereof (save to the extent explicitly otherwise stated), that the reproduction and publication thereof by Stellenbosch University will not infringe any third party rights and that I have not previously in its entirety or in part submitted it for obtaining any qualification.

Christie Dorfling 20 November 2012

ABSTRACT

Sulphuric acid/oxygen pressure leaching is typically employed on Base Metal Refineries (BMRs) to selectively dissolve base metals from platinum group metal (PGM) bearing nickel-copper matte. Optimal operation of this processing step requires an understanding of the system chemistry and the effects of process variables on base metal and PGM leaching behaviour. This project aimed to aid in the development of an improved understanding of the high pressure leaching system.

The effects of temperature, pressure, acid concentration, and solid to liquid ratio on the leaching behaviour were determined experimentally using a two litre autoclave. For conditions comparable to that typically used at the Western Platinum Ltd. BMR, changes in the acid concentration had the largest effect on the copper leaching behaviour. Increasing the initial acid concentration from 140 g H_2SO_4/ℓ to 165 g H_2SO_4/ℓ resulted in the copper dissolution decreasing from 88.7% to 75.3% on average for the experiments performed at different temperatures (116°C, 130°C) and pressures (7 bar, 9 bar), and with different solids contents (80 g/ℓ, 130 g/ℓ). In the case of the other precious metals (OPMs), temperature was determined to be the process variable with the largest effect on the leaching kinetics. The average percentage rhodium dissolution achieved after seven hours of leaching at different conditions (pressure, acid concentration, and solids content were varied) increased from 58.3% at 116°C to 83.6% at 130°C. Similar effects were observed for ruthenium (96.2% dissolution at 130°C; 79.4% dissolution at 116°C) and iridium (81.8% dissolution at 130°C; 46.9% dissolution at 116°C). The rate of copper leaching was found to be limited by the rate of oxygen transfer from the gaseous phase to the liquid phase, while the remainder of the reactions were chemical reaction limited. The extent of OPM leaching was found to be dependent on the rate and extent of copper leaching.

A set of 21 chemical reactions was proposed to describe the leaching behaviour, and the shape factors and reaction rate constants were determined by the method of least squares to minimise the error between the predicted concentrations and the experimental data. Apart from direct base metal leaching reactions, six cationic exchange reactions contribute to the leaching of copper sulphides and nickel sulphides by precipitation of OPM oxides. Three leaching reactions for each of the OPMs (one for sulphide phases, one for metallic phases, and one for oxide phases) resulted in satisfactory modelling of the system behaviour. Activation energies of -26.2 kJ/mol and -5.9 kJ/mol were calculated for the digenite acid

leaching reaction and the covellite direct oxidation reaction, respectively, which confirmed that the rates of these reactions were mass transfer limited. The activation energies for the remainder of the base metal leaching reactions exceeded 30 kJ/mol. The activation energies of the reactions accounting for rhodium sulphide leaching, rhodium leaching, and rhodium oxide leaching, were calculated to be 64.2 kJ/mol, 138.5 kJ/mol, and 116.2 kJ/mol, respectively. Similar activation energies were calculated for the respective Ru and Ir leaching reactions. The rate of OPM sulphide leaching was typically an order of magnitude and three orders of magnitude larger than the rate of OPM leaching reactions and OPM oxide leaching reactions, respectively.

The autoclave at the Western Platinum Ltd. BMR was modelled assuming a monosized distribution of the feed and approximating the autoclave as four ideal continuously stirred tank reactors. The steady state solution employed the sequential modular approach in MATLAB, while the dynamic simulation involved solving a set of 217 differential equations derived from mass and energy balances simultaneously in MATLAB. The model was used successfully to evaluate the effects that changes in the leaching temperature, leaching pressure, acid feed rate, and solids feed rate have on the extent of base metal and OPM leaching in the autoclave. The optimum operating conditions depend on the flow rates and compositions of the feed streams. A feed stream containing 10.3 wt% solids (825 kg solids/h) and an acid addition rate of 28.6 kg/h were considered as typical operating conditions for model-based analysis. More than 95% copper dissolution and no OPM dissolution were predicted when performing the pressure leaching at a pressure of 8 bar and a temperature of approximately 123°C. Decreasing the pressure resulted in lower copper dissolution when OPM leaching started to occur. Increasing the temperature resulted in reduced copper leaching, while decreasing the temperature resulted in a longer OPM leaching period and hence higher OPM dissolution. Model-based analysis furthermore showed that the relative amounts and relative leaching rates of digenite and covellite significantly influence the percentage copper dissolution achieved when noticeable OPM leaching start to occur.

OPSOMMING

Swawelsuur/suurstof hoë druk loging word tipies op Basis Metaal Raffinaderye (BMRe) gebruik om basis metale selektief op te los vanuit platinum groep metaal (PGM) bevattende nikkel-koper mat. Optimale bedryf van hierdie prosesstap vereis 'n begrip van die sisteem se chemie en die effekte wat proses veranderlikes op die logingsgedrag van basis metale en PGMe het. Hierdie projek het ten doel gehad om 'n beter begrip van die hoë druk loging sisteem te ontwikkel.

Die effekte van temperatuur, druk, suur konsentrasie, en vastestof tot vloeistof verhouding op die logingsgedrag is eksperimenteel met behulp van 'n twee liter outoklaaf bepaal. Vir toestande vergelykbaar met dié wat tipies by die Western Platinum Bpk. BMR gebruik word, het veranderinge in die suurkonsentrasie die grootste effek op die logingsgedrag van koper gehad. Verhoging van die aanvanklike suurkonsentrasie van 140 g H_2SO_4/ℓ na 165 g H_2SO_4/ℓ het tot gevolg gehad dat die gemiddelde koper oplossing afgeneem het van 88.7% na 75.3% vir die eksperimente wat by verskillende temperature (116°C, 130°C) en drukke (7 bar, 9 bar), en met verskillende vastestof inhoud (80 g/ℓ, 130 g/ℓ), uitgevoer is. In die geval van die ander edelmetale (AEM) is bevind dat die temperatuur die prosesveranderlike met die grootste effek op die logingskinetika is. Die gemiddelde persentasie rodium oplossing wat na sewe ure se loging by verskillende toestande (druk, suurkonsentrasie, en vastestof inhoud is varieer) behaal is, het toegeneem van 58.3% by 116°C na 83.6% by 130°C. Soortgelyke effekte is waargeneem vir rutenium (96.2% oplossing by 130°C; 79.4% oplossing by 116°C) en iridium (81.8% oplossing by 130°C; 46.9% oplossing by 116°C). Dit is bevind dat die tempo van koper loging beperk is deur die tempo van suurstof oordrag vanaf die gas na die vloeistoffase, terwyl chemiese reaksies beperkend was vir die res van die reaksies. Die mate van AEM loging was afhanklik van die tempo en mate van koper loging.

'n Stel van 21 reaksies is voorgestel om die logingsgedrag te beskryf, en die vorm faktore en reaksie tempo konstantes is bepaal deur middel van die metode van kleinste kwadrate om die fout tussen die voorspelde konsentrasies en die eksperimentele data te minimeer. Afgesien van die direkte basis metaal logingsreaksies het ses kationiese uitruilingsreaksies bygedra tot die loging van kopersulfiede en nikkelsulfiede deur presipitasie van AEM oksiede. Drie logingsreaksies vir elk van die AEMe (een vir die sulfied fase, een vir die metaal fase, en een vir die oksied fase) het bevredigende modellering van die sisteem se gedrag tot gevolg gehad. Aktiveringsenergieë van -26.2 kJ/mol en -5.9 kJ/mol is bereken vir die $Cu_{1.8}S$ suur

logingsreaksie en die CuS direkte oksidasie reaksie, onderskeidelik, wat bevestig het dat die tempo's van hierdie reaksies deur massa oordrag beperk is. Die aktiveringsenergieë vir die res van die basis metaal logingsreaksies het 30 kJ/mol oorskry. Die aktiveringsenergieë vir die reaksies wat die rodiumsulfied loging, rodium loging, en rodiumoksied loging beskryf is as 64.2 kJ/mol, 138.5 kJ/mol, en 116.2 kJ/mol, onderskeidelik, bereken. Soortgelyke aktiveringsenergieë is bereken vir die onderskeie Ru en Ir logingsreaksies. Die tempo van AEM sulfied loging was tipies 'n ordegrootte en drie ordegroottes groter as die tempo van AEM logingsreaksie en AEM oksied logingsreaksies, onderskeidelik.

Die outoklaaf by die Western Platinum Bpk. BMR is gemodelleer deur 'n enkelgrootte verspreiding vir die voer te aanvaar en die outoklaaf as vier ideale kontinu geroerde tenk reaktore te benader. Die oplossing vir gestadige toestande het die sekwensiële modulêre benadering toegepas in MATLAB, terwyl die dinamiese simulasie die gelyktydige oplos van 217 differensiale vergelykings, wat vanaf massa- en energiebalanse afgelei is, in MATLAB behels het. Die model is suksesvol gebruik om die effekte wat veranderinge in die logingstemperatuur, logingsdruk, suur voertempo, en vastestof voertempo op die mate van basis metaal en AEM loging in die outoklaaf het, te bepaal. Die optimale bedryfstoestande is afhanklik van die vloeitempo's en samestellings van die voerstrome. 'n Voerstroom wat 10.3 massa% vastestof (825 kg vastestof per uur) bevat en 'n suur voertempo van 28.6 kg/h is as tipiese bedryfstoestande beskou vir model-gebaseerde analises. Meer as 95% koper oplossing sonder enige AEM oplossing is voorspel wanneer die loging by 'n druk van 8 bar en 'n temperatuur van ongeveer 123°C uitgevoer word. 'n Vermindering van die druk het tot gevolg gehad dat laer koper loging behaal is toe AEM loging begin plaasvind het. 'n Verhoging in die temperatuur het laer koper loging tot gevolg gehad, terwyl laer temperature 'n langer AEM logingsperiode en gevolglik hoër AEM loging tot gevolg het. Model-gebaseerde analises het verder getoon dat die relatiewe hoeveelhede en relatiewe tempo's van loging van $Cu_{1.8}S$ en CuS 'n beduidende invloed het op die persentasie koper wat geloog is wanneer beduidende AEM loging begin plaasvind.

ACKNOWLEDGEMENTS

I wish to express my appreciation to the following people:

- My supervisors, Prof Steven Bradshaw and Prof Guven Akdogan, for their support and guidance.
- Prof Jacques Eksteen, previously from Western Platinum Ltd. (Lonmin Plc), for financial support as well as technical advice.
- Mr Nico Steenekamp from Western Platinum Ltd. Base Metal Refinery, for process information and technical advice.
- Mr Elton Thyse, for assistance with the mineralogical analyses.
- The technical and administrative staff at the Department of Process Engineering at Stellenbosch University.

TABLE OF CONTENTS

LIST OF FIGURES

LIST OF TABLES

1 INTRODUCTION

1.1 Background

The processing of platinum bearing Ni-Cu ores for the extraction of platinum group metals (PGMs) involves comminution, flotation, smelting, and converter treatment of the furnace matte. Hydrometallurgical processes are widely used by platinum producers for the treatment of the PGM bearing converter matte at their base metal refineries to separate the base metals and platinum group metals. These processes have proven to be efficient in the recovery of base metals to produce a high-grade PGM solids residue suitable for further treatment in the PGM refinery. The leaching system employing sulphate media together with oxygen as oxidising agent, in particular, has established itself as the preferred processing route for nickel-copper mattes with a high PGM content (Muir and Ho, 2006).

According to Lamya and Lorenzen (2006), the leaching processes involve an initial or first stage leaching process which can be performed at atmospheric or high pressures (or both), followed by a second stage pressure leaching step. In the first stage leaching step converter matte is treated primarily to achieve nickel dissolution and copper precipitation. The purpose of the second stage pressure leaching is to dissolve the copper in the converter matte and the copper precipitated during the first leaching step, as well as to dissolve any nickel that has not been removed in the upstream leaching steps. The dissolution of PGMs must be limited, since the PGMs are to be recovered from the leaching residue.

Studies have been conducted to investigate the leaching mechanisms and kinetics of base metals in different leaching environments. In general, however, the kinetics of the second stage leaching process are poorly understood because of the complex nature of the leaching chemistry and the diverse mineralogy of the first stage residue to be leached. As a result, these processes are seldom operated at the optimal leaching conditions. The high pressure leaching stages, in particular, are often operated at suboptimal conditions due to the poor fundamental understanding of the PGM leaching behaviour under these conditions. This results in insufficient copper dissolution, which results in low grade PGM rich matte being fed to the downstream processing steps, and excessive PGM leaching, which results in a high PGM inventory and increased PGM losses. The other precious metals (OPMs), namely rhodium, ruthenium, and iridium, are reported to be the PGMs undergoing the largest percentage dissolution in the second stage high pressure leach (Steenekamp, 2009).

1.2 Objective and scope

In order to allow the development of a better understanding of the operation of the pressure leach stage, the following objectives had to be achieved:

- Perform batch leach tests to develop an understanding of the effects that the key process variables have on the leaching behaviour of the PGMs in the second stage leach.
- Propose a set of chemical reactions that can be used to describe the leaching behaviour in the high pressure sulphuric acid/oxygen leaching environment, and subsequently quantify the reaction kinetics in terms of the most important process variables.
- Develop a model that can be used to simulate the dynamic behaviour of the pressure leaching stages, and use the model as a basic tool to assist with the prediction of autoclave behaviour.

1.3 Scientific contributions

The scientific contribution of this work can be summarised as follows:

- An improved understanding of the effects of various operating variables on the leaching behaviour of other precious metals in a high pressure sulphuric acid/oxygen leaching system has been developed. Published information regarding the leaching behaviour of OPMs is limited. This is the first study providing detailed information about the interdependencies between process variables and the effects of changes in variables such as leaching pressure, acid concentration, and solid to liquid ratio on the leaching rates of OPMs.
- Based on experimental data generated at different sets of operating conditions, a set of reactions was proposed to describe the leaching behaviour of the other precious metals. Kinetic rate constants were determined for these reactions. This allows the estimation of leaching kinetics at various temperatures, pressures, acid concentrations, and solid to liquid ratios. While reaction kinetics have previously been quantified for the leaching of base metals in pressure leaching systems, no reaction kinetic data could be found for the leaching of other precious metals. The calculation of the reaction rate constants and activation energies for the reactions involving other precious metals is hence a novel contribution to the existing knowledgebase.
- The kinetic rate constants were used to develop a dynamic model of the autoclave used for the second and third stage high pressure leaching at the Western Platinum Ltd. Base Metal

Refinery. Leaching systems have been modelled using various modelling techniques previously. This is, however, a first attempt to predict the dynamic response of the other precious metals' concentrations in the leach solution to changes in the leaching temperature, leaching pressure, acid feed rate, and solid to liquid feed ratio.

1.4 Thesis structure

Section 2 presents an overview of the base metal refining operations followed by a literature survey on the aspects related to the pressure leaching step. These include base metal and OPM chemistry, the effects of operating conditions on the leaching behaviour, leaching reactions, reaction kinetics, and modelling of leaching reactors. The experimental equipment and methodology are discussed in Section 3, followed by a discussion of the experimental results in Section 4. The work performed to propose feasible leaching reactions and to determine the reaction kinetics is presented in Section 5, while the aspects regarding the development of the autoclave model are discussed in Section 6. The thesis is concluded with a summary of the main conclusions and recommendations in Section 7.

The appendices contain a list of nomenclature (Appendix A), the hazard identification analysis for the experimental setup (Appendix B), results and sample calculations (Appendix C – Appendix F), a list of the publications arising from the thesis (Appendix G), and an electronic copy of the MATLAB code that was developed as part of the project (Appendix H).

2 LITERATURE REVIEW

2.1 Process description

Lamya (2007) classified the process steps that are typically followed during the processing of PGM bearing minerals into the following five categories:

2.1.1 Comminution

Comminution constitutes crushing and grinding with the objective of reducing the particle size of the ore in order to liberate the valuable minerals. Mills can be operated in either a closed circuit configuration, in which case the milled ore is classified and fed to the downstream process only once the desired size has been achieved, or open circuit operation, in which case the mill discharge is fed to the downstream process without any recirculation of oversized particles. Several studies have been performed to investigate the effect of ore particle size distribution on the performance of downstream physical separation processes (Trahar, 1981; Venkoba Rao, 2007) and specifically the flotation of PGM bearing minerals from the UG2 and Merensky reefs (Feng and Aldrich, 1999).

2.1.2 Physical concentration

These processes are used to separate gangue material from valuable ore minerals and could involve either flotation or gravity separation. Flotation, which relies on the surface properties of different minerals to achieve separation, is mainly used to recover base metal sulphides. Chemical reagents such as frothers and collectors can be used to modify the surface properties of different minerals in order to improve the efficiency of the flotation separation process. Studies investigating the effect of flotation cell agitation (Deglon, 2005), flotation chemistry (Buswell *et al.*, 2002; Miller *et al.*, 2005; Wiese *et al.*, 2008), and ore surface characteristics (Shackleton *et al.*, 2007) on the recovery of PGM bearing minerals in flotation processes have been conducted. Gravity separation can be used if the densities of the PGM bearing minerals are high and if these minerals are not associated with gangue to a great extent. Xiao and Laplante (2004) presented an overview of the gravity separation techniques applicable to different ore types. Xiao *et al.* (2009) proposed a methodology to predict the amount of gravity recoverable PGMs in minerals.

2.1.3 Pyrometallurgical concentration

Pyrometallurgical concentration follows physical separation and is used to concentrate the base metals and PGMs into a sulphide matte. During the first smelting step, dried flotation concentrate is fed to a furnace where a molten matte containing base metal sulphides, PGMs,

and some gangue minerals is produced together with an iron-rich gangue slag phase containing silicates and oxides. The typical compositions of the furnace mattes produced by the four platinum producers in South Africa are summarised in Table 2.1. Jones (2005) presented a general overview of PGM smelting operations in Southern Africa. Numerous studies have investigated, inter alia, the sulphide capacity of PGM smelter slag (Du Toit *et al.*, 2006) as well as the chemistry of furnace slag and the solubility of chromium in furnace slag (Nell, 2004). Lamya (2007) discussed the melting characteristics of silicates, base metal sulphides, and platinum group minerals.

Table 2.1. Typical analyses of the furnace mattes produced by the South African platinum producers (adapted from Jones, 2000).

	Co (%)	**Cr (%)**	**Cu (%)**	**Fe (%)**	**Ni (%)**	**S (%)**	**PGM (g/t)**
Amplats Waterval	0.5	0.5	9.5	43	18	28	670
Amplats Union	0.4	2.3	8.4	45	14	30	1000
Impala	0.4		16.2	35	20	28	1070
Lonmin Merensky	0.5	0.25	10.5	40	18	30	1090
Lonmin UG2	0.5	0.32	10.8	38	19	31	2750
Northam	0.4		8.5	44	17	29	780

The furnace matte is then treated in a converter to remove iron and sulphur to produce a concentrated matte consisting primarily of nickel sulphides, copper sulphides, and small amounts of precious metals and impurities such as selenium, tellurium, and lead (Jones, 2005). The typical compositions of the converter mattes produced by South African platinum producers are given in Table 2.2.

Table 2.2. Typical analyses of the converter mattes produced by the South African platinum producers (adapted from Jones, 2000).

	Co (%)	**Cu (%)**	**Fe (%)**	**Ni (%)**	**S (%)**	**PGM (g/t)**
Amplats Waterval	0.5	27	3.0	48	22	2160
Impala	0.4	31	0.5	47	21	3430
Lonmin	0.6	29	1.4	48	20	6060
Northam	0.5	28	1.0	52	19	2620

A general overview of converter operation was given by Jones (2005). Kyllo and Richards (1998a) developed a kinetic model of Peirce-Smith converters, taking into account factors such as mass transfer, heat transfer, and chemical reactions taking place between the phases present in the converter. It was found that mass-transfer rates and related factors had the biggest impact on the model predictions. The effects of gas flow rate, oxygen enrichment of

the injected gas, tuyere submergence and diameter, and slag skimming procedures on converter operation have also been investigated (Kyllo and Richards, 1998b).

The matte can either be cooled slowly or granulated in water. The slow cooling process allows the formation of a Ni-Cu-Fe alloy containing the majority of the PGMs together with a nickel-copper matte with a very low PGM content, which allows magnetic separation of PGMs. Trevorites and magnetite, which do not dissolve during subsequent base metal leaching steps, are however also formed, leading to contamination of the PGM concentrate. Water granulation of the converter matte can be used instead of slow cooling to reduce ferrite formation during the cooling of the converter matte (Steenekamp and Dunn, 1999). The preferred PGM separation process hence determines the preferred converter matte cooling mechanism. Anglo Platinum, for example, utilises magnetic separation to remove PGMs prior to base metal leaching and therefore relies on slow cooling of converter matte. The rest of the South African platinum producers transfer the rapidly cooled converter matte directly to the hydrometallurgical process plant, where PGMs are recovered in the base metal refining residue (Cramer, 2001).

2.1.4 Hydrometallurgical extraction

There is greater variation in the hydrometallurgical processing plant between different platinum producers than in the processing steps discussed in the previous sections. Lamya (2007) discussed the hydrometallurgical processing plants of Rustenburg Base Metals Refinery (Anglo Platinum), Western Platinum Ltd. Base Metal Refinery (Lonmin Plc), and Impala Platinum. Of particular interest to this study is the hydrometallurgical process at the Western Platinum Ltd. BMR. A flow diagram of this process is shown in Figure 2.1.

At the Western Platinum Ltd. Base Metals Refinery, the converter matte is sent to a ball mill operated in a closed circuit configuration with hydrocyclone classification to reduce the matte particle size to a fineness of nine to twelve percent +75 µm (Bircumshaw, 2008). This slurry is fed to the first stage atmospheric leach. The first stage leaching process consists of five agitated tanks in series. Apart from the slurry being fed to the leaching circuit, fresh sulphuric acid and spent electrolyte from the electrowinning circuit are fed to the first tank. Pure oxygen is also sparged into the first two tanks (Lamya, 2007). The atmospheric leaching is performed at a temperature between 85°C and 95°C. The copper in the electrolyte is precipitated during the leaching process, while approximately 70% of the nickel in the matte fed to the first leaching tank is dissolved (Bircumshaw, 2008). The slurry discharged from the first stage

leaching circuit is sent to a solid-liquid separator, and the recovered liquid is fed to a filter where the liquid solution is separated to be fed to the nickel crystallisation plant where nickel sulphate crystals are recovered as the product (Steenekamp and Dunn, 1999). The solids recovered from the solid-liquid separator are fed to a horizontal autoclave together with spent electrolyte, sulphuric acid, and filtrate from one of the downstream batch leaching processes.

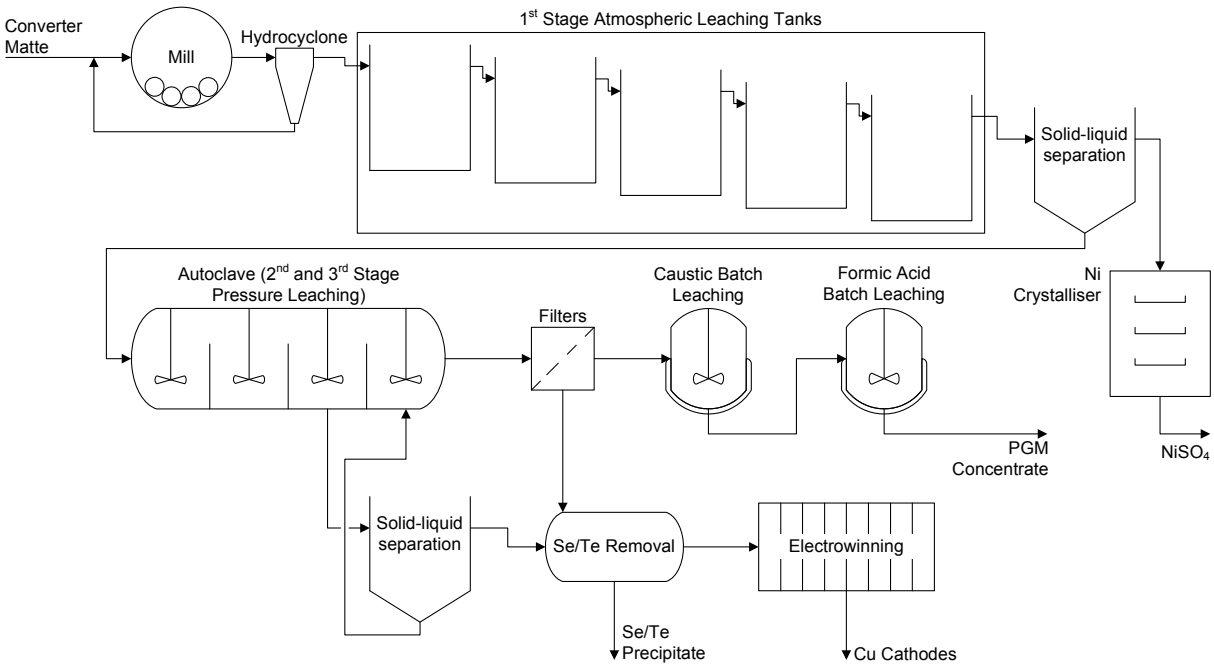

Figure 2.1. Flow diagram of the Western Platinum Ltd. Base Metal Refinery (redrawn from Bircumshaw, 2008).

The pressure leaching process configuration consists of two autoclaves that can be operated in parallel, depending on the rate at which converter matte is fed to the leaching circuit. If the matte feed rate exceeds 26 t/day, the feed to the autoclaves is divided into two streams with the same flow rates to be fed to the respective autoclaves. The autoclaves are carbon steel, lead lined vessels with brick linings. The design specifications included a maximum temperature of 165°C and a maximum pressure of 1000 kPa. The high pressure leaching is typically performed at a temperature between 115°C and 145°C, a pressure between 600 kPa and 700 kPa, and a sulphuric acid concentration of approximately 35 g/ℓ (Steenekamp and Dunn, 1999; Bircumshaw, 2008).

The first three compartments of each autoclave constitute the second stage high pressure leaching. The slurry removed from the third compartment is sent to a solid-liquid separator where solid residue is recovered to be returned to the fourth autoclave compartment together with returned spent electrolyte. The fourth autoclave compartment constitutes the third stage leach, and is employed to increase the grade of the concentrate for specific operating

conditions. The solid concentrate containing the PGMs is recovered from the slurry discharged by means of filtering. This solid residue is upgraded further through high pressure caustic batch leaching (to remove selenium, tellurium, arsenic, and sulphur) and atmospheric formic acid batch leaching (to remove any remaining nickel and iron in the PGM concentrate) (Bircumshaw, 2008). The liquid components of both the second stage leach and the third stage leach discharge slurry are sent through a pipeline reactor for selenium and tellurium removal, where dissolved PGMs also precipitate (Steenekamp and Dunn, 1999). The precipitated residue is reprocessed to recover the valuable components, while the liquid solution is sent to the copper electrowinning circuit.

The majority of the base metals, iron, and selenium in the autoclave feed stream are leached into solution during the second and third stages of leaching, while the PGMs remain in the solid residue. The oxygen used as oxidising agent is added to the second and third compartments in the second stage leach as well as to the third stage leach. The reactions whereby sulphide minerals are oxidised are highly exothermic, necessitating the implementation of a temperature control strategy to prevent the autoclave from reaching unacceptably high temperatures. Strategies that have been employed include the addition of recycled spent electrolyte to avoid overheating and the recycling of hot slurry from the first autoclave compartment to flash steam in order to release energy. Cooling coils are utilised in the second and third autoclave compartment to control the leaching temperature and prevent excessive dissolution of PGMs (Steenekamp and Dunn, 1999). A more detailed discussion of the autoclave configuration is presented in Section 6.1.

2.1.5 Refining of PGM concentrate

The upgraded PGM concentrate produced by the pressure caustic batch leaching and atmospheric formic acid batch leaching is dried and dispatched to the Precious Metal Refinery. Bernardis *et al.* (2005) presented an overview of the techniques used for the refining of platinum group elements.

2.2 Base metal leaching chemistry

The leaching of solids in an aqueous solution can be a physical, chemical, electrochemical, reductive, or electrolytic process, depending on the nature of the solid (Habashi, 1999). The chemistry of and leaching mechanisms for the dissolution of base metals have been discussed for various leaching environments. It is recognised that the thermodynamics of leaching systems are important if the equilibrium speciation and potential intermediate reactions are

important considerations. Eh-pH diagrams, for example, have been presented by several authors as an indication of the thermodynamics in specific leaching systems (Lamya, 2007; Van Schalkwyk, 2011). Given the fact that the leaching kinetics were of primary interest in this study and given the difficulty associated with obtaining reliable reduction-oxidation potential and pH measurements at the high pressure leaching conditions (high temperature, highly acidic, and highly oxidative conditions), this aspect of the leaching system is not discussed further.

2.2.1 First stage atmospheric leaching

Lamya and Lorenzen (2006) studied the leaching behaviour of Ni-Cu matte in a sulphuric acid/copper sulphate solution as encountered in the pre-leach stage at the Impala Platinum BMR. The process is non-oxidative and proceeds at atmospheric pressure. The predominant mineral phases in the matte that was studied were Ni_3S_2, Cu_2S, $Cu_{1.96}S$, and Ni alloy. It was found that the partial dissolution of Ni, Fe, and Co occurs as a result of galvanic interaction between Ni alloys and sulphide minerals, direct acid attack, and a cementation process during which simultaneous precipitation of aqueous copper is achieved. The cementation process was found to be responsible for the leaching of the nickel alloy and iron according to reaction 2.1 and reaction 2.2, respectively:

$$Ni + Cu^{2+} \rightarrow Cu + Ni^{2+} \quad [2.1]$$

$$Fe + Cu^{2+} \rightarrow Cu + Fe^{2+} \quad [2.2]$$

Dissolution of Ni_3S_2 to form NiS through cementation reactions further contributed to the precipitation of copper, according to the following reactions:

$$Ni_3S_2 + Cu^{2+} \rightarrow Cu + 2NiS + Ni^{2+} \quad [2.3]$$

$$Ni_3S_2 + 2Cu^{2+} \rightarrow Cu_2S + NiS + 2Ni^{2+} \quad [2.4]$$

$$Ni_3S_2 + Ni + 4Cu^{2+} \rightarrow 2Cu_2S + 4Ni^{2+} \quad [2.5]$$

Rademan *et al.* (1999) reported that the rate of copper precipitation in atmospheric leaching increases if the ratio of acid to copper in the spent electrolyte is increased, while this also leads to maximum nickel extraction. Leaching by direct acid attack of the nickel-iron alloy, NiS, and FeS is possible in the absence of oxidising reagents, as shown by reactions 2.6 to 2.8. The rates of these reactions are highly dependent on the acid concentration.

$$Ni\text{-}Fe + 4H^{+} \rightarrow Ni^{2+} + Fe^{2+} + 2H_2 \quad [2.6]$$

$$NiS + 2H^{+} \rightarrow Ni^{2+} + H_2S \quad [2.7]$$

$$FeS + 2H^{+} \rightarrow Fe^{2+} + H_2S \quad [2.8]$$

It was observed that the pH of the leaching solution rose noticeably as soon as copper precipitation was completed. This was attributed to the fact that some leaching occurred as a result of a cementation process as long as copper precipitation proceeded. Once all the copper had precipitated, however, the leaching occurred only by direct acid attack, hence leading to an increase in pH (Lamya and Lorenzen, 2006).

In the presence of small amounts of oxygen, oxidative dissolution of the nickel, iron, and their sulphides as well as oxidation of ferrous iron could occur according to the following reactions (Lamya and Lorenzen, 2006; Van Schalkwyk *et al.*, 2011):

$$Ni + 2H^{+} + \tfrac{1}{2}O_2 \rightarrow Ni^{2+} + H_2O \quad [2.9]$$

$$Fe + 2H^{+} + \tfrac{1}{2}O_2 \rightarrow Fe^{2+} + H_2O \quad [2.10]$$

$$Ni_3S_2 + 2H^{+} + \tfrac{1}{2}O_2 \rightarrow Ni^{2+} + 2NiS + H_2O \quad [2.11]$$

$$2Fe^{2+} + 2H^{+} + \tfrac{1}{2}O_2 \rightarrow 2Fe^{3+} + H_2O \quad [2.12]$$

The amount of oxygen in solution was found to be critical to achieve the desired leaching behaviour. An oxygen shortage hinders the oxidation and dissolution of iron while excess oxygen has a negative impact on copper precipitation (Rademan *et al.*, 1999). In the absence of oxygen, the oxidation of ferrous iron can also proceed by reaction with dissolved copper, according to reaction 2.13. Ferric iron enhances the rate of nickel dissolution according to leaching reaction 2.14.

$$Fe^{2+} + Cu^{2+} \rightarrow Cu^{+} + Fe^{3+} \quad [2.13]$$

$$Ni_3S_2 + 2Fe^{3+} \rightarrow 2Fe^{2+} + 2NiS + Ni^{2+} \quad [2.14]$$

It is hence possible that the oxidation of ferrous ions could become the rate limiting step for nickel dissolution if the concentrations of cupric ions and oxygen are low, as was observed by Hofirek and Kerfoot (1992). While iron dissolution occurs primarily in the first stage atmospheric leach, and most of the iron is dissolved (Kerfoot *et al.*, 1986), iron precipitation

could also occur. Iron precipitation has been observed if the pH of the leaching solution increased to values above three, forming ferric hydroxide or ferric sulphate according to reaction 2.15 and reaction 2.16, respectively (Lamya and Lorenzen, 2006):

$$Fe^{3+} + 3H_2O \rightarrow Fe(OH)_3 + 3H^+ \quad [2.15]$$

$$Fe^{3+} + HSO_4^- + H_2O \rightarrow Fe(OH)SO_4 + 2H^+ \quad [2.16]$$

Precious metals that enter the first stage atmospheric leach in solution as a result of recycled spent electrolyte are generally precipitated in the first stage leach together with copper (Kerfoot *et al.*, 1986). This was confirmed by Van Schalkwyk *et al.* (2011), who also confirmed that the mechanism by which this precipitation occurs in the first stage leach is not well understood.

2.2.2 First stage pressure leaching

Rademan *et al.* (1999) performed studies to develop a better understanding of the behaviour of nickel-copper matte in a high pressure acid/oxygen leaching environment. More specifically, the dissolution of base metals in the first stage pressure leach at Impala Platinum Refineries was investigated. Given the similarity between the compositions of the material being fed to atmospheric leaching and the first stage pressure leaching, several of the nickel dissolution reactions observed by Lamya and Lorenzen (2006) discussed in Section 2.2.1also occur in the first stage pressure leaching. Rademan *et al.* (1999) proposed a reaction mechanism for the first stage pressure acid/oxygen leaching of nickel-copper matte. It was determined that all the reactions contributing to the leaching process are electrochemical in nature, and that the leaching process observed during the batch experiments could be divided into three stages.

2.2.2.1 Reaction mechanism – stage 1

The first stage of the leaching process in the first stage pressure leaching was proposed to involve the leaching of Ni according to reaction 2.9 and the leaching of Ni_3S_2 according to reaction 2.11. In addition, Cu^{2+} ions are precipitated in the form of Cu_2S and have a catalytic effect on the dissolution of Ni from Ni_3S_2 to form NiS (reaction 2.4) and the dissolution of nickel from nickel alloy (reaction 2.5). The presence of H_2SO_4 and O_2 can lead to the direct leaching of copper from Cu_2S to form $Cu_{1.8}S$ according to the following reaction:

$$5Cu_2S + 2H^+ + ½O_2 \rightarrow Cu^{2+} + 5Cu_{1.8}S + H_2O \quad [2.17]$$

Some of the copper ions that are formed as a result of the above leaching reaction will immediately be precipitated as a result of reaction 2.4 and reaction 2.5 taking place. The precipitation of Cu^{2+} ions as a result of these reactions with Ni_3S_2 was proposed as a reason why Ni_3S_2 and not Cu_2S is leached during the initial leaching stages. Provis *et al.* (2003) also indicated that the presence of less oxidised species such as Ni alloy and Ni_3S_2 in the leaching solution reduces the dissolution rate or prevent dissolution of several other species because of galvanic inhibition of the more highly oxidised species. It was reported that the following reaction could occur if the Cu^{2+} ions are present in a low concentration (Provis *et al.*, 2003):

$$Ni + 2NiS \rightarrow Ni_3S_2 \quad [2.18]$$

Metallic iron dissolves together with metallic nickel in this initial stage of the high pressure leaching process according to reaction 2.10. Iron sulphide present in the matte fed to the first stage pressure leach is leached together with the Ni_3S_2:

$$Ni_3S_2 \cdot FeS + 2H^+ + \tfrac{1}{2}O_2 \rightarrow 3NiS + Fe^{2+} + H_2O \quad [2.19]$$

2.2.2.2 Reaction mechanism – stage 2

During the second stage of the proposed leaching reaction mechanism, nickel is selectively leached to form different nickel sulphide mineral phases while copper is leached and precipitated simultaneously to form different copper sulphide mineral phases. The following reactions describing the dissolution of copper were believed to occur:

$$25Cu_{1.96}S + 8H^+ + 2O_2 \rightarrow 4Cu^{2+} + 25Cu_{1.8}S + 4H_2O \quad [2.20]$$

$$16Cu_2S + 2H^+ + \tfrac{1}{2}O_2 \rightarrow Cu^{2+} + Cu_{31}S_{16} + H_2O \quad [2.21]$$

$$10Cu_{31}S_{16} + 44H^+ + 11O_2 \rightarrow 22Cu^{2+} + 160Cu_{1.8}S + 22H_2O \quad [2.22]$$

During this second stage of the proposed reaction mechanism, reaction 2.11 proceeds via the production of Ni_7S_6 as an intermediate product:

$$3Ni_3S_2 + 4H^+ + O_2 \rightarrow 2Ni^{2+} + Ni_7S_6 + 2H_2O \quad [2.23]$$

$$Ni_7S_6 + 2H^+ + \tfrac{1}{2}O_2 \rightarrow Ni^{2+} + 6NiS + H_2O \quad [2.24]$$

Provis *et al.* (2003) reported that the intermediate species Ni_7S_6 and $Cu_{31}S_{16}$ are only present in small quantities for short periods of time. The NiS produced in the above reactions is leached further to form Ni_3S_4:

$$4NiS + 2H^+ + \tfrac{1}{2}O_2 \rightarrow Ni^{2+} + Ni_3S_4 + H_2O \quad [2.25]$$

Provis *et al.* (2003) proposed that the reaction 2.26 also contributes to the leaching of NiS, since it was required to accurately model the behaviour of the system. Because the concentration of Cu^{2+} in the system is very low if Ni_3S_2 is present, this reaction only takes place after all Ni_3S_2 has been removed.

$$NiS + Cu^{2+} \rightarrow CuS + Ni^{2+} \quad [2.26]$$

2.2.2.3 Reaction mechanism – stage 3

Simultaneous leaching of nickel and copper occurs during the third and final stage of the proposed leaching mechanism. As soon as all the Ni_3S_2 has been leached and the Cu_2S and $Cu_{1.96}S$ have been converted to $Cu_{1.8}S$ and CuS, copper leaching proceeds according to reaction 2.27 and 2.28:

$$5Cu_{1.8}S + 8H^{+} + 2O_2 \rightarrow 4Cu^{2+} + 5CuS + 4H_2O \quad [2.27]$$

$$5Cu_{1.8}S + 8Fe^{3+} \rightarrow 4Cu^{2+} + 5CuS + 8Fe^{2+} \quad [2.28]$$

The leaching of nickel during this third stage occurs according to reactions 2.29 and 2.30:

$$2Ni_3S_4 + 2H_2O + 15O_2 \rightarrow 6Ni^{2+} + 4H^{+} + 8SO_4^{2-} \quad [2.29]$$

$$2Ni_3S_4 + 6Cu^{2+} + 2H_2O + 3O_2 \rightarrow 6Ni^{2+} + 6CuS + 4H^{+} + 2SO_4^{2-} \quad [2.30]$$

From reaction 2.17, reactions 2.20 to 2.22 and reactions 2.27 and 2.28, it follows that the leaching of copper from Cu_2S to form CuS proceeds in two primary steps, with $Cu_{1.8}S$ being formed as an intermediate product. This proposed leaching path whereby an intermediate species is formed during the first reaction step and the final conversion to CuS is achieved in the second step was used to explain the different rates of leaching observed during initial and latter stages of the process.

2.2.3 Second stage pressure leaching

The second stage pressure leach essentially comprises the leaching of copper that enters the leaching system in the converter matte and copper that has been precipitated in the first stage leaching, as well as nickel that has not been dissolved in the upstream leaching stages. Steenekamp and Dunn (1999) classified the most important reactions taking place during the second stage high pressure leaching into two groups. Two reactions comprise the first group that represents the leaching of the first stage leach hydrolysis products:

$$Cu(OH)_2CuSO_4 + H_2SO_4 \rightarrow 2CuSO_4 + 4H_2O \quad [2.31]$$

$$2Fe(OH)SO_4 + H_2SO_4 \rightarrow Fe_2(SO_4)_3 + 2H_2O \quad [2.32]$$

The second group of reactions involve the oxidation of sulphide minerals, which, in addition to reaction 2.11, include reactions 2.33 to 2.35. Reaction 2.34 presents a simplified overall leaching reaction for Cu_2S, disregarding the formation of intermediate copper sulphide species in the dissolution process.

$$NiS + 2O_2 \rightarrow NiSO_4 \quad [2.33]$$

$$2Cu_2S + 2H_2SO_4 + 5O_2 \rightarrow 4CuSO_4 + 2H_2O \quad [2.34]$$

$$CuS + 2O_2 \rightarrow CuSO_4 \quad [2.35]$$

Grewal *et al.* (1992) studied the high pressure oxidative leaching of a copper refinery residue containing copper, predominantly as Cu_2S and $Cu_{1.96}S$, as well as precious metals. In correspondence with the copper leaching mechanism proposed by Rademan *et al.* (1999), it was determined that various intermediate copper sulphide species such as $Cu_{1.76}S$ were formed during the copper dissolution. The further leaching of these compounds to form CuS were however much faster than the leaching of CuS itself. The proposed reaction pathway therefore considered the dissolution of Cu_2S and $Cu_{1.96}S$ to occur via two steps, with the formation of CuS as an intermediate product. In the presence of acid, the dissolution of Cu_2S in the first step followed the reaction 2.36, which is the combined overall reaction for reaction 2.17 and reaction 2.27 proposed by Rademan *et al.* (1999):

$$Cu_2S + H_2SO_4 + \tfrac{1}{2}O_2 \rightarrow CuS + CuSO_4 + H_2O \quad [2.36]$$

If excess acid was available the dissolution of CuS produced in reaction 2.36 could occur simultaneously according to reaction 2.37. The formation of elemental sulphur did, however, occur rarely under normal operating conditions. Under oxidising conditions, the sulphur was oxidised to yield an overall CuS leaching reaction similar to reaction 2.35. In acid depleted leaching solutions, the leaching of Cu_2S was found to occur according to reaction 2.38, where after CuS leaching again proceeded according to reaction 2.35.

$$CuS + H_2SO_4 + \tfrac{1}{2}O_2 \rightarrow CuSO_4 + H_2O + S \quad [2.37]$$

$$Cu_2S + \tfrac{1}{2}CuSO_4 + \tfrac{1}{2}O_2 + 2H_2O \rightarrow CuS + \tfrac{1}{2}CuSO_4 \cdot 2Cu(OH)_2 \quad [2.38]$$

Kerfoot *et al.* (1986) indicated that conducting the second stage pressure leach at too low a temperature could lead to the formation of elemental sulphur, which in turn will reduce the base metal leaching kinetics and will have a detrimental effect on the quality of the PGM concentrate. The temperature selection must allow any sulphur that form to be oxidised to

sulphuric acid. Increasing the temperature too much, on the other hand, would lead to faster PGM dissolution.

Ruiz *et al.* (2007) investigated the high pressure sulphuric acid/oxygen leaching of white metal containing 76% Cu, 2.2% Fe, and 20.2% S. In order to prevent the chemical reactions from becoming too complex, stoichiometric Cu_2S was considered to be the only copper phase present in the material to be leached. The results agreed with the earlier observations of Grewal *et al.* (1992) that the leaching of chalcocite and other non-stoichiometric copper-sulphides (typically djurleite and digenite) occurs in two stages with the formation of covellite as an intermediate product. Ruiz et al. (2007) proposed reaction 2.36 as the only pathway for chalcocite dissolution, but considered both reaction 2.35 and reaction 2.37 as potential mechanisms for CuS dissolution. Assuming that the investigated system always had excess acid, the exclusion of reaction 2.38 was reasonable. Both the iron content of the white metal (2.2%) and the ratio of solids to liquid were considered to be too low for the iron to have a significant impact on the leaching behaviour of the system. The majority of the sulphur present in the form of sulphides in the white metal was furthermore oxidised to sulphate, with only small amounts of elemental sulphur being produced.

Padilla *et al.* (2008) investigated the dissolution of sulphidised chalcopyrite in a high pressure sulphuric acid environment. Leaching of CuS was reported to occur by the same overall reactions reported above (reaction 2.35 and reaction 2.37). It was however noticed that Fe^{3+} is an oxidising agent that can assist with the leaching of metal sulphides, similar to the observations reported by Hofirek and Kerfoot (1992) for atmospheric leaching. An indirect leaching mechanism was therefore proposed for systems where ferric ions are present whereby metal sulphides are oxidised by Fe^{3+} where after the produced Fe^{2+} is re-oxidised by oxygen. The degree to which this influences the overall leaching rate has not been determined (Padilla *et al.*, 2008). Chu and Lawson (1991) and Grewal *et al.* (1992) confirmed the observation that the presence of iron in the leaching solution increases the copper leaching rate because of the fact that the iron acts as an oxygen carrier, while Clément *et al.* (1992) ascribed the effect that iron concentration has on the leaching behaviour to the effect of iron concentration on slurry viscosity, which in turn will affect gas-liquid mass transfer.

2.3 Platinum group metal chemistry

2.3.1 General properties

The platinum group metals comprise platinum, palladium, rhodium, ruthenium, iridium, and osmium. Overviews of the physical and mechanical properties of these metals are given by Renner (1992) as well as Seymour and O'Farrelly (2006). While all the platinum group metals can exist in numerous oxidation states depending on the compound that they form part of, the most common oxidation states for the respective PGMs are: Ru (+2/+3/+4), Rh (+3), Pd (+2), Os (+2/+4), Ir (+3/+4), and Pt (+2/+4) (Renner, 1992; Housecroft, 1999; Giandomenico, 2006).

The platinum group metals show a high resistance to dissolution by sulphuric acid. Apart from palladium (at a rate of approximately 1 $mg/cm^2 \cdot h$) and rhodium (at a rate of approximately 0.1 $mg/cm^2 \cdot h$ if the rhodium is in a finely divided form), none of the platinum group metals show noticeable dissolution in 96% sulphuric acid at 100°C. In cases where PGMs have been alloyed with base metals, the base metals can be dissolved to form dispersed noble-metal black, which can be dissolved more easily than the bulk PGMs. Dissolution of rhodium in this form by hot sulphuric acid leads to the formation of rhodium sulphate, $Rh_2(SO_4)_3$ (Renner, 1992; Goldberg and Hepler, 1968).

One of the reasons why platinum group metals exhibit such a high resistance to corrosion is the fact that a thin protective oxide film forms on the metal when in aqueous media under oxidising conditions (Seymour and O'Farrelly, 2006). According to Hartley (1991), eight PGM oxides have been identified; these include the dioxides of all the PGMs (hydrated forms can also exist) as well as ruthenium tetroxide, RuO_4, and osmium tetroxide, OsO_4. Several authors (Renner, 1992; Hartley, 1991; Goldberg and Hepler, 1968; Giandomenico, 2006) made reference to additional oxides such as PtO, Pt_2O_3, PtO_3, PdO, Rh_2O_3, and Ir_2O_3. According to Renner (1992), concentrated hydrobromic acid is the only reagent that can directly dissolve oxides of the PGMs. Because the oxides of PGMs are less soluble than the pure metals, reduction of these compounds is required to enhance dissolution (Renner, 1992).

In addition to the two rhodium oxides mentioned above, Rh can also be found as Rh_2S_3 and $RhSe_2$ (Hartley, 1991; Giandomenico, 2006). Although some studies reported the existence of $Rh(OH)_3$, it is most likely that the detected compound was a hydrated form of Rh_2O_3 (Rard, 1985). Ruthenium occurs widely as laurite, RuS_2, and it has been proposed that lower

sulphides do not form (Rard, 1985). Other ruthenium containing compounds relevant to this study include $RuTe_2$ and $RuSe_2$ (Giandomenico, 2006). Compounds of iridium include hydroxides ($Ir(OH)_3$ and $Ir(OH)_4$), sulphides (IrS, Ir_2S_3, IrS_2, and IrS_3), as well as selenides and tellurides. Osmium occurs as OsS_2, $OsSe_2$, and $OsTe_2$ in addition to the oxides. The most common palladium and platinum sulphides, selenides, and tellurides include PdS, PtS, PdS_2, PtS_2, PdSe, $PdSe_2$, PdTe, and $PdTe_2$. The hydroxide compounds, $Pd(OH)_2$ and $Pt(OH)_2$, can also be formed in addition to aforementioned compounds (Giandomenico, 2006). Reference is not made to halides, borides, silicides, and phosphides here, although these compounds also exist for platinum group metals (Giandomenico, 2006). In general, reverse hydrolysis of PGM hydroxide complexes that might be present will occur spontaneously at varying rates when present in an acidic solution (Renner, 1992). The presence of hydrolysed PGM compounds in the leaching solution is thus unlikely.

Selective reduction and cementation of PGMs by base metals is not possible, but zinc, iron, and aluminium have been used for collective cementation of precious metals from aqueous solutions (Renner, 1992). Examples of these applications include the recovery of rhodium from waste rinsing water using zinc powder (Aktas, 2011), using zinc powder for the recovery of PGMs from cyanide leach solutions (Huang *et al.*, 2007), and the utilisation of iron powder for PGM cementation from a sulphuric acid leach solution (Vyazovoy *et al.*, 2010). Limited information about the precipitation reaction mechanisms and kinetics is available.

Platinum group metals exist in many different chemical forms in solution due to their tendency to form complexes and to undergo hydrolysis, hydration, and redox transformations (Aleksenko *et al.*, 2001). Aqua regia and hydrochloric acid are most often used for the dissolution of platinum and palladium. The behaviour of PGMs in these solutions and the chemistry of PGM chloro-, ammonia-, and amine complexes are consequently well understood. There is, however, very limited, and often contradictory, information regarding the behaviour of PGMs in sulphate media available in the published literature. The other precious metals (OPMs), namely rhodium, ruthenium, and iridium, are reported to be the PGMs undergoing the largest percentage dissolution in the second stage high pressure leaching process (Steenekamp, 2009). The focus of the remainder of the thesis will thus be on these three precious metals.

2.3.2 Rhodium species in sulphuric acid solution

As discussed in Section 2.3.1, rhodium primarily occurs in the +3 oxidation state. Gulliver and Levason (1982) reported that chemical oxidation can be used to produce Rh^{4+} species in solution from Rh_2O_3 or $(Rh(H_2O)_6)^{3+}$. The resulting Rh^{4+} ions have, however, not been identified.

Belyaev *et al.* (2009) investigated the formation of rhodium sulphate complexes in aqueous solutions. In solutions with pH values lower than 1.6, a complex with a double sulphate bridge, $[(H_2O)_4Rh(\mu\text{-}SO_4)_2Rh(H_2O)_4]^{2+}$, and an ion pair of Rh^{3+} and SO_4^{2-} were found to be the predominant stable species. As the pH value was increased to between 1.6 and 3.5, a hydroxide ion was substituted for one of the sulphate bridges of some of the double sulphate bridge complexes, resulting in the formation of an additional complex $[(H_2O)_4Rh(\mu\text{-}SO_4)(\mu\text{-}OH)Rh(H_2O)_4]^{3+}$. Giandomenico (2006) reported the existence of soluble rhodium sulphate, $Rh_2(SO_4)_3 \cdot xH_2O$, in two forms, namely a red form containing coordinated sulphate and a yellow form containing hexaaqua ions, $(Rh(H_2O)_6)^{3+}$.

2.3.3 Ruthenium species in sulphuric acid solution

Ruthenium tetroxide (RuO_4) is formed by the oxidation of aqueous solutions of ruthenates, or by reaction of ruthenium metal with a strong oxidising agent in a hot solution (Goldberg and Hepler, 1968; Iwakura *et al.*, 1977). Ruthenium tetroxide is a strong oxidising agent that will oxidise water when in solution. The solubility of RuO_4 in water varies between 0.1 mol/ℓ and 0.14 mol/ℓ, and behaves like a weak acid when dissolved in water (Rard, 1985). When ruthenium tetroxide is reduced in sulphuric acid, an unstable intermediate species, RuO_2^{2+}, could form. RuO_2^{2+} gradually decomposes to Ru^{+4} and RuO_4 (Rard, 1985). Iwakura *et al.* (1977) also reported that RuO_4 is very unstable in acidic solutions and that it will readily be reduced to lower oxidations states.

In general, the oxidation state of Ru will depend on the strength of the acid. For sulphuric acid concentrations of 0.5 mol/ℓ and lower, Ru^{4+} will dominate the system, while oxidation states +3 or +3.5 would be dominant for higher acid concentrations. The stoichiometry of the sulphate complexes that could form at high acid concentrations is not known. Under these conditions, the monomeric form of Ru^{3+} is the most stable, and any polymeric Ru^{3+} present will gradually convert to monomers. Complex formation between ruthenium in the +3 oxidation state and available sulphate ions occurs according to equation 2.39 and equation 2.40 (Rard, 1985).

$$Ru^{3+} + SO_4^{2-} \rightarrow RuSO_4^{+} \quad [2.39]$$

$$RuSO_4^{+} + SO_4^{2-} \rightarrow Ru(SO_4)_2^{-} \quad [2.40]$$

Similar to the Ru^{3+} species, Ru^{4+} can polymerise to form $Ru_4(OH)_{12}^{4+}$, but the monomer $Ru(OH)_2^{2+}$ is the most stable species at pH values below three. This species combines with available sulphate ions to form $Ru(OH)_2SO_4$ (Rard, 1985). Hartley (1991) also reported the stepwise reduction of tetrameric species to species with average oxidation states of +3.75, +3.5, and eventually +3. Rard (1985) suggested that a number of simple ruthenium sulphate complexes such as $RuSO_4$, $Ru(SO_4)^{+}$, $Ru(SO_4)_2^{-}$ and $Ru(OH)_2(SO_4)$, as well as a number of tetrameric forms with average ruthenium valences of between 3.5 and 4, exist in aqueous sulphuric acid solutions.

Martin (1952) reported that the reduction of RuO_4 in sulphuric acid can lead to the formation of Ru^{6+}, but that these species generally decompose to form Ru^{4+} and Ru^{8+}. If Ru^{6+} are present, it was predicted that it would be as a result of ruthenyl radicals (RuO_2^{2+}) being present. According to Goldberg and Hepler (1968), Ru^{+6} would typically occur in the form of ruthenates (RuO_4^{2-}); these species are, however, highly unstable in acidic solutions. The presence of Ru^{6+} in sulphuric acid solutions, if at all, was consequently predicted to be in the form of $[RuO_2(SO_4)_2]^{-2}$ (Goldberg and Hepler, 1968).

Apart from RuO_4, some reports indicate the formation of hydrated oxides approaching the composition of RuO, while others report that Ru(OH), $Ru(OH)_2$, and $RuO{\cdot}H_2O$ form. $RuO_2{\cdot}2H_2O$ and $Ru(OH)_3{\cdot}H_2O$ are both theoretically metastable, with $RuO_2{\cdot}2H_2O$ that should spontaneously dehydrate and $Ru(OH)_3{\cdot}H_2O$ that should disproportionate to RuO_2, Ru, and H_2O (Rard,1985).

2.3.4 Iridium species in sulphuric acid solutions

According to Jones (2004), the chemistry of iridium compounds is similar to that of rhodium compounds, while there are also some correlations with ruthenium complexes. As was the case with rhodium, no compound containing iridium in the +8 or +7 oxidation state has reliably been identified, while information regarding Ir^{6+}compounds is limited to the existence of hexafluorides and possibly some oxide species. Pentafluorides and anionic hexafluorides are the only well characterised compounds of iridium in the +5 oxidation state (Gulliver and Levason, 1982).

In the absence of halide ions, the Ir^{4+} species that exist in solution are not well defined. The oxidation of Ir^{3+} in solution could lead to the formation of $(IrO(OH))^{+}$, $(IrO)^{2+}$, or oxo-centred trimers such as $(Ir_3O(SO_4)_9)^{10-}$. Levason (1991) indicated that Ir^{3+} is thermodynamically very stable, and that the oxidation of Ir^{3+} to produce Ir^{4+} complexes is hence very difficult. While some reports of Ir^{4+} sulphate complexes are available, there exists no certainty as to the existence of any mononuclear species. The structure and complete formulae of the polynuclear sulphate complexes depend on the reagents and production or dissolution route, but typically contain an $Ir_3O(SO_4)_6$ group with various combinations of iridium oxidation states, e.g. $Ir^{3+}Ir^{4+}Ir^{4+}$ or $Ir^{3+}Ir^{3+}Ir^{4+}$ (Gulliver and Levason, 1982; Abovskaya *et al.*, 2006). Giandomenico (2006) also noted that the platinum group metals in lower oxidation states tend to form complexes with sulphur and phosphorous, while the PGMs in higher oxidation states are more likely to form complexes with oxygen and fluorine.

2.4 Variables influencing leaching kinetics

Prosser (1996) presented a comprehensive overview of the factors that may affect the rates at which reactions in a leaching system proceed. These include system variables such as temperature, physical and chemical properties of the leach solution as well as the solid phase, and additional system-specific phenomena. The most commonly investigated effects relevant to the BMR leaching stages are discussed in the subsequent sections.

2.4.1 First stage atmospheric leaching

In a study related to the work discussed in Section 2.2.1, the influences that initial copper ion concentration, initial acid concentration, temperature, stirring rate, particle size distribution, and pulp density have on the first stage atmospheric leaching and copper cementation were investigated (Lamya and Lorenzen, 2005; Lamya and Lorenzen, 2006). Different steps were found to be rate controlling for the different leaching paths and for different temperatures. The rate of metal dissolution by direct acid attack was limited by the rate of diffusion while the rate of chemical reactions limited the rate of metal dissolution in the case of the cementation process.

Apart from the degree of agitation, all the investigated operating parameters had an effect on the rate of copper precipitation. This confirmed the assumption that diffusion of ions through the leaching solution to the solid-liquid interface was not the rate limiting step. The rate of copper cementation was found to decrease as the initial copper ion concentration increased up

to a value of 36 g/ℓ, above which the concentration did not influence the cementation rate. This observation was attributed to the changes in the copper activity, solution viscosity, and diffusivity of the copper ions brought about by the increased copper ion concentration. An increase in the initial acid concentration caused some of the precipitated copper to dissolve again, causing the overall rate of copper precipitation to decrease with increasing acid concentration. Above a specific acid concentration, the rates of copper precipitation and dissolution were believed to be equal, with changes in acid concentration not influencing the cementation rate further. Initial increases in the solid content of the pulp caused the cementation rate to increase due to increased matte surface area where precipitation could take place. Above a specific solids content threshold, further increases in the solids content caused the cementation rate to decrease due to lower mass transfer rates through the larger quantity of matte in the leaching mixture. A decrease in the size of the matte particles led to a larger cathodic surface area and hence an increased cementation rate. In general, the copper precipitation proceeded at a faster rate as the temperature was increased.

2.4.2 First stage pressure leaching

Rademan *et al.* (1999) determined that the rates of nickel dissolution and copper precipitation were very fast during the initial stages of the leaching. As leaching progressed, the porosity of the matte particles increased, leading to improved leaching efficiency. It was found that Ni was leached selectively during initial stages because heazlewoodite (Ni_3S_2) was present, which allowed a substitution reaction to take place whereby copper ions were precipitated as Cu_2S while nickel ions were leached into solution (refer to reaction 2.4 and reaction 2.5).

If the formation of H_2S in the oxidation half-reactions of reaction 2.4 and reaction 2.5 was faster than the oxidation of H_2S, H_2S accumulated in the system and reduced the Ni leaching rate. The formation and accumulation of H_2S can be prevented, and the dissolution rate hence increased, by the presence of silver, cupric, or ferric ions that lead to the rapid formation of intermediate products. While Rademan *et al.* (1999) reported that H_2S was detected and had an inhibiting influence on the leaching reactions when the Cu^{2+} ion concentration became too low, Provis *et al.* (2003) suggested that the Cu^{2+} concentration will always be high enough to prevent the formation of H_2S from having a significant impact on the leaching kinetics.

2.4.3 Second stage pressure leaching

Ruiz *et al.* (2007) investigated the effect of stirring speed, temperature, sulphuric acid concentration, oxygen partial pressure, particle size distribution of the feed, and leaching time

on the leaching of white metal. It was found that sulphur in the matte was predominantly oxidised to sulphate, and the dissolution of copper was unaffected by the acid concentration at concentrations above 0.05 mol/ℓ and the oxygen partial pressure at values above 608 kPa. The temperature did however have a significant impact on the leaching kinetics.

2.4.3.1 Temperature

The effect of temperature on the dissolution of copper from the white metal was investigated for a system with sufficient agitation and oxygen supply, and with a sulphuric acid concentration of 0.2M. Two distinct rates of copper dissolution were observed at temperatures lower than 130°C. Copper dissolution occurred very fast during the first 30 minutes until dissolution of approximately 40% was achieved, where after the rate of dissolution decreased. The two different dissolution rates were believed to be indicative of the two different stages comprising the overall copper dissolution, with CuS being formed as an intermediate product during the rapid initial reaction. At temperatures above 130°C, there was no clear distinction between different dissolution rates because the two reaction stages overlapped and considerably faster leaching of CuS was achieved. The temperature was the variable with the most significant influence on the leaching behaviour of the white metal. At temperatures below 130°C the dissolution was incomplete after five hours while dissolution was completed within 90 minutes at a temperature of 150°C.

Fugleberg *et al*. (1995) investigated the dissolution of rhodium during a high pressure copper leaching stage to determine the most important operating parameters. Of acidity, oxygen pressure, and temperature, the latter was identified as the parameter with the largest influence on rhodium dissolution, causing the dissolution to increase from 10% at 115°C to 80-90% at 140°C. No additional information regarding the leaching reactions and leaching kinetics were published.

2.4.3.2 Acid concentration

In a system with sufficient agitation and an oxygen partial pressure of 1013 kPa at a temperature of 105°C, the total amount of copper that was dissolved after two hours increased as the acid concentration increased. A maximum dissolution of 48% was achieved using 0.5M sulphuric acid. For a sufficiently agitated system operated with an oxygen partial pressure of 608 kPa at a temperature of 150°C, more than 90% copper dissolution was achieved after one hour of leaching for all acid concentrations between 0.025M and 0.3M. It was however observed that maximum copper dissolution was achieved at a concentration of around 0.05M,

where after dissolution decreased slightly with increasing acid concentration. This observation was ascribed to the fact that oxygen solubility decreases with increasing sulphuric acid concentration (Ruiz *et al.*, 2003; Tromans, 1998).

2.4.3.3 Dissolved oxygen concentration

As discussed in Section 2.2, the leaching reactions are dependent on oxygen to proceed. Ruiz *et al.* (2007) investigated the effect of oxygen pressure on the copper dissolution at temperatures of 130°C and 150°C. At the lower temperature, the oxygen partial pressure had a very small effect on the copper dissolution rate. At the higher temperature, however, increasing the oxygen partial pressure from 203 kPa to 608 kPa significantly increased the copper dissolution rate, but further increasing the oxygen partial pressure did not have an influence on the copper dissolution. At high temperatures the leaching reactions proceed at a much faster rate, hence requiring a higher rate of oxygen addition for the reactions to occur. At the low oxygen partial pressure, the availability of oxygen and the transfer of oxygen to the reaction surfaces are limiting the rate at which the leaching reactions can proceed. The importance of oxygen overpressure to achieve fast copper dissolution from copper sulphide phases was also reported by Baghalha *et al.* (2007) and Chu and Lawson (1991).

The rate of oxygen mass transfer from the gaseous phase to the liquid phase is influenced by numerous factors, some of which include the gas flow rate, mixing intensity, reactor configuration, composition and physical properties of the liquid phase, and the oxygen solubility in the liquid phase. The rate of oxygen transfer from the gaseous phase to the liquid phase, r_{O_2} can be calculated using Equation 2.41:

$$r_{O_2} = k_L \cdot a \cdot \left(C_{O_2,Eq} - C_{O_2,Liq}\right) \qquad [2.41]$$

where k_L is the oxygen mass transfer coefficient, a is the interfacial area per unit volume, and $C_{O_2,Eq}$ and $C_{O_2,Liq}$ are the dissolved oxygen concentration in the liquid at equilibrium and the dissolved oxygen concentration present in the bulk liquid, respectively. According to Cheng (1994), the liquid mass transfer coefficient and the specific interfacial area are usually grouped together to simplify the analysis of oxygen mass transfer. Cheng (1994) discussed the effect of the impeller design, agitation speed, temperature, pressure, and solid content of the slurry on the rate of oxygen transfer, and evaluated these effects using an experimental setup applicable to hydrometallurgical studies. Given the complexity involved with the accurate determination of the mass transfer coefficient, $k_L.a$, it is typically treated as an adjustable model parameter in autoclave modelling work (Cheng, 1994).

The dissolved oxygen concentration in the liquid at equilibrium, in turn, is influenced by the solution temperature, oxygen partial pressure, and the solution composition. Tromans (1998a) developed an equation based on thermodynamics to estimate the solubility of oxygen in water as a function of oxygen partial pressure and temperature:

$$C'_{O_2,Eq} = P_{O_2} \cdot f(T) \qquad [2.42]$$

where $C'_{O_2,Eq}$ is the molal concentration of the dissolved oxygen, P_{O_2} is the oxygen partial pressure, and the temperature dependant function, *f(T)*, is given by Equation 2.43:

$$f(T) = \exp\left(\frac{0.046T^2 + 203.35T \cdot \ln\left({}^{T}/_{298}\right) - (299.378 + 0.092T)(T - 298) - 20591}{8.3144T}\right) \qquad [2.43]$$

This correlation was shown to be valid for temperatures from 273 K to 616 K and pressures up to 60 atm. In further work, Tromans (1998b) proposed that Equation 2.42 be modified to account for the reduced water content available to interact with oxygen if inorganic solutes are present in the water:

$$C'_{O_2,Eq} = \phi_{eff} \cdot P_{O_2} \cdot f(T) \qquad [2.44]$$

For solutions containing z different solutes, the effective water fraction available for oxygen interaction, ϕ_{eff}, is given by Equation 2.45:

$$\phi_{eff} = \phi_1 \left(\prod_{2}^{z} \phi_i\right)^q \qquad [2.45]$$

where ϕ_1 is the available water fraction calculated for the solute with the most significant effect on oxygen solubility. The fraction of water available for oxygen interaction calculated for a specific solute i, ϕ_i, is given by Equation 2.46:

$$\phi_i = \left(\frac{1}{1 + \kappa_i (\mathrm{C}'_\mathrm{i})^{y_i}}\right)^{\eta_i} \qquad [2.46]$$

Tromans (1998b) determined values for the coefficient and exponents in Equation 2.45 and Equation 2.46 for a range of solutes for which experimental data at 298 K and an oxygen partial pressure of one atmosphere are available in literature. A value of 0.8 was assigned to parameter q in Equation 2.45 based on 21 solutes examined during the study. The parameters for the solutes that are relevant to this study are shown in Table 2.3.

Table 2.3. Parameters to estimate oxygen solubility in inorganic solutions according to equation 2.45 and equation 2.46 (Tromans, 1998b).

Solute	κ	y	η
H_2SO_4	2.01628	1.253475	0.168954
$NiSO_4$	2.23207	1.115617	0.222794
$CuSO_4$	2.23207	1.115617	0.222794

2.4.3.4 Degree of agitation

The rate of agitation will only have a major effect on the leaching kinetics if the rate of oxygen mass transfer from the gaseous phase to the liquid phase is the rate determining step for the leaching reaction. As discussed in Section 2.4.3.3, the rate of oxygen mass transfer is dependent on various factors, including the reactor design. The effect of the rate of agitation could hence vary between different experimental setups for the same leaching system. For the experimental set-up and conditions described by Ruiz *et al.* (2007), the stirring rate only had an influence on the overall copper dissolution achieved after two hours if the stirring rate was below 600 rpm. At higher stirring rates, the agitation of the leaching solution was sufficient so that mass transfer and oxygen distribution did not limit the rate of copper dissolution.

2.4.3.5 Particle size distribution of feed

Ruiz *et al.* (2007) investigated the leaching behaviour of four different ranges of particle sizes. At the conditions studied, it was concluded that particle size did not have a significant effect on the rate of copper leaching. Slightly lower dissolution was, however, achieved for the range of largest particle sizes, possibly because of diffusion effects within the particles becoming more significant. In general, the particle size distribution is expected to affect the leaching kinetics if the rate of mass transfer between the liquid phase and solid phase limits the rate at which the leaching reactions proceed, or if chemical reaction rate controlled reactions are characterised by slow diffusion in the solid phase (Fogler, 1999).

2.5 Reaction kinetics

2.5.1 Rate expressions

Dissolution mechanisms consist of numerous steps, any one or more of which can control the overall reaction rate. These steps include the following (Crundwell, 1995; Jackson, 1986; Levenspiel, 1972):

- the transfer of gaseous reactants to the leaching solution and the dissolution of these reactants in the leaching solution;
- the transport of reactants through the solution to the particle surface;

- the diffusion of reactants through the porous product or inert component layer (if a shrinking core model is assumed);
- the occurrence of the chemical or electrochemical reactions responsible for the metal dissolution at the reaction interface (this step can in itself be subdivided into a number of steps including the adsorption of reactants, desorption of products, and the transfer of electrons and ions);
- the diffusion of reaction products through the product or inert component layer remaining on the solid particle core (again, only if a shrinking core model is assumed); and
- the transport of the products from the particle surface to the leaching solution.

The form of the rate expression describing the reaction kinetics depends on the rate controlling mechanism, and has been described in various sources (Levenspiel, 1972; Prosser, 1996; Fogler, 1999; Crundwell, 2005; Lamya, 2007; Van Schalkwyk, 2011). According to Habashi (1999), simplified forms of the rate expressions referred to above can be used for dissolution reactions in aqueous systems, as encountered in leaching processes. For diffusion-controlled processes in general, the rate of dissolution is given by Equation 2.47:

$$\frac{dn_i}{dt} = -A \cdot k_d \cdot C_i \qquad [2.47]$$

where A is the reaction surface area of the solid, n_i is the molar amount of reactant i in the system, k_d is the rate constant for a diffusion controlled process, and C_i is the concentration of reactant i in the bulk of the solution, assuming that the stoichiometric coefficient of reactant i is unity. For these types of processes, the rate of dissolution will be highly dependent on the rate of agitation and less so on the leaching temperature. Chemical reaction controlled processes, however, proceed at rates that are independent of the agitation speed but highly dependent on the leaching temperature. The rate expression for chemical reaction controlled processes suggested by Habashi (1999) is given by Equation 2.48:

$$\frac{dn_i}{dt} = -A \cdot k_c \cdot C_{i,interface} \qquad [2.48]$$

where k_c is the rate constant for a chemically controlled process, $C_{i,interface}$ is the concentration of reactant i at the reaction interface, and the remainder of the symbols defined as before. When the rate of diffusion and the chemical reaction rate are comparable, the general form of the rate expression for a leaching process is given by Equation 2.49:

$$\frac{dn_i}{dt} = -A \cdot k \cdot C_i \qquad [2.49]$$

where k is the overall rate constant, given by Equation 2.50:

$$k = \frac{k_d \cdot k_c}{k_d + k_c} \quad [2.50]$$

A similar rate expression for dissolution of solid particles was presented by Fogler (1999). A more general form of the expression given in Equation 2.49 can be written for any species i, where species i can be a reactant or product in solution with stoichiometric coefficient υ_i ($\upsilon_i < 0$ for reactants and $\upsilon_i > 0$ for reaction products), taking part in a specific reaction. If the leach solution volume, V, is furthermore assumed to remain constant, Equation 2.49 can be written as Equation 2.51 (Choo *et al.*, 2006):

$$\frac{dC_i}{dt} = \frac{\upsilon_i \cdot A \cdot k \cdot \prod C_r^{\alpha_r}}{V} \quad [2.51]$$

where C_r refers to the concentration of each of the reactants on which the reaction rate is dependent, and α_r is the order of the reaction with respect to the specific reactant. For solids taking part in the particular reaction, the rate of change in the molar amount of the solid can be calculated using Equation 2.52:

$$\frac{dn_i}{dt} = \mathrm{V} \cdot \frac{dC_i}{dt} \quad [2.52]$$

For processes that are dependent on temperature, the dependence of the reaction rate constant on the temperature is typically given by the Arrhenius equation:

$$k = k_0 \cdot e^{\left(-E_a/R \cdot T\right)} \quad [2.53]$$

where k_0 is the pre-exponential factor, R is the ideal gas constant, T is the absolute temperature, and E_a the activation energy for the particular reaction. Reactions for which diffusion of reagents or products is the rate determining step are characterised by activation energies smaller than 27 kJ/mol, while reactions where the chemical reaction is the rate determining step are characterised by larger activation energies (Burkin, 2001).

Salmi *et al.* (2010) derived an equation to express the surface area of the solid participating in the reaction, A, as a function of the compound molecular weight, M_w, the molar amount of the solid compound initially in the system, n_0, the molar amount of the solid compound currently in the system, n, a shape factor, f_{sh}, and the original specific surface area, σ, assuming equally sized particles:

$$A = \sigma \cdot M_w \cdot n_0^{1/f_{sh}} \cdot n^{1-1/f_{sh}} \quad [2.54]$$

The original specific surface area is defined as the surface area (A_0) per unit mass (m_0) of the particles initially present in the system, which can be calculated using Equation 2.55:

$$\sigma = \frac{A_0}{m_0} \quad [2.55]$$

The shape factor, f_{sh}, is defined as the product of the area (A_0) to volume (V_0) ratio and the characteristic length (L_0) of the particles initially present in the system, as shown by Equation 2.56:

$$f_{sh} = \frac{A_0}{V_0} \cdot L_0 \quad [2.56]$$

The shape factor will have a value of one, two, and three for particles with the geometry of a slab, cylinder, and sphere, respectively, while irregular shaped particles and particles with rough surfaces or high porosity will have shape factors much larger than three.

2.5.2 Kinetics of PGM-containing matte leaching

Despite the relatively large number of authors that have investigated the leaching behaviour of nickel sulphides and copper sulphides in sulphate leaching environments under various operating conditions (refer to Section 2.2 and Section 2.4), only Rademan (1995), Provis *et al.* (2003) (using the same experimental data as Rademan (1995)), Lamya (2007), Ruiz *et al.* (2007), and Fan *et al.* (2010) were found to have calculated rate constants for the base metal leaching reactions proposed respectively. Lamya (2007) focussed primarily on copper cementation and leaching of the metal alloys during the atmospheric first stage leach, while Fan *et al.* (2010) considered the kinetics of nickel alloy and heazlewoodite leaching at atmospheric conditions. No reactions or rate constants describing the leaching of platinum group metals were found.

Provis *et al.* (2003) developed a semi-empirical model based on the work performed by Rademan *et al.* (1995). It was assumed that the kinetics of the electrochemical leaching reactions could be described using first order rate equations. Although diffusion effects were observed in the experimental data, it was not included on a fundamental level and mass transfer limitation were only accounted for empirically. The effects of varying operating conditions studied by Rademan *et al.* (1999) (i.e. oxygen flow rate, oxygen partial pressure, particle size distribution, leaching solution solids content, and initial acid concentration) were included in the model. It was found that changes in the oxygen flow rate and oxygen partial pressure affect the leaching behaviour only because of the subsequent change in the

concentration of dissolved oxygen in the leaching solution. The effects of iron in the matte on the behaviour of the leaching system were not taken into account in the model. The complexity of the model was further reduced by using only the simplest reaction if a number of reactions were believed to give similar outcomes. The rate determining step was assumed to be either pore diffusion or the chemical reaction. The model predicted that Cu^{2+} would always be present in the system irrespective of the operating conditions and would hence be able to react with H_2S to remove it from the system, meaning that the potential inhibitive effect of H_2S on the leaching could be neglected. Empirical rate constants were determined numerically for all the reactions believed to form part of the leaching mechanism to find the combination of constants that proved to be the most accurate for the various experimental conditions.

According to Ruiz *et al.* (2007), copper leaching from chalcocite at atmospheric pressure and temperatures below 100°C can be well described by shrinking core models that assume the sequential occurrence of the reactions comprising the two-stage leaching mechanism (i.e. firstly the transformation of Cu_2S to CuS as an intermediate compound, and secondly the leaching of CuS to form elemental sulphur or sulphate). These reactions do, however, occur simultaneously for high pressure leaching systems operated at higher temperatures. It was furthermore proposed that both reactions of the two-stage leaching mechanism occur simultaneously and uniformly throughout the matte particles. Modelling was performed based on the assumptions that the chemical reactions are the rate limiting steps for both reaction stages of the leaching mechanism, and that the reaction kinetics can be described by first order expressions. Reaction rate constants were estimated from the experimental data for the reactions contributing to the copper leaching for temperatures from 105°C to 150°C. Activation energies of 55 kJ/mol and 88 kJ/mol were calculated for the first and second stages of the leaching mechanism, respectively. The effect of particle size was not incorporated in the model. It was however reported that the assumption of uniform internal reactions showed deficiencies when larger particles were considered. In these instances, diffusion within the particles was believed to limit the rate of leaching.

2.6 Autoclave modelling

The modelling of ideal, perfectly mixed reactors involves performing mass balances assuming that the temperature and the concentrations of all components are identical throughout the reactor and equal to the conditions in the reactor outlet. The overall mass balance approach is the simplest technique, neglecting the effect of particle size distribution and residence time

distribution on the reactor performance. Although the modelling of reactions for which the rate depends on the available surface area might be less accurate if the particle size distribution of the feed is assumed to be monosized, it does allow easier calculations, is typically considered adequate for initial modelling studies (Nikkhah, 1998), and has been used in several leaching studies.

Lampinen (2010) analysed the leaching of Zn concentrate in a non-ideally mixed continuously stirred tank reactor based on these simplifications. Faris *et al.* (1992) simulated the Sherritt nickel-copper matte acid leach process using the SysCAD software package. The sequential modular simulation approach was followed to solve the material balances as well as the dynamic flow sheets, and the Wegstein method was used to perform the recycle convergence. Although no detail about the reactions and reaction kinetics was given, it was reported that simple rate expressions were used in an overall mass balance approach. Basic simplifications, for example estimating the density of a stream as the weighted average of the densities of the different components or assuming constant heat capacities over the specific temperature ranges, were in general acceptable to perform sufficiently accurate simulations of the leaching process to be used for control and operability studies, control system testing, and personnel training (Faris *et al.*, 1992).

For reactors exhibiting non-ideal behaviour, knowledge about the residence time distribution, particle size distribution in the case of particulate reactors, and quality of mixing needs to be taken into account in the mass balances if highly accurate results are desirable. Fogler (1999) presented several models to estimate the performance of these types of reactors. For systems characterised by first order reactions, the residence time distribution can be used to predict conversions in the reactor. For systems characterised by reactions other than first order reactions, information regarding the degree of micro-mixing is also required (Fogler, 1999). The two extreme cases discussed by Fogler (1999) include complete segregation and complete micro-mixing, also referred to as “maximum mixedness”. The segregation model will predict the highest conversion for reactions with reaction orders greater than one and complete micro-mixing model will predict the lowest conversion for these reactions, while identical performance will be predicted for first order or pseudo first order reactions. This is in agreement with the analysis of Crundwell (1994), who discussed the application of these models to particulate reactors in detail. This study furthermore illustrated that the two

abovementioned models are identical if the leaching rates are zero order or pseudo zero order with respect to the concentration of the reagents in the liquid portion of the slurry.

In general, the differences between the performance predicted by the segregation model and that predicted by the maximum-mixed model will increase as the reaction order with respect to the reagent species in the liquid phase increases. Crundwell (1995) also referred to the three abovementioned methods (overall mass balances, population-balance models (considered to be the equivalent of the maximum mixed model), and segregated flow models) as the most commonly used methods for the modelling of leaching reactors. Both the segregated flow model (Papangelakis *et al.*, 1990; Papangelakis and Demopoulus, 1992a; Papangelakis and Demopoulus, 1992b) and the population balance method (Papangelakis and Demopoulus, 1992b; Baldwin *et al.*, 1995; Rubisov and Papangelakis, 1995) have been used in several studies to predict the performance of leaching reactors where non-ideal characteristics were to be accounted for. Crundwell (1995) considered the population balance method to be the most appropriate for the accurate modelling of leaching reactors.

Dixon (1996) discussed the limitations of both the segregated flow model and the population balance model for the modelling of leaching reactors. When applied to multistage leaching reactors on a tank-by-tank basis, the segregated flow model will not be appropriate if the leaching rate is not indicated by changes in particle sizes. The population balance method is considered more rigorous for the analysis of multistage leaching reactors, but is complex and difficult to apply. For the particular modelling method, the particle size distribution needs to be determined accurately, especially for the small particles. In addition, the derivation of the population balance model assumes perfect mixing in the reactor to which the model is applied. Dixon (1996) stated the above arguments as reasons why the population balance model has not been widely used for leaching reactor analysis, and presented an alternative method to the segregated flow model and population balance model to model the performance of leaching reactors. The proposed method, referred to as the multiple convolution integral, was claimed to address the deficiencies of the aforementioned techniques by mathematical manipulation of the leaching kinetics expressions to allow integration over residence time and particle size distributions. According to Crundwell (2005), however, the multiple convolution integral was simply a different formulation of the segregated flow model.

An alternative approach presented by Fogler (1999) involves modelling a real reactor by combining several ideal reactors. One of the examples presented illustrated how the performance of a stirred tank reactor with dead volume could be estimated using an ideal stirred tank reactor with a bypass stream. To evaluate the appropriateness of the selected combination of ideal reactors to represent the real system, extensive experimental data regarding the residence time distribution and particle size distribution of the solids feed stream are required.

For this project, the modelling of the autoclave was done by performing overall mass and energy balances without considering the particle size distribution of the feed or the residence time distribution of the autoclave. The reasons for the selection of this modelling approach and the assumptions made to simplify the modelling are discussed in detail in Section 6.2.

3 EXPERIMENTAL

3.1 Materials

The converter matte, first stage leach residue, and spent electrolyte were supplied by Lonmin Plc, who collected the material samples from their Western Platinum Ltd. Base Metal Refinery. The chemical compositions of these components are summarised in Table 3.1. The sample analysis techniques that were employed are discussed in Section 3.3.

Table 3.1. Chemical composition of the material supplied by Lonmin Plc.

Species	Converter matte (wt%)	1st stage leach residue (wt%)	Spent electrolyte (mg/ℓ)
Ni	49.5	13	22 800
Cu	26.6	50	25 300
S	22.7	26	
Co		0.13	261
Fe	1.2	0.42	856
Ir		$3.0 \cdot 10^{-2}$	33.6
Rh		$8.8 \cdot 10^{-2}$	56.1
Ru		0.20	193
Pd		0.18	5.3
Pt		0.39	8.0
SO_4^{2-}			113 700

The density of the spent electrolyte was determined to be 1.16 kg/ℓ. The total sulphuric acid concentration of the spent electrolyte was estimated by considering the amounts of sulphate and metal ions present in solution. It was assumed that the four metal ions present in the largest concentrations (i.e., nickel, copper, iron, and cobalt) occur paired with sulphate ions in ratios that allow the respective metallic cation and sulphate anion combinations to have no net charge. It was assumed that the oxidation states of copper, nickel, iron, and cobalt in the spent electrolyte solution are Cu^{2+}, Ni^{2+}, Fe^{3+}, and Co^{2+}, respectively. Based on these assumptions, the amount of sulphate ions not associated with these metallic cations were calculated, and it was assumed that the molar quantity of these sulphate ions was numerically equal to molar amount of sulphuric acid, H_2SO_4, in solution. These calculations yielded a sulphuric acid concentration of 36.4 g/ℓ, which agrees well with the typical operating conditions employed at the Western Platinum Ltd. BMR. Attempts to determine the acid concentration by titration were unsuccessful due to the hydrolysis of metal cations that were present in relatively high concentrations in the solution. Sample calculations are shown in Appendix D.

The converter matte was used as received; the particle size distribution was determined using a sieve analysis, with the results presented in Section 3.4.1. The primary mineralogical phases that were present in the converter matte were heazlewoodite, chalcocite, and nickel-copper alloys. The converter matte density was 5.9 g/cm^3.

The first stage leach residue received from the Western Platinum Ltd. BMR had dried and formed conglomerates before test work with the material could commence. Consequently, the material was treated in a laboratory scale crusher to break up the conglomerates. The first stage leach residue density was determined to be 4.45 g/cm^3.

For leach solutions that required a higher initial acid concentration than the acid concentration in the spent electrolyte, sulphuric acid was added to the spent electrolyte. The sulphuric acid was supplied by Sigma-Aldrich™ (95 – 97%, reagent grade). For leach solutions that required a lower initial acid concentration than the acid concentration in the spent electrolyte, demineralised water produced by a reverse osmosis unit was added to the spent electrolyte. A summary of the amounts of spent electrolyte, demineralised water, sulphuric acid, and matte or first stage leach residue for the respective operating conditions during first stage residue leaching, together with a discussion of the calculation method, is given in Appendix D.

3.2 Experimental equipment

A two litre Büchi Polyclave Type 3 pressure reactor manufactured from Hastelloy was used for the experimental work. A schematic diagram of the experimental setup is shown in Figure 3.1. The autoclave was equipped with a Cyclone 300 magnetic stirrer drive allowing stirrer speeds up to 2000 revolutions per minute (rpm). The stirrer controller allowed the stirrer rate to remain constant at the desired stirring rate, which was set manually. Both an anchor and a blade stirrer were available, but the anchor stirrer was used for all the tests. A quarter-inch Hastelloy tube extending from a standard connector on the reactor cover plate into the reactor was used to sparge oxygen into the leaching solution. The reactor was equipped with a pressure gauge, and the pressure was controlled manually by adjusting the oxygen addition rate. A constant purge stream was maintained through a vent valve located on the reactor cover plate. Three thermocouples were located in the reactor shell, reactor jacket, and in the reactor volume, respectively. These temperature measurements were accepted as inputs by a programmable controller. The controller utilised electric heating elements located around the reactor shell and a switch relay valve controlling the flow of cooling water through the reactor shell to control the reactor temperature. In all instances, the temperature control of the reactor

was performed by setting an appropriate set point for the reactor volume and using the programmable controller to maintain the temperature of the leaching solution close to the specified set point. Samples were taken from the reactor via the bottom drain valve. To prevent the sample leaving the reactor from flashing as a result of the sudden pressure drop, a hose with an additional valve was connected to the drain valve outlet. The sample was kept in the tube space between the drain valve outlet and the additional valve until this sample had cooled down to a temperature below its boiling point. The hazard identification for the experimental setup is given in Appendix B.

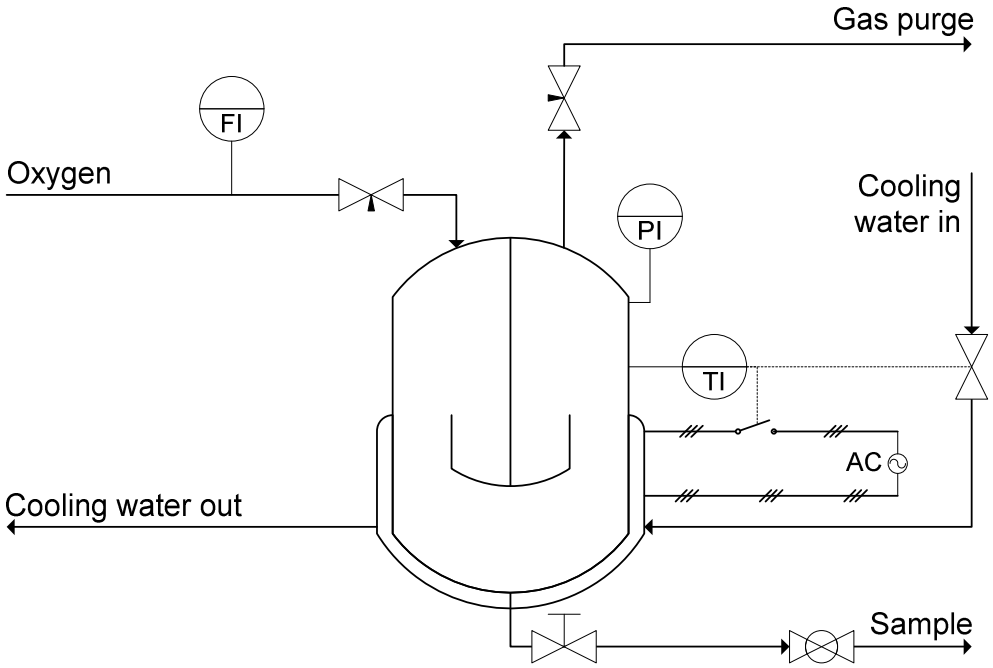

Figure 3.1. Schematic diagram of the experimental setup.

3.3 Experimental procedure

The following experimental procedure was followed:

1. The amounts of spent electrolyte, water, sulphuric acid, and first stage leach residue required to produce one litre of slurry with the desired solids content and initial acid concentration were measured off.
2. The calculated amounts of spent electrolyte, water, and sulphuric acid were added to the autoclave.
3. This liquid mixture was heated to a temperature of 65°C, which is below the normal boiling point of pure water and hence the mixture.
4. The solid material to be leached was added to the liquid mixture after the desired pre-heating temperature set point had been reached.

5. The fully charged reactor was closed, all valves were shut, and the agitator speed set to the desired value (700 rpm) before heating the leaching solution to the desired final leaching temperature.
6. Once the slurry temperature had reached a temperature 10°C below the final operating temperature, the first sample was taken and oxygen was admitted to the autoclave. This point of the procedure was considered to be the start of the experiment for sampling and data analyses purposes.
7. For the validation tests performed on the converter matte, the pressure inside the reactor was increased gradually by opening the oxygen feed valve such that the oxygen feed rate remained constant and equal to the values listed in Section 3.4.1. Once the desired operating pressure had been reached, the pressure was controlled through manual control of the purge valve. For the leaching of the first stage residue, the pressure inside the reactor was increased rapidly by sparging oxygen into the autoclave at a high rate. Once the desired operating pressure had been reached, the purge valve was opened to allow a constant small gas purge, while the pressure was maintained as close to the desired operating pressure as possible by adjusting the oxygen feed valve.
8. Samples were taken at the following time intervals (in minutes) after the time at which initial conditions had been assumed: 5, 10, 20, 40, 80, 120, 160, 200, 240, 300, 360, 420, and 480. In order to prevent any further leaching after sampling, the samples were filtered immediately using 0.45 micron syringe filters.
9. After completion of the reaction, the reactor and leaching solution was cooled to ambient temperature by circulating water through the reactor shell. The reactor was drained through the bottom valve. The reactor was washed by stirring a low concentration sulphuric acid solution in the reactor, followed by the stirring of heated water at 80°C in the reactor to rinse the reactor.

All liquid samples were analysed by Mintek Analytical Services. Inductively coupled plasma optical emission spectrometry (ICP-OES) and inductively coupled plasma mass spectrometry (ICP-MS) were used for analysis of the base metals and platinum group metals, respectively. Four samples of the spent electrolyte were analysed. The standard deviations calculated for the reported concentrations of the different dissolved species, reported as a percentage of the average concentration of the respective species as indicated in Table 3.1, were 5.7% for Ir, 3% for Rh and Pd, 2.8% for Pt, and less than 2% for the remainder of the species.

Solid analyses that were performed include X-ray fluorescence spectrometry (XRF), by Stellenbosch University Central Analytical Facility and Mintek Analytical Services, as well as X-ray diffraction (XRD), by Stellenbosch University Central Analytical Facility and XRD Analytical and Consulting cc. The XRF analysis of multiple samples of first stage leach residue yielded results with standard deviations of less than 3% of the average species content for all the elements reported in Table 3.1. Solid densities were determined using a helium pycnometer (Micromeritics® Accupyc 1330) made available by the Department of Chemical Engineering at the Cape Peninsula University of Technology.

3.4 Experimental planning

3.4.1 Experimental procedure evaluation

In order to be able to compare the results achieved with the proposed experimental setup and procedure with previously published results, initial pressure leaching experiments were conducted on converter matte and not on first stage leach residue. This was done to evaluate the suitability of the proposed setup for pressure leaching tests. The leaching behaviour of base metals during the pressure leaching of converter matte has been researched by Rademan (1995). By comparing the results obtained with the results presented by Rademan (1995) and Rademan *et al.* (1999), the applicability of the proposed experimental procedure and setup could be evaluated. In order to be able to use the results of Rademan *et al.* (1999) as a benchmark against which initial results could be compared, the same operating conditions were employed for these initial tests, as summarised in Table 3.2. In addition to the test performed at these standard conditions, two tests were performed by varying the oxygen flow rate while maintaining the rest of the process conditions constant. The oxygen flow rates that were investigated were 78 and 7.5 g/h per litre leaching solution, respectively. These tests were done to get an indication of the effectiveness of oxygen mass transfer from the gaseous phase to the liquid phase for this specific experimental setup.

Table 3.2. Standard operating conditions for initial leaching tests performed on converter matte, selected in accordance with the work performed by Rademan (1999).

Parameter	**Value**
Temperature	140°C
Total pressure	550 kPa
Oxygen flow rate	14.8 g/h per litre leaching solution
Leaching solution density	1.35 kg/ℓ
Initial H_2SO_4 concentration	103 g/ℓ

The compositions of the converter matte and spent electrolyte used by Rademan (1995) are summarised in Table 3.3. The primary mineral phases present in the Western Platinum Ltd. converter matte and those present in the matte studied by Rademan (1999) were the same, namely nickel alloy, heazlewoodite, and chalcocite. The comparison between the particle size distribution of the converter matte used in this study and that of the matte studied by Rademan (1999) is illustrated in Figure 3.2. The weighted average particle sizes of the material used in this study and of the material used by Rademan (1999) were 144.7 µm and 124.7 µm, respectively. A comparison between the results achieved with the Lonmin converter matte and the results reported by Rademan (1999) is given in Section 4.1.

Table 3.3. The compositions of the converter matte and spent electrolyte used in the study by Rademan et al. (1999).

Species	Converter matte (wt%)	Spent electrolyte (g/ℓ)
Acid (H_2SO_4)	-	103
Nickel	50.7	27.3
Copper	27.4	21.4
Iron	0.54	0.51
Cobalt	0.36	0.22
Sulphur	21.0	-

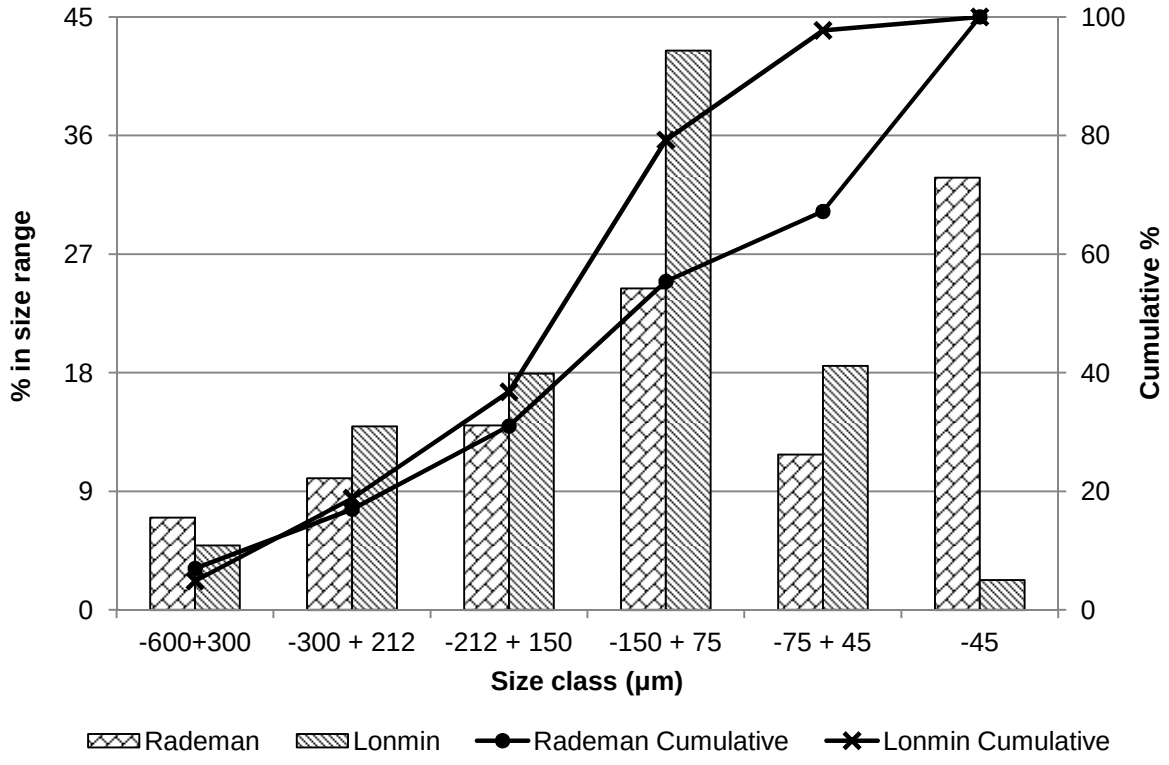

Figure 3.2. Comparison of the particle size distribution of the converter matte used during this study and that used by Rademan et al. (1999).

3.4.2 Leaching of first stage leach residue

The standard operating conditions for the laboratory scale batch leaching process were selected to be as close to the operating conditions encountered on site as possible. The standard operating conditions employed on site are summarised in Table 3.4.

Table 3.4. Summary of the typical operating conditions employed for the second stage leach at the Western Platinum Ltd. BMR.

Variable	Value
Temperature	115 – 145°C
Pressure	600 – 700 kPa
Residence time	4.4 – 7.6 h
Live volume of reactor	28 m^3
Oxygen flow rate	100 – 200 m^3/h
Acid concentration	35 g/ℓ
Solids feed rate	600 – 1000 kg/h
Concentrated acid feed rate	0 – 50 kg/h
Spent flow rate	0.32 – 1.4 ℓ/kg solids fed
Total acid feed rate	0.09 – 0.13 kg/kg solids fed
Spent density	1.2 kg/ℓ

The process variables that could potentially affect the leaching behaviour in the high pressure leaching system are discussed in Section 2.4. Considering the BMR process and the control options that exist on site, the variables that were deemed to be the most important to investigate were the leaching temperature, leaching pressure (which will influence the oxygen partial pressure directly), initial acid concentration, and the solids content of the slurry.

A 2^4 full factorial design was decided upon to determine the relative importance of the effects that each of the four variables have on the metal dissolution behaviour. The values that were used as the high and low values for the respective process variables in this first set of experiments are summarised in Table 3.5.

Table 3.5. Values of the respective process variables for the first set of experiments performed according to a full factorial experimental design.

Variable	High value	Low value
Temperature (°C)	144	116
Pressure (bar,a)	7	5
Initial acid concentration (g/ℓ)	36	26
Solids content (g solids/ℓ)	290	180

Based on the results obtained for these experimental conditions, the experimental conditions were revised and a second set of experiments were performed, again according to a 2^4 full factorial experimental design. The values that were used as the high and low values for the respective process variables in the second set of experiments are summarised in Table 3.6. The results of the first set of experiments and the reasons for selection of the revised experimental conditions are discussed in Section 4.2. The tests were not repeated, but given the robustness and simplicity of the experimental procedure as well as the consistency of results achieved at different operating conditions (as discussed in Section 4.3), it is unlikely that experimental errors affected the results presented.

Table 3.6. Values of the respective process variables for the second set of experiments performed according to a full factorial experimental design.

Variable	**High value**	**Low value**
Temperature (°C)	130	116
Pressure (bar,a)	9	7
Initial acid concentration (g/ℓ)	165	140
Solids content (g solids/ℓ)	130	80

4 EXPERIMENTAL RESULTS AND DISCUSSION

4.1 Evaluation of experimental setup and procedure

As discussed in Section 3.4, the applicability of the experimental setup and procedure for the investigation of high pressure leaching systems was evaluated by first performing pressure leaching tests on converter matte. In this section, these experimental results are compared with the results published by Rademan *et al.* (1999) and anomalies are discussed.

4.1.1 Base metal behaviour

The variations in the nickel, copper, and iron concentrations in the leaching solution for the duration of the experiment performed at the experimental conditions discussed in Section 3.4.1 are shown in Figure 4.1. In addition, the results published by Rademan *et al.* (1999) were scaled so that the initial concentrations of the published results agree with the initial experimental concentrations to allow for easy comparison. Scaling factors of 0.95, 1.2, and 3.44 were used for the nickel, copper, and iron concentrations, respectively.

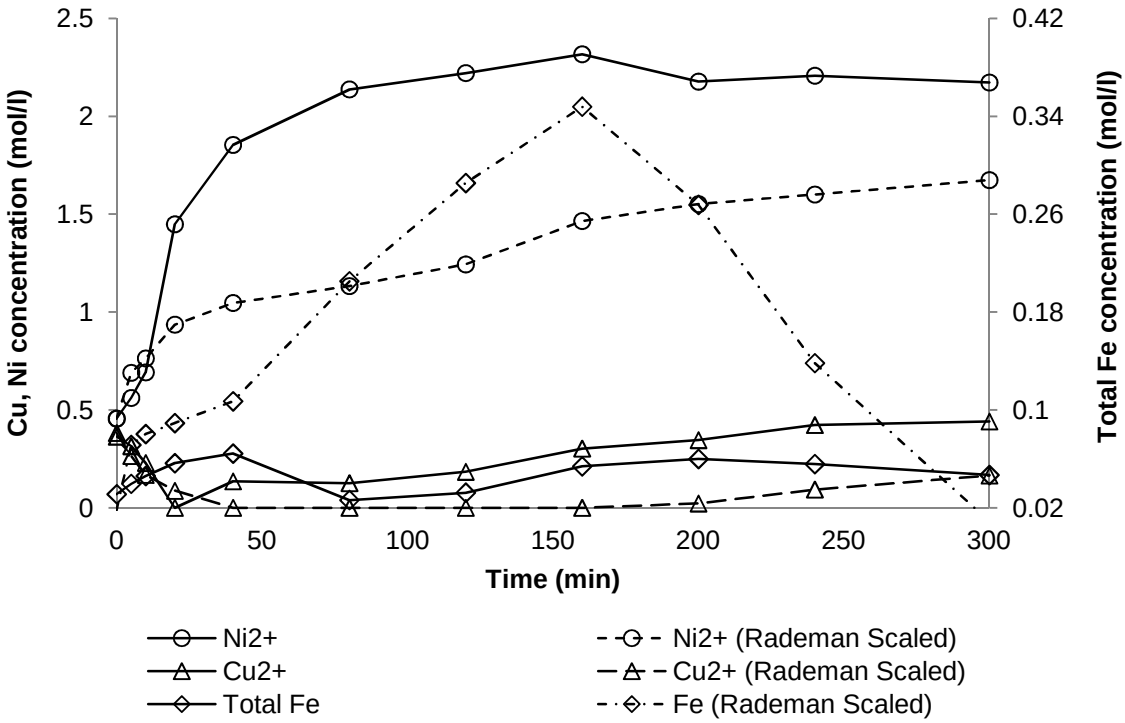

Figure 4.1. Concentrations of nickel, copper, and iron in solution during the leaching experiment, together with scaled results published by Rademan et al. (1999).

Several anomalies are observed when comparing the results of this study with those presented by Rademan *et al.* (1999). Firstly, the concentration of the copper decreased at a slower rate during the early stages of the leaching process, while the nickel concentration increased at a slower rate than that reported. The material leached in the abovementioned study was the

product from the atmospheric repulping stage (first stage leach) and had hence already undergone some degree of leaching after exiting the converter. In this study, the converter matte was treated directly in the high pressure leaching system. The initial dissolution and cementation reactions occurring in the autoclave were therefore what typically would occur in the repulping or first stage atmospheric leach. After approximately 10 minutes, the nickel and copper concentration curves followed trends more comparable to that reported for the initial stages of leaching by Rademan *et al.* (1999). It can be concluded that 10 to 15 minutes of first stage pressure leaching of converter matte had to be allowed to compensate for the absence of the repulping step and to achieve a matte composition more comparable with that used in the abovementioned study. This observation was confirmed by the XRD analyses of the solid samples. Ni_3S_2 and Cu_2S, which are characteristic of converter matte, were found to be the major phases in all the samples taken up to 10 minutes (refer to Table 4.1). It was only from 20 minutes onwards that copper sulphide phases with copper to sulphur ratios of less than two were detected and from 40 minutes onwards that $Cu_{1.8}S$ was detected; Rademan *et al.* (1999) reported the formation of $Cu_{1.8}S$ already after five minutes of first stage pressure leaching.

Secondly, the profile for the iron concentration showed two consecutive stages of dissolution and precipitation, which is in contrast with the observations made by Rademan *et al*. (1999) who reported only a single peak in the iron concentration profile. The fact that untreated converter matte was used as feed material instead of the product from the first stage repulping could possibly also explain this difference. Lamya and Lorenzen (2006) did report that partial dissolution of iron takes place in the repulping stage.

The third noticeable difference concerns the flattening off of the nickel concentration profile after approximately two hours at a concentration of 2.2 mol/ℓ, while Rademan *et al.*, (1999) reported that nickel dissolution continued to occur in the last hour. The nickel dissolution proceeded at a faster rate in the first two hours of the experiment (from 10 minutes onwards) despite the larger particle size distribution of the converter matte used in this study, as discussed in Section 3.4.1. This can possibly be ascribed to better mass transfer of oxygen to the solution given the much smaller reactor volume (2 ℓ autoclave containing 1 ℓ slurry compared with an 82 ℓ autoclave containing 40 ℓ slurry) and relatively high stirring rate. Although Rademan (1995) eliminated the possibility of solid diffusion effects playing a limiting role, it was reported that increased oxygen flow rates enhanced the oxygen to solution mass transfer and consequently the oxygen dependant chemical reactions. The good

oxygen to solution mass transfer achieved in the small reactor at high stirring rates and relatively low oxygen flow rates was further illustrated by the fact that the oxygen flow rate had a negligible effect on the rate of nickel dissolution, as illustrated in Figure 4.2. This also confirmed that the rate of agitation was sufficient to ensure that mass transfer was not the rate limiting factor for this specific process, and that the rate of oxygen mass transfer from the gaseous phase to the liquid phase was faster than the rates generally achieved in typical larger scale autoclaves. Further contributing factors could have been lower nickel alloy and higher Ni_3S_2 content of the converter matte, which has been reported to increase the rate of nickel leaching (Rademan, 1995), and the difference in the iron content of the material used for the difference studies. The iron content of the converter matte and the iron content of the spent electrolyte used in this study (1.2 wt% and 0.86 g/ℓ, respectively) were higher than the iron content of the converter matte and spent electrolyte used by Rademan (1995) (0.54 wt% and 0.51 g/ℓ, respectively). Rademan *et al.* (1999) did report that ferric ions in solution could enhance the rate of nickel dissolution.

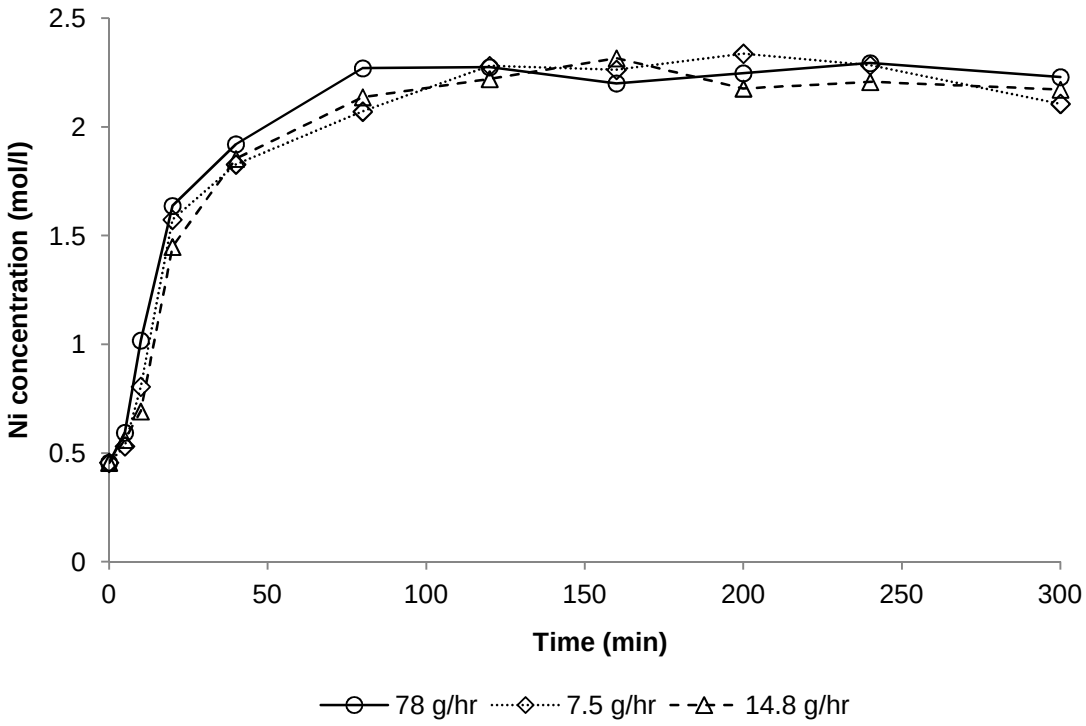

Figure 4.2. Concentration of nickel in solution during leaching experiments performed with varying oxygen flow rates.

Finally, it can be noticed in Figure 4.1 that some degree of copper leaching occurred after 30 minutes and proceeded further from 80 minutes onwards. Data presented by Rademan *et al.* (1999) suggest that the copper concentration of the leaching solution only started to increase after 160 minutes. From the reaction mechanism proposed by Rademan (1995) it is evident that the dissolution of Ni_3S_2 is the main copper cementation reaction. Given the fact

that nickel dissolution proceeded much faster and reached maximum dissolution after approximately two hours in this study, for reasons discussed earlier, it is reasonable to expect that the copper concentration of the leaching solution would have started to increase at an earlier stage. Lamya and Lorenzen (2006) as well as Rademan (1995) also reported that copper cementation decreased as the initial copper concentration of the leaching solution was increased. The fact that the copper concentration of the leaching solution used in this study was 13.6% higher than that reported by Rademan *et al.* (1999) could therefore be an additional factor contributing to the lower degree of copper cementation observed.

XRD analyses of the solid samples were performed to get an indication of the leaching mechanism followed. The major phases that were found to be present in the samples taken at the respective sampling times are summarised in Table 4.1. The complete set of XRD results for the solid samples obtained at the different sampling times is presented in Appendix C.

Table 4.1. Major phases detected in the solid samples using XRD analyses.

Sampling time (minutes)	Major phases
0	Ni_3S_2, Cu_2S
5	Ni_3S_2, Cu_2S
10	Ni_3S_2, Cu_2S
20	$Cu_{1.96}S$
40	$Cu_{1.8}S$, $Cu_{31}S_{16}$
80	$Cu_{1.8}S$, CuS, Ni_3S_4
120	$Cu_{1.8}S$, CuS, Ni_3S_4
160	$Cu_{1.8}S$, Co_2CuS_4
240	CuS, $(Co,Ni)_3S_4$

As mentioned previously, Ni_3S_2 and Cu_2S were determined to be the two major phases in the converter matte, and were found to be present in a ratio of approximately three to one. As leaching proceeded, $Cu_{1.96}S$ was detected as the major copper phase at 20 minutes. $Cu_{1.8}S$ was detected as the major copper phase from 40 minutes to 160 minutes with a small amount of $Cu_{31}S_{16}$ also detected at 40 minutes. CuS was found to be present from 80 minutes onwards, becoming the major copper phase at 240 minutes. Apart from Ni_3S_2 during the initial leaching stages, Ni_3S_4 was the only other nickel phase readily detected by the XRD analysis from 80 minutes onwards. The formation of NiS as an intermediate nickel phase has been reported by numerous studies (Rademan, 1995; Hofirek and Kerfoot, 1992), but the fast nickel dissolution and relatively small amount of NiS expected to be present have made it difficult to confirm the presence of this phase. In general, and particularly for the copper phases, it can be said

that the experimental observations agree well with reaction mechanism proposed by Rademan *et al.* (1999), who concluded that leaching of nickel sulphides and copper sulphides proceed via a number of intermediate sulphides with decreasing nickel to sulphur and copper to sulphur ratios.

4.1.2 Conclusions

The experimental results obtained for the high pressure sulphuric acid/oxygen leaching of converter matte in a Büchi Polyclave Type 3 pressure reactor were compared with high pressure leaching results published by Rademan *et al.* (1999). It was found that 10 to 15 minutes of leaching had to be allowed for the converter matte to reach a composition comparable to that of the repulping stage product. The overall nickel dissolution achieved agreed well with published results, but the reaction rates were observed to be considerably faster. This could be ascribed to improved mass transfer of oxygen to the leaching solution in the small reactor, to the lower nickel alloy and higher Ni_3S_2 content of the feed material, and the higher iron content of the converter matte and spent electrolyte. The oxygen flow rate had a negligible effect on the degree and rate of nickel dissolution. As a result of the faster nickel dissolution, copper cementation occurred to a much lesser extent. In addition, the higher initial copper concentration of the leaching solution also contributed to the reduced copper cementation, as reported by Lamya and Lorenzen (2006) as well as Rademan (1995). XRD analyses of the solid samples confirmed that the general reaction mechanism proposed previously was valid for the studied leaching system.

Although several anomalies were observed between the experimental results generated during the pressure leaching of converter matte and the results published by Rademan (1995) and Rademan *et al.* (1999), these differences were primarily because of variations in the feed material and possibly because of improved mass transfer of gaseous oxygen to the aqueous leach solution in the autoclave used for the current study.

4.2 Leaching of first stage residue: first experimental design

As discussed in Section 2.1, the primary objective of the second stage leach is to dissolve copper and nickel from the first stage leach residue while limiting the dissolution of PGMs. Copper sulphides have been reported to be the major species present in the first stage leach residue, while rhodium is reported to be one the first PGMs to leach (the other PGMs readily leached are ruthenium and iridium) (Steenekamp, 2009). Given the importance of these two species in the second stage leach, the effects of the respective operating variables on the

dissolution of copper and rhodium are discussed qualitatively in Sections 4.2.2.1 to 4.2.2.3, followed by a discussion of the relationships between the leaching of different PGMs in Section 4.2.2.4. The experimental data for the first set of first stage leach residue leaching experiments are given in Appendix C.

4.2.1 High solids content conditions

While the copper concentration in the leach solution was below the copper solubility limit at the typical autoclave conditions, it exceeded the copper solubility at atmospheric conditions. This resulted in difficulties associated with sampling and subsequent analysis, especially during the latter parts of the leaching tests. As a result, no reliable data could be obtained for the tests performed at the high solids content conditions.

The copper solubility in the leach solution was estimated using the OLIAnalyzer® 3.0 software package. A system containing one kilogram water, 35 g H_2SO_4, and varying amounts of $NiSO_4$ and $CuSO_4$ was defined. The amount of $NiSO_4$ was varied between 60 g, 80 g, and 100 g for temperatures of 30°C, 50°C, 70°C, and 90°C at a pressure of 1 atm and 90°C, 110°C, and 130°C at a pressure of 6 atm. For each of these sets of conditions, the $CuSO_4$ addition was gradually increased until a solid copper sulphate phase formed. This point was assumed to represent the maximum copper solubility for the particular conditions, and the corresponding Cu^{2+} concentration was determined. The results are shown in Figure 4.3.

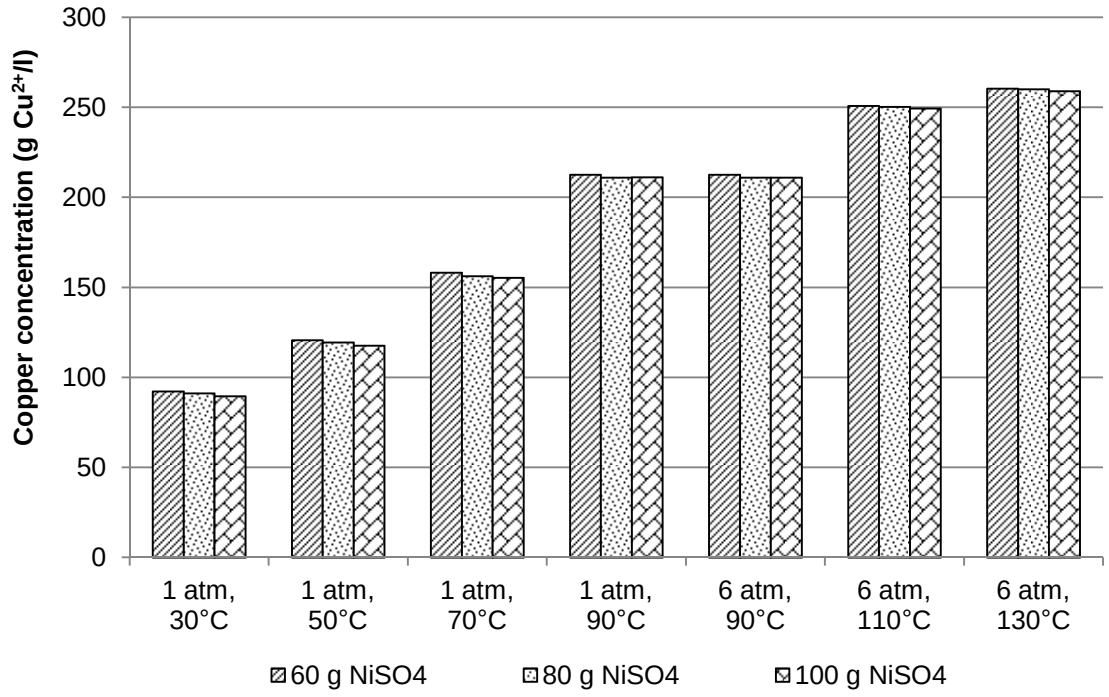

Figure 4.3. Estimated copper solubility in the leach solution as a function of system temperature, pressure, and $NiSO_4$ content.

4.2.2 Low solids content conditions

4.2.2.1 Effect of leaching temperature on metal dissolution

Figure 4.4 to Figure 4.7 show comparisons between the concentration of copper and rhodium over time at the high and low temperature values for specific pressure and acid concentration conditions. From Figure 4.4 and Figure 4.5, it can be seen that the temperature had no significant influence on the extent or rate of copper dissolution if the leaching was performed at a pressure of 7 bar. When the leaching pressure was reduced to 5 bar, the temperature had a noticeable influence on the degree to which copper was leached. At this pressure, higher dissolution of copper was achieved at 116°C than at 144°C, as can be seen in Figure 4.6 and Figure 4.7.

According to the reaction mechanisms discussed in the Section 2.2, dissolved oxygen must be available in the leaching solution for dissolution of copper from digenite and covellite to occur. Hofirek and Kerfoot (1992) further stated that the overall leaching time of copper is determined by reaction 2.36, the rate of which can be increased by increasing the concentration of dissolved oxygen in the leaching solution, or by increasing the temperature if sufficient oxygen is available in the system. Based on results presented by Tromans (1998b) and Kimweri (1990), it is expected that the oxygen solubility in a sulphuric acid solution will increase with an increase in temperature for temperatures above approximately 100°C, if the oxygen partial pressure remains constant. Since the experimental results suggested that a decrease in temperature will lead to increased copper dissolution (refer to Figure 4.6 and Figure 4.7), the effect of temperature on the oxygen partial pressure had to be considered. The atmosphere above the leaching solution in the reactor consisted primarily of water vapour and oxygen. As the leaching temperature was increased, the vapour pressure of water increased while the total pressure was kept constant. Consequently, the partial pressure of oxygen decreased, which resulted in a lower concentration of dissolved oxygen in the solution and consequently a slower copper leaching rate. This effect of temperature and pressure on the water vapour pressure, oxygen partial pressure, and oxygen solubility in pure water is summarised in Table 4.2 to further illustrate the reasoning. The oxygen solubility in pure water was calculated using the model proposed by Tromans (1998b), as discussed in Section 2.4. The addition of solutes to water will reduce the oxygen solubility, but the general dependency on the temperature and pressure will remain similar. The decrease in the oxygen partial pressure as a result of the temperature increase hence had a more significant effect on the leaching rate than the direct effect of temperature on the leaching kinetics.

Table 4.2. Summary of the effect of temperature and pressure on oxygen partial pressure and oxygen solubility in pure water.

Pressure (bar)	Temperature (°C)	$P^*_{H_2O}$ (kPa)	P_{O_2} (kPa)	$[O_2]_{H_2O}$ (mg/ℓ)
5 bar	115	169.1	330.9	84.0
	125	232.1	267.9	70.4
	135	313.0	187.0	51.5
	145	415.4	84.6	25.0
7 bar	115	169.1	530.9	134.6
	125	232.1	467.9	122.7
	135	313.0	387.0	106.1
	145	415.4	284.6	82.6
9 bar	115	169.1	730.9	185.2
	125	232.1	667.9	174.9
	135	313.0	587.0	160.7
	145	415.4	484.6	140.1

In the case of the high pressure operation, the inhibiting effect of the decreasing partial pressure and the direct effect of the higher temperature were of comparable importance. The fact that the leaching rate of copper did not decrease when the temperature was decreased also confirmed that if elemental sulphur formation occurred at the lower temperatures, as suggested by Kerfoot *et al.* (1986), it did not significantly affect the base metal leaching rate. Given the highly oxidising leaching conditions, the formation of elemental sulphur was unlikely. Both Ruiz *et al.* (2007) and Grewal *et al.* (1992) reported that very little, if any, elemental sulphur formation occurred during the leaching of copper sulphide species under typical high pressure oxygen leaching conditions.

Considering the effect of temperature on rhodium dissolution, it can be seen from Figure 4.6 and Figure 4.7 that there was no significant difference in the leaching rate of rhodium if the leaching pressure was kept constant at 5 bar. For the cases where the leaching pressure was maintained at 7 bar, the effect of the temperature on the rhodium leaching was also dependent on the initial acid concentration. For a low initial acid concentration, the degree of rhodium leaching was the same at both temperatures up to 160 minutes, where after the rhodium concentration in the leaching solution at 144°C exceeded the concentration in the solution at 116°C (shown in Figure 4.4). In the case of the high initial acid concentration, it was only after 240 minutes that the amount of rhodium leached at different operating temperatures started to differ. Figure 4.5 shows that higher rhodium dissolution was observed for the leaching performed at 116°C than for the leaching performed at 144°C.

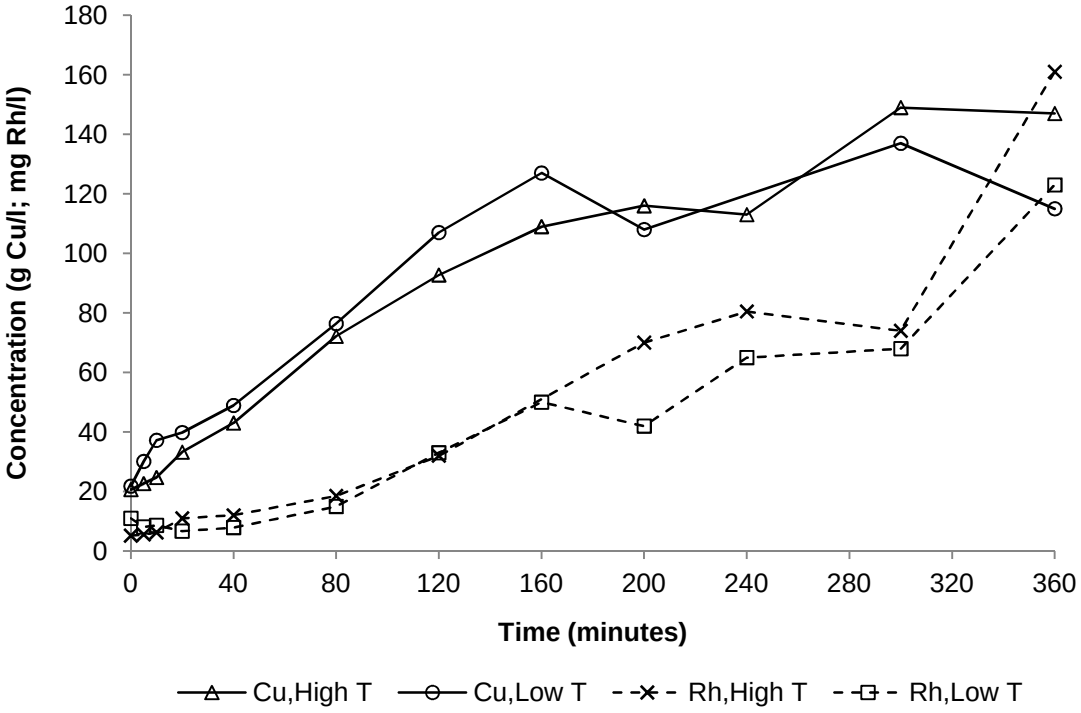

Figure 4.4. Concentration of Cu and Rh in solution as a function of leaching time and temperature at 7 bar and an initial acid concentration of 26 g/ℓ (High T: 144°C; Low T: 116°C).

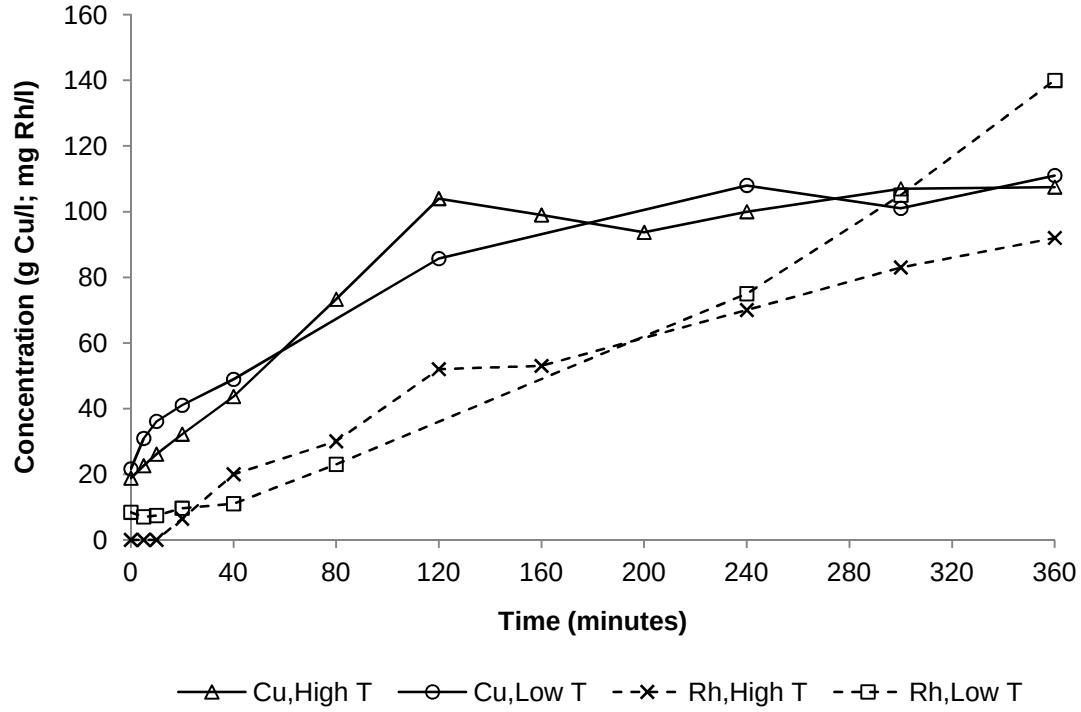

Figure 4.5. Concentration of Cu and Rh in solution as a function of leaching time and temperature at 7 bar and an initial acid concentration of 36 g/ℓ (High T: 144°C; Low T: 116°C).

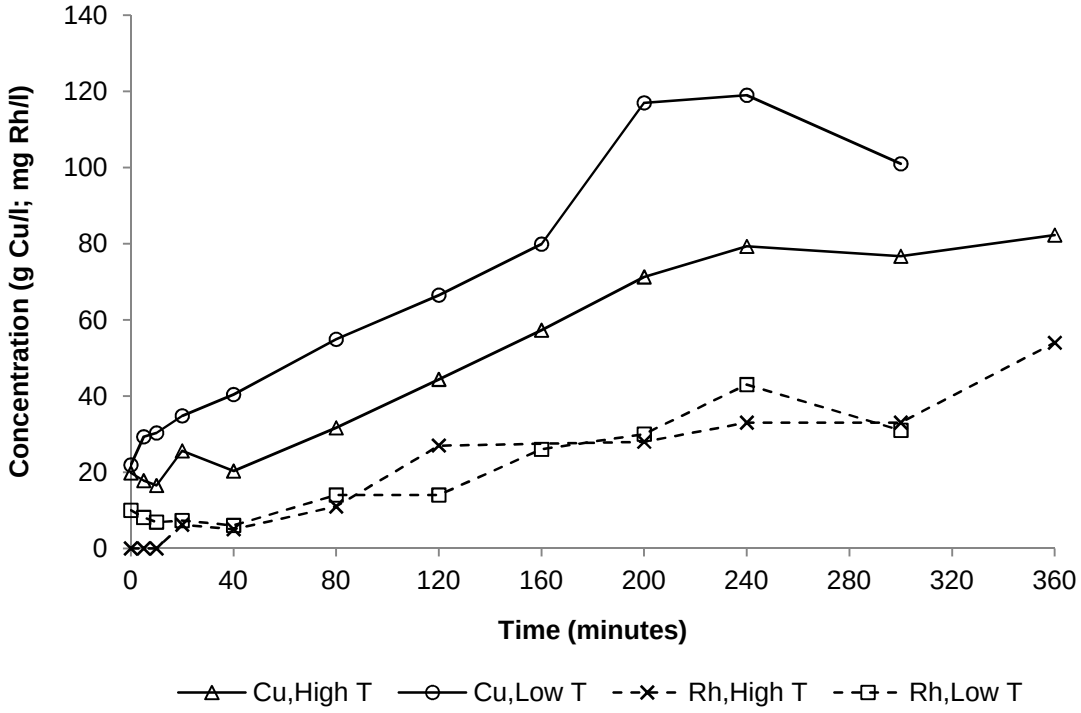

Figure 4.6. Concentration of Cu and Rh in solution as a function of leaching time and temperature at 5 bar and an initial acid concentration of 26 g/ℓ (High T: 144°C; Low T: 116°C).

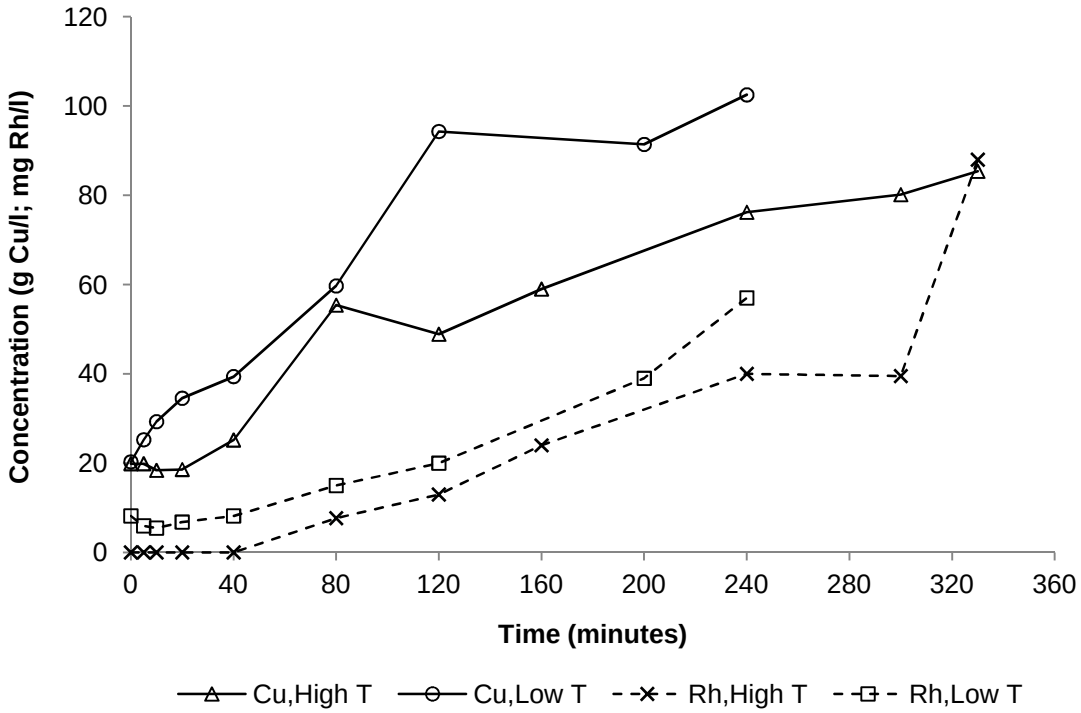

Figure 4.7. Concentration of Cu and Rh in solution as a function of leaching time and temperature at 5 bar and an initial acid concentration of 36 g/ℓ (High T: 144°C; Low T: 116°C).

4.2.2.2 Effect of leaching pressure on metal dissolution

Figure 4.8 to Figure 4.11 show comparisons between the concentration of copper and rhodium over time at the high and low pressure values for specific temperature and acid concentration conditions. It can be seen that the effect of pressure on the leaching of copper was more significant when the leaching was performed at 144°C than when it was performed at 116°C. At the high operating temperature in particular, the degree of copper leaching was considerably higher when the leaching pressure was increased. The reasoning to explain this observation is similar to that used to explain the temperature effects. At the low temperature conditions, the water vapour pressure was relatively low and the oxygen partial pressure was hence always high enough to sustain the leaching of copper without being the limiting factor. At higher temperatures, the water vapour pressure increased. When the total leaching pressure was decreased, the oxygen partial pressure decreased to a value where the availability of dissolved oxygen in the leaching solution became a reaction limiting factor. The fact that there were noticeable differences between the leaching of rhodium at 5 bar and at 7 bar for all the temperature and initial acid conditions could be an indication that the kinetics of the PGM leaching reactions are influenced by the oxygen partial pressure over a wider partial pressure range than the copper dissolution.

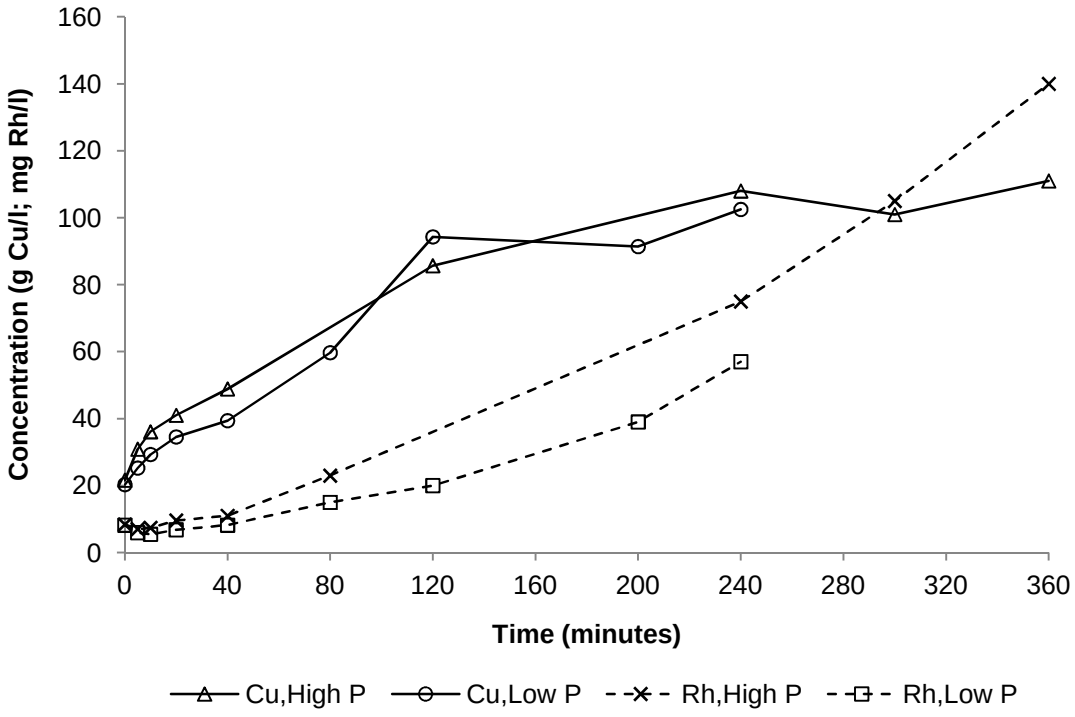

Figure 4.8. Concentration of Cu and Rh in solution as a function of leaching time and pressure at 116°C and an initial acid concentration of 36 g/ℓ (High P: 7 bar; Low P: 5 bar).

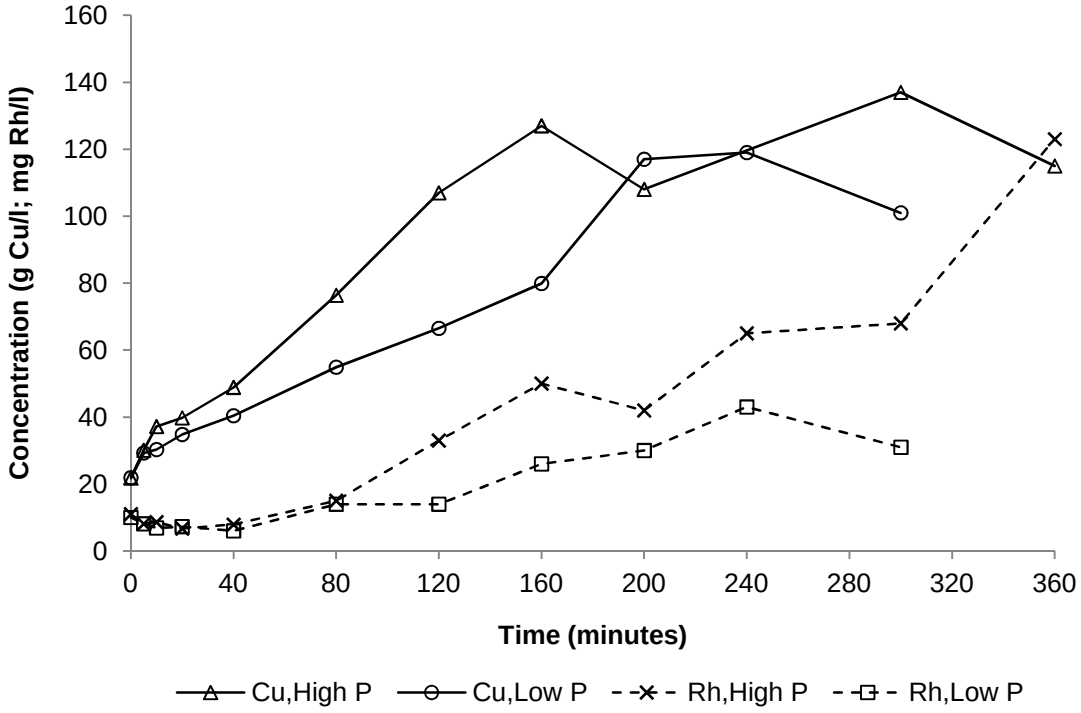

Figure 4.9. Concentration of Cu and Rh in solution as a function of leaching time and pressure at 116°C and an initial acid concentration of 26 g/ℓ (High P: 7 bar; Low P: 5 bar).

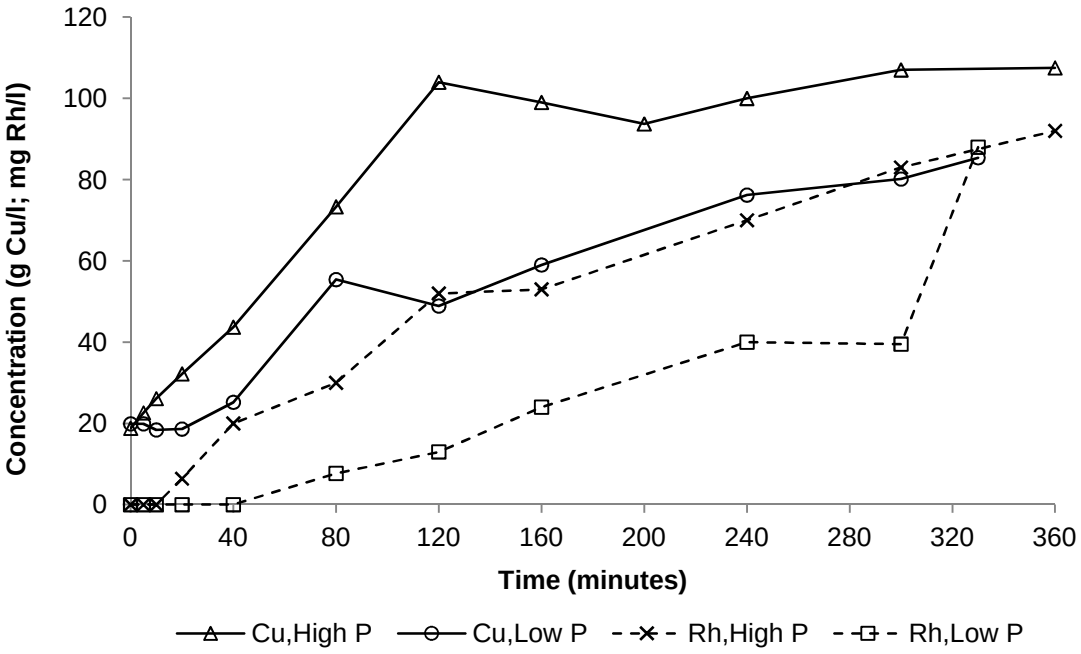

Figure 4.10. Concentration of Cu and Rh in solution as a function of leaching time and pressure at 144°C and an initial acid concentration of 36 g/ℓ (High P: 7 bar; Low P: 5 bar).

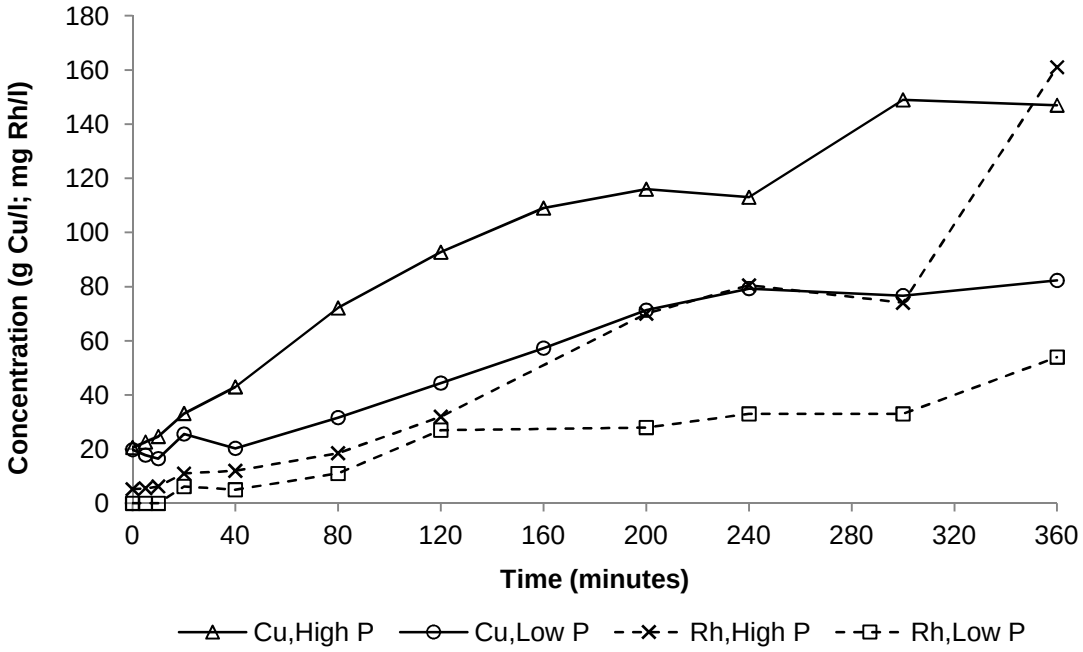

Figure 4.11. Concentration of Cu and Rh in solution as a function of leaching time and pressure at 144°C and an initial acid concentration of 26 g/ℓ (High P: 7 bar; Low P: 5 bar).

4.2.2.3 Effect of initial acid concentration on metal dissolution

Figure 4.12 and Figure 4.13, as well as Figure 4.15 and Figure 4.16, show comparisons between the concentration of copper and rhodium over time at the high and low initial acid values for specific conditions of temperature and pressures. In Figure 4.12 and Figure 4.13 it can be seen that, for the leaching experiments performed at 7 bar, a lower initial acid concentration resulted in increased dissolution of copper once copper leaching had been completed after five to six hours. This is in agreement with the observations made by Ruiz *et al.* (2007), who reported a slight decrease in copper dissolution when the acid concentration increases above an optimum level due to decreased oxygen solubility. Hofirek and Kerfoot (1992) reported that precipitation of iron from solution is possible at acid concentrations below 30 g/ℓ, and that acid is released during these precipitation reactions. It was also suggested that iron might act as an electron carrier and thereby influence the oxidation mechanism.

The concentration of iron in the leaching solution for the four sets of experimental conditions illustrated in Figure 4.12 and Figure 4.13 is shown in Figure 4.14. It can be seen that precipitation of iron from solution occurred to a much greater extent for the low acid operating conditions than for the high acid operating conditions, which is in agreement with the observations reported in literature and discussed above. As a result of this iron precipitation reaction that occurred, acid was released, which in turn could enhance the

leaching of copper according to reaction 2.27 and reaction 2.37. At high initial acid concentrations, however, the reactions involving iron occurred to a much lesser extent and did not influence the copper leaching behaviour. Given the relatively low iron concentration in the leach solution compared to the copper concentration, however, the effect of acid on oxygen solubility was expected to have a more significant influence on the copper leaching behaviour than the iron precipitation.

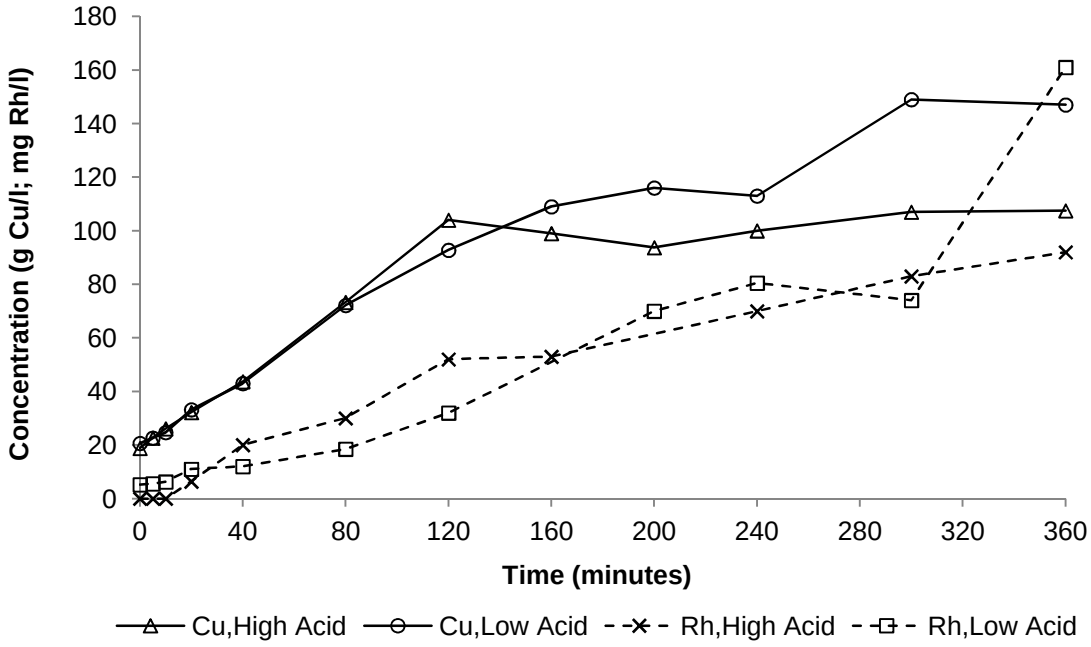

Figure 4.12. Concentration of Cu and Rh in solution as a function of leaching time and initial acid concentration at 144°C and 7 bar (High Acid: 36 g/ℓ; Low Acid: 26 g/ℓ).

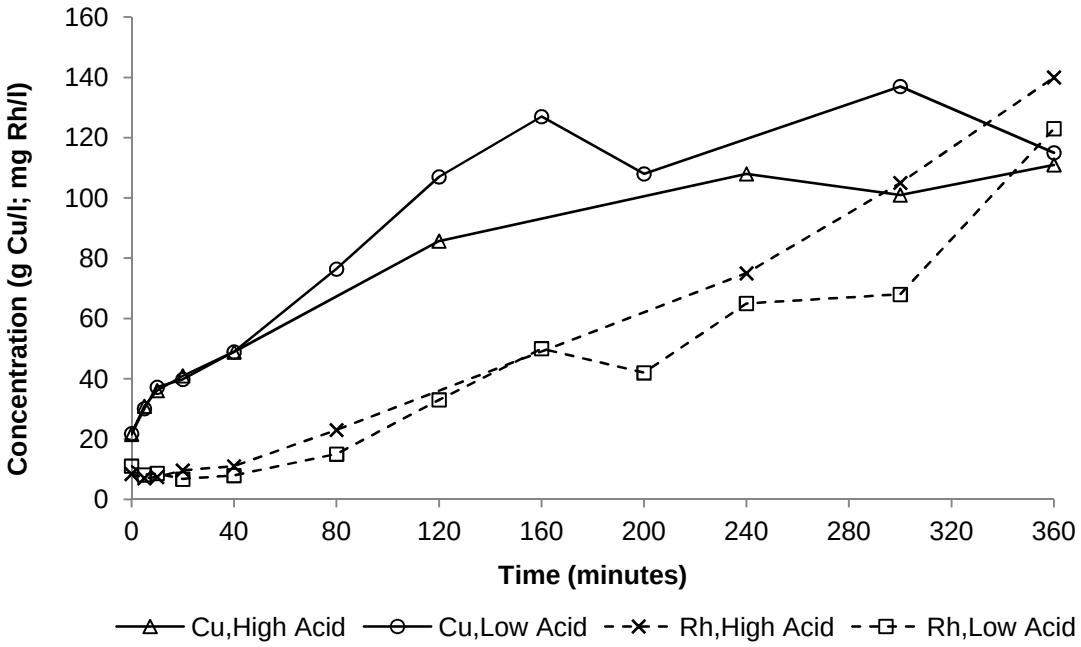

Figure 4.13. Concentration of Cu and Rh in solution as a function of leaching time and initial acid concentration at 116°C and 7 bar (High Acid: 36 g/ℓ; Low Acid: 26 g/ℓ).

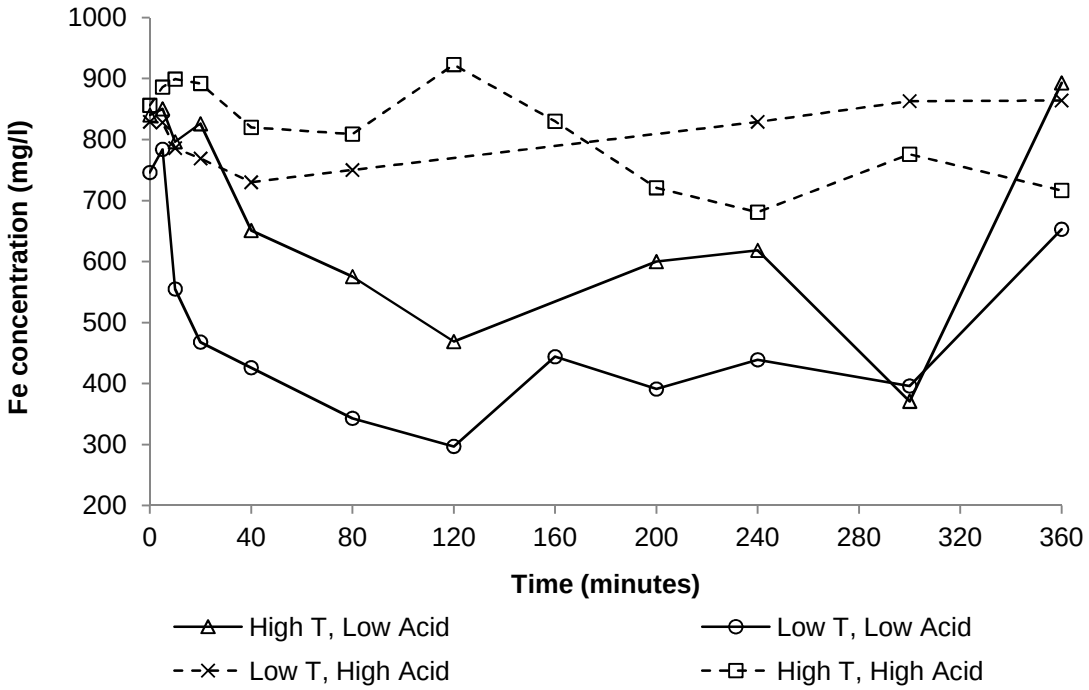

Figure 4.14. Concentration of Fe in solution as a function of leaching time, temperature and initial acid concentration at 7 bar (High T: 144°C; Low T: 116°C; High Acid: 36 g/ℓ; Low Acid: 26 g/ℓ).

In Figure 4.15 and Figure 4.16 it can be seen that the initial acid concentration had a negligible effect on the copper dissolution for the leaching experiments performed at a pressure of 5 bar. The concentration of copper in solution at the end of the leaching was also lower for these experiments than for the experiments performed at 7 bar. This suggested that the availability of oxygen in the leaching solution at the lower pressure limited the copper dissolution to such an extent that the acid concentration did not influence the leaching.

For all the operating conditions, the leaching of rhodium initially proceeded at approximately the same rate for the high and low initial acid concentrations. It was only during the latter stages of the leaching process that the kinetics of rhodium dissolution changed for different acid concentrations and that the leaching rate of rhodium typically increased noticeably. One possible explanation involves the changing limiting factor as leaching progressed and the simultaneous occurrence of leaching reactions competing for the available oxygen in the leaching solution. The concentration of copper in the leaching solution typically reached a constant value after 160 minutes for the high pressure leaching conditions and after 200 to 240 minutes for the low pressure leaching conditions. Up to this time, the dissolved oxygen was consumed preferentially by the copper dissolution reactions and there was hence a limited amount of oxygen available for rhodium dissolution. The acid concentration was therefore not the factor limiting the rhodium leaching during the initial stages. When copper

dissolution had been completed, however, the PGM dissolution reactions were the only reactions requiring oxygen and oxygen availability were no longer the factor limiting the leaching kinetics. This resulted in faster PGM dissolution in general, with the concentration of acid in the solution being the rate determining factor at that time instance. Higher acid concentrations in the leaching solution at this stage of the leaching process hence lead to higher dissolution of PGMs.

As discussed for the dissolution of copper, iron precipitation reactions could increase the acid concentration in the leaching solution. It was also noted that iron precipitation did occur during the experiment performed with a low initial acid concentration at 144°C and 7 bar, but not during the experiment performed with a high initial acid concentration at the same temperature and pressure conditions. This explained why the rhodium dissolution after 360 minutes of leaching with a low initial acid concentration exceeds the rhodium dissolution observed for the experiment with the high initial acid concentration and the same temperature and pressure conditions (shown in Figure 4.12). For the experiments performed at 5 bar, limited iron precipitation was observed and the acid concentration throughout the leaching process was dependent solely on the initial acid concentration. At these low pressure operating conditions, the rhodium concentration in solution at the termination of the process was hence higher for the high initial acid conditions than for the low acid conditions, as shown in Figure 4.15 and Figure 4.16.

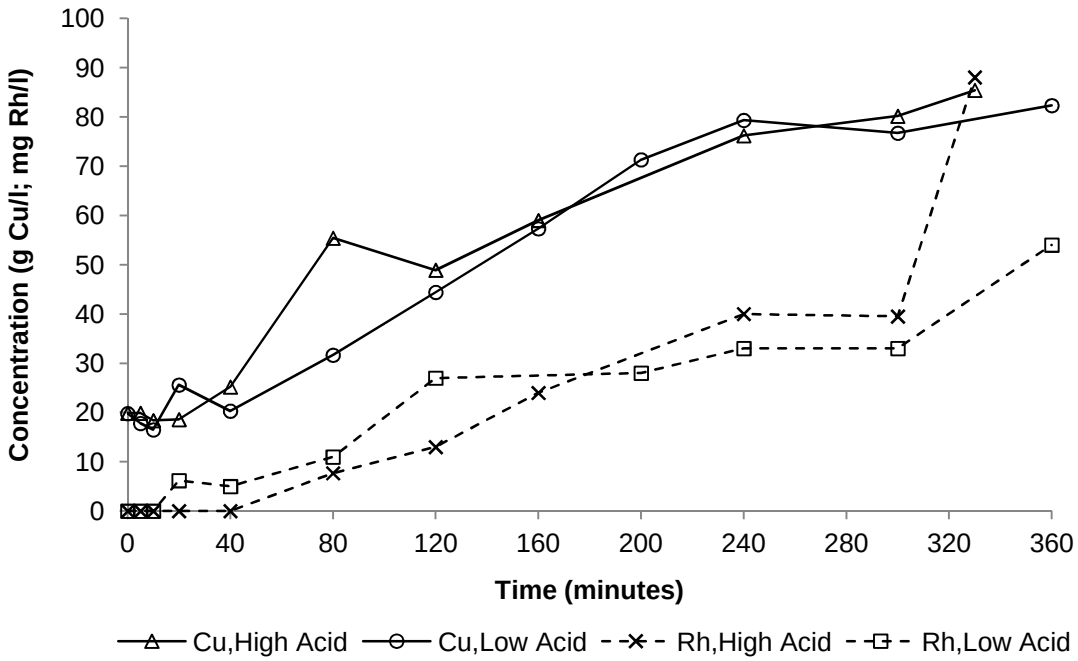

Figure 4.15. Concentration of Cu and Rh in solution as a function of leaching time and initial acid concentration at 144°C and 5 bar (High Acid: 36 g/ℓ; Low Acid: 26 g/ℓ).

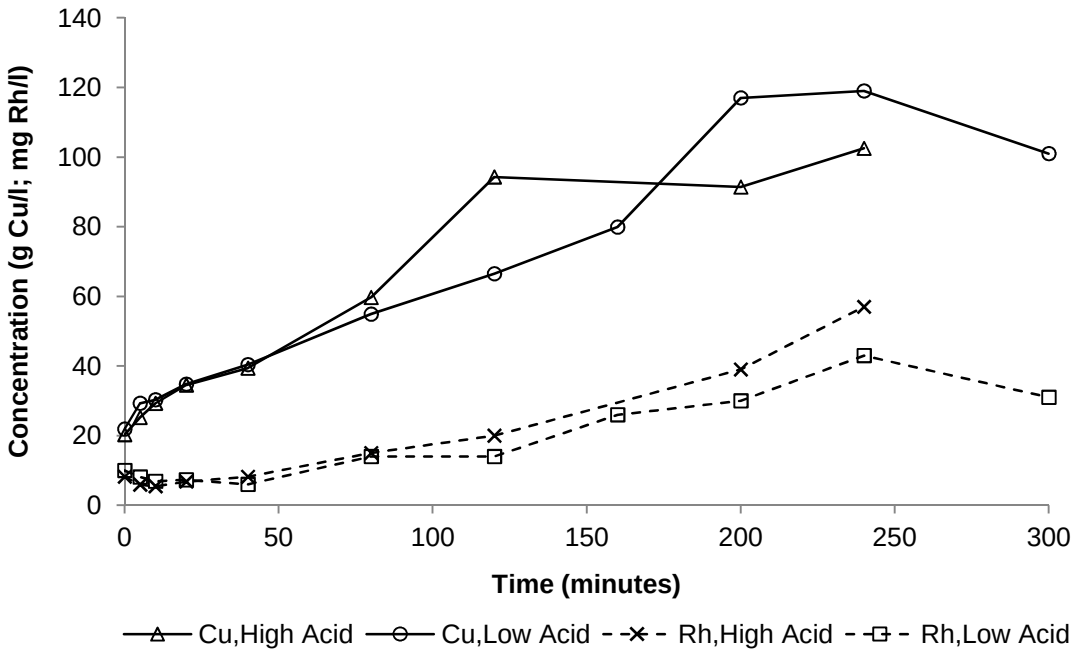

Figure 4.16. Concentration of Cu and Rh in solution as a function of leaching time and initial acid concentration at 116°C and 5 bar (High Acid: 36 g/ℓ; Low Acid: 26 g/ℓ).

4.2.2.4 Comparison of the leaching behaviour of the PGMs

The interactions that exist between the effects that different leaching temperatures, leaching pressures, and initial acid concentrations have on the dissolution of rhodium have been discussed. Similar effects were, however, observed for all the other PGMs present in the first stage leach residue. Figure 4.17 illustrates the percentage dissolution achieved for the different PGMs after six hours (or five hours in case of test 1e and test 1f) at the various combinations of operating conditions. The operating conditions corresponding to specific test numbers are given in Appendix C, and are repeated in Table 4.3 for clarity.

It can be seen that, in general, the different PGMs responded similarly to the variations in operating conditions if the percentage dissolution at the end of leaching was considered as the evaluation criterion. For Rh, Ru, Ir, Pd, and Pt, the largest percentage dissolution was achieved during test 1a, followed by test 1c, and then test 1b. All the PGMs showed low percentage dissolutions during test 1e and test 1h. Osmium showed to highest resistance to dissolution, with 8.2% dissolution achieved on average for the eight tests under consideration; platinum showed the second highest resistance to dissolution, with 20.2% dissolution achieved on average. These results agreed with the earlier statement that the other platinum group metals (Rh, Ru, and Ir) generally exhibit a higher tendency to dissolve in the pressure leaching system than platinum (Steenekamp, 2009). The behaviour of palladium, on the other hand, appeared to contradict this statement for tests 1(a) to 1(d) in particular; the percentage

dissolution values calculated for palladium for these tests were comparable to that of rhodium and ruthenium. Given the relatively high percentage palladium dissolution, its dissolution could potentially be significant and were hence identified for further investigation together with Rh, Ru, and Ir in the tests that were performed subsequently. The fact that a percentage dissolution value of more than 100% was calculated for iridium can possibly be ascribed to an analytical error in the solids analysis, with the actual amount of Ir present in the first stage leach residue being higher than the reported value. The calculations done to determine the percentage dissolution values are discussed in Appendix D. The percentage extraction values calculated at the respective sampling time instances for the different operating conditions are also summarised in Appendix D.

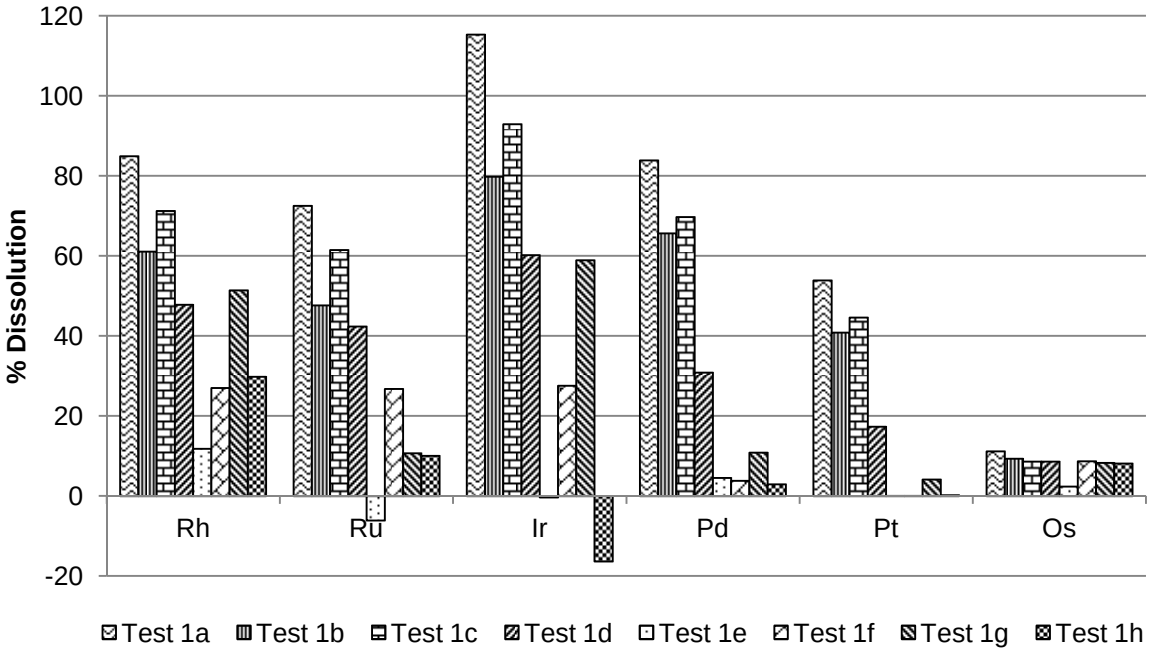

Figure 4.17. Comparison of the percentage dissolutions achieved for the different PGMs during the first set of leaching experiments (low solids content) performed on the first stage leach residue.

Table 4.3. Experimental conditions for the first set of leaching experiments (low solids content) performed on the first stage leach residue.

	Temperature (°C)	**Pressure (bar)**	**Initial [M_{H2SO4}] (g/ℓ)**	**Solids content (g solids/ℓ)**
Test 1a	144	7	26	180
Test 1b	116	7	26	180
Test 1c	116	7	36	180
Test 1d	144	5	36	180
Test 1e	116	5	26	180
Test 1f	116	5	36	180
Test 1g	144	7	36	180
Test 1h	144	5	26	180

In addition to considering the effects that changes in the various operating conditions had on the percentage dissolution achieved after a specific leaching time, the effects on the relative leaching rates of the different PGMs also had to be considered. The concentrations of Rh, Ru, and Ir in the leaching solution are shown as a function of time for test 1a and test 1d in Figure 4.18 to illustrate the similarities in the trends observed for the different PGMs. For all elements, the degree of metal precipitation during the initial leaching stages was greater during test 1d than during test 1a. The leaching rate and extent of dissolution also appeared to be greater during test 1a than during test 1d for the metals under consideration. Similar trends were observed when comparing the leaching behaviour of Rh, Pd, and Pt during these two tests, as shown in Figure 4.19. In general, it can thus be said that the discussion of the effects of operating conditions on the leaching behaviour of Rh in Section 4.2.2.1 to Section 4.2.2.3 is applicable to the platinum group metals in general. The experimental data and the calculated percentage dissolution values are given in Appendices C and D, respectively.

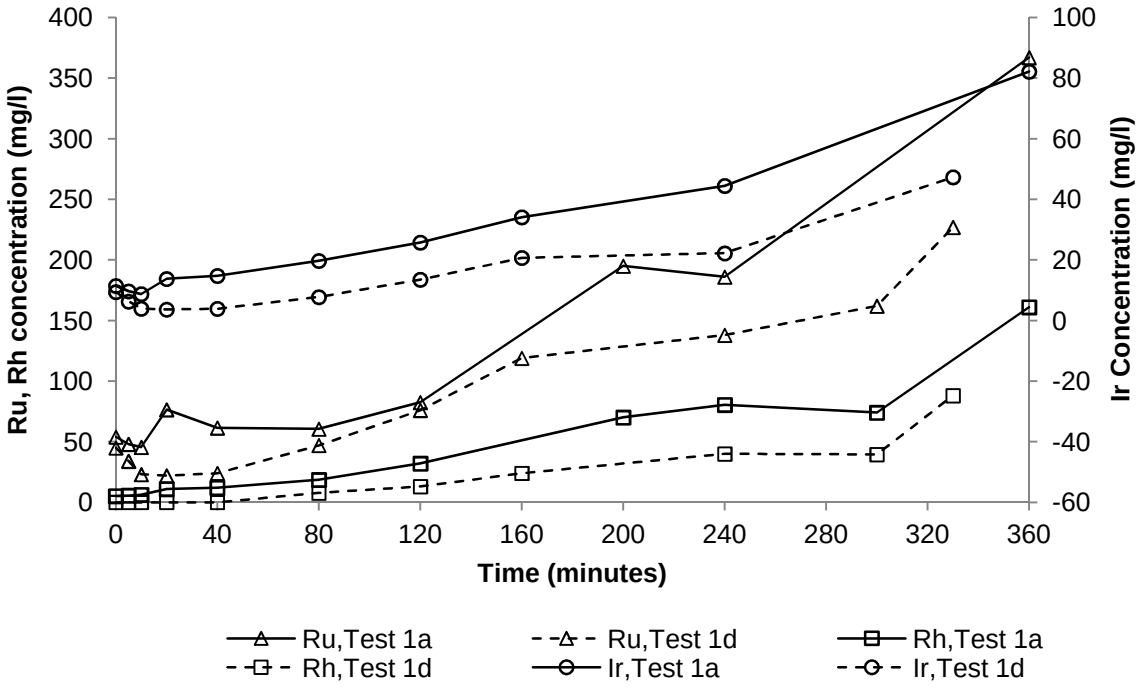

Figure 4.18. Concentration of Rh, Ru, and Ir in solution as a function of leaching time for test 1a and test 1d.

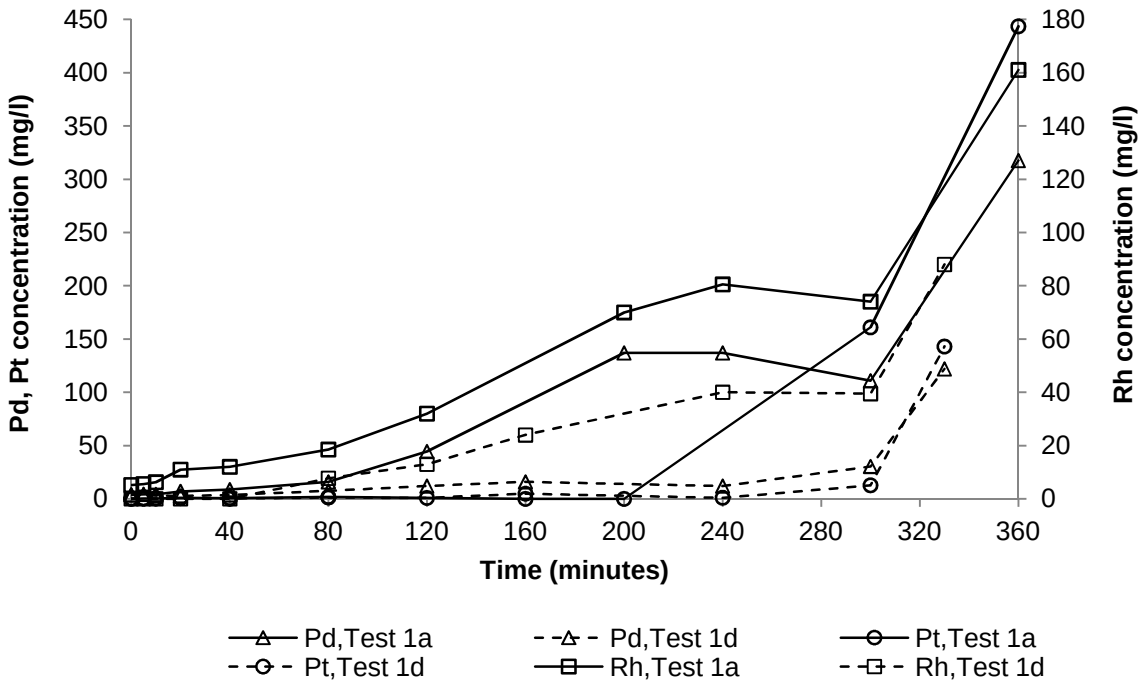

Figure 4.19. Concentration of Rh, Pd, and Pt in solution as a function of leaching time for test 1a and test 1d.

4.2.3 Conclusions

From the experimental results discussed above, it can be concluded that copper dissolution was insufficient when leaching was performed at a pressure of 5 bar and a temperature of 144°C. At this combination of temperature and pressure conditions the oxygen partial pressure of approximately 96 kPa was too low to ensure sufficient oxygen availability for the copper dissolution to proceed. The highest copper dissolution was achieved at a pressure of 7 bar, a temperature of 144°C, and an initial acid concentration of 26 g/ℓ. These leaching conditions did, however, also correspond to the highest rhodium dissolution. If these conditions are to be used, the residence time in the autoclave must be limited to prevent excessive OPM leaching. The copper concentration in the leach solution did not change noticeably after five hours, while the Rh concentration increased from approximately 75 mg/ℓ to 160 mg/ℓ during the sixth hour of leaching.

Leaching processes operated at the remaining combinations of conditions resulted in comparable copper dissolution, with the average final copper concentration for the remaining high pressure conditions being 8.8% higher than for the remaining low pressure conditions. The average final rhodium concentration was however 62.7% lower for the remaining low pressure conditions than for the remaining high pressure conditions. The lowest Rh dissolution was observed for the leaching performed at a pressure of 5 bar, a temperature of 116°C, and an initial acid concentration of 26 g/ℓ.

At higher leaching temperatures, the oxygen partial pressure, which influences the dissolved oxygen content of the solution, decreased to such an extent that oxygen availability limited the copper leaching. If copper leaching is to be enhanced by increasing the operating temperature, the oxygen partial pressure must be maintained above its rate limiting level.

The initial acid concentration in the leaching solution influenced the dissolution of copper if the dissolved oxygen content was sufficiently high. The effects of reduced oxygen solubility at increased acid concentration and of iron precipitation reactions occurring at low acid conditions on copper dissolution were more significant than the direct effect that acid concentration had on the leaching behaviour.

The limiting factor governing the Rh leaching rate changed as leaching progressed. Since both copper and PGM dissolution depend on oxygen to proceed, the copper dissolution and rhodium leaching competed for dissolved oxygen during the initial stages of the process. As copper dissolution approached completion, more oxygen became available for PGM dissolution, with acid concentration that became the rate determining factor during the latter stages of the process.

In order to determine the direct effects of the various process variables on the leaching kinetics, the experimental conditions had to be revised to avoid the secondary effects mentioned above.

4.3 Leaching of first stage residue: second experimental design

As discussed in Section 4.2, the experimental conditions had to be revised in order to be able to quantify the direct effects of the various process variables on the leaching kinetics. More specifically, the following changes had to be made to the experimental conditions:

- The solid to liquid ratio had to be reduced to maintain the dissolved metal content of the leaching solution at levels that would not lead to excessive crystallisation during sampling, as was the case with the high solids content experiments for the first experimental design.
- The operating pressure had to be increased and/or the leaching temperature decreased in order to operate at conditions where oxygen availability was not the limiting factor, which would allow the quantification of the effect of temperature on PGM dissolution.

- The initial acid concentration had to be increased to maintain the pH at a low enough value to prevent iron precipitation from occurring, since iron precipitation is rarely observed on site. Instead of using an initial acid concentration corresponding to the acid concentration of the leach solution on site (25 g/ℓ to 35 g/ℓ), the initial acid concentration was adjusted so that the final acid concentration in the batch tests would correspond to the typical acid concentration in the site leach solution. In order to obtain an estimate of the initial acid concentration required for the batch tests to obtain a final acid concentration larger than 35 g/ℓ, the following assumptions were made:
  - All the copper in the first stage leach residue was initially present as digenite, and leached according to reaction 2.27.
  - The covellite produced in reaction 2.27 was leached according to reaction 2.37.
  - All the nickel in the first stage leach residue was initially present as millerite, and leached according to reaction 2.25.

  The leaching reactions of PGMs were not taken into account, since the base metals were present in much larger concentrations in the first stage leach residue. The assumptions above furthermore allowed a conservative estimation of the acid requirements, since not all the base metal leaching occurred according to acid leaching reactions, and a portion of the copper was present as covellite in the first stage leach residue. Any acid required for PGM leaching would hence not have reduced the final acid concentration to below the required level of 35 g/ℓ.

A summary of the revised experimental conditions used for the second set of experiments performed according to a full factorial experimental design is given in Table 3.6. The experimental data for the second set of first stage leach residue leaching experiments are given in Appendix C.

4.3.1 Evaluation of revised experimental conditions

4.3.1.1 Reduced solid to liquid ratio

The revised experimental conditions allowed the selection of feed material amounts requiring 80 g and 130 g solids to be added per litre of leach solution, respectively. These conditions allowed samples to be taken without crystallisation occurring; by the time the samples had reached the analytical laboratory, however, copper sulphate had started to precipitate. As a result, the copper concentrations reported for the samples taken during the latter stages of the

respective leaching tests in particular were below the actual concentrations and appeared erratic.

This behaviour was more profound for the high solids content tests (Figure 4.20) than for the low solids content tests (Figure 4.21), as would be expected given the fact that the tests with the higher solid to liquid ratio would yield higher actual dissolved metal concentrations. In addition, the low solids content tests yielded realistic percentage copper dissolution values between 70.0% (test 2g) and 94.9% (test 2n). A table summarising the experimental conditions for the respective tests is given in Appendix C, but is repeated in Table 4.4 for clarity. The concentrations of the remainder of the elements conformed to observations made during the first experimental design, and yielded realistic percentage dissolution values. The behaviour of the remainder of the metals is discussed in Section 4.3.2, together with the effects that the various process variables have on the copper leaching for the low solids content tests.

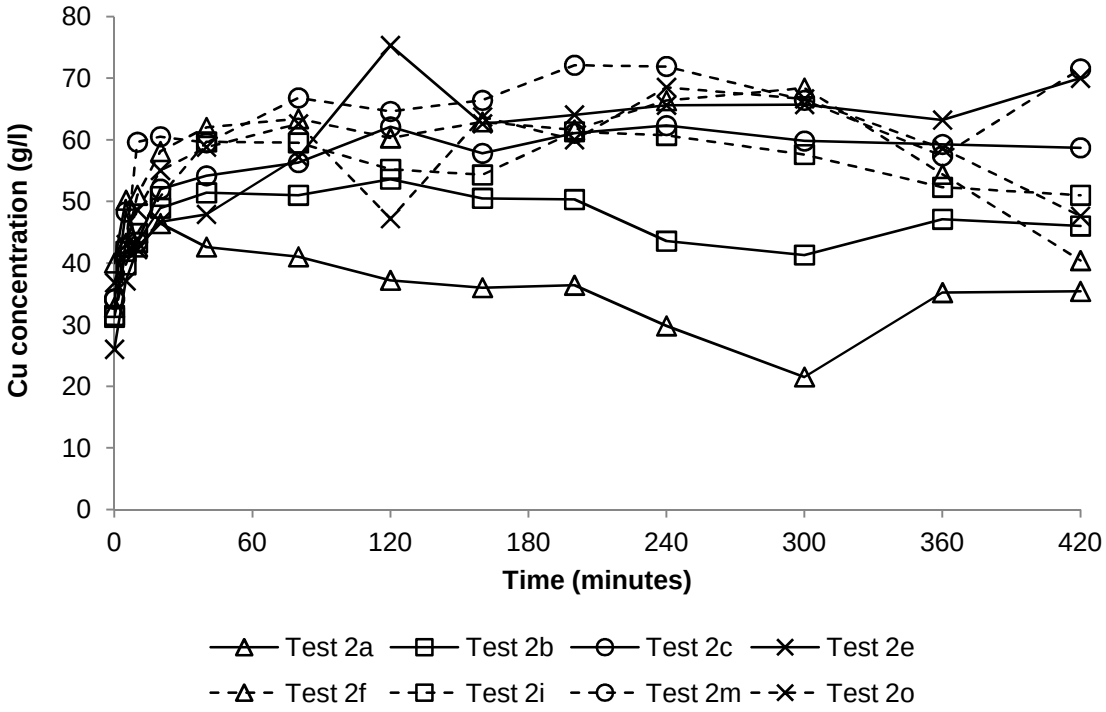

Figure 4.20. Concentration of Cu in solution as a function of leaching time for the tests performed at a solids content of 130 g/ℓ.

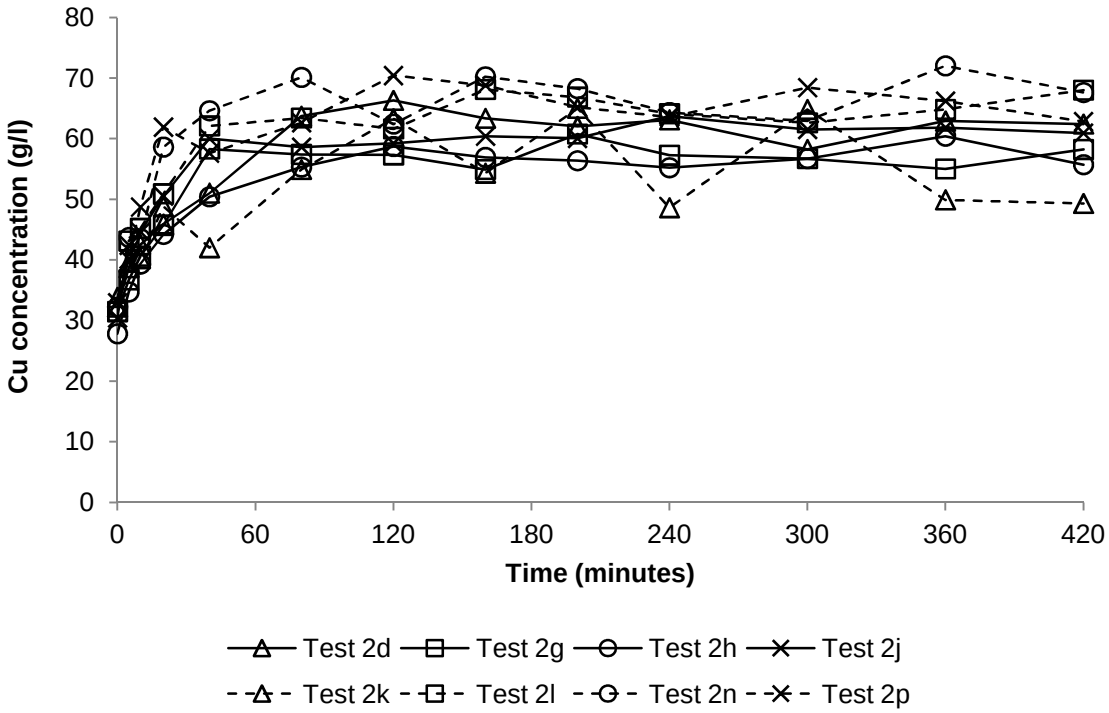

Figure 4.21. Concentration of Cu in solution as a function of leaching time for the tests performed at a solids content of 80 g/ℓ.

Table 4.4. Experimental conditions for the second set of leaching experiments performed on the first stage leach residue.

	Temperature (°C)	**Pressure (bar)**	**Initial [M_{H2SO4}] (g/ℓ)**	**Solids content (g solids/ℓ)**
Test 2a	116	9	165	130
Test 2b	130	9	165	130
Test 2c	116	7	165	130
Test 2d	130	7	140	80
Test 2e	130	7	140	130
Test 2f	130	9	140	130
Test 2g	130	9	165	80
Test 2h	116	7	165	80
Test 2i	116	9	140	130
Test 2j	116	9	165	80
Test 2k	130	7	165	80
Test 2l	130	9	140	80
Test 2m	130	7	165	130
Test 2n	116	9	140	80
Test 2o	116	7	140	130
Test 2p	116	7	140	80

4.3.1.2 Increased oxygen partial pressure

A summary of the estimated oxygen partial pressures for the respective experimental conditions is given in Table 4.5. Unlike the first experimental design, in which case the temperature had an insignificant effect on the rhodium leaching because the secondary oxygen partial pressure effect was more significant than the primary temperature effect, the second experimental design results indicated that temperature was the operating variable with the largest influence on the rhodium leaching kinetics.

This is in agreement with the observation of Fugleberg *et al*. (1995), as discussed in Section 2.4.3, and confirmed that the oxygen availability was no longer the rate limiting factor for the rhodium leaching reactions. Despite the earlier observation that the oxygen partial pressure at which oxygen availability was no longer the rate limiting factor is higher for PGM leaching than for copper leaching, the copper dissolution did appear to be dependent on the total system pressure during the second experimental design; this dependence is discussed in Section 4.3.2.

Table 4.5. A summary of the estimated oxygen partial pressures for the respective combinations of pressure and temperature conditions.

	Temperature (°C)	Pressure (bar)	P_{O2} (bar)
First experimental design	116	5	3.25
	116	7	5.25
	144	5	0.96
	144	7	2.96
Second experimental design	116	7	5.25
	116	9	7.25
	130	7	4.30
	130	9	6.30

4.3.1.3 Increased initial acid concentration

The reason for increasing the initial acid concentration was to ensure that the final acid concentration in the leaching system was sufficiently high to avoid iron precipitation, as iron precipitation is not observed on site. From Figure 4.22 and Figure 4.23 it can be seen that no significant iron precipitation occurred at any of the operating conditions, and the objective for changing the initial acid concentration was hence achieved. In general, the rate and extent of iron leaching increased for the second experimental design compared with the first experimental design because of the increased acid concentration in the leach solution.

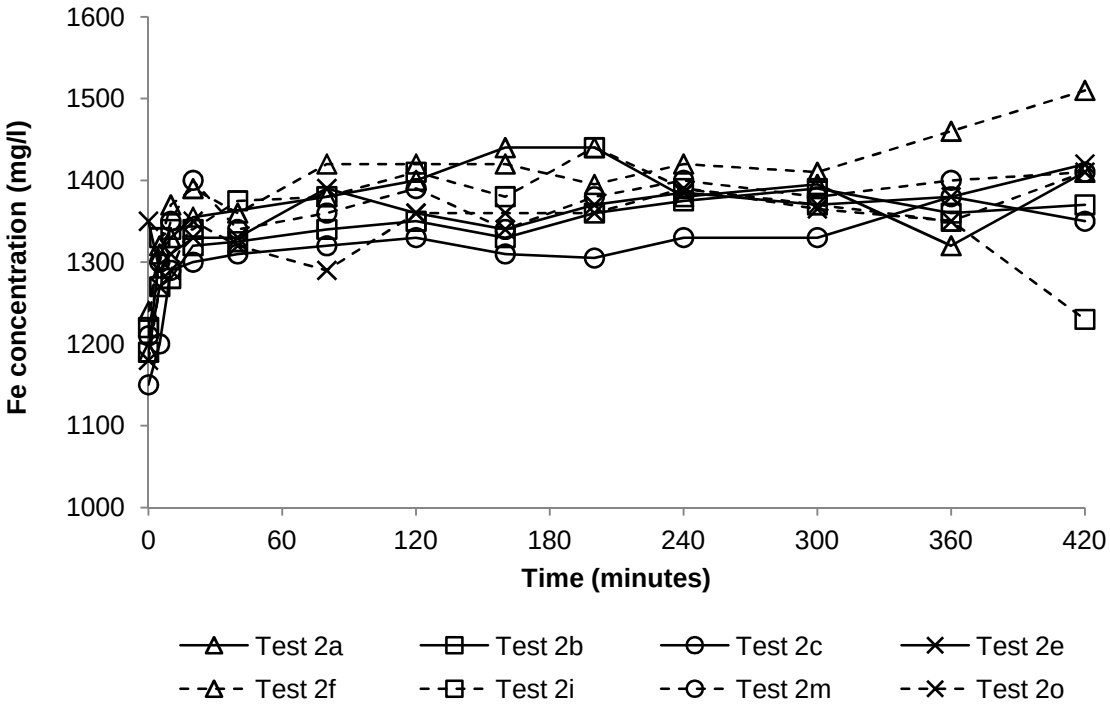

Figure 4.22. Concentration of iron in solution as a function of leaching time for the tests performed at a solids content of 130 g/ℓ.

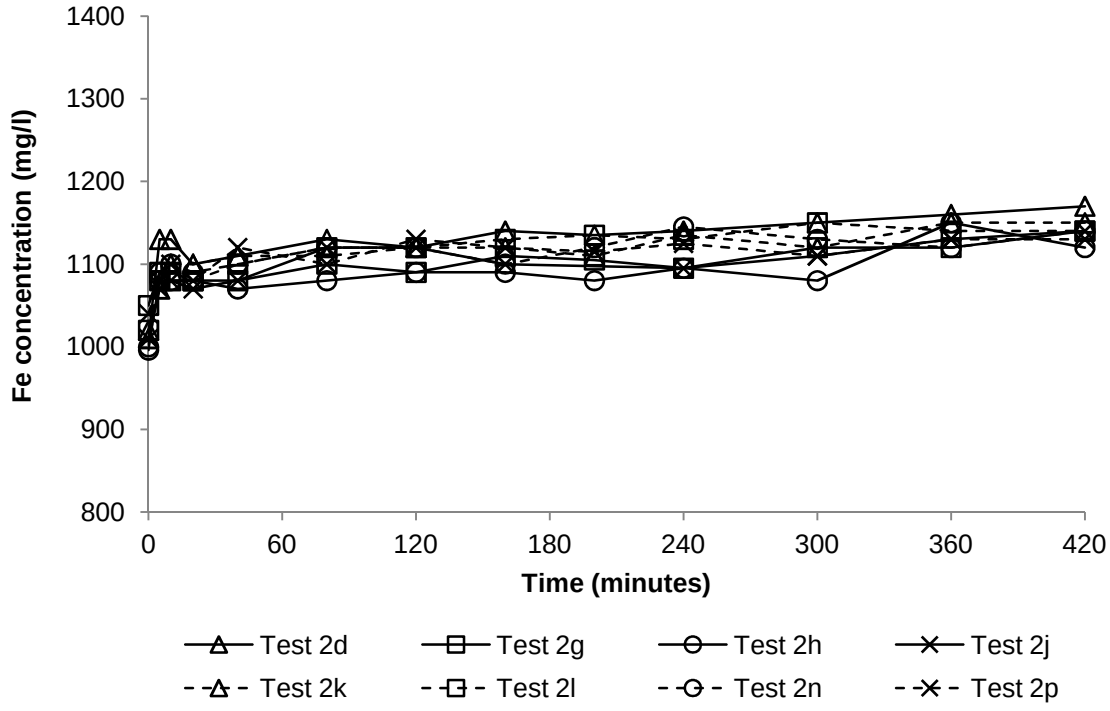

Figure 4.23. Concentration of iron in solution as a function of leaching time for the tests performed at a solids content of 80 g/ℓ.

4.3.2 Effects of various process variables on leaching behaviour

4.3.2.1 Effect of slurry solids content on metal dissolution

Figure 4.24 and Figure 4.25 show the amount of dissolved rhodium as a function of time for tests performed at the high temperature (130°C) and low temperature (116°C), respectively. For both the high temperature and the low temperature tests, the tests performed at the higher solids content (130 g/ℓ, indicated by solid lines on the respective figures) resulted in larger dissolved rhodium concentrations after seven hours of leaching, as would be expected given the fact that there was more rhodium available to dissolve. The intermittent sampling intervals during the initial stages of the leaching experiments limited the accuracy with which the rhodium precipitation period could be determined; in general, however, it can be said that the period of precipitation was longer for a high solids content test than for the low solids content test performed at the same pressure and initial acid concentration. Given the dependence of the OPM precipitation period on the leaching behaviour of the copper sulphides, as discussed in Section 4.2.2, this suggested that increasing the solid to liquid ratio did not increase the rate of copper leaching. A longer leaching time was therefore required for the larger amount of copper sulphides to be dissolved to the extent where OPM leaching started to occur. The fact that an increase in the solid-liquid interfacial area did not result in increased copper leaching rates indicated that the availability of oxygen in solution, and more specifically the rate of mass transfer from the gaseous phase to the liquid phase, was the rate determining factor for the copper leaching reactions. The limited oxygen availability could have limited the rate of copper leaching for two reasons: the dissolution of the copper sulphide phases according to reaction 2.27 and reaction 2.35 is dependent on the availability of dissolved oxygen, and Padilla *et al.* (2008) suggested that metal sulphide leaching could proceed via reactions with Fe^{3+}, in which case oxygen is required to return the Fe^{2+} to the Fe^{3+} state to sustain the reaction with the metal sulphide. The exact mechanism whereby the copper leaching proceeded could not be determined from the available data.

The subsequent OPM leaching over the period 60 to 120 minutes proceeded at a faster rate for a high solids content test compared to the low solids content test performed at the same temperature, pressure, and initial acid concentration. This could be attributed to the larger solid-liquid interfacial area as a result of the larger solid to liquid ratio. Inconsistent copper analyses achieved for the high solids content tests as a result of copper sulphate precipitation that occurred during sample transportation meant that the inferred effect of the percentage solids in the slurry on copper dissolution could not be verified.

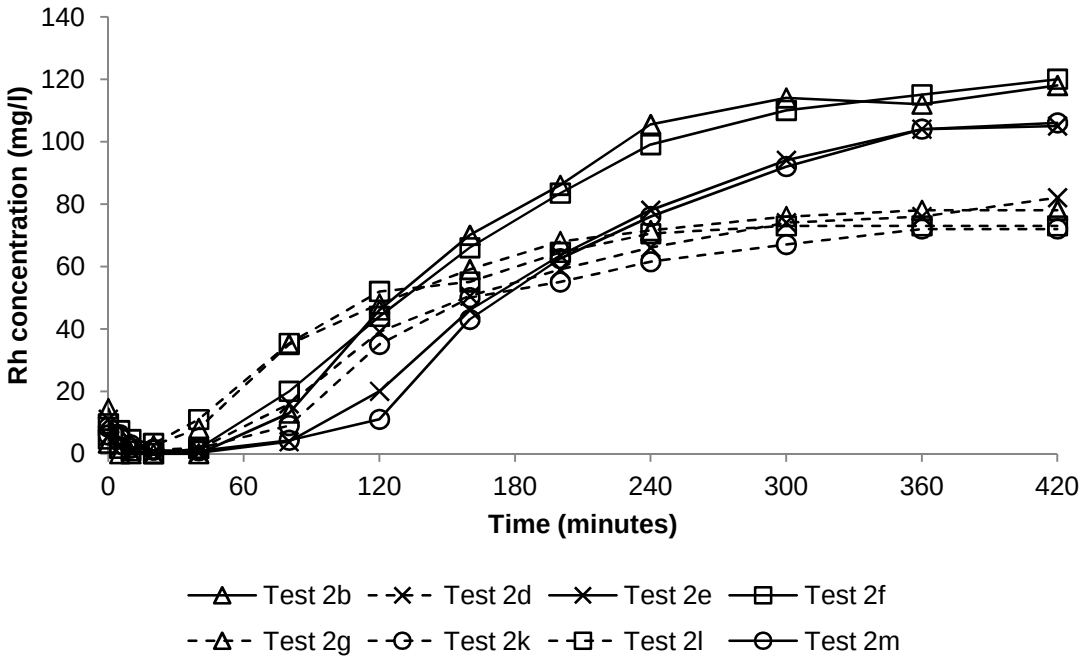

Figure 4.24. Concentration of Rh in solution as a function of leaching time for the tests performed at 130°C.

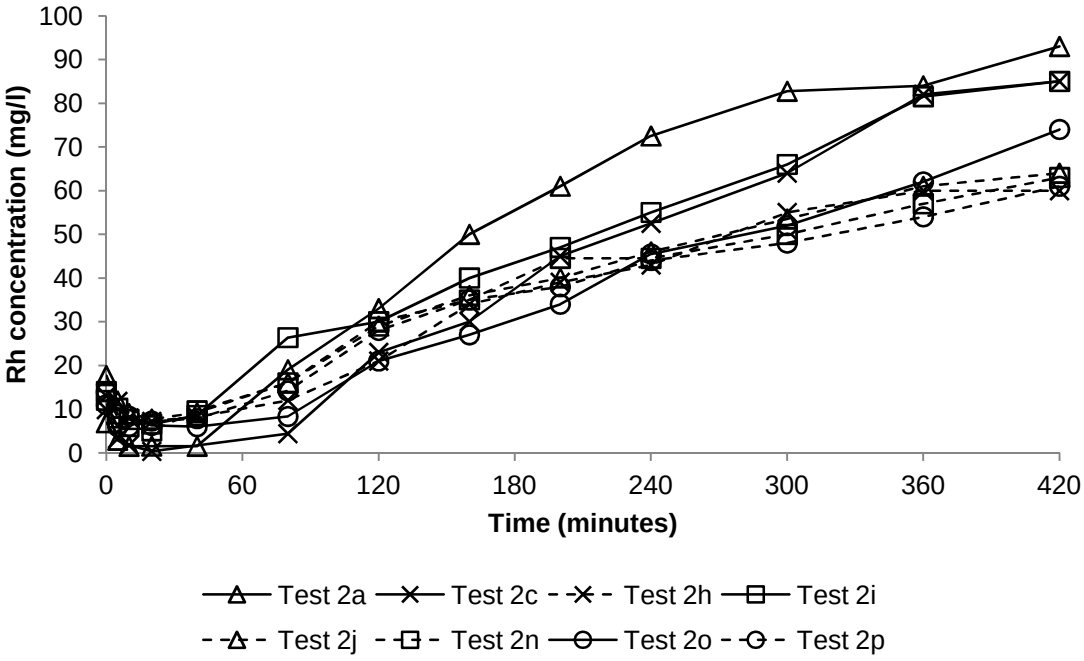

Figure 4.25. Concentration of Rh in solution as a function of leaching time for the tests performed at 116°C.

4.3.2.2 Effect of leaching temperature on metal dissolution

Figure 4.26 to Figure 4.29 show comparisons between the concentration of copper and rhodium over time at the high and low temperature conditions for the low solids content tests and specific conditions of pressure and initial acid concentration. The temperature did not affect the rate or extent of copper leaching significantly, which was a further indication that

the rates of the copper leaching reactions were not chemical reaction controlled. In the case of rhodium, however, a change in temperature affected both the rhodium precipitation during the initial leaching stages as well as the subsequent rhodium dissolution, irrespective of the pressure and initial acid concentration. Although changing the temperature did not affect the duration of the initial precipitation stage noticeably, increasing the temperature did result in faster rhodium precipitation and hence lower rhodium concentrations in solution during the first 40 minutes of the tests. The subsequent leaching proceeded at a faster rate for the tests performed at 130°C compared to the tests performed at 116°C. This is in agreement with the results reported by Fugleberg *et al.* (1995), who indicated that temperature is the process variable with the largest effect on rhodium leaching, and that the dissolution increases significantly as the temperature is increased (10% dissolution at 115°C to 80-90% dissolution at 140°C). The average percentage rhodium dissolution achieved after seven hours of leaching for the low solids content tests performed at 130°C was 84.0% compared to 59.7% for the tests performed at 116°C. Similar effects were observed for the tests performed at the higher solid to liquid ratio; for these tests, the average percentage rhodium dissolution was 83.2% at 130°C and 57.0% at 116°C.

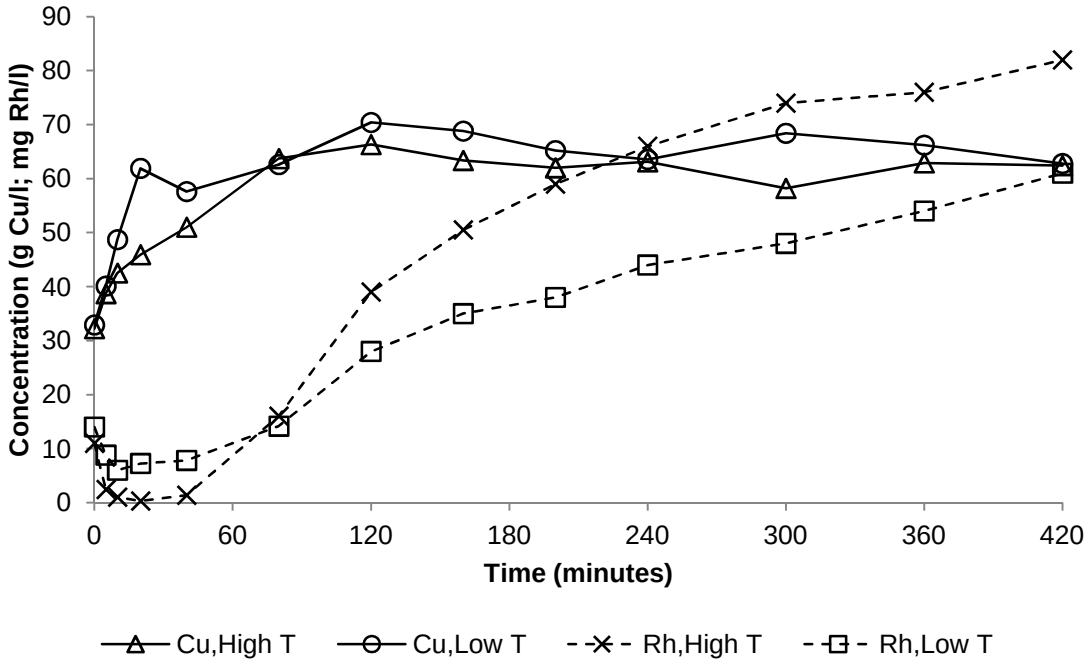

Figure 4.26. Concentration of Cu and Rh in solution as a function of leaching time and temperature at 7 bar, an initial acid concentration of 140 g/ℓ, and a solids content of 80 g/ℓ (High T: 130°C; Low T: 116°C).

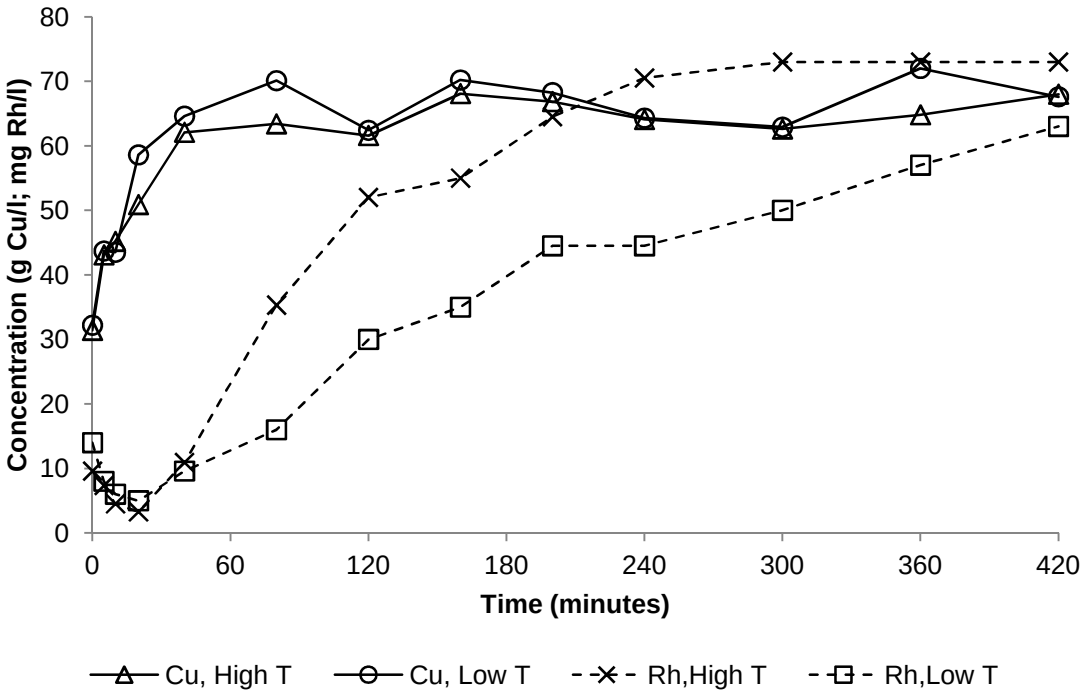

Figure 4.27. Concentration of Cu and Rh in solution as a function of leaching time and temperature at 9 bar, an initial acid concentration of 140 g/ℓ, and a solids content of 80 g/ℓ (High T: 130°C; Low T: 116°C).

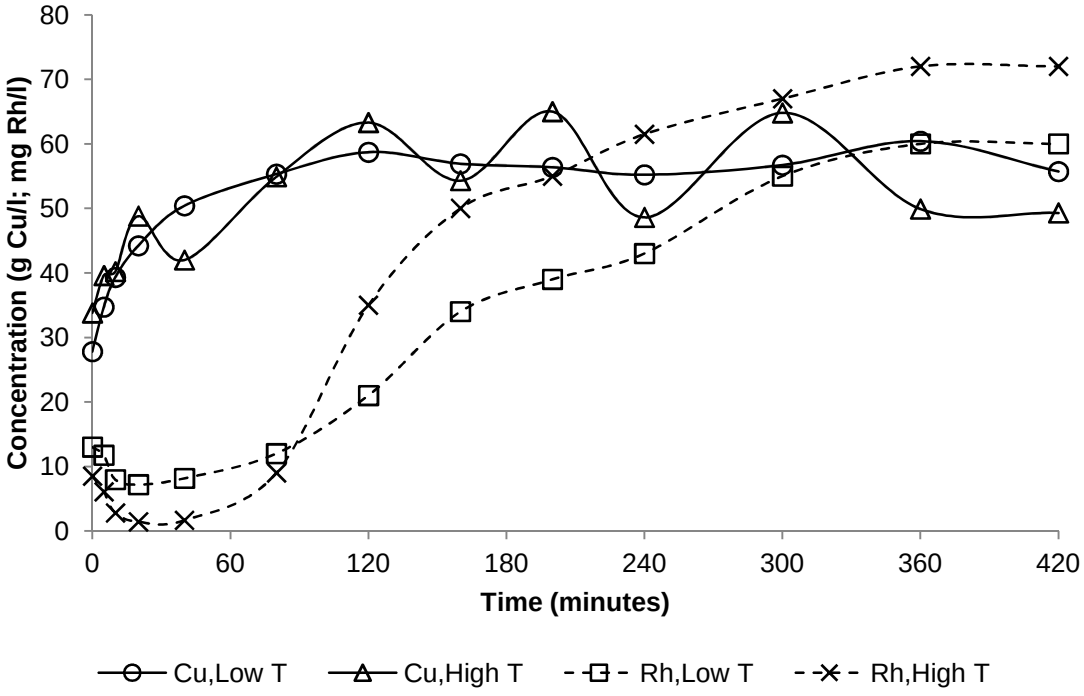

Figure 4.28. Concentration of Cu and Rh in solution as a function of leaching time and temperature at 7 bar, an initial acid concentration of 165 g/ℓ, and a solids content of 80 g/ℓ (High T: 130°C; Low T: 116°C).

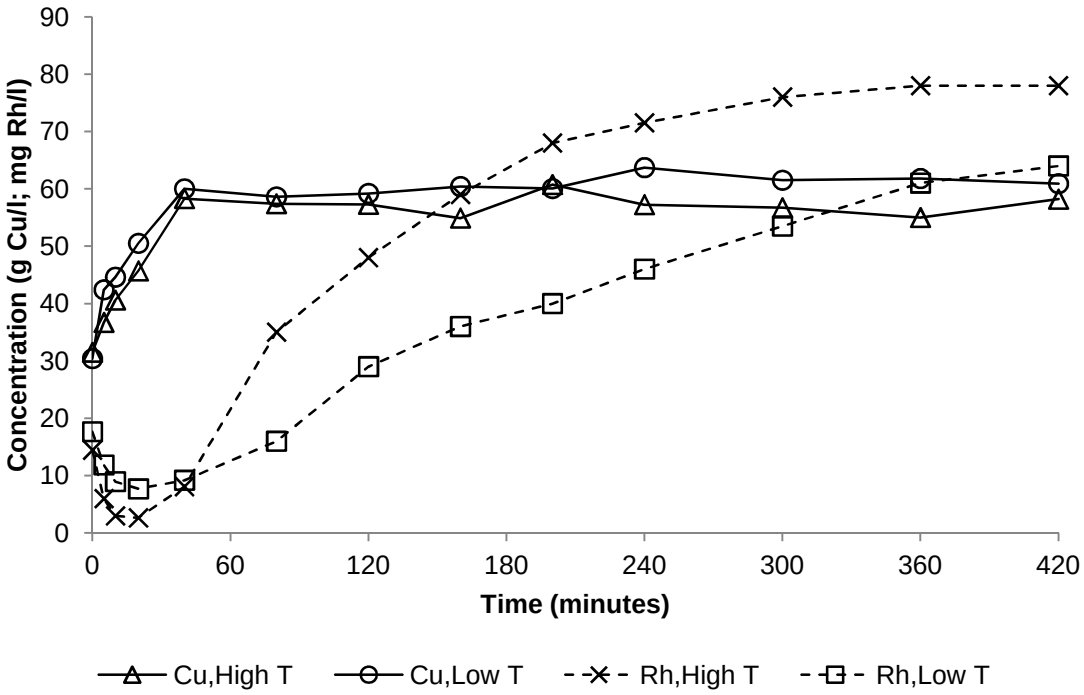

Figure 4.29. Concentration of Cu and Rh in solution as a function of leaching time and temperature at 9 bar, an initial acid concentration of 165 g/ℓ, and a solids content of 80 g/ℓ (High T: 130°C; Low T: 116°C).

4.3.2.3 Effect of leaching pressure on metal dissolution

When considering the effects that the operating pressure had on the leaching behaviour, the dependence of the rhodium leaching on copper leaching as discussed in Section 4.2 was confirmed. The effect of pressure on the rhodium leaching behaviour was also dependent on the other operating conditions.

When leaching was performed at 116°C with an initial acid concentration of 140 g/ℓ (Figure 4.30), the pressure affected neither the rhodium leaching behaviour nor the rate and extent of the copper leaching. For the test performed at 116°C with an initial acid concentration of 165 g/ℓ (Figure 4.32), the effect of pressure on the copper leaching rate was more noticeable, with the high pressure resulting in faster leaching kinetics due to the higher dissolved oxygen concentration. As a result, the equilibrium copper concentration was reached after approximately 40 minutes for the high pressure test compared to 120 minutes for the low pressure test. The pressure effect was more noticeable at the high initial acid concentration compared with the low initial acid concentration for the tests performed at 116°C because the higher acid concentration reduced the oxygen solubility of the leaching solution. At the low initial acid concentration, the oxygen availability remained sufficient to not be the rate determining factor, irrespective of the leaching pressure. At the higher initial acid

concentration, the reduced oxygen solubility caused the oxygen availability to become the rate determining factor. Increasing the overall pressure resulted in an increased oxygen partial pressure and hence an increased oxygen solubility, which subsequently resulted in a faster leaching rate. Considering the rhodium behaviour at these conditions, the initial leaching rate appeared to be faster for the high pressure test than for the low pressure test. During the latter stages of the batch test, however, the Rh leaching for the high pressure test and the Rh leaching for the low pressure test proceeded at similar rates.

The effect of pressure on the rhodium leaching was however more profound for the tests performed at 130°C (Figure 4.31 and Figure 4.33). While the pressure did not affect the rate at which the rhodium leaching proceeded, the precipitation period during the initial stages of the leaching process was longer for the tests performed at a pressure of 7 bar compared to the tests performed at 9 bar. In addition, the time required for the copper to reach the equilibrium dissolved copper concentration was longer for the low pressure tests than the higher pressure tests. The copper behaviour could once again be attributed to the oxygen availability. For a specific operating pressure, the oxygen partial pressure in the system decreased as the temperature was increased, due to the fact that the water vapour pressure increased. At the higher temperature, the oxygen availability was the rate determining factor irrespective of the initial acid concentration. By increasing the pressure, the oxygen partial pressure, and hence the oxygen availability, was increased, which allowed the equilibrium dissolved copper concentration to be achieved faster.

It can furthermore be concluded that the rhodium leaching started to proceed at an appreciable rate only once the copper dissolution had almost been completed. This confirmed the earlier observation that copper and rhodium competed for the available oxygen during the initial leaching stages, with the available oxygen preferentially being used for copper leaching. One possible reason why overall leaching of OPMs is not observed during the initial leaching stages is because the OPM precipitation reactions that occur in the presence of base metal sulphides are thermodynamically more favourable than the OPM leaching reactions. This is investigated in more detail in Section 5.2. It is furthermore possible that the majority of the leachable OPM species occur as inclusions inside the base metal sulphide matrix, and that the base metals need to be leached to an appreciable extent to allow the acid and dissolved oxygen required for OPM dissolution to reach the solid-liquid reaction interface.

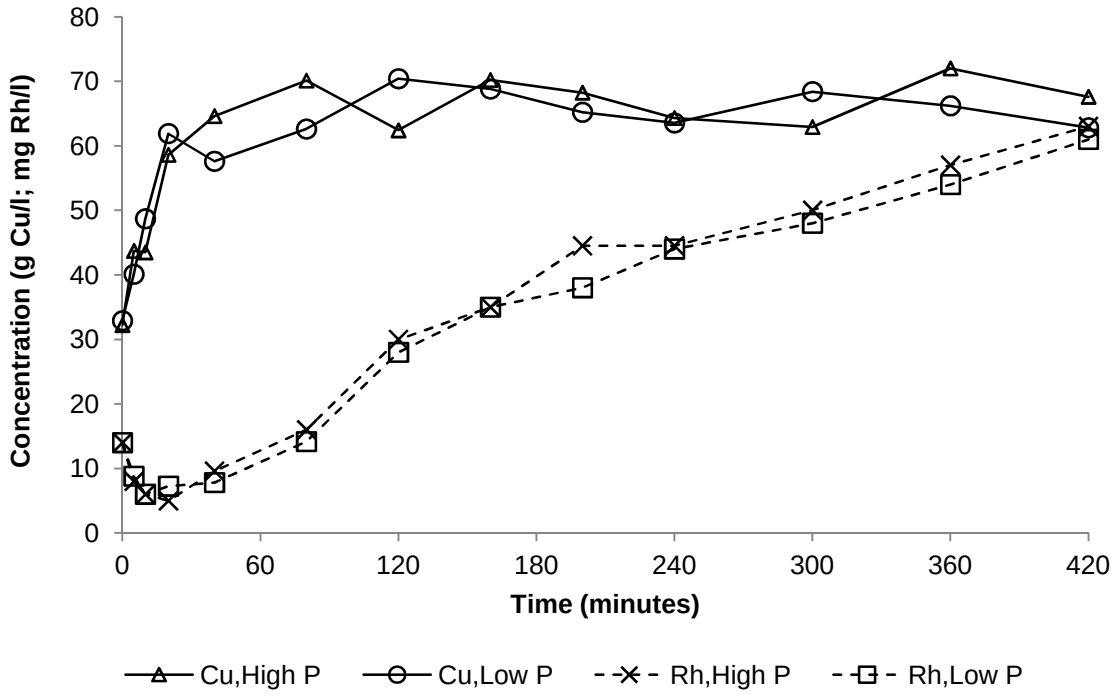

Figure 4.30. Concentration of Cu and Rh in solution as a function of leaching time and pressure at 116°C, an initial acid concentration of 140 g/ℓ, and a solids content of 80 g/ℓ (High P: 9 bar; Low P: 7 bar).

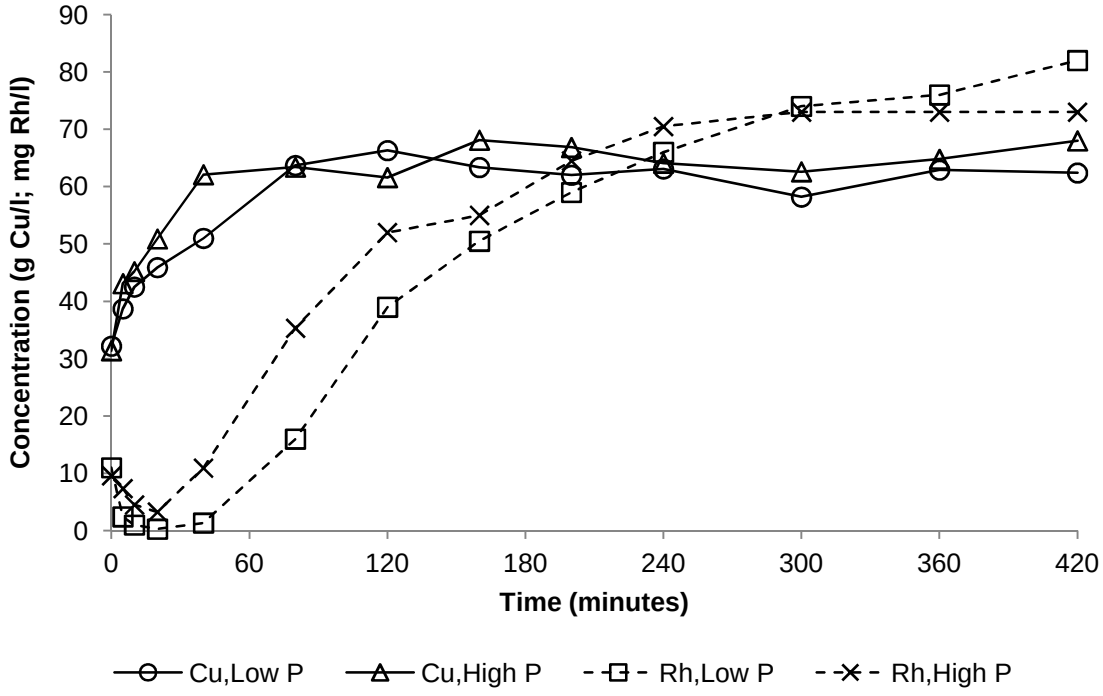

Figure 4.31. Concentration of Cu and Rh in solution as a function of leaching time and pressure at 130°C, an initial acid concentration of 140 g/ℓ, and a solids content of 80 g/ℓ (High P: 9 bar; Low P: 7 bar).

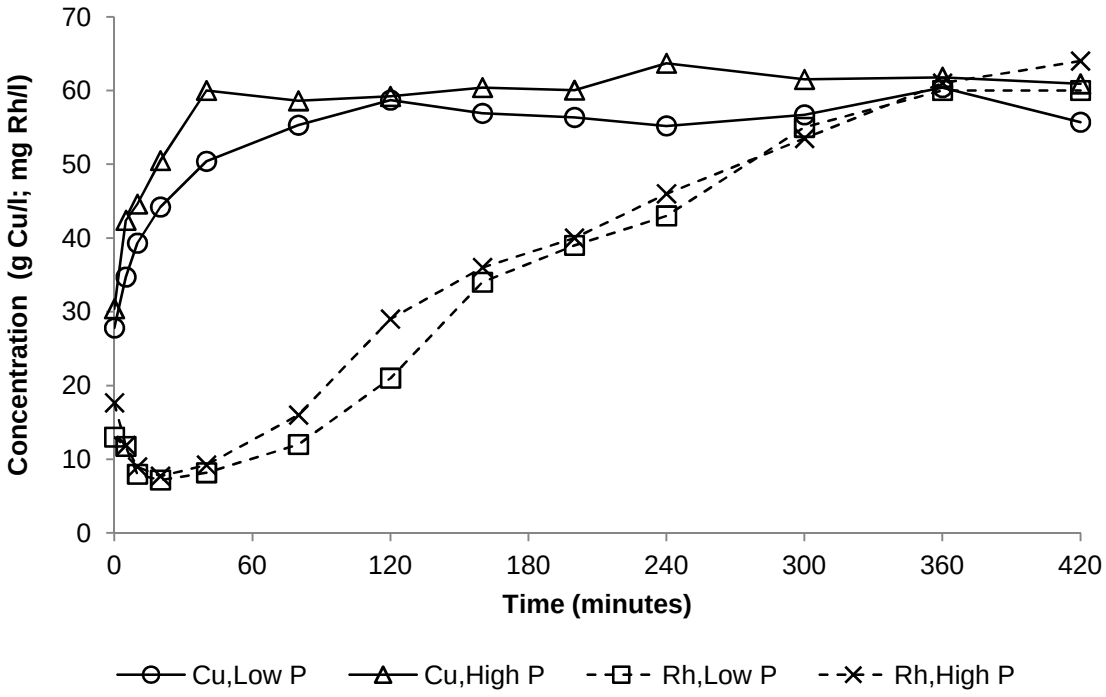

Figure 4.32. Concentration of Cu and Rh in solution as a function of leaching time and pressure at 116°C, an initial acid concentration of 165 g/ℓ, and a solids content of 80 g/ℓ (High P: 9 bar; Low P: 7 bar).

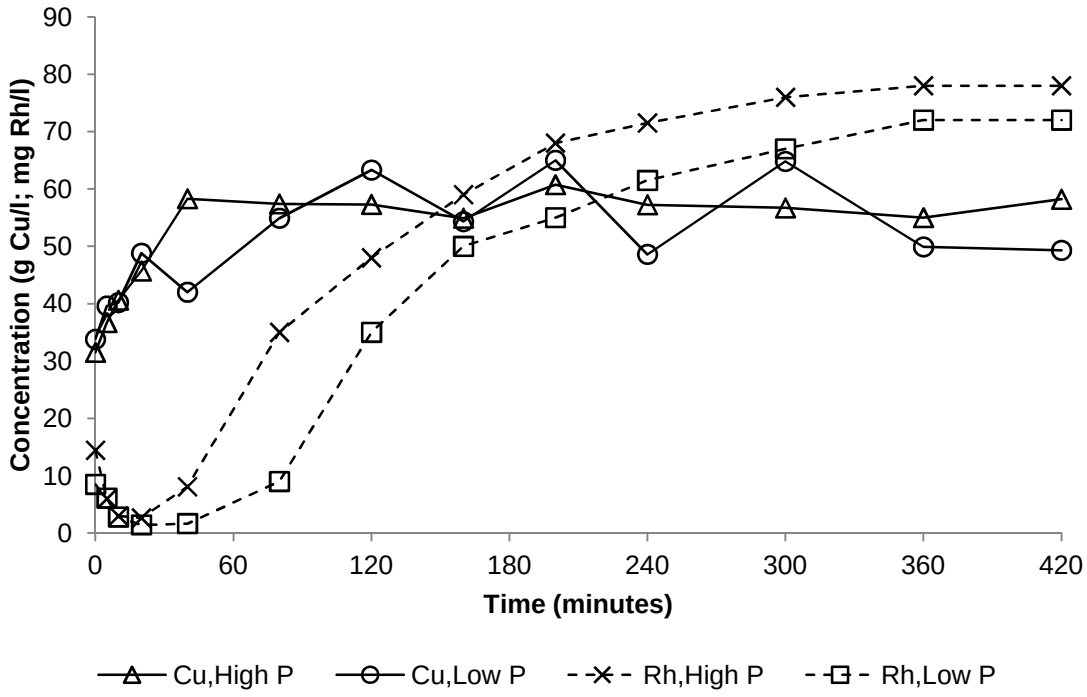

Figure 4.33. Concentration of Cu and Rh in solution as a function of leaching time and pressure at 130°C, an initial acid concentration of 165 g/ℓ, and a solids content of 80 g/ℓ (High P: 9 bar; Low P: 7 bar).

Although no reliable copper analyses could be obtained for the tests performed with the higher solid to liquid ratio, the results for the rhodium illustrate the same behaviour as for low solids content tests: the precipitation time during the initial leaching stages was longer for the tests performed at the lower pressure, but the leaching rate was not affected by the change in pressure. Unlike the low solids content tests, however, this trend was also observed for the test performed at 116°C with an initial acid concentration of 140 g/ℓ, indicating that oxygen availability was also the rate determining factor at these experimental conditions.

4.3.2.4 Effect of initial acid concentration on metal dissolution

The effect that the initial acid concentration had on the leaching behaviour of copper and rhodium at various temperature and pressure conditions are shown in Figure 4.34 to Figure 4.37. The rate of copper dissolution in all the tests was significantly faster than at the conditions investigated in the first experimental design, and this could be attributed to the fact that the initial acid concentration in the second experimental design was 3.9 to 6.3 times larger than in the first experimental design.

For the range of initial acid concentrations investigated in the second experimental design, the tests with the lower initial acid concentration yielded a higher maximum copper dissolution for the low initial acid conditions (88.7% on average) than for the high initial acid conditions (75.3% on average). Although the copper leaching rate increased from the first experimental design to the second experimental design due to the higher initial acid concentration, the increase in initial acid concentration from 140 g/ℓ to 165 g/ℓ for the second experimental design had a negative effect on the copper leaching behaviour. It could thus be concluded that an optimum initial acid concentration existed where the rate and extent of copper leaching were a maximum. This is in agreement with the findings of Ruiz *et al.* (2003), as discussed in Section 2.4.3, who attributed the existence of an optimum acid concentration to the effect of acid concentration on oxygen solubility. For the range of conditions investigated, the decrease in oxygen solubility as a result of the increased acid concentration was more significant than the direct effect of the higher acid concentration on the leaching kinetics. The rhodium leaching behaviour was not affected noticeably by the change in the initial acid concentration.

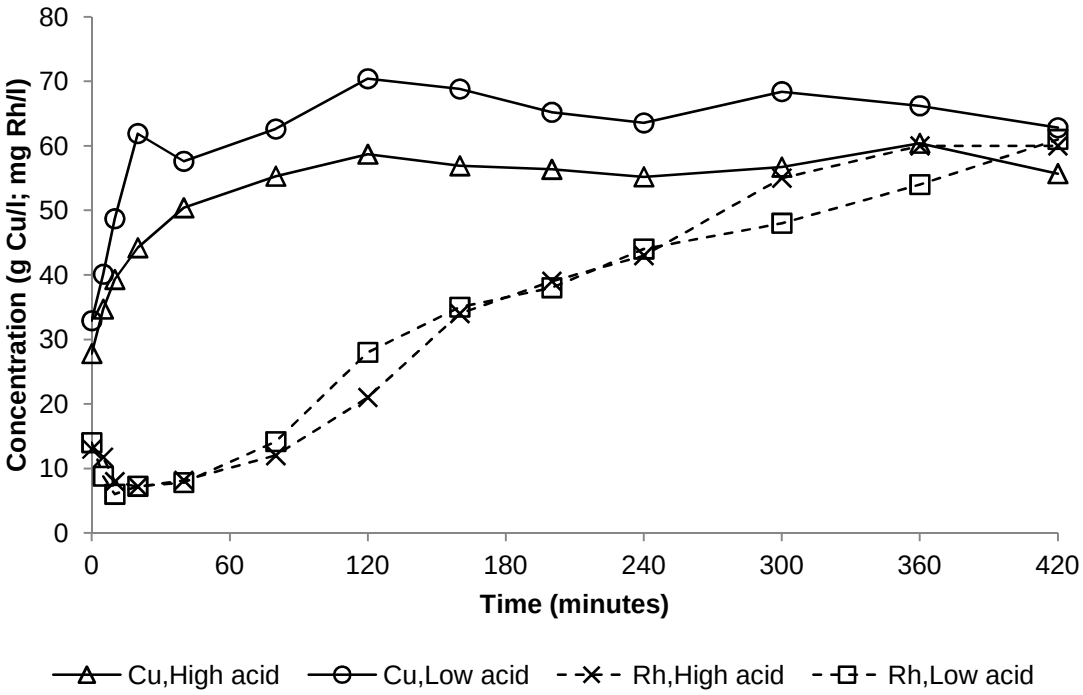

Figure 4.34. Concentration of Cu and Rh in solution as a function of leaching time and initial acid concentration at 116°C, 7 bar, and a solids content of 80 g/ℓ (High Acid: 165 g/ℓ; Low Acid: 140 g/ℓ).

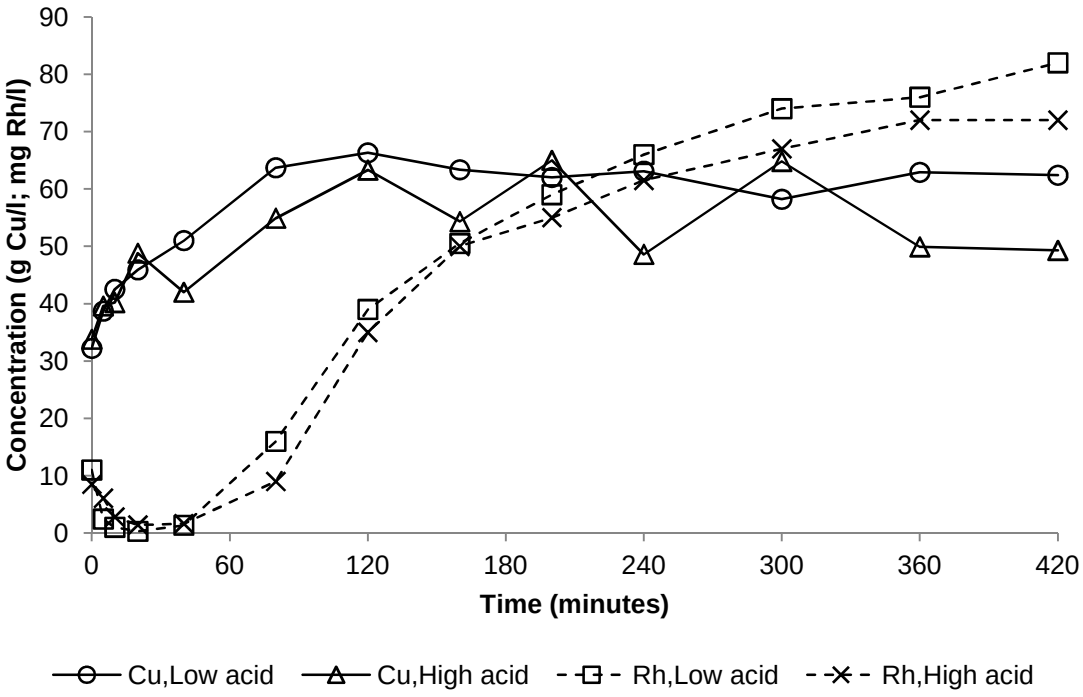

Figure 4.35. Concentration of Cu and Rh in solution as a function of leaching time and initial acid concentration at 130°C, 7 bar, and a solids content of 80 g/ℓ (High Acid: 165 g/ℓ; Low Acid: 140 g/ℓ).

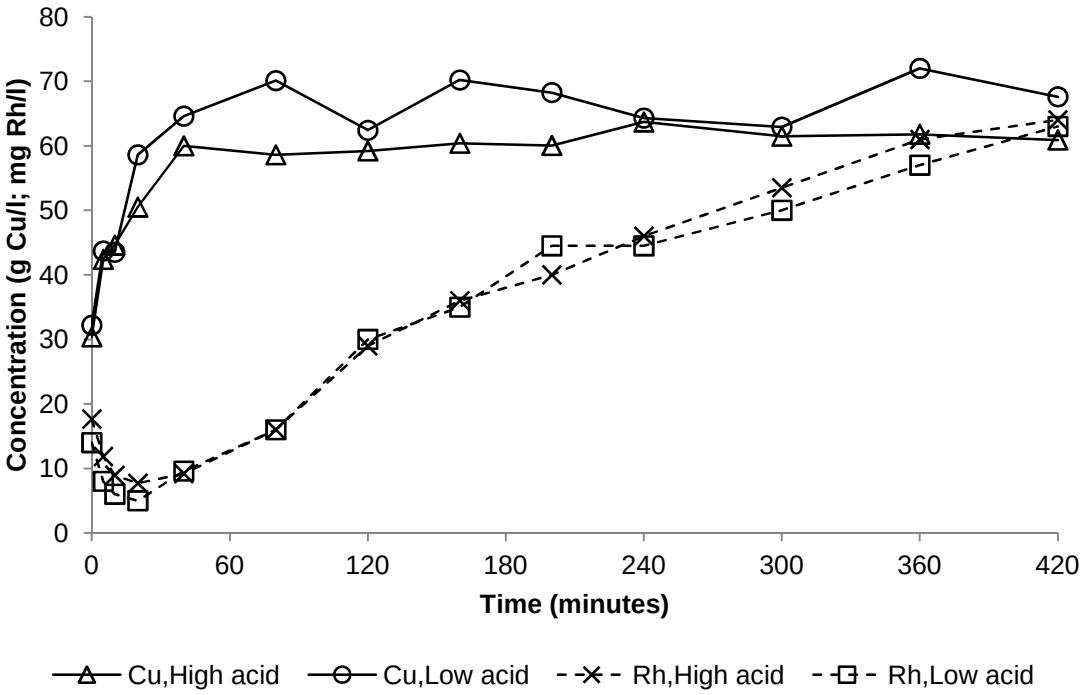

Figure 4.36. Concentration of Cu and Rh in solution as a function of leaching time and initial acid concentration at 116°C, 9 bar, and a solids content of 80 g/ℓ (High Acid: 165 g/ℓ; Low Acid: 140 g/ℓ).

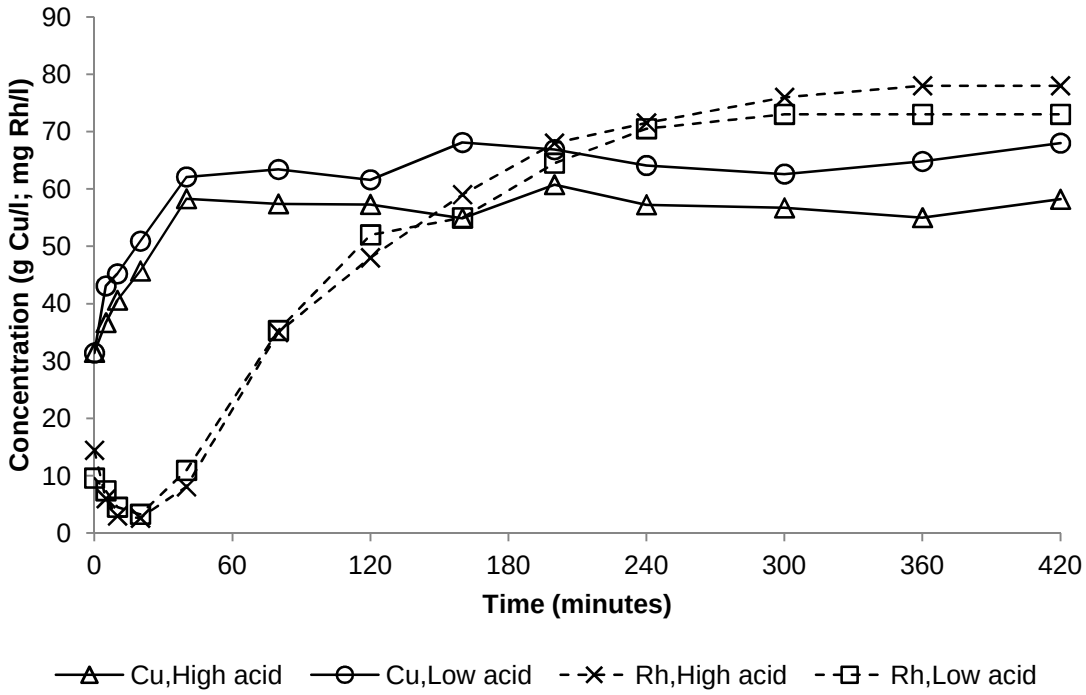

Figure 4.37. Concentration of Cu and Rh in solution as a function of leaching time and initial acid concentration at 130°C, 9 bar, and a solids content of 80 g/ℓ (High Acid: 165 g/ℓ; Low Acid: 140 g/ℓ).

4.3.3 Analysis of variance

Analysis of variance was performed in order to quantify the effects that the leaching temperature, pressure, initial acid concentration, and solids content had on the leaching behaviour of the system, and to identify interactions between these process variables in order to validate the qualitative observations discussed in Section 4.3.2. The response variable for the analysis performed on the copper behaviour was the maximum percentage copper dissolution achieved over the seven hour leaching period (the copper dissolution values calculated for the high solids content tests were omitted from the analysis). The percentage metal dissolution achieved after seven hours of leaching was used as the response variable for the other precious metals (Rh, Ru, and Ir). The *p*-values obtained for the various process variables as well as the second-order interactions when considering the different response variables are summarised in Table 4.6. In the case of copper leaching, the initial acid concentration was the process variable with the statistically most significant effect on the copper dissolution, as indicated by the relatively small p-value for this main effect compared with the p-values calculated for the remainder of the main and interaction effects. This is in agreement with the qualitative observations discussed in Section 4.3.2, where it was noted that the initial acid concentration was the only process variable with a noticeable effect on the extent of copper leaching. The interaction between the pressure and the initial acid concentration was the most significant interaction effect; the second-order interaction effects were, however, not considered to be statistically significant, as can be seen from the relatively large p-values calculated for the interaction effects compared to the main effects. These observations are also illustrated graphically in the main effects plot (Figure 4.38(a)) and the interaction plots (Figure 4.39) for Cu dissolution.

Table 4.6. Summary of the p-values calculated for the main effects and second-order interaction effects of process variables on the different response variables.

	p-value			
	Cu	**Rh**	**Ru**	**Ir**
Temperature (T)	0.169	<0.001	0.003	<0.001
Pressure (P)	0.424	0.022	0.359	0.306
Acid (A)	0.094	0.575	0.858	0.872
Solids content (S)	-	0.278	0.754	0.878
TP	0.691	0.943	0.514	0.565
TA	0.883	0.070	0.596	0.894
TS	-	0.294	0.829	0.364
AP	0.357	0.675	0.671	0.478
SP	-	0.008	0.591	0.387
SA	-	0.035	0.281	0.227

Temperature was the only process variable that had a statistically significant main effect on the leaching of all the OPMs. This further confirmed that the temperature was the process variable with the largest effect on the OPM dissolution behaviour, as discussed in Section 4.3.2. With the exception of the effect of interactions between pressure and slurry solids content and between the initial acid concentration and slurry solids content on Rh dissolution, none of the second-order interactions were found to have a significant effect on the OPM dissolution behaviour. The main effects plot and the interaction plots for Rh dissolution illustrate these observations regarding the main effects and the interaction effects in Figure 4.38(b) and Figure 4.40 respectively.

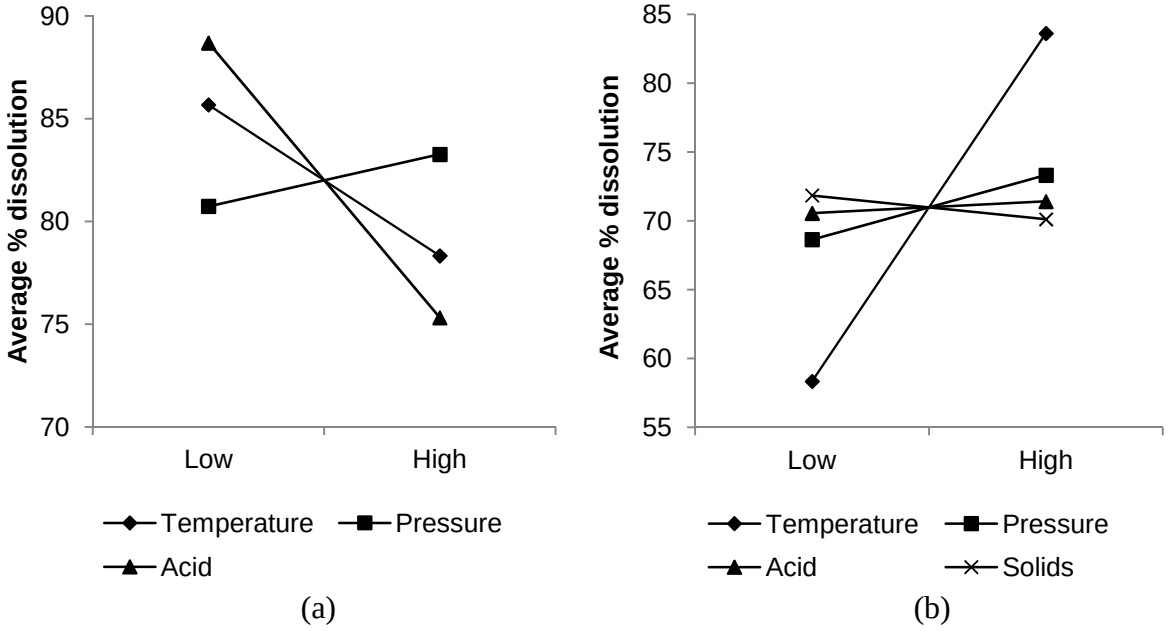

Figure 4.38. Main effects plots showing the effects that changes in the different process variables have on the average percentage dissolution of (a) Cu and (b) Rh.

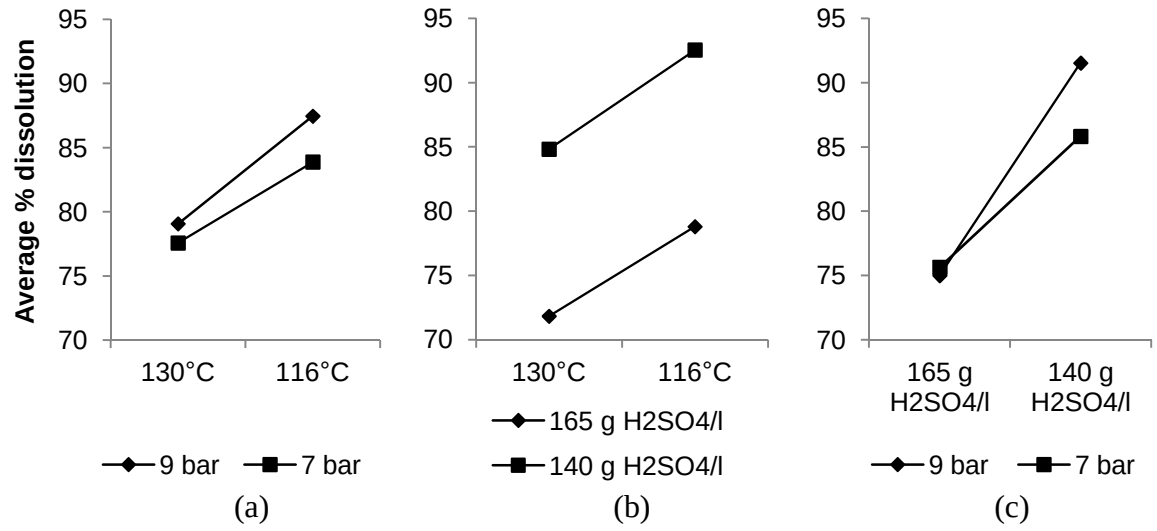

Figure 4.39. Interaction plots showing the effects of interactions between (a) temperature and pressure, (b) temperature and acid concentration, and (c) acid concentration and pressure on the percentage copper dissolution.

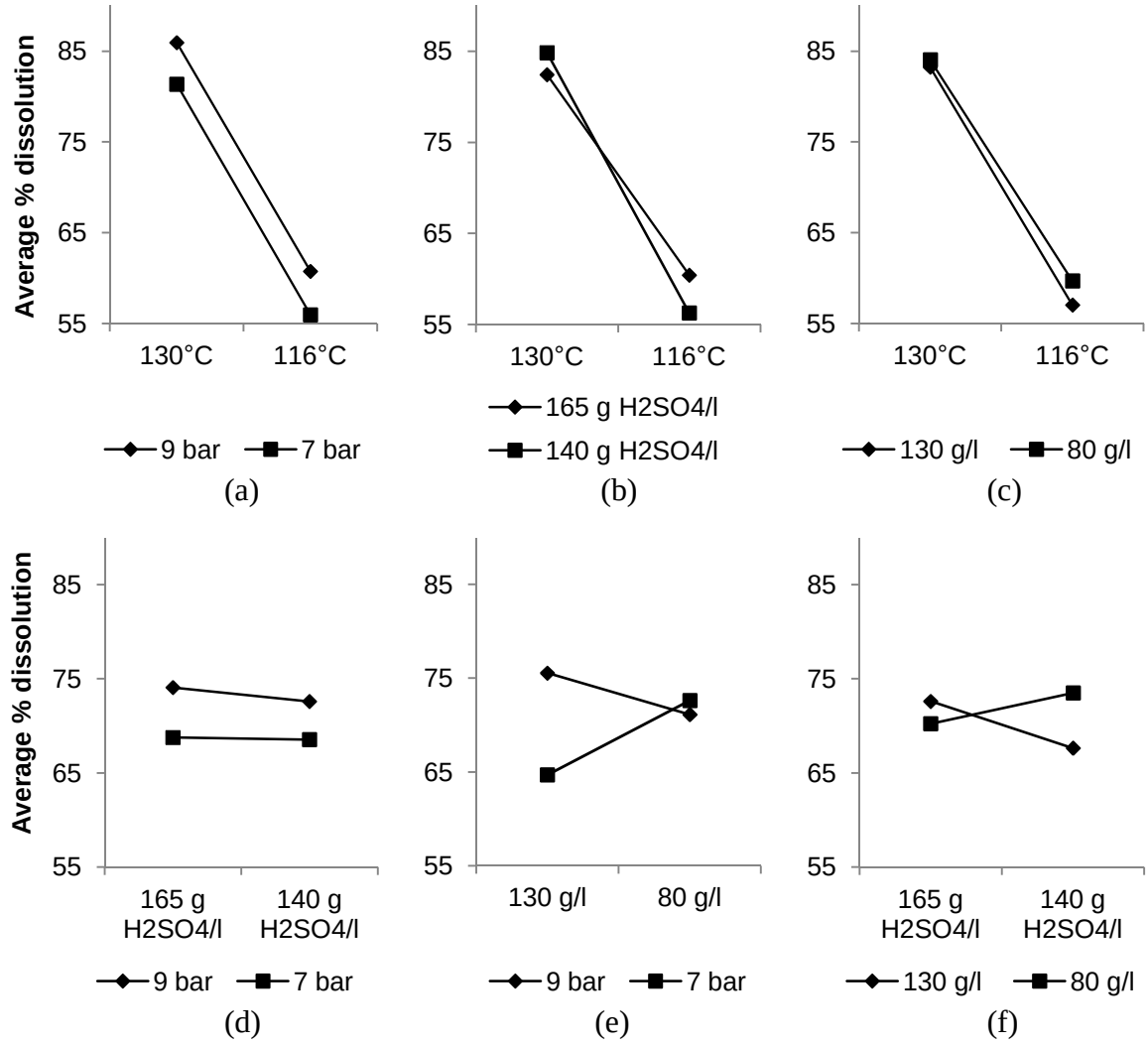

Figure 4.40. Interaction plots showing the effects of interactions between (a) temperature and pressure, (b) temperature and acid concentration, (c) temperature and solids content, (d) pressure and acid concentration, (e) pressure and solids content, and (f) acid concentration and solids content on the percentage rhodium dissolution.

4.3.4 Comparison of the leaching behaviour of the PGMs

The effects that the various process variables had on the leaching behaviour of rhodium were discussed in Section 4.3.2. Similar effects were, however, also observed for the remainder of the OPMs. The percentage metal dissolution achieved after seven hours of leaching under the various sets of leaching conditions are illustrated in Figure 4.41. In general, similar trends were observed for Rh, Ru, and Ir, indicating that changing the operating conditions between the respective tests had similar effects on the extent of leaching of these three metals. This is in agreement with the results obtained with the regression analyses, which identified the same process variable to have a statistically significant effect on the leaching extent for all the OPMs.

It was noted in Section 4.2.2 that the extent of Pd leaching was comparable to that of the OPMs under the conditions investigated in the first experimental design, and was hence identified for further investigation as it could potentially contribute noticeably to the total PGMs in solution. For the range of conditions investigated during the second experimental design, the percentage Pd dissolution achieved after seven hours of leaching was lower than that of Rh, Ru, and Ir for all the tests, as shown in Figure 4.41. On average, 40.3% Pd dissolution was achieved compared to 71.0% for Rh, 87.8% for Ru, and 64.4% for Ir.

The correlation between the extent of Pd leaching and that of the other precious metals (Rh, Ru, and Ir) for the different sets of operating conditions was furthermore not clear (Figure 4.41). A regression analysis utilising the percentage Pd dissolution after seven hours as the response variable indicated that pressure (*p*-value of 4.32×10^{-3}) and temperature (*p*-value of 2.72×10^{-2}) were the process variables with a statistically significant effect on the Pd leaching behaviour if a significance level of 0.05 was chosen. For a significance level of 0.01, the leaching pressure was the only statistically significant process variable. The effect of pressure on the extent of Pd leaching was therefore more significant than for the OPMs, for which temperature was the only process variable with a statistically significant effect, as discussed in Section 4.3.3.

In addition to comparing the extent of metal leaching achieved after seven hours of leaching, the effect of changes in the process variables on the relative leaching kinetics also had to be considered. The similar leaching behaviour of the other precious metals at different sets of process conditions is illustrated for test 2i and test 2m, as an example, in Figure 4.42. During test 2m (130°C, 7 bar, 165 g H_2SO_4/ℓ, and a solids content of 130 g/ℓ), Ru, Rh, and Ir exhibited faster precipitation kinetics during the initial stages of the leach, a longer precipitation period, faster leaching kinetics, and a greater extent of leaching after seven hours than during test 2i (116°C, 9 bar, 140 g H_2SO_4/ℓ, and a solids content of 130 g/ℓ). Similar comparisons can be made for the remainder of the tests; in general, it can therefore be said that the discussion regarding the effects of various process variables on the leaching behaviour of rhodium (Section 4.3.2) is also applicable to ruthenium and iridium.

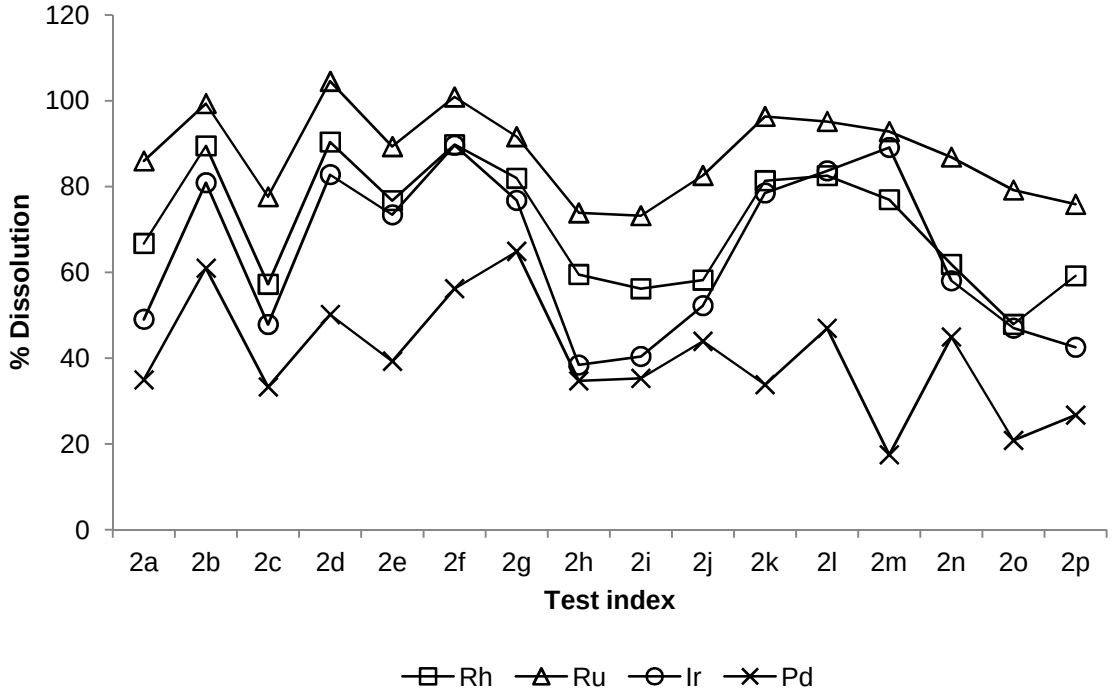

Figure 4.41. Comparison of the dissolution of Rh, Ru, Ir, and Pd after seven hours of leaching during the second set of leaching experiments performed on the first stage leach residue.

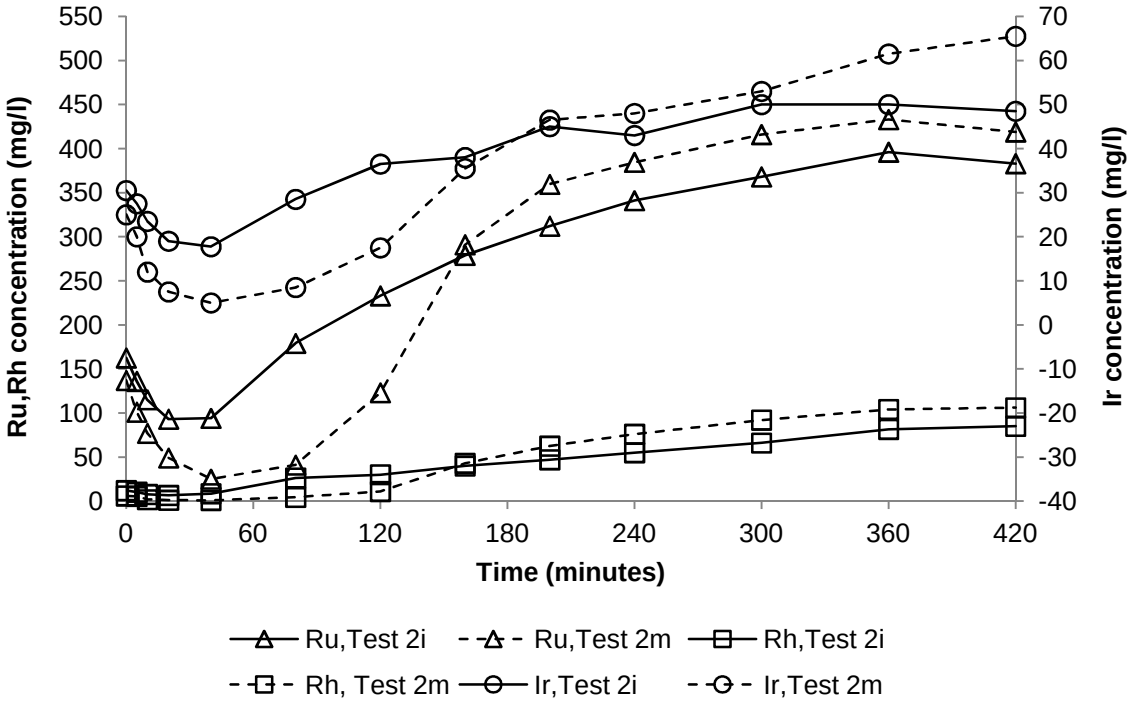

Figure 4.42. Concentration of Rh, Ru, and Ir in solution as a function of leaching time for test 2i and test 2m.

It has already been established that, under the conditions investigated, the percentage Pd leaching achieved after seven hours of leaching was lower than that of the other precious metals. Comparing the leaching kinetics of Pd to the leaching kinetics of Rh (representing OPMs in general), several differences were observed. Figure 4.43 illustrates the relative leaching behaviour of these two components for a number of tests (Figure 4.44 shows the data during the first 80 minutes of the respective tests in more detail). The first difference was the fact that no noticeable precipitation of Pd occurred during the initial leaching stages. Secondly, for any specific set of operating conditions, the leaching of Pd only started to proceed at a noticeable rate at a later stage compared to Rh. For the tests shown in Figure 4.43, Pd leaching only started approximately 80-120 minutes after Rh leaching had done so. Given the plant observation that Pd does not leach to a significant extent (discussed in Section 4.2.2), that the Pd leaching has been shown to proceed from a later point in time than the other precious metals, and taking into account that the Pd concentration in the spent electrolyte is typically an order of magnitude smaller that than of the other precious metals (Table 3.1), the leaching reactions of Pd was not be considered in the remainder of the study.

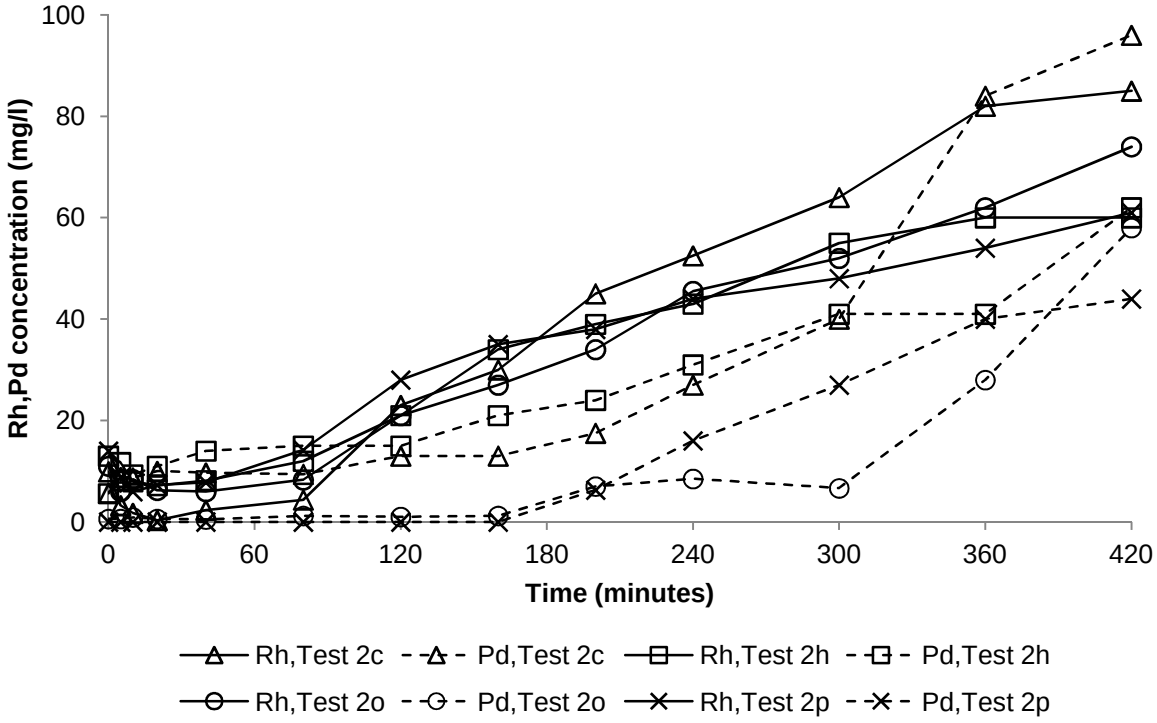

Figure 4.43. Concentration of Rh and Pd in solution as a function of leaching time for tests 2c, 2h, 2o, and 2p.

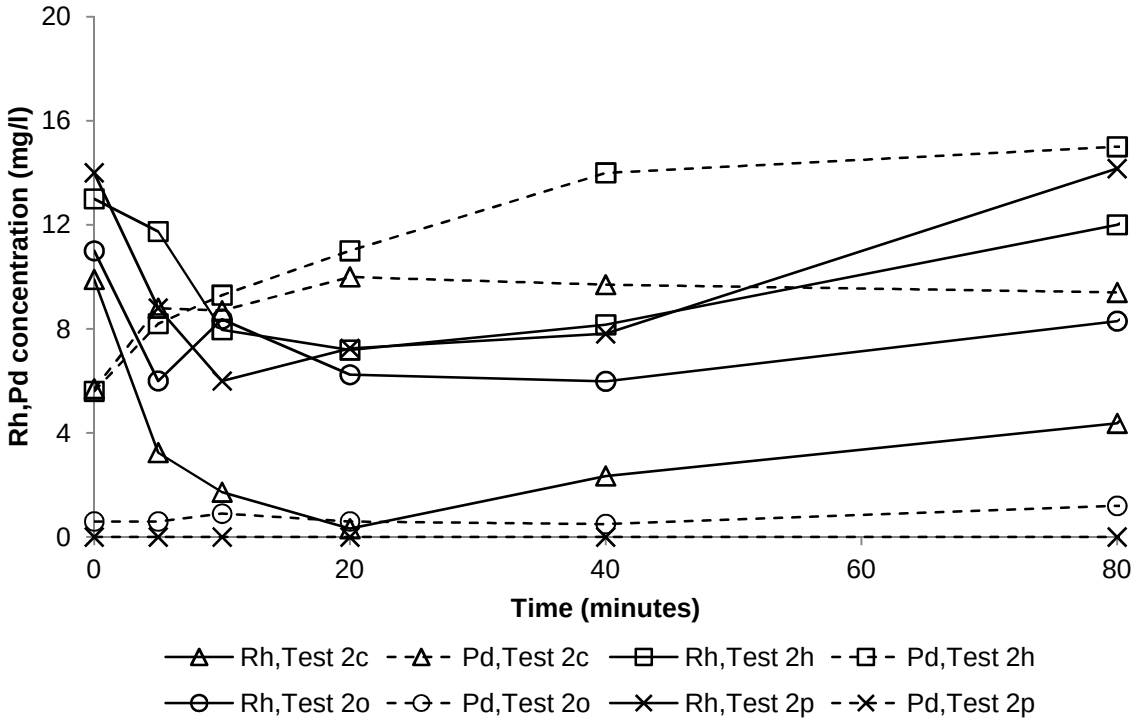

Figure 4.44. Concentration of Rh and Pd in solution as a function of leaching time for the first 80 minutes of tests 2c, 2h, 2o, and 2p.

5 LEACHING REACTIONS AND KINETICS

5.1 Mineralogy of the first stage leach residue

The PGM containing matte entering the hydrometallurgical circuit from the Peirce Smith converter contains base metals primarily as heazlewoodite (Ni_3S_2), chalcocite (Cu_2S), and Cu-Ni alloy, while inert phases such as trevorite ($NiFe_2O_4$) and magnetite (Fe_3O_4) are also present (Van Schalkwyk *et al.*, 2011). The metallic phases are typically the first to dissolve (Lamya, 2007). Leaching of heazlewoodite by copper cementation could lead to the formation of millerite (NiS) (reaction 2.3 and reaction 2.4), while the oxidative conditions in the first two tanks of the atmospheric leaching stage could also contribute to millerite formation (reaction 2.11). Millerite can undergo further leaching to form either polydymite (Ni_3S_4) according to reaction 2.25, or dissolve completely by cementation with copper, yielding covellite (CuS), as shown in reaction 2.26.

Any copper leaching that occurs in the atmospheric leaching stage is likely to proceed according to reaction 2.17 and reactions 2.20 to 2.22, with the formation of digenite ($Cu_{1.8}S$) as an intermediate leaching product. Apart from the covellite formation as a result of cementation reactions with nickel sulphides (reaction 2.26 and reaction 2.30), it is also formed during leaching of digenite, according to reaction 2.27. Although Steenekamp and Dunn (1999) presented a leaching reaction for a copper hydrolysis product, Van Schalkwyk (2011) did report that copper hydrolysis will only occur at relatively high pH values of between 4.5 and 6, which is higher than the typical operating conditions of the first stage leach. This is in agreement with the report by Lamya (2007), which indicated copper oxides and basic copper sulphates ($Cu_3(OH)SO_4$) to be stable only at pH values larger than four.

Based on the above discussion, the primary phases present in the first stage leach residue being fed to the second stage pressure leach are expected to be millerite and polydymite in the case of nickel sulphides and digenite and covellite in the case of the copper sulphides. This is in agreement with the findings of Van Schalkwyk (2011), who investigated the effect of various atmospheric first stage leach process variables on the leaching behaviour of Peirce Smith converter matte supplied by Lonmin. The dominance of these phases in the first stage leach residue supplied by Lonmin was confirmed by XRD analysis. The results are presented in Appendix C.

Considering the discussion of the iron behaviour during the first stage leach in Section 2.2.1, the majority of the iron that can be leached will be dissolved in the first stage leach. Depending on the conditions in the first stage leach, however, iron hydrolysis might result in the precipitation of iron in the form of $Fe(OH)_3$ or $Fe(OH)SO_4$ (reaction 2.15 and reaction 2.16). No distinction could be made between these two phases during the analysis of the first stage leach residue supplied by Lonmin, but Steenekamp and Dunn (1999) did report that the leachable iron typically enters the second stage leach as $Fe(OH)SO_4$.

The phases described above are the primary phases of the respective metals. Minor phases, such as telluride and sellenide compounds, were not taken into consideration in the analysis, and the leaching behaviour of these minor elements was not evaluated.

5.2 Leaching reactions

The leaching of base metals from PGM-containing matte under various leaching conditions in base metal refinery processes has been investigated in numerous studies (Van Schalkwyk *et al.*, 2011; Lamya, 2007; Lamya and Lorenzen, 2006; Lamya, 2005; Provis, 2003; Steenekamp and Dunn, 1999; Fugleberg *et al.*, 1995; Hofirek and Nofal, 1995; Rademan, 1995; Hofirek and Kerfoot, 1992), as discussed in Section 2.2. Based on these studies, the base metal leaching reactions that are dominant in the second stage pressure leach were identified.

5.2.1 Nickel

Since the second stage pressure leach is performed under oxidising conditions, leaching of millerite proceeds according to reaction 2.25 and reaction 2.33 rather than reaction 2.7. Furthermore, since no reduction in the copper concentration in solution was observed while nickel leaching proceeded during the leaching of the first stage leach residue, it can be concluded that no overall copper precipitation occurred. Therefore, in order to simplify the reaction scheme and reduce the number of kinetic constants that had to be determined, reactions involving nickel leaching by cementation with copper (reaction 2.26 and reaction 2.30) were not considered; leaching of polydymite occurs according to reaction 2.29. The reactions that were considered during the determination of reaction kinetic constants in order to account for the dissolution of nickel are summarised as reaction one to three in Table 5.3 for clarity. The reaction numbers in the first column are assigned to allow clear numbering and explanation during the discussion of the determination of the kinetic constants.

5.2.2 Copper

Leaching of digenite could proceed by either reaction 2.27 or reaction 2.28, or both. Reaction 2.28 was proposed by Rademan *et al.* (1999) because of the observation that iron acts as an electron carrier in base metal leaching processes. The high pressure leaching tests were performed at highly oxidative conditions with a high initial acid concentration. If the reaction whereby Fe^{2+} is oxidised to Fe^{3+} was considered together with reaction 2.28, it would yield reaction 2.27 as the overall leaching reaction. It was therefore assumed that reaction 2.27 represents the dissolution of the digenite. Given the oxidative conditions at which the leach is performed, the sulphides are most likely to be oxidised to sulphates without the formation of elemental sulphur. Milbourne *et al.* (2003) furthermore indicated that the formation of elemental sulphur will prevent PGM leaching; in the tests performed, the OPMs leached relatively fast once the OPM precipitation reactions had been completed, which confirmed that it was unlikely that elemental sulphur was present. Grewal *et al.* (1992) also indicated that the formation of elemental sulphur during the leaching of covellite very rarely occurs under typical operating conditions. As such, the primary covellite leaching reaction is reaction 2.35. In summary, the two reactions considered to account for copper sulphide leaching from the first stage leach residue are listed as reaction 4 and reaction 5 in Table 5.3. Reactions proposed to take place between copper sulphides and dissolved PGMs are discussed in Section 5.2.4.

5.2.3 Iron

As discussed, the leachable iron in the first stage leach residue is in the form of the hydrolysis product, $Fe(OH)SO_4$, and leaching occurs according to reaction 2.32, shown as reaction 6 in Table 5.3.

5.2.4 Other precious metals

As was discussed in Section 5.2.2, elemental sulphur was not considered to form as a reaction product. Lamya (2007) furthermore reported that hydrogen and hydrogen sulphide formation can be prevented by maintaining sufficient oxygen in the leaching system. Given the fact that oxygen is sparged into the second stage pressure leach continuously, the formation of hydrogen and hydrogen sulphide is unlikely, and were hence not considered as reaction products.

The OPMs in solution were all considered to be present in the +3 oxidation state, based on the discussion of OPM complexes and oxidation states in Section 2.3. OPM solid compounds that

were considered include the sulphides, oxides, and metals. The reactions describing the behaviour of the OPMs in the leach solution can be divided into those accounting for the precipitation of OPMs during the initial leaching stages and those accounting for the dissolution of the metals during the latter stages of the process.

5.2.4.1 Precipitation reactions

Milbourne *et al.* (2003) reported that hydrated ferric iron precipitates are reactive towards dissolved PGMs. For this particular study, it was observed that the iron leaching during the initial stages of the leaching process proceeded at a much faster rate than the OPM precipitation. In addition, there was no apparent correlation between iron leaching period and the period over which PGM precipitation occurred. The iron concentration in solution is shown as a function of time for the various combinations of operating conditions in Figure 4.22 and Figure 4.23. In the light of the above, it was concluded that reactions between the iron hydroxide precipitate and dissolved OPMs did not contribute significantly to OPM precipitation, and that iron leaching proceeded primarily according to reaction 2.32.

As discussed in Section 2.3, reverse hydrolysis is likely to occur given the relatively high acid concentration in the second stage pressure leach (Renner, 1992). As such, precipitation by hydrolysis was not considered as feasible reactions to include in the proposed reaction scheme.

Given the above considerations, precipitation of the OPMs during the initial stages of the leaching process had to proceed primarily via precipitation reactions similar to the cementation and metathesis reactions by which copper precipitates in the first stage leach. In the formulation of these overall cationic exchange reactions, all base metal sulphides were assumed to dissolve directly without the formation of intermediate base metal sulphide phases. A summary of all the reactions considered is given in Table 5.1, together with the corresponding Gibbs free energy change. The Gibbs free energy changes for the respective reactions were calculated at 130°C, the typical operating temperature of the second stage pressure leach, using HSC Chemistry® version 6.12. Where thermodynamic data for specific species had not been included in the HSC Chemistry® main database, thermodynamic data collected from literature were added to the database. Thermodynamic data were added to the HSC Chemistry® database for Ru^{3+} (Sassani and Shock, 1998), RhO_2 (Jacob and Prusty, 2010), and Cu_9S_5 (Etienne, 1970; Grønvold *et al.*, 1987). Data for Rh^{3+} and Ru^{3+} complexes in aqueous solutions are available in literature (Sassani and Shock, 1998). However, because

the complexes present in solution and the extent to which different complexes take part in the reactions were not determined, the proposed reactions were written in terms of the ion forms of the respective OPMs. The ion forms were subsequently used to calculate the Gibbs free energy changes for reactions involving rhodium and ruthenium. According to McGeorge *et al.* (2009), complexes of these ions would be more stable than the ions. The differences in the Gibbs free energy changes of the respective reactions would however remain the same. No appropriate data could be found for Ir^{3+} species, and the Gibbs free energy changes for reactions involving iridium could therefore not be calculated.

Table 5.1. Reactions considered for OPM precipitation, together with the corresponding Gibbs free energy (kJ/mol OPM^{3+}).

Rhodium reactions		**ΔG° (kJ/mol)**
$4Rh^{3+} + Cu_9S_5 + 8H^+ + SO_4^{2-} \rightarrow 2Rh_2S_3 + 9Cu^{2+} + 4H_2O$	[5.1]	-186.6
$8Rh^{3+} + 3Cu_9S_5 + 30O_2 \rightarrow 8Rh + 27Cu^{2+} + 15SO_4^{2-}$	[5.2]	-1256.7
$8Rh^{3+} + 3Cu_9S_5 + 36O_2 \rightarrow 4Rh_2O_3 + 27Cu^{2+} + 15SO_4^{2-}$	[5.3]	-1396.5
$8Rh^{3+} + 3Cu_9S_5 + 38O_2 \rightarrow 8RhO_2 + 27Cu^{2+} + 15SO_4^{2-}$	[5.4]	-1444.7
$2Rh^{3+} + 3CuS \rightarrow Rh_2S_3 + 3Cu^{2+}$	[5.5]	-168.5
$8Rh^{3+} + 3CuS + 12H_2O \rightarrow 8Rh + 3Cu^{2+} + 24H^+ + 3SO_4^{2-}$	[5.6]	-105.8
$2Rh^{3+} + CuS + 3H_2O + 2O_2 \rightarrow Rh_2O_3 + Cu^{2+} + 6H^+ + SO_4^{2-}$	[5.7]	-320.6
$2Rh^{3+} + CuS + 3H_2O + 2.5O_2 \rightarrow 2RhO_2 + Cu^{2+} + 6H^+ + SO_4^{2-}$	[5.8]	-368.7
$2Rh^{3+} + 3NiS \rightarrow Rh_2S_3 + 3Ni^{2+}$	[5.9]	-288.2
$8Rh^{3+} + 3NiS + 12H_2O \rightarrow 8Rh + 3Ni^{2+} + 24H^+ + 3SO_4^{2-}$	[5.10]	-135.7
$2Rh^{3+} + NiS + 3H_2O + 2O_2 \rightarrow Rh_2O_3 + Ni^{2+} + 6H^+ + SO_4^{2-}$	[5.11]	-360.5
$2Rh^{3+} + NiS + 3H_2O + 2.5O_2 \rightarrow 2RhO_2 + Ni^{2+} + 6H^+ + SO_4^{2-}$	[5.12]	-408.6
$10Rh^{3+} + 4Ni_3S_4 + 4H_2O \rightarrow 5Rh_2S_3 + 12Ni^{2+} + 8H^+ + SO_4^{2-}$	[5.13]	-266.3
$10Rh^{3+} + Ni_3S_4 + 16H_2O \rightarrow 10Rh + 3Ni^{2+} + 32H^+ + 4SO_4^{2-}$	[5.14]	-130.2
$2Rh^{3+} + Ni_3S_4 + 4H_2O + 7.5O_2 \rightarrow Rh_2O_3 + 3Ni^{2+} + 8H^+ + 4SO_4^{2-}$	[5.15]	-1267.0
$2Rh^{3+} + Ni_3S_4 + 4H_2O + 8O_2 \rightarrow 2RhO_2 + 3Ni^{2+} + 8H^+ + 4SO_4^{2-}$	[5.16]	-1315.2
Ruthenium reactions		**ΔG° (kJ/mol)**
$16Ru^{3+} + 5Cu_9S_5 + 56H^+ + 7SO_4^{2-} \rightarrow 16RuS_2 + 45Cu^{2+} + 28H_2O$	[5.17]	-198.6
$8Ru^{3+} + 3Cu_9S_5 + 30O_2 \rightarrow 8Ru + 27Cu^{2+} + 15SO_4^{2-}$	[5.18]	-1210.0
$8Ru^{3+} + 3Cu_9S_5 + 38O_2 \rightarrow 8RuO_2 + 27Cu^{2+} + 15SO_4^{2-}$	[5.19]	-1464.7
$8Ru^{3+} + 15CuS + 8H^+ + SO_4^{2-} \rightarrow 8RuS_2 + 15Cu^{2+} + 4H_2O$	[5.20]	-176.0
$8Ru^{3+} + 3CuS + 12H_2O \rightarrow 8Ru + 3Cu^{2+} + 24H^+ + 3SO_4^{2-}$	[5.21]	-59.1
$2Ru^{3+} + CuS + 3H_2O + 2.5O_2 \rightarrow 2RuO_2 + Cu^{2+} + 6H^+ + SO_4^{2-}$	[5.22]	-388.7
$8Ru^{3+} + 15NiS + 8H^+ + SO_4^{2-} \rightarrow 8RuS_2 + 15Ni^{2+} + 4H_2O$	[5.23]	-325.6
$8Ru^{3+} + 3NiS + 12H_2O \rightarrow 8Ru + 3Ni^{2+} + 24H^+ + 3SO_4^{2-}$	[5.24]	-89.0
$2Ru^{3+} + NiS + 3H_2O + 2.5O_2 \rightarrow 2RuO_2 + Ni^{2+} + 6H^+ + SO_4^{2-}$	[5.25]	-428.6
$2Ru^{3+} + Ni_3S_4 \rightarrow 2RuS_2 + 3Ni^{2+}$	[5.26]	-298.3
$10Ru^{3+} + Ni_3S_4 + 16H_2O \rightarrow 10Ru + 3Ni^{2+} + 32H^+ + 4SO_4^{2-}$	[5.27]	-83.5
$2Ru^{3+} + Ni_3S_4 + 4H_2O + 8O_2 \rightarrow 2RuO_2 + 3Ni^{2+} + 8H^+ + 4SO_4^{2-}$	[5.28]	-1335.1

Iridium reactions	
$4Ir^{3+} + Cu_9S_5 + 8H^+ + SO_4^{2-} \rightarrow 2Ir_2S_3 + 9Cu^{2+} + 4H_2O$	[5.29]
$16Ir^{3+} + 5Cu_9S_5 + 56H^+ + 7SO_4^{2-} \rightarrow 16IrS_2 + 45Cu^{2+} + 28H_2O$	[5.30]
$8Ir^{3+} + 3Cu_9S_5 + 30O_2 \rightarrow 8Ir + 27Cu^{2+} + 15SO_4^{2-}$	[5.31]
$8Ir^{3+} + 3Cu_9S_5 + 36O_2 \rightarrow 4Ir_2O_3 + 27Cu^{2+} + 15SO_4^{2-}$	[5.32]
$8Ir^{3+} + 3Cu_9S_5 + 38O_2 \rightarrow 8IrO_2 + 27Cu^{2+} + 15SO_4^{2-}$	[5.33]
$2Ir^{3+} + 3CuS \rightarrow Ir_2S_3 + 3Cu^{2+}$	[5.34]
$8Ir^{3+} + 15CuS + 8H^+ + SO_4^{2-} \rightarrow 8IrS_2 + 15Cu^{2+} + 4H_2O$	[5.35]
$8Ir^{3+} + 3CuS + 12H_2O \rightarrow 8Ir + 3Cu^{2+} + 24H^+ + 3SO_4^{2-}$	[5.36]
$2Ir^{3+} + CuS + 3H_2O + 2O_2 \rightarrow Ir_2O_3 + Cu^{2+} + 6H^+ + SO_4^{2-}$	[5.37]
$2Ir^{3+} + CuS + 3H_2O + 2.5O_2 \rightarrow 2IrO_2 + Cu^{2+} + 6H^+ + SO_4^{2-}$	[5.38]
$2Ir^{3+} + 3NiS \rightarrow Ir_2S_3 + 3Ni^{2+}$	[5.39]
$8Ir^{3+} + 15NiS + 8H^+ + SO_4^{2-} \rightarrow 8IrS_2 + 15Ni^{2+} + 4H_2O$	[5.40]
$8Ir^{3+} + 3NiS + 12H_2O \rightarrow 8Ir + 3Ni^{2+} + 24H^+ + 3SO_4^{2-}$	[5.41]
$2Ir^{3+} + NiS + 3H_2O + 2O_2 \rightarrow Ir_2O_3 + Ni^{2+} + 6H^+ + SO_4^{2-}$	[5.42]
$2Ir^{3+} + NiS + 3H_2O + 2.5O_2 \rightarrow 2IrO_2 + Ni^{2+} + 6H^+ + SO_4^{2-}$	[5.43]
$10Ir^{3+} + 4Ni_3S_4 + 4H_2O \rightarrow 5Ir_2S_3 + 12Ni^{2+} + 8H^+ + SO_4^{2-}$	[5.44]
$2Ir^{3+} + Ni_3S_4 \rightarrow 2IrS_2 + 3Ni^{2+}$	[5.45]
$10Ir^{3+} + Ni_3S_4 + 16H_2O \rightarrow 10Ir + 3Ni^{2+} + 32H^+ + 4SO_4^{2-}$	[5.46]
$2Ir^{3+} + Ni_3S_4 + 4H_2O + 7.5O_2 \rightarrow Ir_2O_3 + 3Ni^{2+} + 8H^+ + 4SO_4^{2-}$	[5.47]
$2Ir^{3+} + Ni_3S_4 + 4H_2O + 8O_2 \rightarrow 2IrO_2 + 3Ni^{2+} + 8H^+ + 4SO_4^{2-}$	[5.48]

From Table 5.1 it can be seen that there are numerous reactions that could potentially contribute to the precipitation behaviour of the OPMs. Although reactions one to five in Table 5.3 would dominate the base metal behaviour due to the relatively low concentration OPMs in solution, all the OPM precipitation reactions also contribute to the leaching of the base metals. Experimental determination of the relative extents of reaction for the reactions listed in Table 5.1 was hence not feasible, while calculation of all the reaction rate constants would not yield sensible results.

In order to simplify the analysis and reduce the number of reactions for which rate constants had to be determined, the Gibbs free energy for the respective reactions were considered to determine which reactions are the most favourable. McGeorge *et al.* (2009) used a similar approach to identify the most favourable rhodium precipitate to form during the precipitation of Rh and Cu from an acidic base metal sulphate solution using an excess of thiosulphate.

From the values presented in Table 5.1, the formation of rhodium oxides as precipitate by reaction with digenite (reactions 5.3 and 5.4) and polydymite (reactions 5.15 and 5.16) is the most favourable. Reaction 5.2, which leads to the formation of metallic rhodium, has a Gibbs

free energy comparable with that of the rhodium oxide formation reactions mentioned above. Further oxidation of the rhodium would, however, yield the same overall reaction as reaction 5.4. For the purpose of kinetic modelling, reaction 5.4 and reaction 5.16 were selected to account for rhodium precipitation. This is in agreement with observations made at the Western Platinum Ltd. BMR that the solids residue leaving the second stage pressure leach contains PGM oxides (Eksteen, 2011).

The results obtained for the potential ruthenium precipitation reactions are similar to the results discussed for rhodium: the reactions between dissolved ruthenium and digenite and between dissolved ruthenium and polydymite yielding ruthenium dioxide as precipitate (reaction 5.19 and reaction 5.28, respectively) are the most favourable from a thermodynamic perspective.

Although no Gibbs free energy changes could be calculated for the reactions proposed for iridium precipitation, it is expected that the behaviour of iridium will be similar to that of rhodium and ruthenium. This is based on the fact that the behaviour of all three metals during the leaching process was similar, as discussed in Section 4.3, and there is similarity between Gibbs free energy values calculated for the rhodium precipitation reactions and the ruthenium precipitation reactions. For this reason, reaction 5.33 and reaction 5.48 were included in the set of proposed reactions for which the kinetic rate constants were determined.

The reactions included in the kinetic modelling of the system to account for the precipitation of OPMs during the initial stages of the leaching process are summarised as reactions seven to twelve in Table 5.3.

5.2.4.2 Dissolution reactions

Dissolution of the metallic species, metal sulphides, and metal oxides had to be accounted for. Various sulphide and oxide species can be present in the feed to the second stage leach. However, in order to simplify the kinetic modelling and to limit the number of reactions for which reaction rate constants had to be determined, a single oxide and a single sulphide were considered to represent all oxides and sulphides, respectively, for a specific OPM. The compounds that were selected are common OPM compounds, namely Rh_2S_3, RhO_2, RuS_2, RuO_2, Ir_2S_3, and IrO_2. The leaching reactions proposed to account for the dissolution of these species, together with the Gibbs free energy calculated for the respective reactions are shown in Table 5.2.

Table 5.2. Reactions considered for OPM dissolution, together with the corresponding Gibbs free energy (kJ/mol OPM^{3+}).

OPM dissolution reactions		ΔG° (kJ/mol)
$Rh_2S_3 + 6O_2 \rightarrow 2Rh^{3+} + 3SO_4^{2-}$	[5.49]	-730.5
$4Rh + 3O_2 + 12H^+ \rightarrow 4Rh^{3+} + 6H_2O$	[5.50]	-119.0
$2RhO_2 + 6H^+ \rightarrow 2Rh^{3+} + 3H_2O + 0.5O_2$	[5.51]	69.1
$4RuS_2 + 2H_2O + 15O_2 \rightarrow 4Ru^{3+} + 6SO_4^{2-} + 4H^+ + 2SO_4^{2-}$	[5.52]	-947.8
$4Ru + 3O_2 + 12H^+ \rightarrow 4Ru^{3+} + 6H_2O$	[5.53]	-165.7
$2RuO_2 + 6H^+ \rightarrow 2Ru^{3+} + 3H_2O + 0.5O_2$	[5.54]	89.0
$Ir_2S_3 + 6O_2 \rightarrow 2Ir^{3+} + 3SO_4^{2-}$	[5.55]	-
$4Ir + 3O_2 + 12H^+ \rightarrow 4Ir^{3+} + 6H_2O$	[5.56]	-
$2IrO_2 + 6H^+ \rightarrow 2Ir^{3+} + 3H_2O + 0.5O_2$	[5.57]	-

Table 5.3. Summary of the final set of reactions proposed to describe the leaching behaviour in the second stage pressure leach.

Reaction 1	$4NiS + 2H^+ + ½O_2 \rightarrow Ni^{2+} + Ni_3S_4 + H_2O$	[2.25]
Reaction 2	$NiS + 2O_2 \rightarrow Ni^{2+} + SO_4^{2-}$	[2.33]
Reaction 3	$2Ni_3S_4 + 2H_2O + 15O_2 \rightarrow 6Ni^{2+} + 4H^+ + 8SO_4^{2-}$	[2.29]
Reaction 4	$Cu_9S_5 + 8H^+ + 2O_2 \rightarrow 4Cu^{2+} + 5CuS + 4H_2O$	[2.27]
Reaction 5	$CuS + 2O_2 \rightarrow Cu^{2+} + SO_4^{2-}$	[2.35]
Reaction 6	$Fe(OH)SO_4 + H^+ \rightarrow Fe^{3+} + SO_4^{2-} + H_2O$	[2.32]
Reaction 7	$8Rh^{3+} + 3Cu_9S_5 + 38O_2 \rightarrow 8RhO_2 + 27Cu^{2+} + 15SO_4^{2-}$	[5.4]
Reaction 8	$2Rh^{3+} + Ni_3S_4 + 4H_2O + 8O_2 \rightarrow 2RhO_2 + 3Ni^{2+} + 8H^+ + 4SO_4^{2-}$	[5.16]
Reaction 9	$8Ru^{3+} + 3Cu_9S_5 + 38O_2 \rightarrow 8RuO_2 + 27Cu^{2+} + 15SO_4^{2-}$	[5.19]
Reaction 10	$2Ru^{3+} + Ni_3S_4 + 4H_2O + 8O_2 \rightarrow 2RuO_2 + 3Ni^{2+} + 8H^+ + 4SO_4^{2-}$	[5.28]
Reaction 11	$8Ir^{3+} + 3Cu_9S_5 + 38O_2 \rightarrow 8IrO_2 + 27Cu^{2+} + 15SO_4^{2-}$	[5.33]
Reaction 12	$2Ir^{3+} + Ni_3S_4 + 4H_2O + 8O_2 \rightarrow 2IrO_2 + 3Ni^{2+} + 8H^+ + 4SO_4^{2-}$	[5.48]
Reaction 13	$Rh_2S_3 + 6O_2 \rightarrow 2Rh^{3+} + 3SO_4^{2-}$	[5.49]
Reaction 14	$4Rh + 3O_2 + 12H^+ \rightarrow 4Rh^{3+} + 6H_2O$	[5.50]
Reaction 15	$2RhO_2 + 6H^+ \rightarrow 2Rh^{3+} + 3H_2O + 0.5O_2$	[5.51]
Reaction 16	$4RuS_2 + 2H_2O + 15O_2 \rightarrow 4Ru^{3+} + 6SO_4^{2-} + 4H^+ + 2SO_4^{2-}$	[5.52]
Reaction 17	$4Ru + 3O_2 + 12H^+ \rightarrow 4Ru^{3+} + 6H_2O$	[5.53]
Reaction 18	$2RuO_2 + 6H^+ \rightarrow 2Ru^{3+} + 3H_2O + 0.5O_2$	[5.54]
Reaction 19	$Ir_2S_3 + 6O_2 \rightarrow 2Ir^{3+} + 3SO_4^{2-}$	[5.55]
Reaction 20	$4Ir + 3O_2 + 12H^+ \rightarrow 4Ir^{3+} + 6H_2O$	[5.56]
Reaction 21	$2IrO_2 + 6H^+ \rightarrow 2Ir^{3+} + 3H_2O + 0.5O_2$	[5.57]

5.3 Kinetic modelling

5.3.1 Rate expressions

The calculation of reaction kinetics and the subsequent modelling were performed based on the results obtained during the second experimental design, as these conditions were the best representation of the conditions typically encountered on site.

The general form of the rate expression typically used for the kinetic modelling of leaching and cementation reactions (Equation 2.51, adapted from Choo *et al.*, 2006) was used for the determination of the leaching kinetics in the second stage leach. For this expression to be used, the volume of the leach solution had to remain constant while the leaching progressed. In order for this condition to be satisfied, the dissolved metal concentrations as determined using ICP analysis were adjusted to compensate for the solution volumes lost as a result of the sampling that was done at fixed intervals. This data adjustment is discussed in Appendix D.

Estimating the solid surface area available for reactions introduced uncertainty. The first stage leach residue fed to the second stage leach contains particles consisting of numerous mineralogical phases. Van Schalkwyk (2011) reported that embedded alloy phases can be leached from a base metal sulphide matrix under certain conditions during the first stage leach, resulting in porous particles and possible disintegration. Leaching of sulphide phases in the second stage could proceed in a similar fashion. Van Schalkwyk (2011) did report the possible presence of embedded copper sulphide vein-like structures in the first stage leach residue which, when leached in the second stage leach, would result in porous particles without necessarily affecting the particle sizes. Rademan *et al.* (1999) made reference to increased particle porosity as leaching progressed, which resulted in improved leaching kinetics. Prosser (1996) also suggested that the solid-solution interfacial area is one of the process variables most difficult to measure and control. The particle size distribution of the solid feed was hence not a good indication of the solid surface available for chemical reactions to take place due to the possibility of porous particle structure existing or of components existing as discrete inclusions inside particles, which is the case for the OPM components. Figure 5.1 shows scanning electron microscope images of solids remaining after two hours of high pressure leaching. Both the porous structure of the solid particles and the discrete PGM rich inclusions (represented by the bright phases on the image) are evident from these images. The solid surface area available for reactions to take place was hence estimated using the approach described by Salmi *et al.* (2010), as discussed in Section 2.5. This implies that the solid surface area available for reaction was proportional to the amount of the particular solid species present in the system, rather than being dependent on the size distribution of particles which consisted of a range of phases.

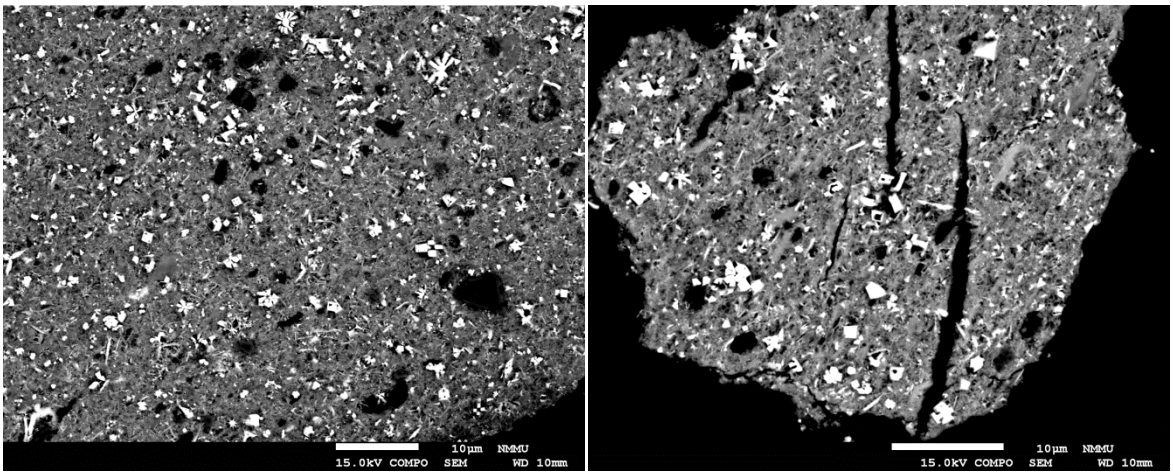

Figure 5.1. SEM images of solid material remaining after two hours of high pressure sulphuric acid/oxygen leaching, showing particle porosity and PGM inclusions.

The reaction rates were assumed to be dependent on the concentration of the reactants present as dissolved species in the solution. As a first estimation, the dependence of the reaction rates on the concentration of the dissolved species was taken to be a first order dependence. Several of the proposed reactions listed in Table 5.3 depend on the dissolved oxygen content of the leach solution. Provis *et al.* (2003) reported that changes in the oxygen flow rate and oxygen partial pressure affected leaching behaviour because of the subsequent change in the dissolved oxygen concentration of the leach solution. Considering Equation 2.41, the dissolved oxygen concentration at a specific instance in time is proportional to the dissolved oxygen concentration at equilibrium for the specific process conditions. For reactions dependent on the dissolved oxygen concentration, the oxygen solubility at equilibrium for specific process conditions was included in the rate expressions. The correlation develop by Tromans (1998b) to estimate oxygen solubility in solutions as a function of temperature, solution composition, and oxygen partial pressure has been used in the analysis of high pressure leaching environments (Padilla *et al.*, 2008), and was also used in this study to estimate the dissolved oxygen concentration at equilibrium as a function of the abovementioned process variables.

If the constants in Equation 2.51 and Equation 2.54 are included in the rate constant, k, Equation 2.51 can be simplified to Equation 5.58:

$$\frac{dC_i}{dt} = \upsilon_i \cdot k \cdot n_0^{1/f_{sh}} \cdot n^{1-1/f_{sh}} \cdot \prod C_r^{\alpha_r} \qquad [5.58]$$

where C_i refers to the concentration of species i in solution, υ_i is the stoichiometric coefficient of species i in the particular chemical reaction, k is the rate constant, n_0 and n are the molar amount of solid participating in the reaction that is present in the system per unit slurry volume initially and at the given time instance, respectively, f_{sh} is the particle shape factor, C_r

is the concentration of the dissolved species on which the reaction rate is dependent, and α_r is the order of the reaction with respect to the specific reactant.

5.3.2 Calculation of kinetic constants

In order to determine the reaction rate constants, mass balances were performed for the respective species present in the batch experimental leaching system to calculate the change in concentrations over time. The resulting set of differential equations, given by Equation 5.59 to Equation 5.79, was solved numerically by the 4th order Runge-Kutta method in Microsoft Excel®. This numerical method is discussed in Appendix D.5. Of the expressions predicting the concentration dissolved species in solution, the expressions for the concentration of Rh^{3+} (Equation 5.67), Ru^{3+} (Equation 5.71), and Ir^{3+} (Equation 5.75) contain the most fitted parameters; these parameters include five rate constant pre-exponential factors, five activation energies, and five shape factors. The number of data sets available for each of these dissolved species is 16, which confirms that positive degrees of freedom were maintained in all instances.

$$\frac{dC_{NiS}}{dt} = -4r_1 - r_2 \quad [5.59]$$

$$\frac{dC_{Ni_3S_4}}{dt} = r_1 - 2r_3 - r_8 - r_{10} - r_{12} \quad [5.60]$$

$$\frac{dC_{Ni^{2+}}}{dt} = r_1 + r_2 + 6r_3 + 3r_8 + 3r_{10} + 3r_{12} \quad [5.61]$$

$$\frac{dC_{Cu_9S_5}}{dt} = -r_4 - 3r_7 - 3r_9 - 3r_{11} \quad [5.62]$$

$$\frac{dC_{CuS}}{dt} = 5r_4 - r_5 \quad [5.63]$$

$$\frac{dC_{Cu^{2+}}}{dt} = 4r_4 + r_5 + 27r_7 + 27r_9 + 27r_{11} \quad [5.64]$$

$$\frac{dC_{Fe^{3+}}}{dt} = r_6 \quad [5.65]$$

$$\frac{dC_{Fe(OH)SO_4}}{dt} = -r_6 \quad [5.66]$$

$$\frac{dC_{Rh^{3+}}}{dt} = -8r_7 - 2r_8 + 2\,r_{13} + 4r_{14} + 2r_{15} \quad [5.67]$$

$$\frac{dC_{RhO_2}}{dt} = 8r_7 + 2r_8 - 2r_{15} \quad [5.68]$$

$$\frac{dC_{Rh}}{dt} = -4r_{14} \quad [5.69]$$

$$\frac{dC_{Rh_2S_3}}{dt} = -r_{13} \quad [5.70]$$

$$\frac{dC_{Ru^{3+}}}{dt} = -8r_9 - 2r_{10} + 4r_{16} + 4r_{17} + 2r_{18} \quad [5.71]$$

$$\frac{dC_{RuO_2}}{dt} = 8r_9 + 2r_{10} - 2r_{18} \quad [5.72]$$

$$\frac{dC_{Ru}}{dt} = -4r_{17} \quad [5.73]$$

$$\frac{dC_{RuS_2}}{dt} = -4r_{16} \quad [5.74]$$

$$\frac{dC_{Ir^{3+}}}{dt} = -8r_{11} - 2r_{12} + 2\,r_{19} + 4r_{20} + 2r_{21} \quad [5.75]$$

$$\frac{dC_{IrO_2}}{dt} = 8r_{11} + 2r_{12} - 2r_{21} \quad [5.76]$$

$$\frac{dC_{Ir}}{dt} = -4r_{20} \quad [5.77]$$

$$\frac{dC_{Ir_2S_3}}{dt} = -r_{19} \quad [5.78]$$

$$\frac{dC_{H^+}}{dt} = -2r_1 + 4r_3 - 8r_4 - r_6 + 8(r_8 + r_{10} + r_{12}) - 12(r_{14} + r_{17} + r_{20}) - 6(r_{15} + r_{18} + r_{21}) + 4r_{16} \quad [5.79]$$

The shape factors for the respective solid components and the reaction rate constants were determined by the method of least squares; the Solver-function in Microsoft Excel® was used to minimise the sum of the squared differences between the model predicted concentrations and the experimental concentrations of Ni, Cu, Fe, Rh, Ru, and Ir in solution. This method to determine rate constants is typically preferred when dealing with complex systems involving multiple reactions (Fogler, 1999). The rate constants were determined separately for the eight

tests performed at 130°C and the eight tests performed at 116°C. The dependence of the rate constant on temperature was assumed to be given by the Arrhenius equation (Equation 2.53).

5.4 Reaction rate constants

The rate expressions for the reactions proposed to describe the leaching behaviour of the base metals and OPMs in the second stage pressure leach are summarised in Table 5.4. It was found that the rates of direct oxidation of millerite and covellite (reaction 2 and reaction 5, respectively) were best described by a second order dependence on the dissolved oxygen concentration. The conclusion from the qualitative observations that the rates of the copper leaching reactions (reactions 4 and 5) were determined by the rate of oxygen transfer from the gaseous phase to the liquid phase allowed the omission of the solid surface parameter from the rate expressions for these two reactions.

Based on the qualitative observation that the initial acid concentration did not affect the rate or extent of the OPM leaching, the OPM leaching reactions (reactions 14, 15, 17, 18, 20, and 21) were assumed to be of zero order with respect to the acid concentration. This could be attributed to the fact that the acid was generally present in large amounts of excess compared to the OPM solid phases. The OPM leaching reactions (reactions 10, 11, and 12) were furthermore assumed to proceed only once the Cu_9S_5 remaining in the system reached 1% of the initial Cu_9S_5 amount to account for the preferential leaching of Cu phases during the initial leaching stages. All the copper and nickel leaching reactions were assumed to proceed simultaneously. The pre-exponential factors and activation energies for the respective reactions are summarised in Table 5.5, and the shape factors determined for the respective solid components are summarised in Table 5.6.

Studies that have previously investigated the kinetics of base metal sulphide leaching in a sulphuric acid system include those by Rademan (1995), Provis *et al.* (2003), Lamya (2007), Ruiz *et al.* (2007), and Fan *et al.* (2010). Fan *et al.* (2010) did, however, not report rate constants for specific reactions, while Lamya (2007) focussed on the copper cementation reactions and the direct acid attack of metallic phases, rather than the leaching of millerite, polydymite, digenite, and covellite, which were of primary interest in this study. Ruiz *et al.* (2007) presented simple rate expressions excluding the effects of the acid concentration and dissolved oxygen concentration on the reactions rates. Rademan (1995) and Provis *et al.* (2003) included the effect of the oxygen in the rate expressions by the inclusion of an “effective oxygen partial pressure”, which was dependent on the flow rate of oxygen to the

leaching system. Because of the different forms of the rate expressions used in this study and in previous studies, direct comparison of the rate constants to previously reported values was not sensible.

The activation energies for the two copper sulphide leaching reactions (reaction 4 and reaction 5) are both negative with relatively small absolute values (<30 kJ/mol), indicating that the chemical reaction was not the rate controlling mechanism and that an increase in temperature would cause the leaching rate to decrease. Based on the literature review presented in Section 2.4, it was expected that an increase in temperature would increase the rate of copper leaching. For the given range of operating conditions, however, the decrease in the oxygen partial pressure as a result of the higher temperature was more significant than the effect on the reaction rate constant. As a result, the reaction rate decreased as the temperature was increased, and the effect of the decreasing oxygen partial pressure to some extent masked the real effect of the temperature on the rate constant. If the activation energies were artificially forced to remain positive, the rate expressions for reaction 4 and reaction 5 had to have a higher order dependence on the dissolved oxygen concentration in order to accurately predict the experimental data.

At lower temperatures and higher pressures, an increase in temperature is likely to result in faster copper dissolution. The negative values should thus be seen as apparent activation energies for the given range of operating conditions that allow the best prediction of the experimental data. In addition, Rademan (1995) also reported negative apparent activation energies for copper sulphide leaching reactions. The relatively large positive activation energies (>34 kJ/mol) for the remainder of the reactions confirmed that the rates of these reactions were likely to be chemical reaction controlled, as discussed previously. The correlations between the activation energies calculated for the leaching reactions of the Rh compounds, Ru compounds, and Ir compounds confirmed that the leaching mechanisms of the different OPMs are similar.

As discussed in Section 2.5, the shape factor is an indication of the surface area to volume ratio of the particles under consideration. The SEM images in Figure 5.1 illustrate the porous structure of the particles. The porosity increased the surface to volume ratio of the particles, which explains why shape factors larger than three were calculated for some of the base metal phases. The OPM phases, which are indicated by the bright phases in Figure 5.1, occur as

irregularly shaped inclusions which are mostly non-porous. The shape factors between 1.9 and 3.4 for the OPM alloy and the OPM sulphide phases are in agreement with this observation. The fact that shape factors much larger than three were calculated for the OPM oxide phases can be ascribed to the fact that the oxide phases were formed by the cationic exchange reactions (reaction 7 to reaction 12 in Table 5.3), resulting in very small, well dispersed occurrences of these phases.

Table 5.4. Rate expressions for the proposed reactions.

$r_1 = k_1 \cdot C_{H^+} \cdot C'_{O_2,Eq} \cdot \left(n_0^{1/f_{sh}} \cdot n^{1-1/f_{sh}}\right)_{NiS}$	[5.80]
$r_2 = k_2 \cdot C'^{\,2}_{O_2,Eq} \cdot \left(n_0^{1/f_{sh}} \cdot n^{1-1/f_{sh}}\right)_{NiS}$	[5.81]
$r_3 = k_3 \cdot C'_{O_2,Eq} \cdot \left(n_0^{1/f_{sh}} \cdot n^{1-1/f_{sh}}\right)_{Ni_3S_4}$	[5.82]
$r_4 = k_4 \cdot C_{H^+} \cdot C'_{O_2,Eq}$	[5.83]
$r_5 = k_5 \cdot C'^{\,2}_{O_2,Eq}$	[5.84]
$r_6 = k_6 \cdot C_{H^+} \cdot \left(n_0^{1/f_{sh}} \cdot n^{1-1/f_{sh}}\right)_{Fe(OH)SO_4}$	[5.85]
$r_7 = k_7 \cdot C_{Rh^{3+}} \cdot C'_{O_2,Eq} \cdot \left(n_0^{1/f_{sh}} \cdot n^{1-1/f_{sh}}\right)_{Cu_9S_5}$	[5.86]
$r_8 = k_8 \cdot C_{Rh^{3+}} \cdot C'_{O_2,Eq} \cdot \left(n_0^{1/f_{sh}} \cdot n^{1-1/f_{sh}}\right)_{Ni_3S_4}$	[5.87]
$r_9 = k_9 \cdot C_{Ru^{3+}} \cdot C'_{O_2,Eq} \cdot \left(n_0^{1/f_{sh}} \cdot n^{1-1/f_{sh}}\right)_{Cu_9S_5}$	[5.88]
$r_{10} = k_{10} \cdot C_{Ru^{3+}} \cdot C'_{O_2,Eq} \cdot \left(n_0^{1/f_{sh}} \cdot n^{1-1/f_{sh}}\right)_{Ni_3S_4}$	[5.89]
$r_{11} = k_{11} \cdot C_{Ir^{3+}} \cdot C'_{O_2,Eq} \cdot \left(n_0^{1/f_{sh}} \cdot n^{1-1/f_{sh}}\right)_{Cu_9S_5}$	[5.90]
$r_{12} = k_{12} \cdot C_{Ir^{3+}} \cdot C'_{O_2,Eq} \cdot \left(n_0^{1/f_{sh}} \cdot n^{1-1/f_{sh}}\right)_{Ni_3S_4}$	[5.91]
$r_{13} = k_{13} \cdot C'_{O_2,Eq} \cdot \left(n_0^{1/f_{sh}} \cdot n^{1-1/f_{sh}}\right)_{Rh_2S_3}$	[5.92]
$r_{14} = k_{14} \cdot C'_{O_2,Eq} \cdot \left(n_0^{1/f_{sh}} \cdot n^{1-1/f_{sh}}\right)_{Rh}$	[5.93]
$r_{15} = k_{15} \cdot \left(n_0^{1/f_{sh}} \cdot n^{1-1/f_{sh}}\right)_{RhO_2}$	[5.94]
$r_{16} = k_{16} \cdot C'_{O_2,Eq} \cdot \left(n_0^{1/f_{sh}} \cdot n^{1-1/f_{sh}}\right)_{RuS_2}$	[5.95]
$r_{17} = k_{17} \cdot C'_{O_2,Eq} \cdot \left(n_0^{1/f_{sh}} \cdot n^{1-1/f_{sh}}\right)_{Ru}$	[5.96]
$r_{18} = k_{18} \cdot \left(n_0^{1/f_{sh}} \cdot n^{1-1/f_{sh}}\right)_{RuO_2}$	[5.97]
$r_{19} = k_{19} \cdot C'_{O_2,Eq} \cdot \left(n_0^{1/f_{sh}} \cdot n^{1-1/f_{sh}}\right)_{Ir_2S_3}$	[5.98]
$r_{20} = k_{20} \cdot C'_{O_2,Eq} \cdot \left(n_0^{1/f_{sh}} \cdot n^{1-1/f_{sh}}\right)_{Ir}$	[5.99]
$r_{21} = k_{21} \cdot \left(n_0^{1/f_{sh}} \cdot n^{1-1/f_{sh}}\right)_{IrO_2}$	[5.100]

Table 5.5. Parameters to calculate the rate constants for the proposed reactions.

Rate constant, $k_i = k_{i,0} \cdot \exp(-E_{a,i}/R \cdot T)$		
Reaction	**Pre-exponential factor, $k_{i,0}$**	**Activation energy, $E_{a,i}$ (kJ/mol)**
Reaction 1	2.33×10^{9}	78.5
Reaction 2	4.76×10^{8}	41.1
Reaction 3	1.68×10^{10}	87.4
Reaction 4	7.52×10^{-5}	-26.2
Reaction 5	5.45×10	-5.9
Reaction 6	1.43×10^{3}	34.3
Reaction 7	4.66×10^{9}	59.5
Reaction 8	1.89×10^{8}	64.6
Reaction 9	7.34×10^{8}	56.1
Reaction 10	1.20×10^{5}	52.1
Reaction 11	2.18×10^{17}	120.9
Reaction 12	2.38×10^{6}	48.5
Reaction 13	7.10×10^{8}	64.2
Reaction 14	2.99×10^{17}	138.5
Reaction 15	1.25×10^{12}	116.2
Reaction 16	9.16×10^{6}	52.8
Reaction 17	1.44×10^{16}	124.3
Reaction 18	9.29×10^{14}	134.1
Reaction 19	1.20×10^{10}	72.4
Reaction 20	2.47×10^{22}	175.1
Reaction 21	3.09×10^{24}	209.2

Table 5.6. Shape factors for the respective solid species participating in the reactions.

NiS	1.6
Ni_3S_4	1.0
Cu_9S_5	3.3
$Fe(OH)SO_4$	3.4
Rh_2S_3	1.9
Rh	2.6
RhO_2	>> 3
RuS_2	2.7
Ru	1.9
RuO_2	>> 3
Ir_2S_3	2.1
Ir	3.4
IrO_2	>> 3

Graphs illustrating the comparison between the experimentally determined metal concentrations and the model predicted concentrations for test 2i and test 2n are shown in Figure 5.2 and Figure 5.3, respectively. Similar graphs for the other 14 tests are shown in Appendix E. The model was able to satisfactorily predict the precipitation of the OPMs during the initial leaching stages and the subsequent OPM dissolution once copper dissolution had proceeded to a sufficient extent. As can be seen from Figure 5.2 and Figure 5.3, the model typically predicted higher copper concentrations than the experimentally determined values, especially for the tests performed with the high solid to liquid ratio. This was primarily due to the precipitation of copper sulphate from the samples which resulted in the reported copper concentrations being less than the actual concentration, as discussed in Section 4.3.

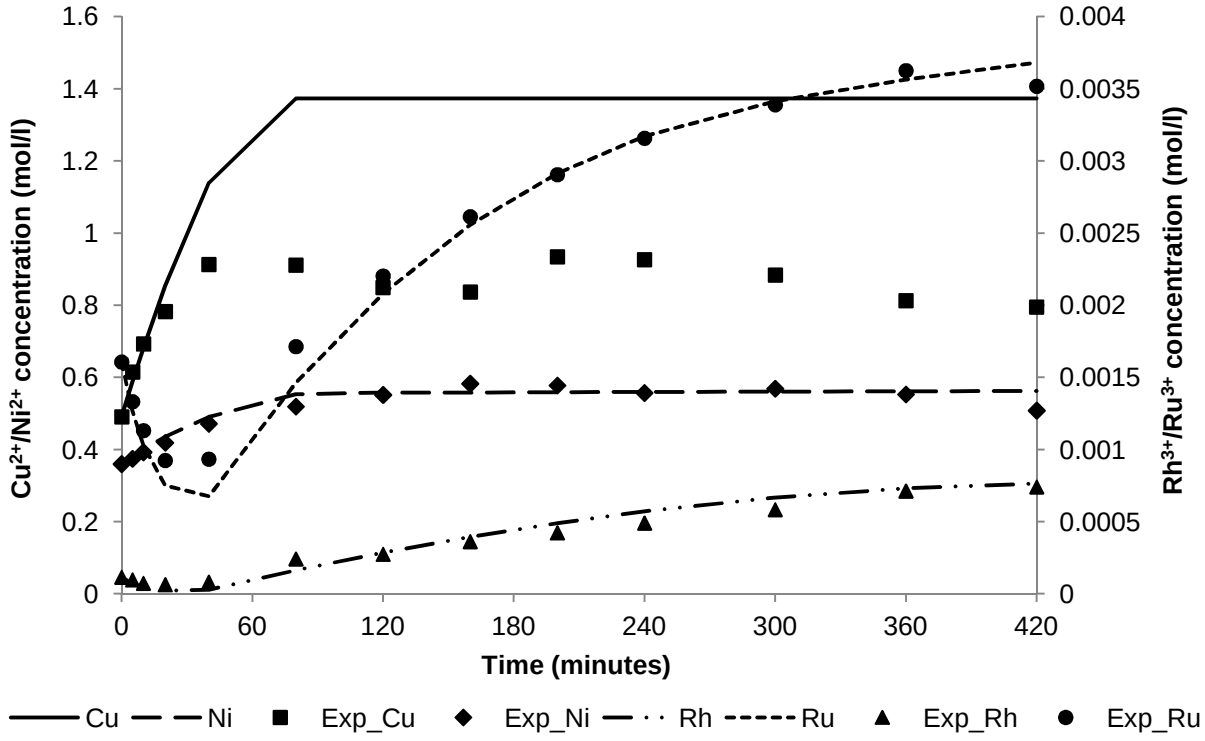

Figure 5.2. Comparison of the model predicted metal concentrations as a function of leaching time and the experimental metal concentrations after correction for sampling losses for test 2i ($T = 116°C$; $P = 9$ bar; $[M_{H2SO4}] = 140g/\ell$; solids content = 130 g/ℓ)

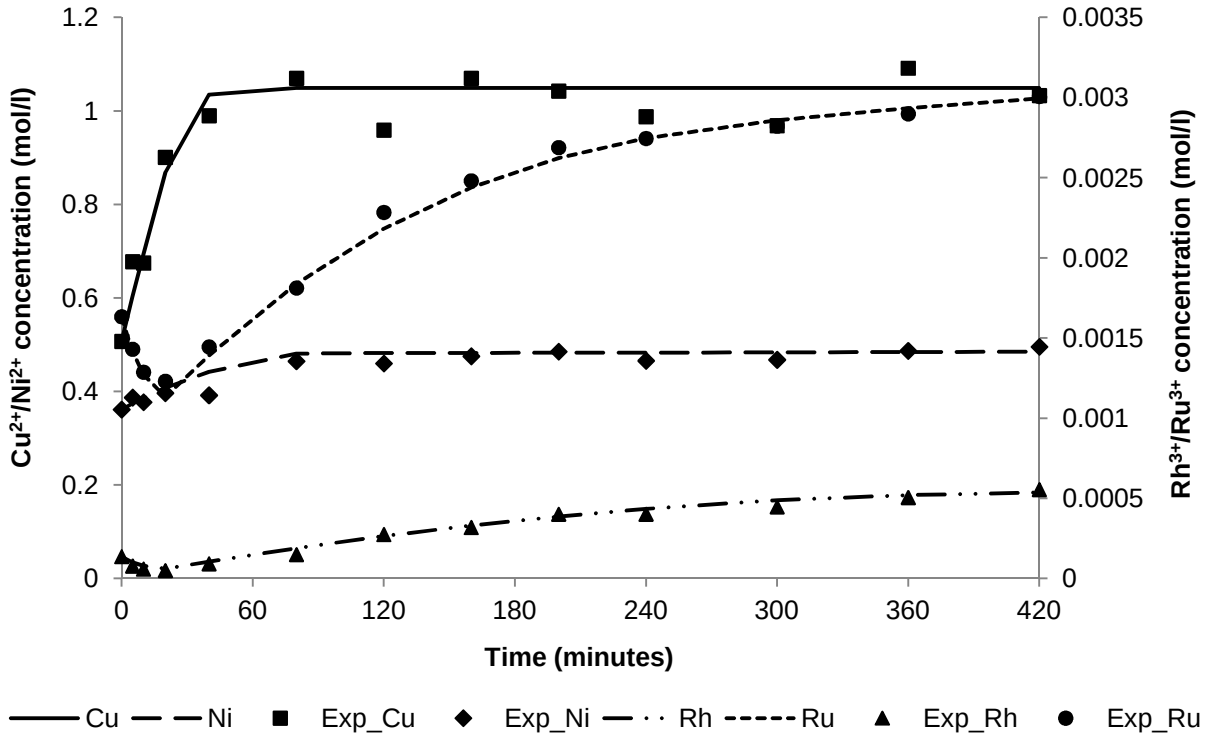

Figure 5.3. Comparison of the model predicted metal concentrations as a function of leaching time and the experimental metal concentrations after correction for sampling losses for test 2n (T = 116°C; P = 9 bar; [M_{H2SO4}] = 140g/ℓ; solids content = 80 g/ℓ)

The goodness of fit of the proposed models was quantified by calculation of the coefficient of determination, R^2, for the models according to Equation 5.101:

$$R^2 = 1 - \frac{\sum(y_n - \hat{y}_n)^2}{\sum(y_n - \bar{y})^2} \qquad [5.101]$$

where y_n is the n^{th} experimental value, $\hat{y}_n$ is the n^{th} model predicted value, and $\bar{y}$ is the mean of the experimental values. The coefficients of determination calculated for the models used to predict the concentrations of the dissolved species shown in Figure 5.2 and Figure 5.3 as well as in Figure E.1 to Figure E.14 for each of the tests are summarised in Table 5.7. The fact that coefficients of determination less than zero were calculated in some instances for the model used to predict the copper concentration confirms the qualitative observation that the model provides a poor fit for the copper concentration. In general, the closer the coefficient of determination is to one, the better the fit of the model. From the values presented in Table 5.7, it can thus be said that the proposed models are appropriate to predict the concentration of nickel and OPMs in solution.

Table 5.7. Coefficient of determination calculated to quantify the goodness of fit of the models used to predict the concentrations of the respective dissolved species and the respective tests.

Test #	Cu	Ni	Rh	Ru
2a	<0	0.91	0.98	0.97
2b	<0	0.94	0.98	0.98
2c	<0	0.83	0.97	0.98
2d	0.69	0.77	0.96	0.99
2e	0.44	0.97	1.00	0.98
2f	<0	0.95	0.99	0.99
2g	0.17	0.70	0.99	0.98
2h	0.69	0.66	0.96	0.92
2i	<0	0.92	0.95	0.98
2j	0.69	0.53	0.96	0.94
2k	<0	0.93	0.98	0.96
2l	0.80	0.93	0.98	0.99
2m	<0	0.97	0.97	0.98
2n	0.85	0.83	0.98	0.99
2o	<0	0.97	0.96	0.99
2p	0.65	0.90	0.97	0.98
Overall	<0	0.95	0.98	0.98

5.5 Predicted effect of process variables on reaction rates

The expressions derived to calculate the reaction kinetics were used to evaluate the effects that the leaching temperature, leaching pressure, and acid concentration have on the kinetics of the respective reactions. The composition of the solid phase was assumed to be the same as that of the first stage residue, and a typical liquid composition of 700 mg/ℓ Fe, 19.1 g/ℓ Ni, 23.8 g/ℓ Cu, 160 mg/ℓ Ru, 30 mg/ℓ Rh, and 25 mg/ℓ Ir was selected to evaluate the rates predicted by the kinetic expressions.

The effect of temperature and pressure on the rate of digenite leaching according to reaction 4 is illustrated in Figure 5.4. As discussed, this reaction rate decreases as the temperature is increased and/or the pressure is decreased over the investigated range of conditions. Changing the temperature or pressure has similar effects on the rate of covellite leaching according to reaction 5. The effect of acid concentration on these leaching rates is shown in Figure 5.5. The rate of reaction 4 depends on both the acid concentration and the oxygen availability in the system. The direct effect of increasing the acid concentration on the particular reaction rate is more significant than the decreased oxygen solubility resulting from the increased acid concentration, resulting in slightly faster leaching kinetics. In the case of reaction 5, acid does

not participate in the leaching of covellite, and the reaction rate is only dependent on the oxygen availability. For this reason, the decreased oxygen solubility caused by the increased acid concentration leads to slower kinetics for reaction 5.

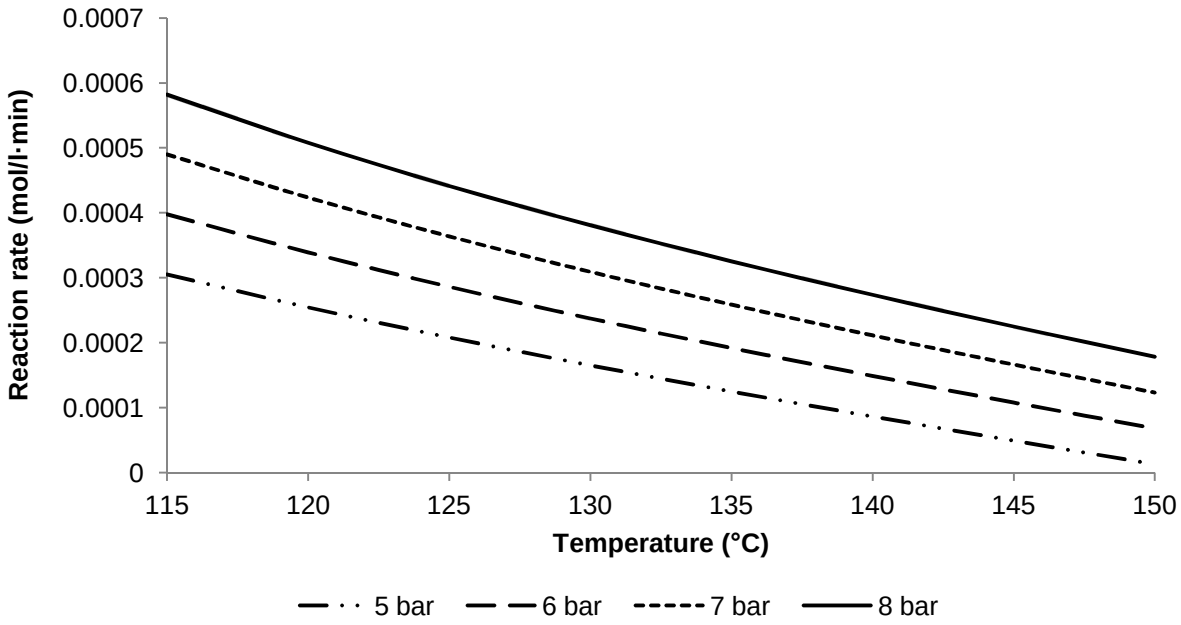

Figure 5.4. The predicted rate of reaction 4 shown as a function of temperature and pressure (acid concentration: 30 g/ℓ; solid content: 80 g/ℓ).

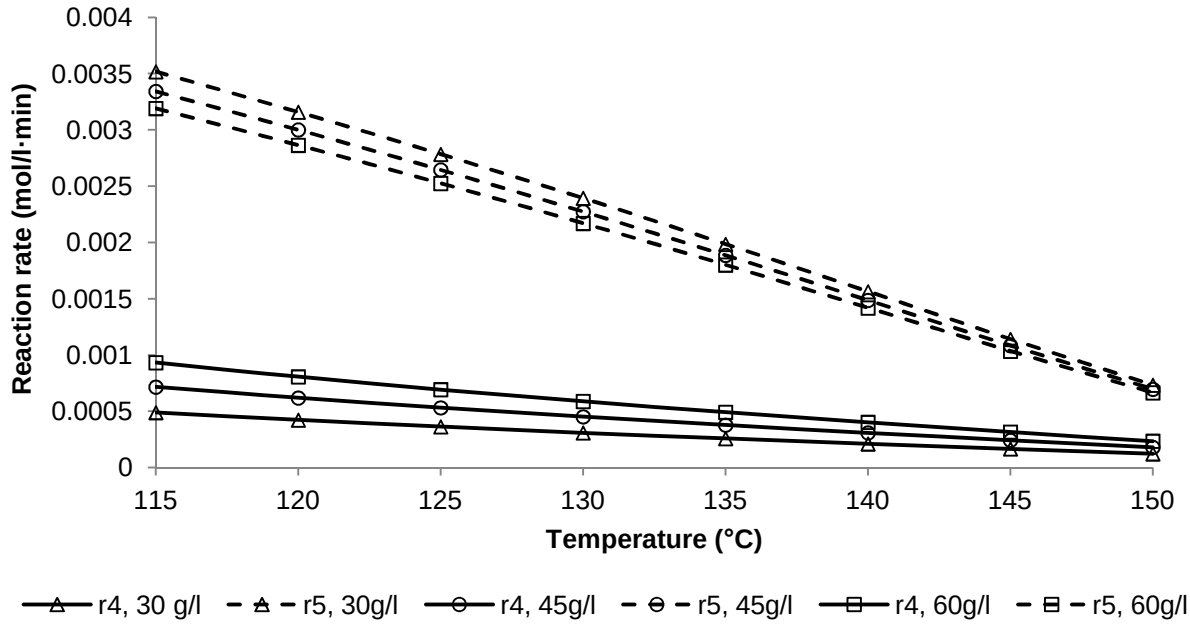

Figure 5.5. The predicted rates of reaction 4 and reaction 5 shown as a function of temperature and acid concentration (pressure: 7 bar; solid content: 80 g/ℓ).

The effects that changing the temperature, pressure, and/or acid concentration have on the rate at which reaction 13 proceeds are shown in Figure 5.6. Given the dependence of this reaction on oxygen availability, increasing the pressure results in faster leaching kinetics. As discussed in Section 4.3, increasing the temperature results in faster leaching kinetics. This trend is, however, only observed as long as the oxygen partial pressure is maintained at a sufficient level to ensure that oxygen availability does not become the rate determining factor. The predicted rates for leaching performed at 5 bar and at 6 bar start to decrease at temperatures above 138°C and 145°C, respectively, due to the associated decrease in the oxygen partial pressure as the water vapour pressure increases at a constant total pressure. Since acid does not participate in reaction 13, an increase in the acid concentration resulted in a decreased reaction rate due to the reduced oxygen solubility. Similar trends were observed for the rates of reactions 7-12, reaction 14, reactions 16-17, and reactions 19-20. Although reactions 14, 17, and 20 include acid as a reagent, the rate expressions for these reactions were determined to be zero order expressions with respect to the acid concentration, as discussed in Section 5.3.1. Consequently, increasing the acid concentration also resulted in slower kinetics for these reactions due to the dependence of these reactions on the availability of oxygen. The rates of reactions 15, 18, and 21 increased as the temperature was increased, but these rates were not affected by changes in the pressure or changes in the acid concentration.

The effects of temperature and pressure on the kinetics of reactions 1-3, as well as the effect of acid concentration on the kinetics of reactions 2 and 3 are similar to those discussed for reaction 13 with reference to Figure 5.6. The effect of changes in the acid concentration on the kinetics of reaction 1 was, however, found to be more significant compared with the reactions discussed above, primarily because acid was identified as a reagent required for this leaching reaction to proceed. Figure 5.7 illustrates that the direct effect of the increased acid concentration on the reaction rate is more significant than the effect of the decreased oxygen solubility, subsequently resulting in faster leaching rates.

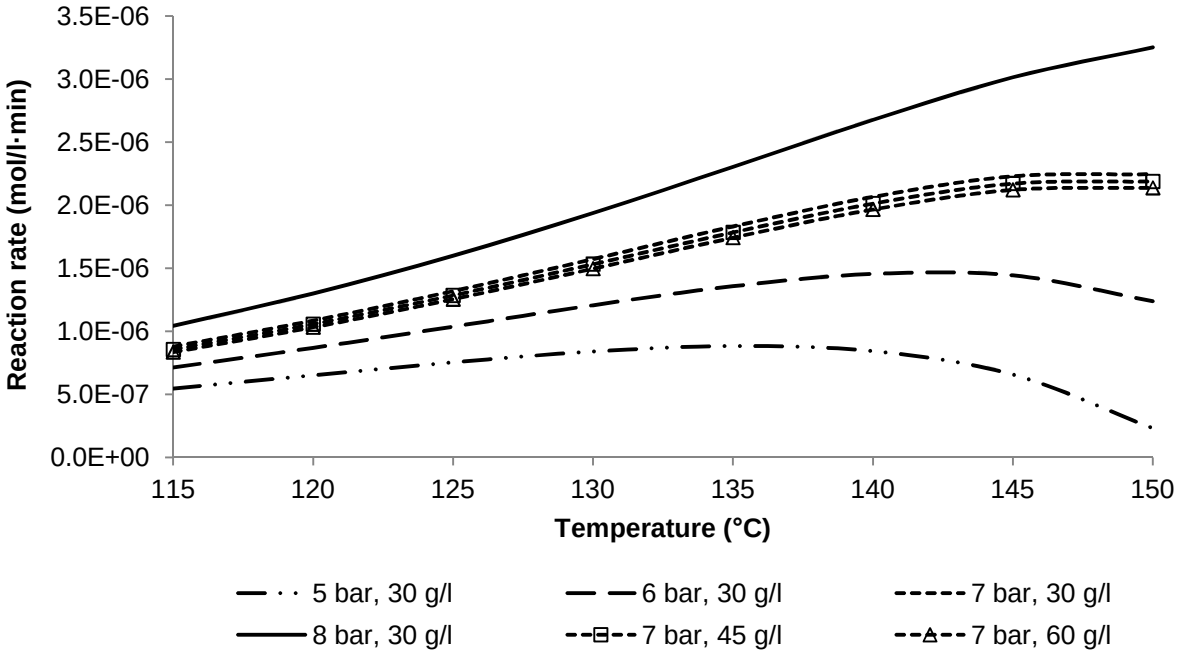

Figure 5.6. The predicted rates of reaction 13 shown as a function of temperature, pressure, and acid concentration (solid content: 80 g/ℓ).

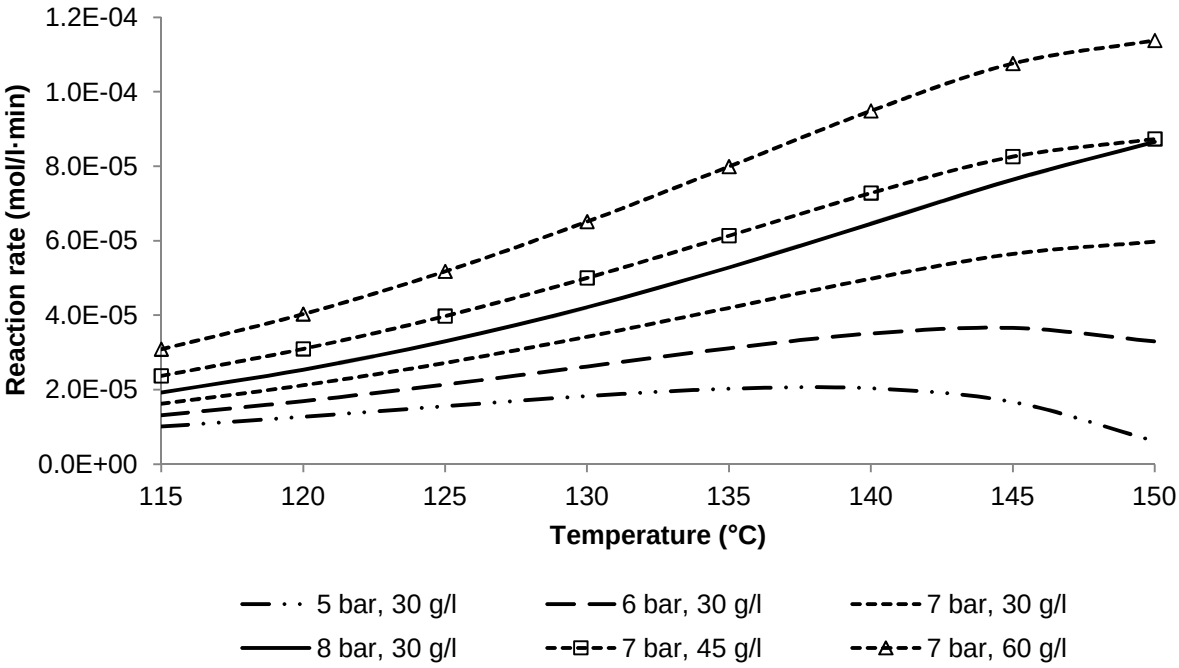

Figure 5.7. The predicted rate of reaction 1 as a function of temperature, pressure, and acid concentration (solid content: 80 g/ℓ).

The relative reaction rates of the different rhodium leaching reactions at various temperature and pressure conditions are shown in Figure 5.8. The leaching rate of rhodium sulphide is generally an order of magnitude larger than the leaching rate of metallic rhodium and two to three orders of magnitude larger that the leaching rate of rhodium oxide at lower

temperatures, but these differences decrease as the temperature is increased; this is due to the higher dependence of the leaching rates of metallic rhodium and rhodium oxide on temperature, as indicated by the larger activation energies of these reactions compared to the OPM sulphide leaching reactions. These observations are similar to those made for the ruthenium and iridium leaching reactions, and agree with the expected behaviour considering the discussion in Section 2.3 regarding the solubility of different OPM phases.

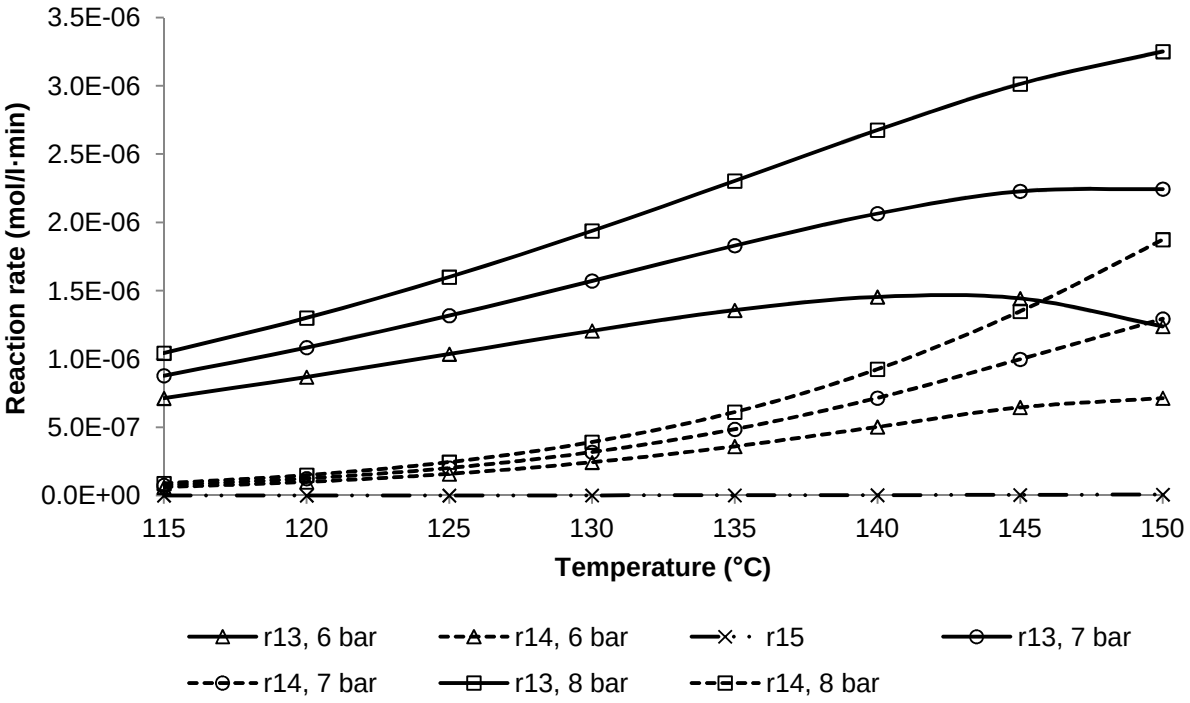

Figure 5.8. The predicted rates of reaction 13, reaction 14, and reaction 15 as a function of temperature and pressure (acid concentration: 30 g/ℓ; solid content: 80 g/ℓ).

6 MODELLING OF THE PRESSURE LEACHING STAGES

6.1 Background

The proposed set of reactions and the reaction rate constants determined using the batch experiments were utilised to model the dynamic behaviour of the autoclave used at the Western Platinum Ltd. BMR. A schematic overview of the pressure leaching stages with the relevant unit operations and streams is presented in Figure 6.1.

The first stage leach residue (stream 1) is first sent to a slurry preparation tank where fresh water, acid, filtrate from the formic acid leach, and spent electrolyte are added to control the metal content and acid concentration of the leach solution leaving the second stage leach. The filtrate from the formic acid leach is essentially a dilute sulphuric acid stream containing small amounts of iron and nickel; for modelling purposes, this filtrate was made up by specifying appropriate values for the fresh water (stream 3) and acid (stream 4) feed streams.

The combined stream leaving the slurry preparation tank is sent to the flash recycle tank. The primary reason for the flash recycle tank is to assist with the temperature control in the first compartment of the autoclave. A portion of the slurry in the first autoclave compartment is recycled to the flash recycle tank (stream 9). The recycle stream has a temperature similar to that in the autoclave, which is higher than the boiling point of water at atmospheric pressure. As a result, a portion of the liquid in the recycle stream evaporates when the recycle stream enters the flash recycle tank via a flash valve, losing energy in the process. Cooling is required in the first autoclave compartment because the leaching reactions occurring in the second stage leach are highly exothermic. In addition to the slurry recycle stream, the gas purge stream drawn from the first autoclave apartment to prevent the accumulation of impurities in the vapour space of the autoclave (stream 8) passes through the flash recycle tank. For modelling purposes, it was assumed that all the spent electrolyte, water, and fresh acid that are fed to the autoclave are added to the slurry preparation tank, although these components may also be added to the flash recycle tank. While the distribution of the addition of these components between the slurry preparation tank and the flash recycle tank will have an effect on the dynamic behaviour of the feed end of the autoclave, it will not affect the overall material balances.

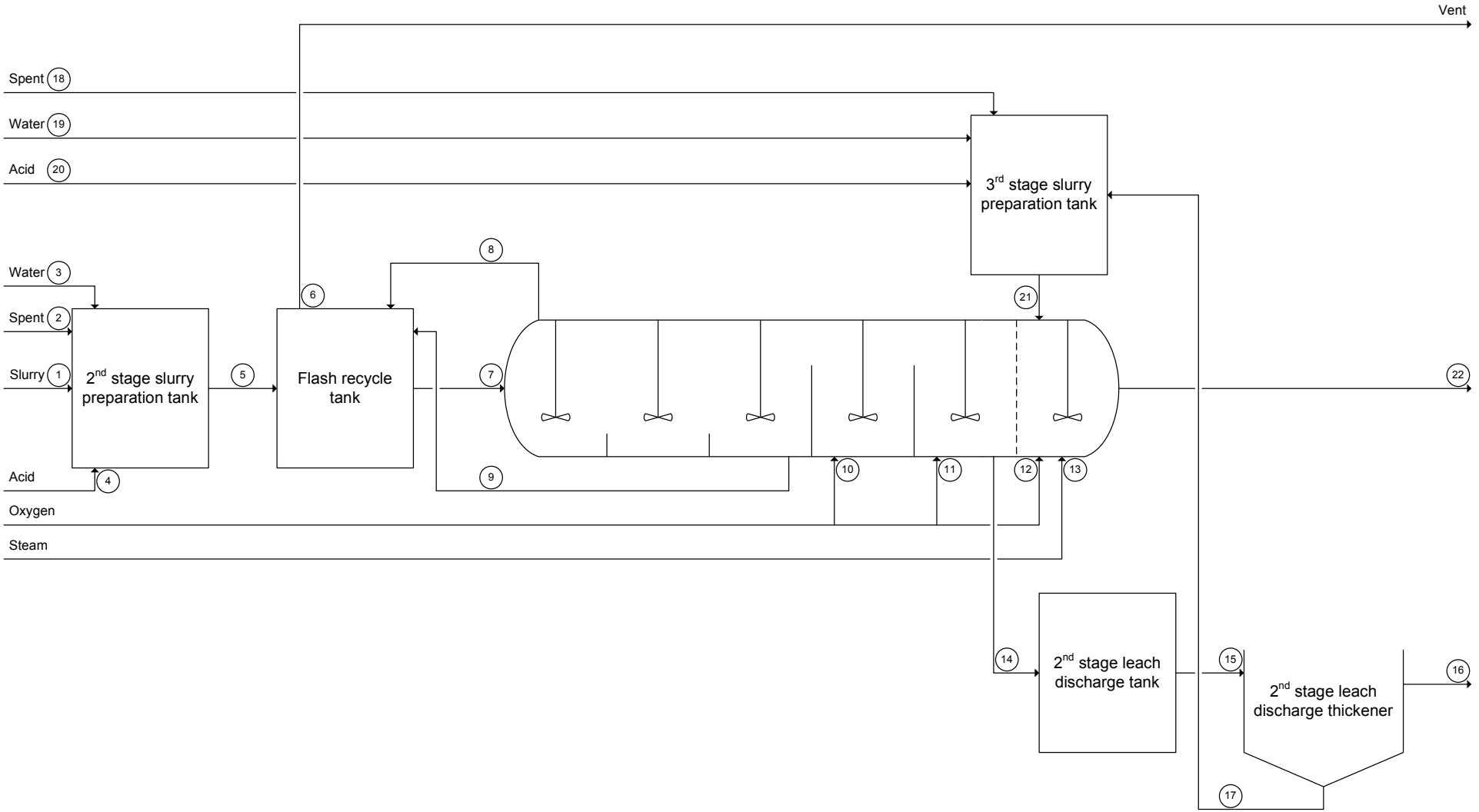

Figure 6.1. Schematic diagram of the second and third stages of leaching at the Lonmin BMR, as used to perform the dynamic modelling.

The stream leaving the flash recycle tank (stream 7) serves as the feed stream to the autoclave. The autoclave consists of four compartments, of which the first three encompass the second stage leach while the fourth compartment constitutes the third leaching stage at the Western Platinum Ltd. BMR. The first three compartments are separated by overflow weirs, which allow slurry to flow through the second stage leach. The third compartment and the fourth compartment are separated by a partitioning wall that does not allow slurry transfer between the second stage leach and the third stage leach; there is, however, an opening connecting the vapour spaces of the compartments, allowing the transfer of vapours between the second and third stage leach. Oxygen is added to the last three compartments of the autoclave (streams 10, 11, and 12). Temperature control in the second and third compartments is achieved by means of cooling water flowing through cooling coils. The slurry leaving the third autoclave compartment (stream 14) passes to a discharge tank and thickener, where the pregnant copper sulphate leach solution is recovered for downstream treatment in the Se/Te removal section and electrowinning. The thickener underflow is fed to the third stage slurry preparation tank, where fresh water (stream 19), acid (stream 20), and spent electrolyte (stream 18) are added to achieve the desired operating conditions in the third stage leach. Because the extents of reactions are relatively small in the third stage leach, it is typically required that energy be added to this leaching stage to maintain the desirable operating temperature. This is achieved by spraying steam directly into the fourth compartment (stream 13). Stream 22, the slurry stream leaving the third stage leach, is sent to downstream treatment units to recover the pregnant copper sulphate leach solution and to further improve the grade of the solids residue.

The process variables that can be manipulated to achieve the desired operational objectives of maximum base metal leaching and minimum PGM leaching include the leaching temperature, the pressure in the autoclave, the acid concentration in the leach solution, and the residence time. Analyses of the solids residue leaving the second stage leach and the third stage leach, analyses of the leach solutions, as well as the redox potential of the leach solutions are monitored to evaluate the autoclave performance. There is, however, a long waiting time for the analytical results, meaning that rapid control to achieve the desired leaching performance is not possible (Steenekamp, 2009b).

6.2 Assumptions and simplifications

In order to simplify both the steady state and dynamic modelling of the autoclave, the following assumptions were made:

- Mass transfer between the liquid and vapour phases is limited to the transfer of oxygen to the liquid phase as a result of oxygen being consumed in the leaching reactions, as well the evaporation or condensation of water. The implications of this assumption can be summarised as follows:
  - The vapour phases in the autoclave compartments and in the flash recycle tank (stream 6) consist of water vapour and oxygen only. To validate this, a sample flash drum calculation was done using Aspen Plus® 2006. A process stream with a composition similar to that of the recycle stream was sent to an adiabatic flash drum operated at a pressure of 1 bar; the results in Table 6.1 confirmed that water is essentially the only component that evaporates during flashing.

    Table 6.1. Sample flash drum calculation results generated using Aspen Plus® 2006.

	Feed	**Vapour product**	**Liquid product**
Temperature (°C)	140.0	100.9	100.9
Pressure (bar)	7	1	1
Mass flow (kg/h)			
H_2O	3446.5	206.32	3186.18
H_2SO_4	170	<0.001	170
Cu^{2+}	240		240
Ni^{2+}	140		140
Fe^{3+}	3.5		3.5

  - There are certain subsystems or process units for which the oxygen solubility of the feed stream differ from the oxygen solubility of the system content and product streams. Examples include the difference between the oxygen solubility of the stream entering the autoclave and the slurry inside the autoclave as well as the recycle stream before flashing and after flashing. Given the relatively low oxygen solubility (approximately 90 mg/ℓ at the typical leaching conditions), the effect of oxygen solubility on the mass balance calculations was assumed to be negligible compared to the overall slurry and oxygen flow rates as well as the rate of oxygen consumption in the autoclave.

- The vapour space in the autoclave is saturated with water, which means that the partial pressure of the water at specific operating conditions could be calculated to be approximately equal to the vapour pressure of pure water at the corresponding temperature. This, together with the assumption regarding the liquid-vapour mass transfer, furthermore allowed the calculation of the oxygen partial pressure and the molar composition of the vapour phase.

- The model does not incorporate thermodynamic models to evaluate the speciation in the different process streams or to check that solubility limits of metal salts are not exceeded. Only overall reactions were considered: dissolved metals were assumed to be present as cations with sulphate ions present to balance the charge of the cations, and the acid was assumed to undergo complete dissociation. In a study by Baldwin *et al.* (1995), similar assumptions yielded modelling results that were highly comparable with plant data.

- The heat capacity of the liquid component of the slurry and the heat capacity of the solid component of the slurry were assumed to remain constant over the investigated temperature ranges. The heat capacity of the liquid portion was estimated as the weighted average of the heat capacity of water and that of sulphuric acid. The heat capacity of the solid portion was estimated as the weighted average of the heat capacities of major phases in the solid phase, namely millerite (52.0 J/mol·℃; HSC Chemistry® v. 6.12), polydymite (121.9 J/mol·℃; HSC Chemistry® v. 6.12), digenite (158 J/mol·°C; Etienne, 1970, and Grønvold *et al.*, 1987), and covellite (43.7 J/mol·℃; HSC Chemistry® v. 6.12).

- The densities of the liquid portion and the solid portion of all the slurry streams were assumed to be approximately equal to the density of spent electrolyte and first stage residue, respectively.

- If the second stage leach and third stage leach are operated at different temperatures, heat transfer between the third autoclave compartment and the fourth autoclave compartment is negligible compared to the heats of reaction and external energy transfer due to cooling in the case of the third compartment and due to steam injection in the case of the fourth compartment.

- The standard heats of mixing and the standard heat of dissolution for oxygen were assumed to be negligible compared to the heats of reaction for the chemical reactions, as listed in Table 6.2.

- Heat loss from the autoclave to the environment was assumed to be primarily as a result of free convection and radiation heat losses to the environment.

- It was assumed that no chemical reactions occur in the auxiliary process units (the second stage slurry preparation tank, the flash recycle tank, the second stage leach discharge tank,

the second stage leach discharge thickener, and the third stage slurry preparation tank). Species were hence only considered to be consumed (reagents) or produced (products) in the autoclave compartments.

- Modelling done by performing overall mass and energy balances based on the determined rate expressions, without considering the particle size distribution of the autoclave feed and the residence time distribution of the respective autoclave compartments, yields sufficiently accurate results to achieve the objectives of this project. As discussed in Section 2.6, the population balance method and the segregated flow model are the two methods commonly used for highly accurate modelling of leaching reactors. The literature review did, however, reveal that models derived assuming perfectly mixed ideal reactors with a monosized feed yield results that are sufficient to develop an understanding of the effects of various process variables on the dynamic system behaviour and leaching performance. Ruiz *et al.* (2007) furthermore reported that the particle size distribution of the feed material did not significantly influence the rate of copper sulphide dissolution. It is also known that the first stage residue fed to high pressure leaching stages at the Western Platinum Ltd. BMR has a narrow size distribution with little variation. Furthermore, as reported by Dixon (1996), the segregated flow model will not be appropriate if leaching rates are not indicated by changes in particle sizes. The uncertainty regarding the solid surface area available for reactions to take place in the pressure leaching stages, the increased porosity as leaching progressed, and the presence of certain phases as discrete inclusions in the sulphide matrix were discussed in Section 5.3.1. These factors suggest that the segregated flow model will not yield accurate results for the leaching system under investigation.

  The population balance method has been shown to be sensitive to model parameters, such as residence time distribution and particle size distribution (Crundwell and Bryson, 1992; Crundwell, 1994). Because sufficiently accurate data for these parameters were not available, the application of the population balance method and the increased complexity it introduces could not be justified.

6.3 Modelling

6.3.1 General

The dynamic modelling of the autoclave was done by defining subsystems for which the mass and energy balances could be solved. Each of the auxiliary process units was defined as

subsystems, while the autoclave was divided into four subsystems according to the compartments in the autoclave. Each autoclave compartment was treated as a continuously stirred tank reactor in the model. The division of the second stage leach into the three constituting compartments is a more realistic representation compared to treating the entire second stage leach as a single reactor, since the dividing weirs in the autoclave prevent mixing of the slurry in the respective compartments. This also allowed estimation of percentage metal dissolution at the respective stages of leaching inside the autoclave. The nine defined subsystems, with the corresponding stream numbers, are shown in Appendix F.

The operating conditions that were assumed to be known or specified are the flow rates of the liquid and solid process streams entering the pressure leaching section of the plant (streams 1, 2, 3, 4, 18, 19, and 20) and the temperatures of streams 5 and 21. The flow rate of the flash recycle stream (stream 9) was selected as a further variable for which a fixed value could be specified. The aforementioned flow rates are used as manipulated variables on site to control the operating temperature and extents of leaching in the respective leaching stages. In order to estimate the flow rate of the oxygen streams fed to the autoclave (stream 10, 11, and 12), the theoretical amount of oxygen required for complete dissolution of copper and nickel was calculated for the case where all the nickel is present as NiS and all the copper is present as Cu_9S_5. A fixed percentage excess oxygen was selected to subsequently calculate the total oxygen feed rate to the autoclave, with the distribution of the oxygen between compartment two, compartment three, and compartment four to be specified by the user. The oxygen temperature can also be specified by the user.

The general form of the mass balance for any component *i* with a molecular weight of $M_{w,i}$ is shown in Equation 6.1:

$$\frac{dm_i}{dt} = \sum_{in} \dot{m}_{i,k} - \sum_{out} \dot{m}_{i,k} + V \cdot \sum \upsilon_{i,j} \cdot r_j \cdot M_{w,i} \qquad [6.1]$$

where m_i refers to the mass of component *i* in the system under consideration, $\dot{m}_{i,k}$ refers to the flow rate of component *i* in stream *k*, *V* refers to the system volume, $\upsilon_{i,j}$ is the stoichiometric coefficient of component *i* in reaction *j*, which has a reaction rate of r_j (molar amount per volume·time). For each subsystem, balances were performed for the total mass, the mass of solids, the mass of liquid, the mass of solid species (NiS, Ni_3S_4, Cu_9S_5, CuS, $Fe(OH)SO_4$, Rh_2S_3, Rh, RhO_2, RuS_2, Ru, RuO_2, Ir_2S_3, Ir, and IrO_2) and the mass of dissolved

species (Cu^{2+}, Ni^{2+}, Fe^{3+}, Rh^{3+}, Ru^{3+}, Ir^{3+}, and H_2SO_4). The general form of the energy balance for any particular system is given by Equation 6.2:

$$\frac{dT}{dt} = \frac{\dot{Q} - \dot{W}_{shaft} + \sum_{in} \dot{m}_{i,k} \cdot \hat{H}_{i,k} - \sum_{out} \dot{m}_{i,k} \cdot \hat{H}_{i,k} - V \cdot \sum r_j \cdot \Delta\hat{H}^{\circ}_{rxn,j}}{\sum m_i \cdot C_{p,i}} \qquad [6.2]$$

where T is the temperature of the system, $\dot{Q}$ and $\dot{W}_{shaft}$ are the rates at which energy is transferred to the system and work is done by the system, respectively, $\hat{H}_{i,k}$ is the specific enthalpy of species i in stream k relative to a selected reference state (reactant and product species at 25°C and 1 atm were selected as the reference state for all calculations in this study), and $\Delta\hat{H}^{\circ}_{rxn,j}$ is the standard heat of reaction j. m_i and $C_{p,i}$ are the mass of component i in the system and the heat capacity of component i, respectively. The standard heats of reactions were calculated using HSC Chemistry® version 6.12, and are summarised in Table 6.2. Due to insufficient thermodynamic data for iridium species, the heats of reaction for the reactions involving iridium species were estimated based on the heats of reaction for the comparable reactions involving rhodium and ruthenium species.

Table 6.2. Standard heats of reaction for the respective reactions occurring in the autoclave.

Reaction #	$\Delta\hat{H}^{\circ}_{rxn}$ **(kJ/mol)**
1	-283.8
2	-852.3
3	-6251.2
4	-756.1
5	-765.3
6	-83.1
7	-13685.6
8	-3110.2
9	-13814.1
10	-3142.3
11	-13800.0
12	-3140.0
13	-2037.6
14	-963.0
15	-15.4
16	-5117.3
17	-1139.8
18	16.7
19	-2000.0
20	-1150
21	10.0

The dynamic modelling required that ordinary differential equations, derived by applying Equation 6.1 and Equation 6.2 to the respective subsystems, had to be solved simultaneously. The initial values required to solve this set of differential equations were set equal to the steady state conditions at the initially defined operating conditions. The steady state conditions were determined by setting the left hand sides of Equation 6.1 and Equation 6.2 (the time derivatives of the system mass and temperature, respectively) equal to zero, resulting in algebraic equations to be solved.

6.3.2 Steady state conditions

The solution of the equations to determine the steady state operating conditions was done using the sequential modular approach. A schematic overview of the solution methodology is shown in Figure 6.2. The balances on the second stage slurry preparation tank were solved firstly to determine the flow rate of the fresh slurry feed to the flash recycle tank (stream 5).

In order to calculate the temperature, flow rate, and composition of stream 7, the mass transfer between the vapour and liquid phases in the flash recycle tank had to be determined, and the temperature and composition of the recycle stream (stream 9) had to be known. Based on the assumptions discussed in Section 6.2, it was assumed that the only mass transfer occurring between the liquid phase and the vapour phase in the flash recycle tank is the evaporation of water from the recycle stream. This implies that the vent stream leaving the first autoclave compartment pass through the recycle tank unaffected. Initial guessed values were assigned to the temperature of the recycle stream 9, the mass fraction solids in stream 9, and the composition of both the liquid and solid phases in stream 9.

The temperature, flow rate, and composition of stream 7, as calculated using the guessed properties of stream 9, were used as inputs to subsequently perform mass and energy balances on the first compartment of the autoclave. Because the compartments were treated as ideal continuously stirred tank reactors, the composition and temperature of stream AC1 (the slurry stream flowing from the first autoclave compartment to the second compartment) and the autoclave compartment content were assumed to be equal to that of stream 9. The mass balances required the extent of reaction to be calculated for the respective reactions.

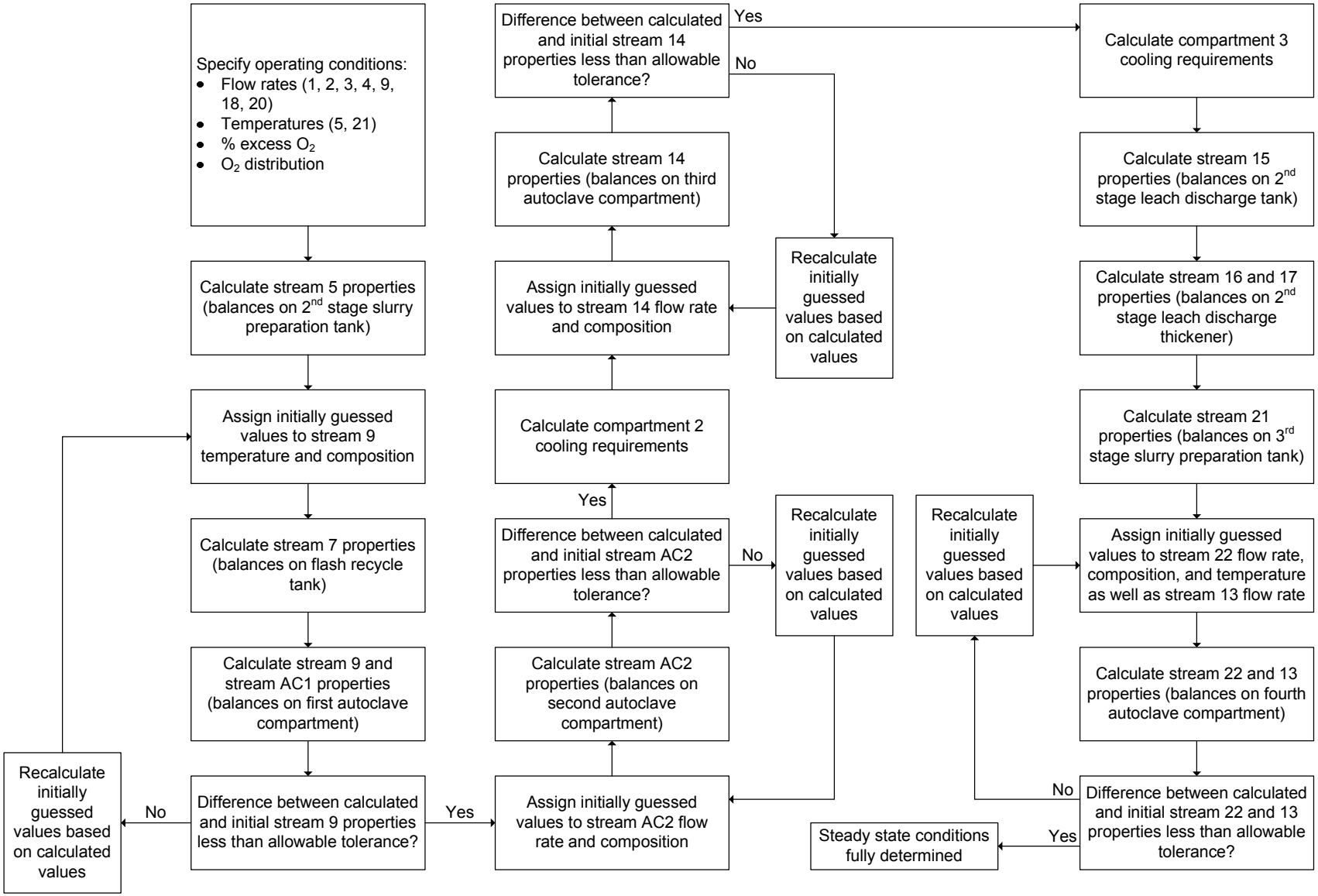

Figure 6.2. Schematic overview of the solution strategy followed to determine the steady state operating conditions of the autoclave.

A schematic overview of the solution strategy that was followed to calculate the extents of reactions is shown in Figure 6.3. This involved calculating the reaction rates for the assumed flow rates and compositions, which were used to calculate the amount of each of the solid components consumed (or produced, in cases where solid species are reaction products). The physical and stoichiometric limitations on the amount of each species that could be consumed or produced were applied. These amounts were used to estimate the extent of reaction for the respective reactions, where after the amounts of dissolved species produced (leaching product) or consumed (reagent) were calculated. For reactions where dissolved species rather than solid species were found to be the limiting reagent, the extent of reaction was recalculated. As a result, the extent of reaction for the reactions depending on dissolved species limited reactions had to be recalculated and it had to be verified that the recalculated extents of reactions were achievable given the calculated reaction rates.

The temperature of stream 9, the mass fraction solids in stream 9, and the composition of both the liquid and solid phases in stream 9 were subsequently calculated and compared to the initial guessed values. Successive substitution was used to iteratively calculate the properties of stream 9 until the user specified convergence criteria were met. These criteria were typically selected that the initial guessed values and the newly calculated values for any of the properties did not differ by more than 0.01%. To prevent the successive substitution method from incrementing the property value with too large steps, the initial values were recalculated using Equation 6.3:

$$x_{new}^{(j)} = x^{(j)} + f \cdot \left(x^{(j+1)} - x^{(j)}\right) \qquad [6.3]$$

where $x^{(j)}$ refers to the initially guessed value for any property x, $x^{(j+1)}$ indicates the recalculated value for the particular property, and $x_{new}^{(j)}$ represents the recalculated initial guess. The multiplication factor, f, was typically selected to be a value between 0.005 and 0.2, depending on the variable to be solved.

The mass and energy balances for the second and third compartments were subsequently solved in a similar fashion. The temperature of these two compartments was assumed to be the same as the temperature calculated for the first compartment. In the case of the second autoclave compartment, the flow rate and composition of stream AC2 (the slurry stream flowing from the second autoclave compartment to the third compartment) were guessed initially, while the flow rate and composition of stream 14 were guessed initially to solve the material balances for the third compartment. Once the material balances had been solved,

energy balances were used to determine the rate at which heat must be removed from the respective compartments to maintain a constant temperature; as discussed, heat removal can be varied by varying the flow rate of water through the cooling coils.

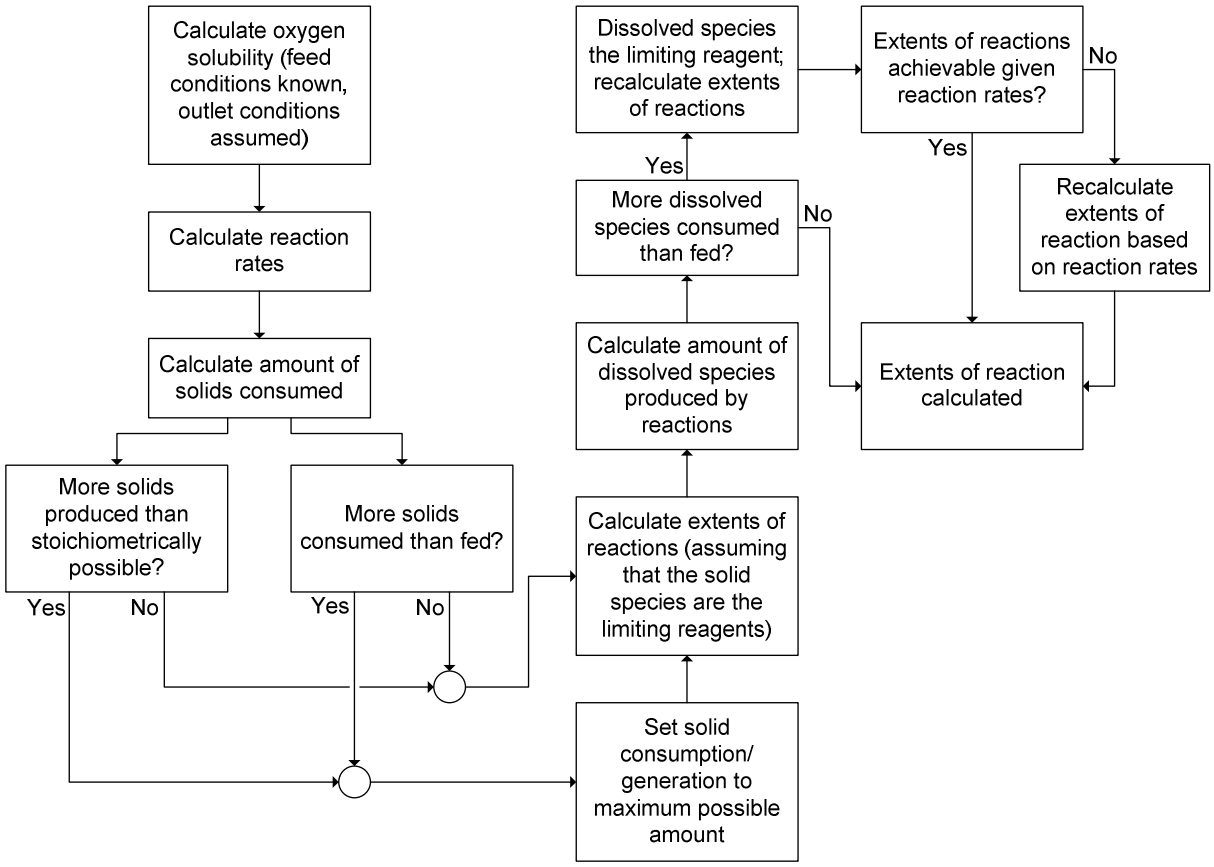

Figure 6.3. Schematic overview of the solution strategy followed to determine the extent of reaction for the respective reactions.

The material balances for the second stage leach discharge tank, the second stage leach discharge thickener, and the third stage slurry preparation tank were solved in succession, assuming that perfect solid-liquid separation is achieved in the thickener. The material and energy balances for the fourth autoclave compartment (third stage leach) were finally solved, again using successive substitution. The temperature, flow rate, and composition of the final discharge stream (stream 22) as well as the flow rate of the steam (stream 13) were assigned guessed values initially, and solved using an approach similar to that used for the autoclave compartments in the second stage leach. The flow rate of steam was calculated by performing an energy balance on the third stage leach based on the assumption that the third stage leach temperature is the same as that of the second stage leach. In cases where a negative steam flow rate was calculate (i.e. where energy had to be removed from the third stage leach to achieve the same temperature as in the second stage leach), the steam flow rate was set to zero and the actual operating temperature of the third stage leach subsequently calculated.

6.3.3 Dynamic modelling

The same assumptions regarding the mass transfer between the vapour and liquid phase in the recycle tank and the temperatures of the respective autoclave compartments discussed for the steady state calculations were applicable to the dynamic modelling. In addition, the dynamics of flow into and out of the respective unit operations had to be incorporated. No process control loops were implemented in the dynamic simulation. The flow rates of material from the auxiliary process units (slurry preparation tanks, flash recycle tank, discharge tank, and discharge thickener) were set proportional to the square root of the mass of slurry in the respective process units. The proportionality constants for the respective process units were calculated based on the initial steady state conditions and user-specified initial steady state volumes in the respective unit operations. Slurry flow between the different compartments in the first three compartments of the autoclave occurs by overflowing weirs with fixed heights between the compartments. Under typical operating conditions, the level in the autoclave is maintained at a level that allows continuous slurry flow between the different compartments. It was hence assumed that there is no accumulation of material in any of the autoclave compartments. The effect of oxygen flow rate on the pressure in the autoclave was not taken into account explicitly. The developed model requires the user to specify a constant operating pressure for the autoclave which will affect the oxygen solubility in the slurry, and hence the reaction rates. It was furthermore assumed that the volume of the vapour space inside the autoclave would remain approximately constant over time, and that there would hence not be accumulation of gaseous components in the vapour space at a constant pressure.

Unless a step change was introduced in the rate of heat removal from the second compartment, the rate of heat removal from the third compartment, or the rate of steam addition to the fourth autoclave compartment at a specific time instance, these variables were kept constant and equal to the rates calculated for the initial steady state conditions for the dynamic simulation. The temperatures of these autoclave compartments were thus not controlled during the dynamic simulation.

The resulting set of 217 ordinary differential equations, which are described in detail in Appendix F, were solved simultaneously making use of an ordinary differential solver in MATLAB. A compact disc containing an electronic copy of the MATLAB code is included in Appendix H.

6.4 Results

6.4.1 Mass balance verification

To verify that the sequential modular approach used to determine the steady state conditions in an iterative manner yielded consistent results, elemental species balances were performed for the overall process using the model calculated flow rates and compositions to check that atomic species were not generated or consumed in the process. Typical operating conditions used on site were assigned to the variables that had to be specified by the user for the model. A summary of the assigned values considered to represent typical operating conditions are listed in Table 6.3. The gangue (non-leachable) material in the solids was treated as an inert component. The liquid portion of the slurry was assumed to consists of the dissolved metals (Cu^{2+}, Ni^{2+}, Fe^{3+}, Rh^{3+}, Ru^{3+}, and Ir^{3+}), sulphuric acid, sulphate ions associated with the metal cations to balance the charge, and the remainder water. The mass flow rates and molar flow rates of the respective species in the different process streams entering and leaving the overall process are summarised in Table 6.4 and Table 6.5, respectively. The atomic species balance results are summarised inTable 6.6, indicating that the calculated steady state conditions are consistent.

Table 6.3. Typical operating conditions assigned to the model user inputs.

Variable	Value
Mass flow: first stage residue (stream 1 solids)	750 kg/h
Volumetric flow: spent electrolyte (stream 1 liquid)	500 l/h
Volumetric flow: spent electrolyte (stream 2)	2500 l/h
Volumetric flow: water (stream 3)	3500 l/h
Volumetric flow: sulphuric acid (stream 4)	28.6 l/h
Mass flow: recycle stream (stream 9)	14400 kg/h
Volumetric flow: spent electrolyte (stream 18)	400 l/h
Volumetric flow: water (stream 19)	800 l/h
Volumetric flow: sulphuric acid (stream 20)	0 l/h
Temperature: autoclave feed (stream 5)	35°C
Temperature: third stage leach feed (stream 21)	35°C
Oxygen excess	10%
Oxygen to compartment 2	55%
Oxygen to compartment 3	20%
Oxygen to compartment 4	25%
Temperature: oxygen (streams 10, 11, 12)	25°C
Temperature: steam (stream 13)	180°C
Autoclave pressure	7 bar

Table 6.4. Overall mass balance for the typical operating conditions specified in Table 6.3.

	IN (kg/h)												OUT (kg/h)			
	#1	#2	# 3	# 4	# 10	# 11	# 12	# 13	# 18	# 19	# 20	Total	#6	#16	#22	Total
H_2SO_4	45.0	225.0		50.4					36.0			356.4		138.6	35.6	174.3
Cu^{2+}	17.5	87.5							14.0			119.0		435.7	42.7	478.3
Ni^{2+}	16.5	82.5							13.2			112.2		180.6	27.9	208.5
Fe^{3+}	0.4	2.1							0.3			2.9		3.1	0.4	3.5
Rh^{3+}	0.0	0.1							0.0			0.2		0.1	0.3	0.4
Ru^{3+}	0.1	0.5							0.1			0.7		0.5	1.0	1.5
Ir^{3+}	0.0	0.1							0.0			0.2		0.1	0.2	0.3
NiS	148.8											148.8			0.5	0.5
Ni_3S_4	29.4											29.4			28.7	28.7
Cu_9S_5	338.1											338.1			0.0	0.0
CuS	170.3											170.3			26.9	26.9
$Fe(OH)SO_4$	1.7											1.7			0.0	0.0
Rh_2S_3	0.3											0.3			0.0	0.0
Rh	0.2											0.2			0.1	0.1
RhO_2												0.0			0.1	0.1
RuS_2	1.0											1.0			0.1	0.1
Ru	0.3											0.3			0.0	0.0
RuO_2												0.0			0.1	0.1
Ir_2S_3	0.1											0.1			0.0	0.0
Ir	0.1											0.1			0.0	0.0
IrO_2												0.0			0.0	0.0
O_2					227.9	82.9	103.6					414.4	36.1			35.1
SO_4^{2-}	54.8	273.8							43.8			372.3		963.0	113.1	1076.1
H_2O	455.7	2278.3	3500.0	2.1					364.5	800.0		7400.6	317.2	5961.6	1155.9	7434.7
Gangue	59.8											59.8			59.8	59.8
Total	1340.0	2950.0	3500.0	52.5	227.9	82.9	103.6	0.0	472.0	800.0	0.0	9528.9	352.3	7683.3	1493.3	9529.0

Table 6.5. Overall mole balance for the typical operating conditions specified in Table 6.3.

	IN (kmol/h)												OUT (kmol/h)			
	#1	#2	# 3	# 4	# 10	# 11	# 12	# 13	# 18	# 19	# 20	Total	#6	#16	#22	Total
H_2SO_4	0.459	2.294		0.514					0.367			3.634		1.414	0.363	1.777
Cu^{2+}	0.275	1.377							0.220			1.873		6.856	0.671	7.527
Ni^{2+}	0.281	1.405							0.225			1.911		3.077	0.474	3.551
Fe^{3+}	0.008	0.038							0.006			0.052		0.055	0.007	0.062
Rh^{3+}	0.0002	0.0012							0.0002			0.0017		0.0007	0.0031	0.0039
Ru^{3+}	0.0010	0.0052							0.0008			0.0071		0.0048	0.0098	0.0147
Ir^{3+}	0.0001	0.0006							0.0001			0.0008		0.0006	0.0010	0.0016
NiS	1.640											1.640			0.006	0.006
Ni_3S_4	0.096											0.096			0.094	0.094
Cu_9S_5	0.462											0.462			0.000	0.000
CuS	1.781											1.781			0.282	0.282
$Fe(OH)SO_4$	0.01007											0.01007			0.00004	0.00004
Rh_2S_3	0.00091											0.00091			0.00008	0.00008
Rh	0.00182											0.00182			0.00054	0.00054
RhO_2												0.00000			0.00073	0.00073
RuS_2	0.00623											0.00623			0.00048	0.00048
Ru	0.00267											0.00267			0.00009	0.00009
RuO_2												0.00000			0.00072	0.00072
Ir_2S_3	0.00030											0.00030			0.00002	0.00002
Ir	0.00041											0.00041			0.00008	0.00008
IrO_2												0.00000			0.00010	0.00010
O_2					7.12	2.59	3.24					12.95	1.10			1.10
SO_4^{2-}	0.57	2.85							0.46			3.88		10.02	1.18	11.20
H_2O	25.29	126.43	194.23	0.12				0.00	20.23	44.40	0.00	410.67	17.61	330.83	64.14	412.58

Table 6.6. Summary of the results achieved by performing atomic species balances for the overall process.

Atomic species	Total in (kmol/h)	Total out (kmol/h)
Cu	7.809E+00	7.809E+00
Ni	3.840E+00	3.840E+00
Fe	6.212E-02	6.212E-02
Rh	5.296E-03	5.296E-03
Ru	1.597E-02	1.597E-02
Ir	1.811E-03	1.811E-03
H	8.287E+02	8.287E+02
O	4.667E+02	4.667E+02
S	1.365E+01	1.364E+01

6.4.2 Steady state model predictions

As discussed in Section 6.1, the process variables that are typically manipulated to achieve the desired operational objectives include the leaching temperature, the leaching pressure, the autoclave residence time, and the acid concentration in the leach solution. The effect that varying these variables would have on the percentage metal dissolution was evaluated by means of the steady state model. The values of the user specified variables that were kept constant were assigned as listed in Table 6.3, while the values of the abovementioned process variables were varied around these listed values. The results are discussed with reference to the copper, nickel and rhodium behaviour in the second stage leach. Although the exact concentration and percentage dissolution values of the ruthenium and iridium differed from that of rhodium, the general trends and behaviour were observed to be the same.

For the range of conditions investigated, the rate of copper leaching in the first three compartments increased as the recycle rate was increased (and as the operating temperature decreased), irrespective of the pressure or acid feed rate. This can be ascribed to the increased oxygen partial pressure as well as the increased rate constants of reactions 4 and 5 at the lower temperatures. The percentage nickel dissolution achieved at various stages of leaching decreased with a decrease in the operating temperature, indicating that the decrease in the reaction rate constants had a more significant effect than the increase in the oxygen partial pressure.

For a given operating temperature, increasing the pressure also resulted in faster copper leaching and hence higher percentage copper dissolution, as shown in Figure 6.4. A distinct

change in the trend of the line representing the percentage copper leaching in the third compartment as the leaching temperature decreased can be observed. This change indicates the temperature below which Cu_9S_5 was completely leached, and where the copper dissolution in the third compartment proceeded solely by means of CuS leaching according to reaction 5. If leaching was performed at a pressure of 6 bar, for example, leaching at temperatures below approximately 110°C would result in complete leaching of Cu_9S_5 in the third compartment, with the remainder of the copper present as CuS. This corresponded to 75% copper dissolution; in the case of leaching performed at 7 bar, the corresponding temperature and percentage copper dissolution were 116°C and 84%, respectively.

Several factors contribute to the fact that the percentage copper dissolution differed at the instant when Cu_9S_5 leaching was completed for the different pressures. Reaction 5, which has a second order dependence on the dissolved oxygen concentration, proceeded faster relative to reaction 4 at higher pressures; it hence contributed more to the overall percentage copper dissolution by the time that Cu_9S_5 had dissolved completely.

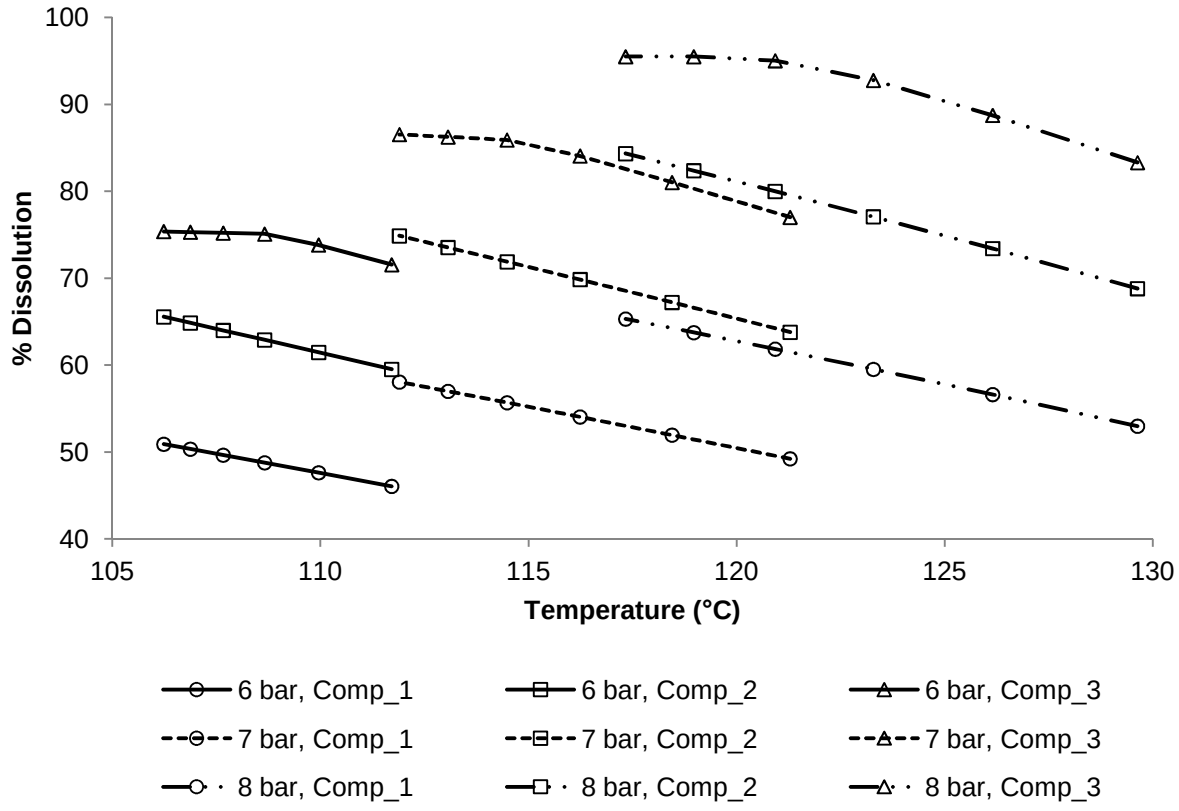

Figure 6.4. Percentage copper dissolution in the different compartments of the second stage leach as a function of leaching temperature and pressure (acid feed rate: 28.6 kg/h; solids feed rate: 825 kg/h).

The effect of temperature on the relative leaching rates depended on the total pressure and solution composition. The reaction rate constant of Cu_9S_5 leaching according to reaction 4 has a larger dependence on temperature than the rate of CuS leaching according to reaction 5 (activation energies of -26.2 kJ/mol and -5.9 kJ/mol, respectively). By performing the leaching at lower temperatures, the reaction 4 rate constant was increased to a larger extent than the reaction 5 rate constant. The lower temperature would, however, also result in a larger oxygen partial pressure which will enhance reaction 5 to a larger extent than reaction 4. By performing the leaching at a higher temperature, the rates of reactions 7, 9, and 11 were also increased. The cationic substitution reactions between the dissolved OPMs and the digenite hence contributed more to the dissolution of digenite than at the lower pressure and temperature conditions. As a result, less CuS was formed, and this allowed a larger portion of copper to be dissolved directly from Cu_9S_5 without producing CuS as an intermediate phase. Given the relative low concentrations of the OPMs, the contribution of this factor to the observed copper leaching behaviour was small compared to the contribution of the aforementioned factors.

Figure 6.5 shows that the rhodium dissolution decreased from compartment to compartment as long as digenite remained present in the leach solution (a negative percentage dissolution indicates that precipitation of rhodium occurred; a decrease in the percentage dissolution hence implies an increased precipitation). The effect of pressure on the rhodium precipitation was not as significant as that of temperature. The percentage dissolution decreased as the leaching temperature was increased due to the faster kinetics of the cationic substitution reactions. The slower kinetics of the digenite leaching according to reaction 4 at the higher operating temperature also allowed the cationic substitution reactions to make a larger contribution towards the digenite leaching, resulting in more OPM precipitation. Under conditions where rhodium dissolution had started to proceed, the increase in rhodium dissolution was proportional to the temperature, with the largest increase in rhodium leaching observed at the highest temperature. This was expected given the dependence of the rate of the chemical reaction controlled OPM leaching reactions on the temperature.

Depending on the values of several operating variables, it was possible for OPM leaching to commence earlier at decreased temperatures compared to increased temperatures, which resulted in a higher extent of OPM leaching at decreased temperatures despite the slower leaching rates. Comparing Figure 6.4 and Figure 6.5, it can be seen that leaching performed at

the low pressure conditions resulted in rhodium leaching to start occurring when only 75% copper dissolution had been achieved. This could be ascribed to the relative amounts of Cu_9S_5 and CuS and relative leaching rates of these two components, as discussed above.

In order to maximise Cu leaching and minimise OPM dissolution, leaching conditions must be selected such that the cationic substitution reactions are faster relative to reaction 4 to increase OPM precipitation and to reduce the formation of CuS as an intermediate species. The reaction rate of covellite leaching (reaction 5) must furthermore be enhanced relative to the leaching rate of digenite by reaction 4 by increasing the pressure, increasing the temperature, and decreasing the acid concentration to ensure that CuS leaching has progressed significantly by the time that the digenite leaching has been completed. The residence time will subsequently have to be adjusted accordingly so that limited time is available for OPM leaching to proceed.

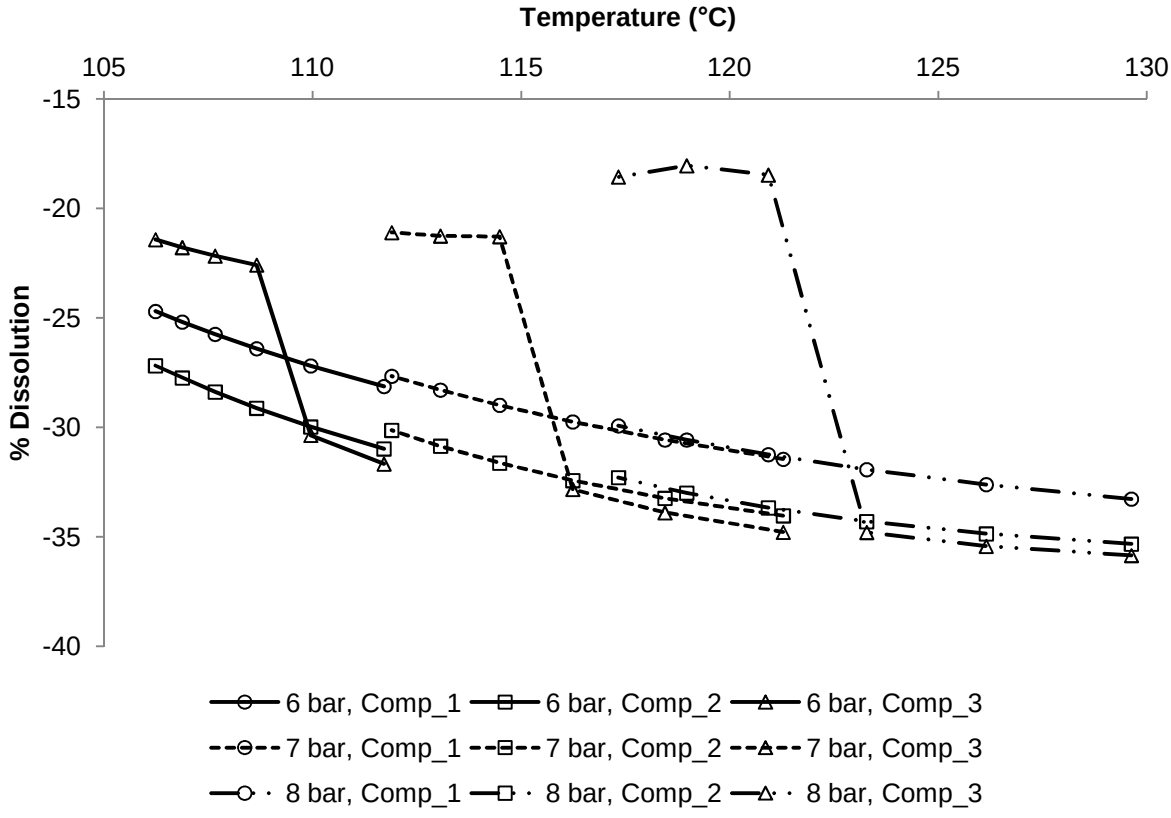

Figure 6.5. Percentage rhodium dissolution in the different compartments of the second stage leach as a function of leaching temperature and pressure (acid feed rate: 28.6 kg/h; solids feed rate: 825 kg/h).

The acid feed rate did not affect the nickel leaching noticeably, as would be expected given the fact that the rates of both reaction 2 and reaction 3 are only dependent on the dissolved oxygen content of the leach solution and not on the acid concentration. For the conditions illustrated in Figure 6.6, the acid feed rate had a limited effect on the percentage copper leaching achieved in the first two autoclave compartments, with the higher acid concentration achieving slightly higher copper dissolution at a particular temperature. In the third compartment, the temperature and percentage copper dissolution at which the rate of copper leaching started to decrease were different for the different acid feed rates. The high acid feed rate (34.3 kg/h) achieved complete digenite leaching at approximately 116°C, corresponding to 84% copper leaching, while the low acid feed rate (22.9 kg/h) achieved complete digenite leaching at approximately 113°C corresponding to 88% copper leaching. This confirmed the earlier observation regarding the relative amounts and leaching rates of digenite and covellite.

At higher acid feed rates, the rate of digenite leaching according to reaction 4 was higher relative to the leaching of covellite and the cationic substitution leaching reactions than at low acid feed rates. As a result, more CuS was produced as an intermediate product, while the rate of CuS leaching was slower relative to the rate of reaction 4, resulting in decreased copper dissolution by the time that digenite leaching had been completed. These were then also the conditions at which significant rhodium leaching started to occur for the respective acid feed rates, as shown in Figure 6.7. Less precipitation of rhodium was predicted when increasing the acid feed rate. This can be ascribed to the fact that the increased acid feed rate increased the leaching rate of reaction 4 relative to the rates of the cationic substitution reactions, effectively reducing the amount of digenite available for OPM precipitation. The precipitation reactions are furthermore dependent on the dissolved oxygen concentration, which decreases as the acid concentration is increased. The limited effect that acid concentration had on the OPM dissolution behaviour could also be ascribed to the effect that the acid concentration has on the oxygen solubility and leaching temperature.

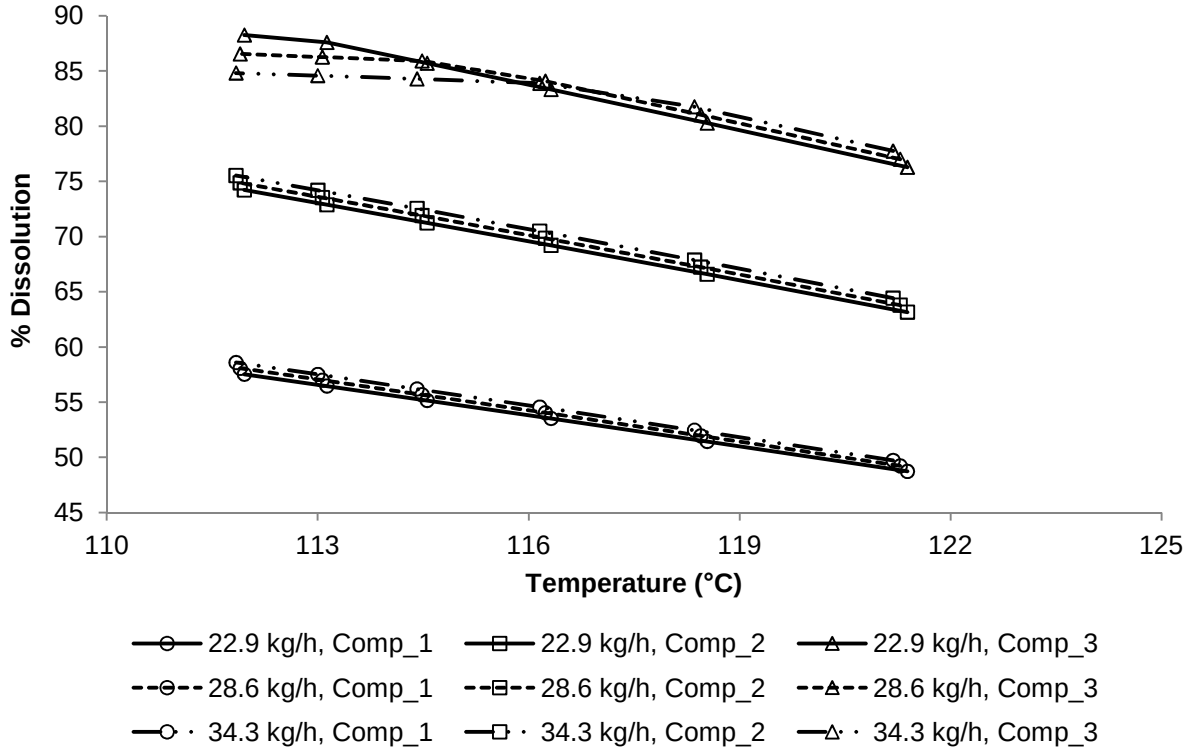

Figure 6.6. Percentage copper dissolution in the different compartments of the second stage leach as a function of leaching temperature and acid feed rate (pressure: 7 bar; solids feed rate: 675 kg/h).

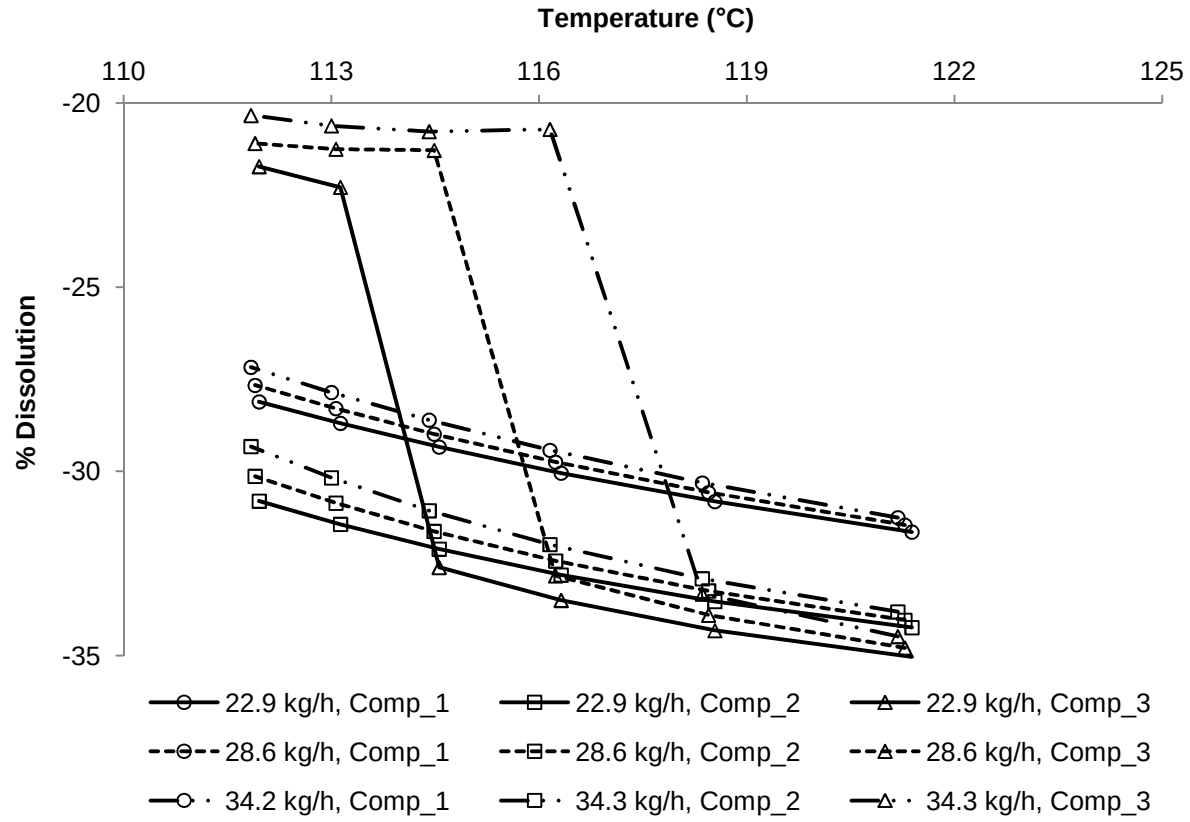

Figure 6.7. Percentage rhodium dissolution in the different compartments of the second stage leach as a function of leaching temperature and acid feed rate (pressure: 7 bar; solids feed rate: 675 kg/h).

The optimum operating conditions are dependent on the rates at which the respective feed streams enter the pressure leaching stage. With reference to Figure 6.4 and Figure 6.5, and for the feed rates specified for the particular analysis, the model suggested that leaching at a pressure of 8 bar and a temperature between 122°C and 124°C would yield the highest copper leaching and the lowest OPM dissolution. Increasing the temperature above this range would result in insufficient copper leaching, while lower temperatures would result in excessive OPM dissolution. Lower pressures would not allow sufficient copper leaching to occur before OPM dissolution started to proceed. Figure 6.6 and Figure 6.7 suggest that the optimum leaching temperature would decrease if the acid feed rate was decreased at a specific pressure. While the acid concentration in solution should be sufficient to sustain the acid dependent base metal leaching reactions, decreasing the acid feed rate could result in a higher percentage copper leaching when OPM dissolution start to proceed.

The effect that variations in the solid feed rate had on the leaching behaviour of copper is shown in Figure 6.8. The percentage copper that dissolved decreased with an increase in solids feed rate, mainly because the percentage dissolution was calculated based on the larger amount of material fed. There was a slight decrease in the amount of copper leached in the first compartment at the higher solids feed rate, and this could be ascribed to the shorter residence time associated with the larger feed rate. The copper leaching rate was not affected significantly because the rates of reactions 4 and 5, which contribute the most to the copper leaching, were not dependent on the available solid surface area. For the low solids feed rate, complete copper dissolution was achieved in the second compartment for temperatures below 121°C. This resulted in rhodium dissolution starting to occur in the second compartment, as shown in Figure 6.9.

The increased solid surface area resulted in faster rhodium precipitation for the increased solids feed rate, resulting in comparable percentage rhodium dissolution values in the first compartment. The percentage dissolution achieved after leaching in the second and third leaching stages was governed by the copper behaviour. The rate and extent of nickel leaching increased with the increased solid flow rate, since the rates of the nickel dissolution reactions were determined to be chemical reaction controlled, and hence dependent on the available solid surface area.

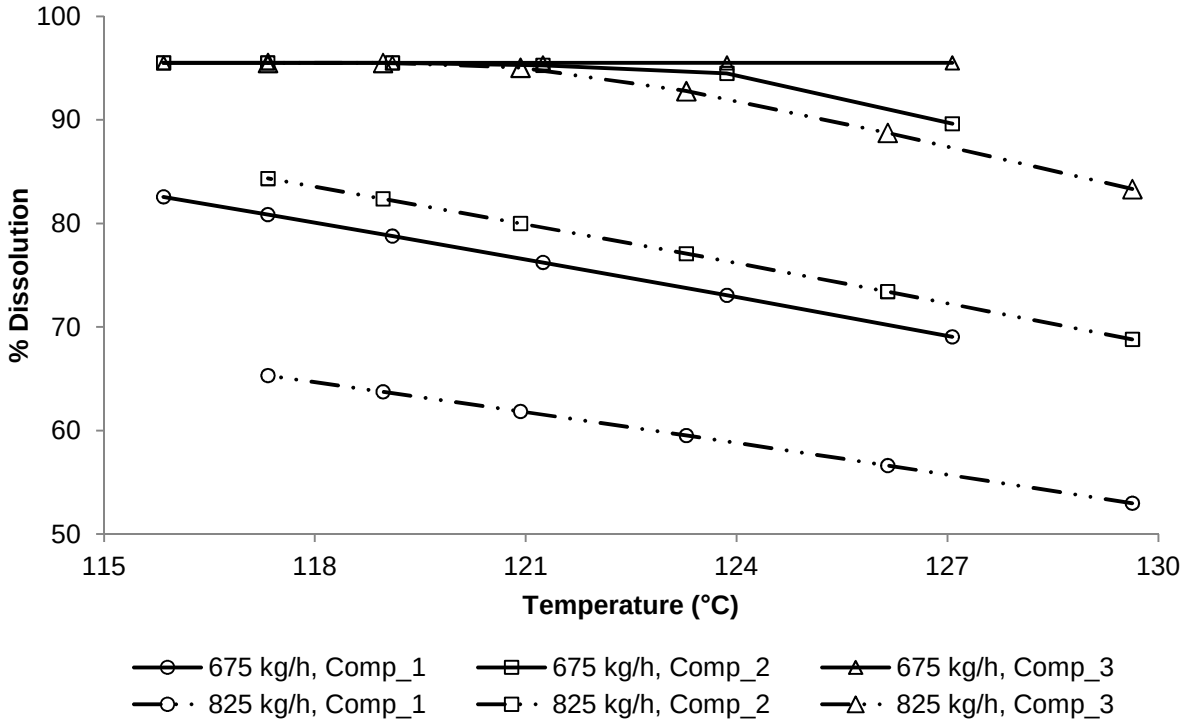

Figure 6.8. Percentage copper dissolution in the different compartments of the second stage leach as a function of leaching temperature and solids feed rate (pressure: 8 bar; acid feed rate: 28.6 kg/h).

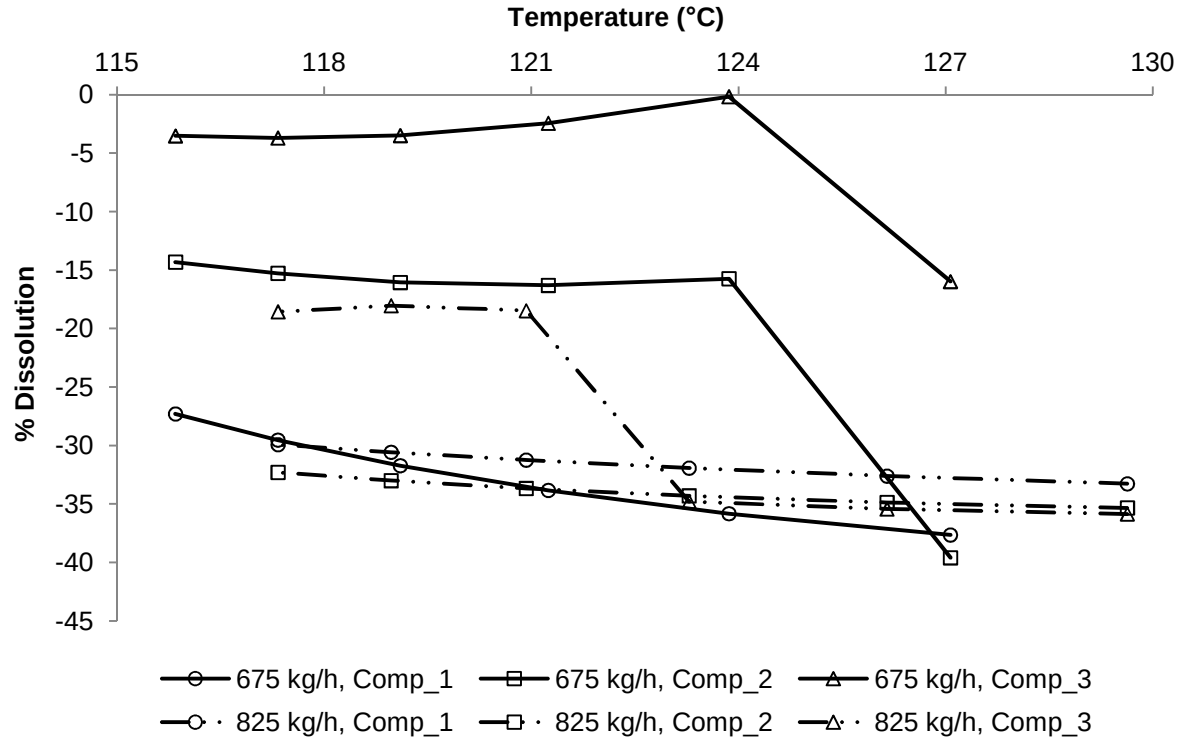

Figure 6.9. Percentage rhodium dissolution in the different compartments of the second stage leach as a function of leaching temperature and solid feed rate (pressure: 8 bar; acid feed rate: 28.6 kg/h).

The general trends and effects observed for the second stage leach were also valid for the third stage leach. There are, in general, numerous interactions between the various variables. For the third stage leach, the performance of the second stage leach will also be important in determining the appropriate operating conditions given the dependency of the third stage leach on the composition and flow rate of the second stage leach residue. For the range of conditions investigated, achieving metal and acid concentrations in the third stage leach solution similar to that produced by the second stage leach proved challenging. In most instances, more than 90% of the copper and 70% of the nickel in the first stage leach residue were leached in the second stage leach. This resulted in a small amount of second stage leach residue with relatively low base metal contents. To achieve high base metal concentrations in the third stage leach solution, the flow rates of the liquid components to the third stage leach had to be kept small, which subsequently resulted in long residence times and high extents of OPM dissolution in the third stage leach. The process flow sheet does, however, make provision for the third stage leach solution to be recycled to the second stage leach. The primary objective when selecting the operating conditions for the third stage leach should hence be to achieve the desired base metal leaching while minimising OPM dissolution rather than producing a leach solution that can be sent to the downstream processing units. The composition of the third stage leach solution recycled to the second stage leach would be similar to the composition of the spent electrolyte.

6.4.3 Modelling of dynamic behaviour

Validation of the accuracy of the dynamic model was not possible due to limited availability of online analysis of different process streams. Interdependencies of process variables that typically vary continuously and simultaneously would furthermore make deconvolution of available data challenging, implying that the effect of changes in specific process variables on the pressure leaching performance would be difficult to quantify. The observed responses achieved with the dynamic model did, however, conform to the process behaviour expected based on the results discussed in Section 4 and Section 5.5. The predicted response of the temperature and composition in the different compartments to changes in the acid feed rate shown in Figure 6.10 is discussed in more detail to illustrate this conformity, while the dynamic responses of the autoclave performance to changes in the solids feed rate (Figure 6.11), the flash recycle rate (Figure 6.11), and the pressure (Figure 6.13) are also shown to illustrate the results achieved with the dynamic model.

An increase in the acid feed rate resulted in a slight increase in the copper concentration in the first compartment, indicating that the effect of the increase in the acid concentration on the rate of reaction 4 was more significant than the effect of the reduced oxygen solubility as a result of the higher acid concentration. Leaching of covellite according to reaction 5, which contributes significantly to the increase in the dissolved copper concentration once digenite has been leached, is only dependent on the dissolved oxygen concentration and not on the acid concentration. As a result, the copper concentration in the second and third compartments, where digenite had leached completely, decreased due to the slower covellite leaching rate resulting from the reduced oxygen solubility. The smaller extent of this exothermic reaction also resulted in a decrease in the temperature of these two compartments. The relatively slow dynamics of the process are illustrated by the fact that the that the process requires in excess of 10 hours to achieve steady state conditions after modification of the operating conditions.

The rhodium concentration in the first autoclave compartment increased as a result of the increase in the acid feed rate. This can be ascribed to the change in the rate of reaction 7 relative to the rate of reaction 4 as well as the dependence of the precipitation reactions on the dissolved oxygen concentration, as discussed in section 3.1. The increase in the rhodium concentration from the first compartment to the second compartment was smaller for the higher acid feed rate, indicating that the leaching of rhodium phases proceeded at a slower rate. This was due to the fact that the rates of the rhodium leaching reactions are not dependent on the acid concentration but the rates of Rh and Rh_2S_3 dissolution are dependent on the dissolved oxygen concentration. The rates of the OPM leaching reactions have also been shown to be highly dependent on the leaching temperature; the decrease in the leaching temperature in the second compartment thus further decreased the rate of OPM leaching. This decrease in the OPM leaching rate as a result of the reduced leaching temperature also resulted in the decrease in the rhodium concentration in the third autoclave compartment.

The amount of covellite that had not been leached in the second stage leach increased because of the slower covellite leaching reaction at the higher acid concentrations. As a result, the extent of the covellite leaching reaction (reaction 4) in the third stage leach was larger, resulting in an increase in the both the copper concentration and the temperature in the fourth compartment. The higher temperature also resulted in faster rhodium leaching and hence higher dissolved rhodium concentrations in the fourth compartment. Decreasing the flow rate

of the acid feed stream had the opposite effects on the temperatures and compositions in the different compartments.

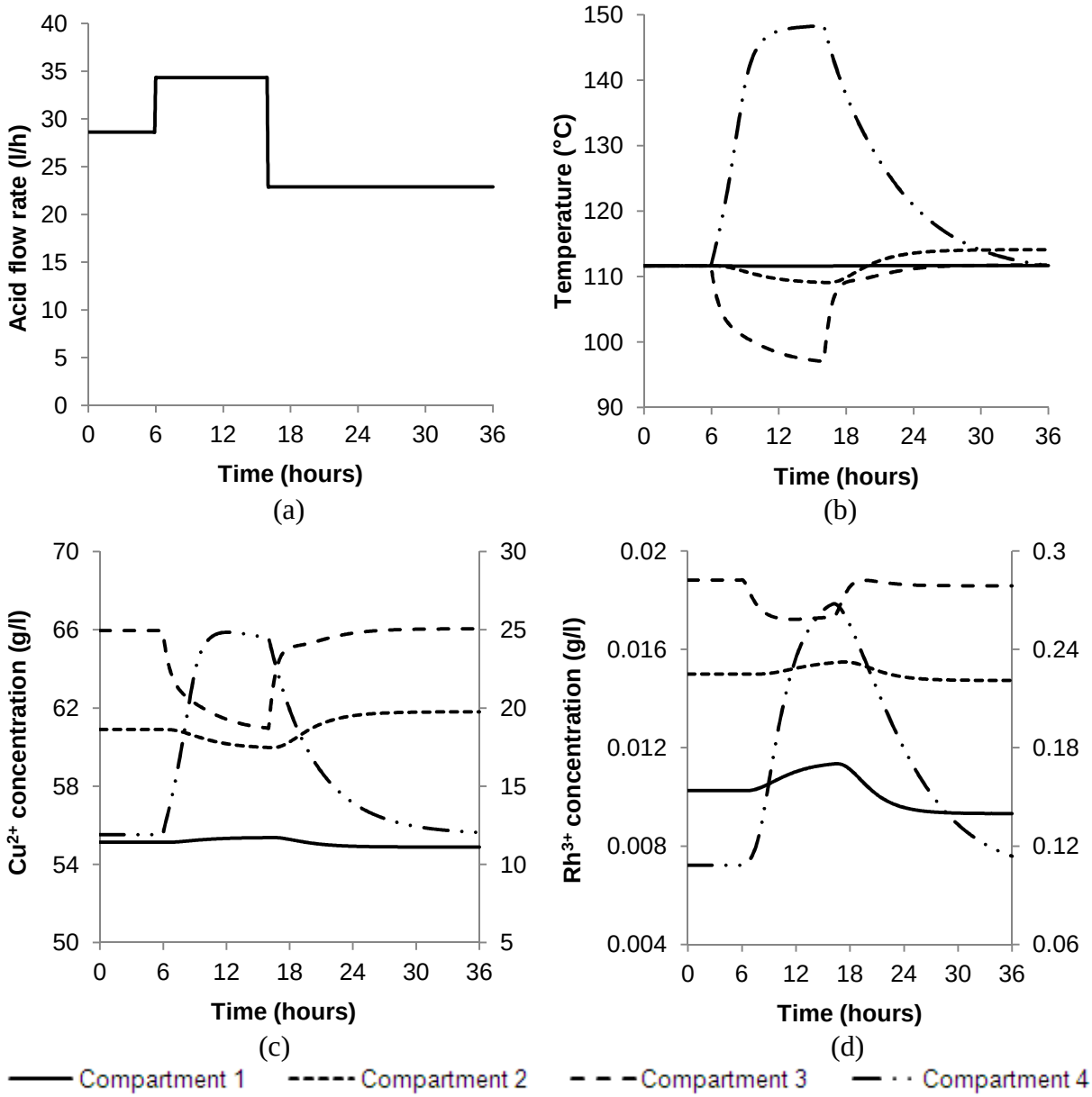

Figure 6.10. Dynamic response of (b) the temperature, (c) dissolved copper concentration, and (d) the dissolved rhodium concentration in the respective autoclave compartments for step changes in the acid feed rate (a). Data for the fourth compartment are shown on the secondary y-axes in (c) and (d).

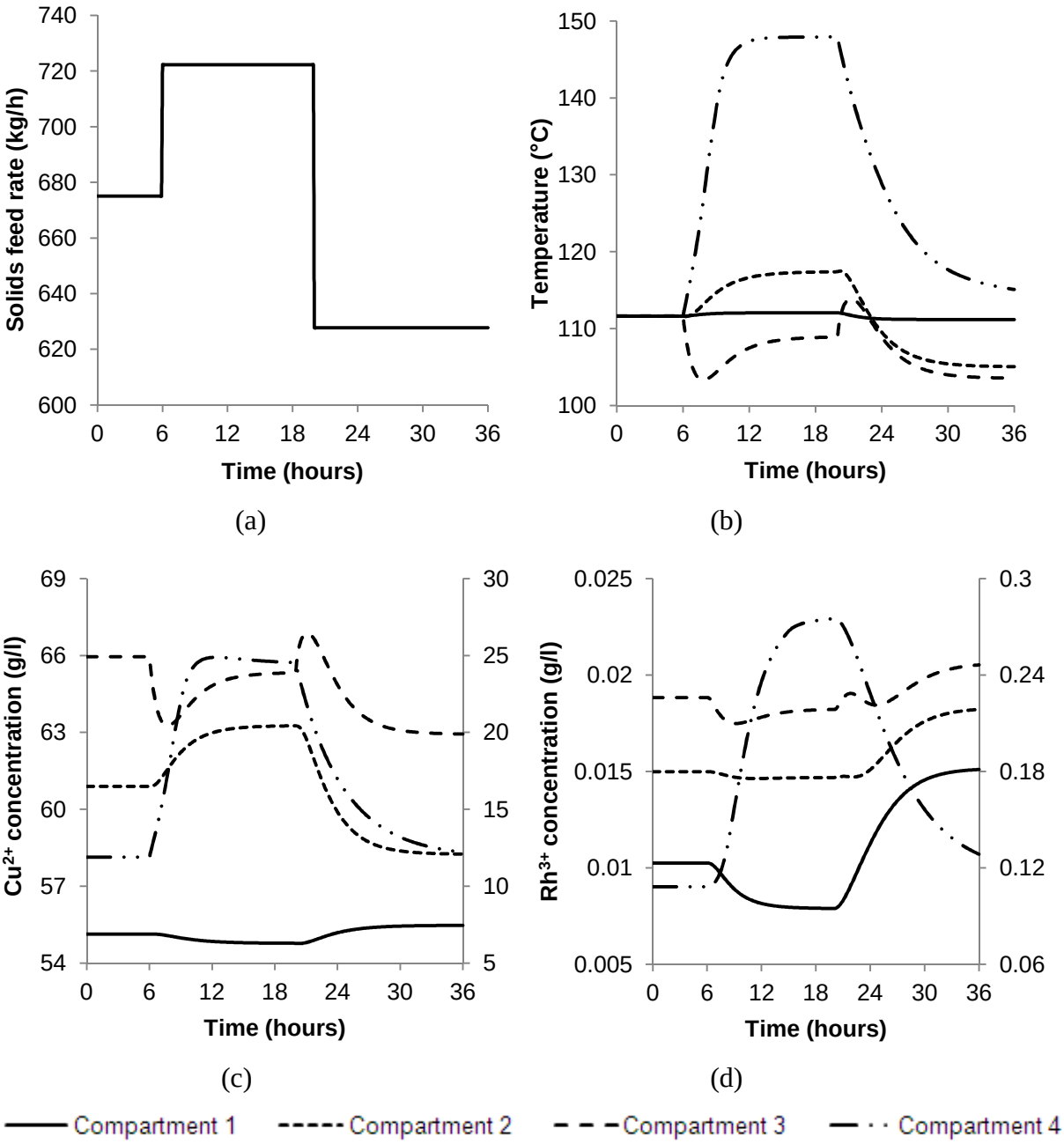

Figure 6.11. Dynamic response of (b) the temperature, (c) dissolved copper concentration, and (d) the dissolved rhodium concentration in the respective autoclave compartments for step changes in the solids feed rate (a). Data for the fourth compartment are shown on the secondary y-axes in (c) and (d).

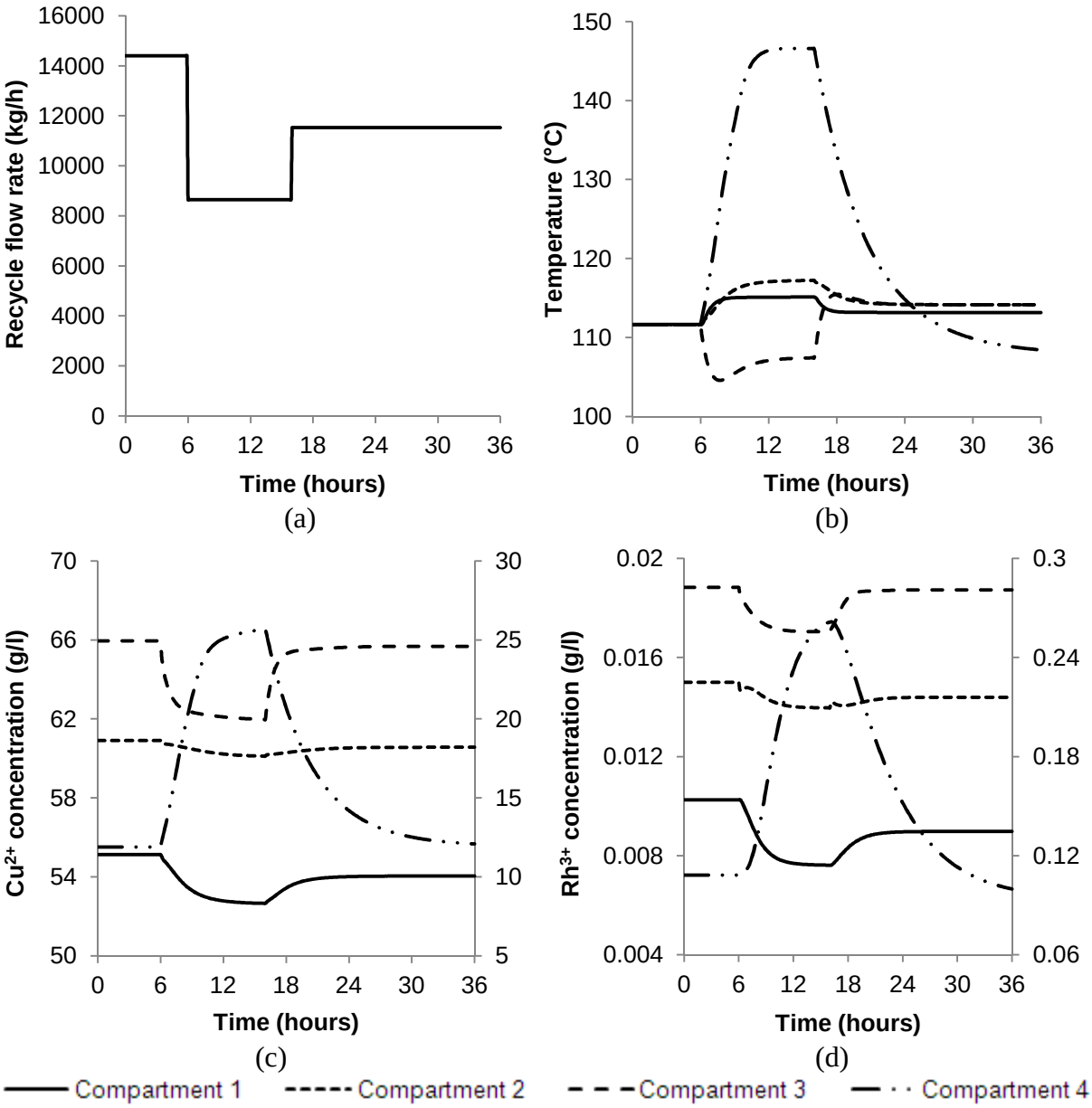

Figure 6.12. Dynamic response of (b) the temperature, (c) dissolved copper concentration, and (d) the dissolved rhodium concentration in the respective autoclave compartments for step changes in the recycle stream flow rate (a). Data for the fourth compartment are shown on the secondary y-axes in (c) and (d).

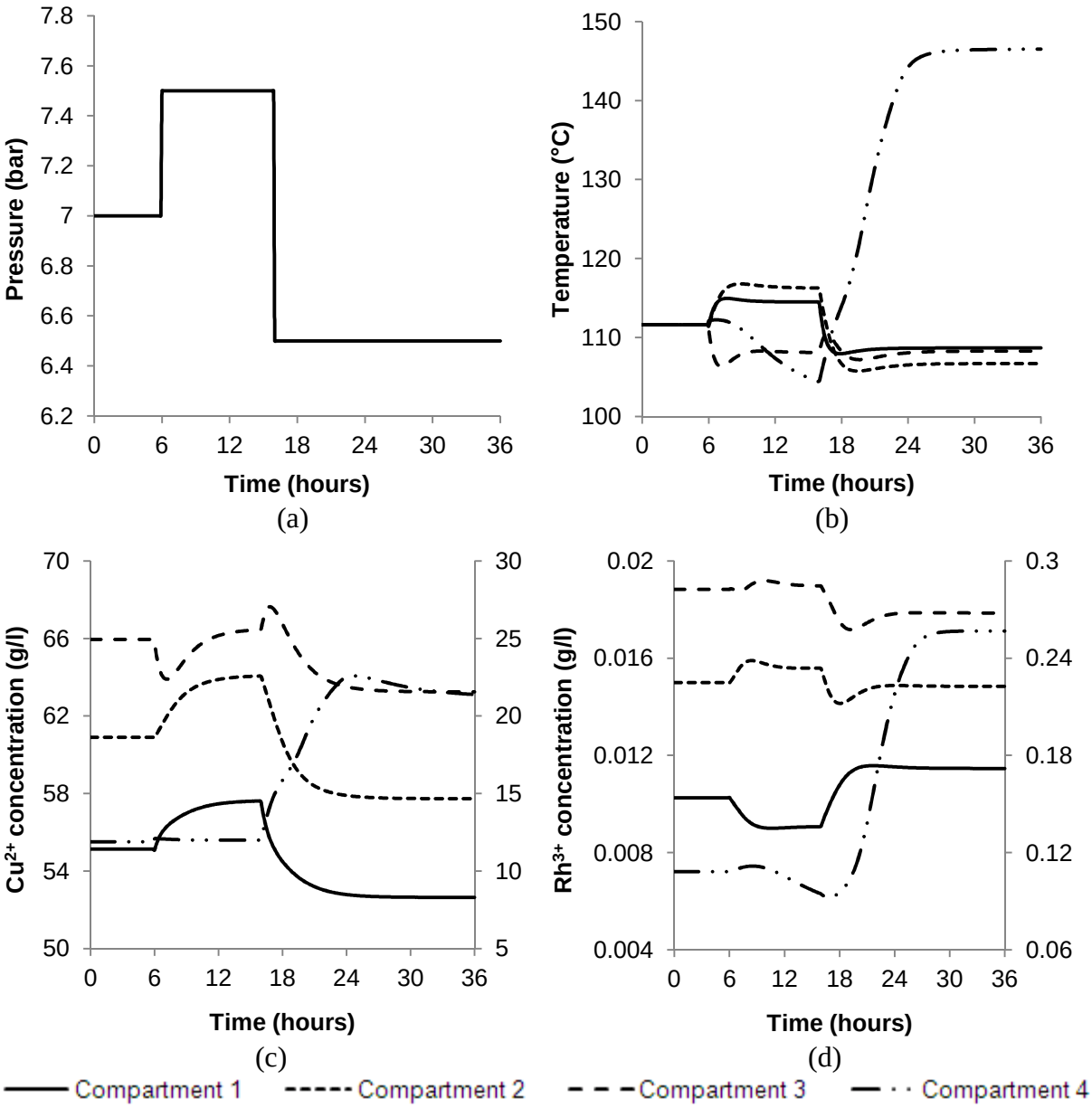

Figure 6.13. Dynamic response of (b) the temperature, (c) dissolved copper concentration, and (d) the dissolved rhodium concentration in the respective autoclave compartments for step changes in the autoclave pressure (a). Data for the fourth compartment are shown on the secondary y-axes in (c) and (d).

7 CONCLUSIONS AND RECOMMENDATIONS

The original scientific contribution of the work, as outlined in Section 1.3, has been illustrated. The calculation of the reaction rate constants and activation energies for the reactions explaining OPM precipitation and OPM leaching is a novel contribution, as is the incorporation of the OPM precipitation and leaching reactions in a model to predict the dynamic response of the leach solution composition, including OPM concentrations, to changes in key process variables.

The objectives of the project outlined in Section 1.2, were achieved. The conclusions are summarised in accordance with the specified objectives.

7.1 Effect of operating conditions on leaching behaviour

Experimental data were analysed to evaluate the effects that temperature, pressure, acid concentration, and solid to liquid ratio have on the leaching behaviour of the first stage leach residue. Under the evaluated conditions, the mass transfer of oxygen from the gaseous phase to the liquid phase limited the rate of the copper dissolution reactions. Given the relatively fast gas to liquid mass transfer achieved in the experimental setup compared with larger scale equipment, the copper dissolution reactions are likely to be oxygen mass transfer limited in larger scale autoclaves. The rates of the remainder of the reactions were determined to be chemical reaction limited.

The set of experimental conditions used for the first experimental designed illustrated the importance of oxygen availability for copper leaching to proceed. At a leaching temperature of 144°C and a total pressure of 5 bar, which corresponds to an oxygen partial pressure of approximately 0.96 bar, only 60-65% copper dissolution was achieved after six hours of leaching. Copper dissolution in excess of 90% was achieved when the pressure (and hence the oxygen partial pressure) was increased by 2 bar; this was due to the increased oxygen solubility in the leach solution. Although the increased pressure also resulted in higher OPM dissolution, the majority of the OPM dissolution occurred during the later part of the experiment after copper leaching had been completed. Under these conditions, the OPM leaching reactions were limited by oxygen availability during the initial leaching stages while copper leaching proceeded; during the latter stages, the acid concentration had a larger effect on the OPM leaching reactions.

The revised experimental conditions used for the second experimental design yielded results that allowed a better understanding of the leaching behaviour at conditions comparable to that typically employed on site. It also confirmed several conclusions drawn from the first set of experiments, such as the preferential leaching of copper sulphide phases during the initial leaching stages. It was furthermore determined that an optimum acid concentration existed, which was dependent on the values of the remainder of the process variables. Increasing the acid concentration enhanced the rate at which acid dependent reactions proceeded; it did, however, also lead to reduced oxygen solubility which was detrimental to oxygen dependent reactions. The effect of solution solids content on the dissolution of copper could be inferred from the rhodium leaching behaviour, given the dependence of the OPM precipitation period on the copper leaching rate.

Of the process variables investigated, the initial acid concentration had the largest effect on the copper leaching rate, while temperature was identified as the process variable with the largest effect on the OPM leaching rate. The percentage copper dissolution achieved during the four experiments that were performed with a slurry solids content of 80 g/ℓ and an initial sulphuric acid concentration of 140 g/ℓ were 13.4 percentage points higher on average than during the four experiments performed with an initial sulphuric acid concentration of 165 g/ℓ. In the case of OPM leaching, the average percentage rhodium dissolution was 25.3 percentage points higher for the eight tests performed at 130°C than for the eight tests performed at 116°C. An analysis of variance was performed to statistically verify the qualitative observations regarding the effects of the respective process variables. The analysis of variance furthermore showed that interaction between the slurry solid content and the leaching pressure and between the slurry solids content and the initial acid concentration were the only two significant interactions affecting rhodium dissolution; no interaction effect was found significant for copper, ruthenium, or iridium dissolution. In general, the dissolution of the different OPMs showed similar responses to changes in the different process variables, while the dissolution of palladium did not exhibit the same behaviour as the OPMs. In general, palladium dissolution proceeded from a later point in time than the OPMs during the batch tests.

7.2 Leaching reactions and kinetics

A set of reactions has been proposed to describe the behaviour of base metals and OPMs in the high pressure sulphuric acid/oxygen leaching environment. The precipitation of OPMs during the initial leaching stages when copper leaching had not proceeded to a significant

extent could be ascribed to cation exchange reactions similar to the cementation and metathesis reactions leading to copper precipitation in the first stage leach.

The reaction rate constants and activation energies determined by means of the method of least squares allowed the realistic prediction of metal concentrations in solution as a function of the leaching time taking into account the effect of the leaching temperature, leaching pressure, slurry solids content, and the acid concentration. It furthermore supported the qualitative observations regarding relative leaching rates and rate controlling mechanisms. The activation energies of -26.2 kJ/mol and -5.9 kJ/mol calculated for the digenite and covellite leaching reactions, respectively, confirmed that the rates of these reactions were mass transfer controlled. The leaching rates of the OPM phases were the fastest for the sulphide phases, then the metallic phases, and finally the oxide phases. The leaching reactions that contributed mostly to the increase in the dissolved OPM concentration changed as leaching progressed, with the fast leaching of sulphide phases dominating the initial leaching followed by the slower leaching of the OPMs and OPM oxides once the sulphide phases had been completely leached. Leaching of the OPM oxide phases showed the largest dependence on the leaching temperature, with activation energies of 116.2 kJ/mol, 134.1 kJ/mol, and 209.2 kJ/mol for rhodium oxide, ruthenium oxide, and iridium oxide, respectively.

7.3 Modelling of the second stage pressure leach

In general, the interaction between the temperature, acid concentration, pressure, and oxygen solubility makes the prediction of the autoclave performance challenging. The model that was developed allows the prediction of the operating temperature as well as the compositions of both the solid and the liquid phases in the different autoclave compartments as a function of the flow rates of the water, spent electrolyte, acid, first stage residue, and oxygen, as well as the recycle stream sent to the flash recycle tank and the autoclave pressure.

While the actual values predicted by the steady state model and dynamic model might differ from the actual plant data under certain operating conditions, the models yield results that can effectively be used to evaluate the effect of changing process conditions on the overall process performance and to assist in the selection of optimum operating conditions. In principle, the knowledge about the pressure leaching process encompassed in the model is of primary importance. It has been illustrated how interdependencies between different process variables could be determined and an improved understanding of the process can be developed by means of the process model. The importance of the relative leaching rates of

digenite and covellite was, for example, illustrated by generating model predictions for different operation scenarios.

7.4 Recommendations

The chemical reactions proposed in this study are overall reactions that disregard the speciation and complex formation in the leach solution. The speciation of the PGM compounds, in particular, is complex. The reactions can be refined if the exact speciation of the PGM compounds in the sulphate leaching system can be determined reliably.

The effects that variations in the composition of the process feed streams would have on the autoclave performance have not been determined explicitly. While the developed model allows the prediction of the autoclave performance for different feed compositions, the applicability of the model to feed streams with compositions significantly different to those used in this study has not been verified. Experimental studies to evaluate the effect that variations in the feed streams would have on the leaching behaviour would be useful.

The effect that the dissolved iron concentration has on the leaching system was taken into account empirically. A detailed study regarding the effect of dissolved iron concentration on the leaching behaviour will be required to quantify the potential catalytic effect of dissolved iron on the leaching reactions.

The rate of oxygen mass transfer was not determined for the autoclave, and was hence only included empirically in the developed model. The rate of mass transfer between the gaseous phase and the liquid phase is reactor specific and a more fundamentally correct model could only be obtained by analysis of the actual equipment on site or a dynamically similar reactor vessel. The rate of mass transfer from the gaseous phase to the liquid phase is most likely to govern the copper leaching rate.

The developed model is a simplified presentation of the autoclave. Important site specific data, e.g. the autoclave residence time distribution and the average particle size distribution of the solids feed, will have to be determined by extensive data collection initiatives if more rigorous models are to be developed and compared to the basic model developed as part of this project.

Evaluating the accuracy of the dynamic model is challenging given the absence of online analytical equipment that would allow regular composition information to be determined, and hence evaluation of the effect of changes in process variables on the product quality. Online instrumentation would be important if the model is to be refined further.

The developed model not only allows for the evaluation of different control strategies, but it can also be used to evaluate the effects that variations in process variables would have on the autoclave performance and to assist with operator training. Model predictive control strategies, in particular, could contribute significantly to improve the operation of the pressure leaching stages.

8 REFERENCES

Abovskaya, N.V., Simanova, S.A., Boichinova, E.S., and Fedorov, M.K., 2006. Sorption recovery of sulphate complexes of iridium on hydrated zirconium dioxide. *Russian Journal of Applied Chemistry*, 79(4):563-567

Aktas, S., 2011. Rhodium recovery from rhodium-containing waste rinsing water via cementation using zinc powder. *Hydrometallurgy*, 106:71-75

Aleksenko, S.S., Gumenyuk, A.P., Mushtakova, S.P., and Timerbaev, A.R., 2001. Speciation studies by capillary electrophoresis – distribution of rhodium(III) complexed forms in acidic media. *Fresenius Journal of Analytical Chemistry*, 370:865-871

American Elements, 2012. *Iridium Sulfate*, http://www.americanelements.com/irs.html, Accessed: 17 January 2012

Baghalha, M., Papangelakis, V.G., and Curlook, W., 2007. Factors affecting the leachability of Ni/Co/Cu slags at high temperature. *Hydrometallurgy*, 85:42-52

Baldwin, S.A., Demopoulos, G.P., and Papangelakis, V.G., 1995. Mathematical modelling of the zinc pressure leach process. *Metallurgical and Materials Transactions B*, 26B:1035-1047

Belyaev, A.V., Fedotov, M.A., and Vorob'eva, S.N., 2009. ^{103}Rh and ^{17}O NMR study of oligomer rhodium(III) sulfates in aqueous solutions. *Russian Journal of Coordination Chemistry*, 35(11):824-829

Bernardis, F.L., Grant, R.A., and Sherrington, D.C., 2005. A review of methods of separation of the platinum-group metals through chloro-complexes. *Reactive & Functional Polymers*, 65:205-217

Bircumshaw, L., 2008. Base Metal Refinery Process Overview. *Lonmin Internal Communication*, 16 April 2008

Burkin, A.R., 2001. *Chemical hydrometallurgy: theory and principles*, Imperial College Press, London, United Kingdom

Buswell, A.M., Bradshaw, D.J., Harris, P.J., and Ekmekci, Z., 2002. The use of electrochemical measurements in the flotation of a platinum group mineral (PGM) bearing ore. *Minerals Engineering*, 15:395-404

Cheng, C.Y., and Lawson, F., 1991. The kinetics of leaching chalcocite in acidic oxygenated sulphate-chloride solutions. *Hydrometallurgy*, 27:249-268

Cheng, T.C., 1994. Measurement of oxygen mass transfer rates in a laboratory batch pressure reaction. *MEng Thesis*, Department of Mining and Metallurgical Engineering, McGill University, Montreal, Canada

Choo, W.L., Jeffrey, M.I., and Robertson, S.G., 2006. Analysis of leaching and cementation reaction kinetics: Correcting for volume changes in laboratory studies. *Hydrometallurgy*, 82:110-116

Chu, Y.C., and Lawson, F., 1991. The kinetics of leaching chalcocite in acidic oxygenated sulphate-chloride solutions. *Hydrometallurgy*, 27:249-268

Clément, C., Tyroler, P.M., Krause, E., and Nissen, N.C., 1992. Total oxidative leaching of Cu_2S-containing residue at Inco Ltd.'s copper refinery: the effect of morphology and viscosity of basic copper sulphate on the leaching of cupric sulphide. *Hydrometallurgy*, 29(1-3):335-356

Cramer, L.A., 2001. The extractive metallurgy of South Africa's platinum ores. *Journal of Minerals, Metals and Materials Society*, October 2001, p.14-18

Crundwell, F.K., 1994. Micro-mixing in continuous particulate reactors. *Chemical Engineering Science*, 49(23):3887-3896

Crundwell, F.K., 1995. Progress in the mathematical modelling of leaching reactors. *Hydrometallurgy*, 39:321-335

Crundwell, F.K., 2005. The leaching number: its definition and use in determining the performance of leaching reactors and autoclaves. *Minerals Engineering*, 18:1315-1324

Crundwell, F.K., and Bryson, A.W., 1992. The modelling of particulate leaching reactors – the population balance approach. *Hydrometallurgy*, 29:275-295

Deglon, D.A., 2005. The effect of egitation on the flotation of platinum ores. *Minerals Engineering*, 18:839-844

Dixon, D.G., 1996. The multiple convolution integral: a new method for modelling multistage continuous leaching reactors. *Chemical Engineering Science*, 51(21):4759-4767

Du Toit, A.J., Gaylard, P., Jahanshahi, S., and Nell, J., 2006. Iron redox-equilibria and sulphide capacity of PGM melter-type slags. *Minerals Engineering*, 19:212-218

Eksteen, J.J., 2011. Consulting metallurgist: Lonmin. *Private communication*, 21 October 2011

Etienne, A., 1970. Electrochemical aspects of the aqueous oxidation of copper sulphides. *PhD Dissertation*, Department of Metallurgy, University of British Columbia, Canada

Fan, C., Li, B., Fu, Y., and Zhai, X., 2010. Kinetics of acid-oxygen leaching of low-sulfur Ni-Cu matte at atmospheric pressure. *Transactions of Nonferrous Metals: Society of China*, 20:1166-1170

Faris, M.D., Moloney, M.J., and Pauw, O.G., 1992. Computer simulation of the Sherritt nickel-copper matte acid leach process. *Hydrometallurgy*, 29:261-273

Feng, D., and Aldrich, C., 1999. Effect of particle size on flotation performance of complex sulphide ores. *Minerals Engineering*, 12(7):721-731

Fogler, H.S., 1999. *Elements of chemical reaction engineering*, Third Edition, Prentice-Hall International, Inc., New Jersey, United States of America

Fugleberg, S., Hultholm, S.E., Rosenback, L., and Holohan, T., 1995. Development of the Hartley Platinum leaching process. *Hydrometallurgy*, 39:1-10

Giandomenico, C.M., 2006. Platinum-group metals, compounds. In: *Kirk-Othmer Encyclopedia of Chemical Technology: Volume 19*, Fifth Edition, Editor: Seidel, A., John Wiley & Sons Inc., New Jersey, United States of America

Goldberg, R.N., and Hepler, L.G., 1968. Thermochemistry and oxidation potentials of the platinum group metals and their compounds. *Chemical Reviews*, 68(2):229-252

Grewal, I., Dreisinger, D.B., Krueger, D., Tyroler, P.M., Krause, E., and Nissen, N.C., 1992. Total oxidative leaching of Cu_2S-containing residue at INCO Ltd.'s copper refinery: laboratory studies on the reaction pathways. *Hydrometallurgy*, 29(1-3):319-333

Grønvold, F., Stølen, S., Westrum, E.F., and Galeas, C.G., 1987. Thermodynamics of copper sulphides III. Heat capacities and thermodynamic properties of $Cu_{1.75}S$, $Cu_{1.80}S$, and $Cu_{1.85}S$ from 5 to about 700K. *Journal of Chemical Thermodynamics*, 19(12):1305-1324

Gulliver, D.J., and Levason, W., 1982. The chemistry of ruthenium, osmium, rhodium, iridium, palladium and platinum in the higher oxidation states. *Coordination Chemistry Reviews*, 46:1-127

Habashi, F., 1999. *Textbook of Hydrometallurgy*, Second Edition, Métallurgie Extractive Québec, Québec, Canada

Hartley, F.R., 1991. The occurrence, extraction, properties and uses of the platinum group metals. In: *Chemistry of the Platinum Group Metals: Recent Developments*, Editor: Hartley, F.R., Elsevier Science Publishers B.V., Amsterdam, The Netherlands

Hofirek, Z., and Kerfoot, D.G.E., 1992. The chemistry of the nickel-copper matte leach and its applications to process control and optimisation. *Hydrometallurgy*, 29(1-3):357-381

Hofirek, Z., and Nofal, P.J., 1995. Pressure leach capacity expansion using oxygen-enriched air at RBMR (Pty) Ltd. *Hydrometallurgy*, 39:91-116

Housecroft, C.E., 1999. *The heavier d-block metals: aspects of inorganic and coordination chemistry*, Oxford University Press, Oxford, Great Britain

Huang, K., Li, Q., and Chen, J., 2007. Recovery of copper, nickel and cobalt from acidic pressure leaching solutions of low-grade sulphide flotation concentrates. *Minerals Engineering*, 20:722-728

Incropera, F.P., and De Witt, D.P., 1996. *Fundamentals of heat and mass transfer*, Fourth Edition, John Wiley and Sons, Inc., New York, United States of America

Iwakura, C., Hirao, K., and Tamura, H., 1977. Anodic evolution of oxygen on ruthenium in acidic solutions. *Electrochimica Acta*, 22:329-334

Jackson, E., 1986. *Hydrometallurgical extraction and reclamation*, Ellis Horwood Limited, Chichester, West Sussex, England

Jacob, K.T., and Prusty, D., 2010. Thermodynamic properties of RhO_2. *Journal of Alloys and Compounds*, 507:L17-L20

Jones, R.T., 2000. Platinum smelting in South Africa. *Mintek*, Available online: http://www.mintek.co.za/Pyromet/Platinum/Platinum.htm, Accessed: 20 May 2009

Jones, R.T., 2005. An overview of Southern African PGM smelting. *Mintek*, Available online: http://www.mintek.co.za/Pyromet/Files/2005JonesPGMsmelting.pdf, Accessed: 20 May 2009

Jones, T., 2004. Iridium plating. *Metal Finishing*, 102(6):87-103

Kakhu, A.I., and Pantelides, C.C., 2003. Dynamic modelling of aqueous electrolyte systems. *Computers and Chemical Engineering*, 27:869-882

Kerfoot, D.G.E., Kofluk, R.P., and Weir, D.R., 1986. Recovery of platinum group metals from nickel-copper-iron matte. *United States Patent*, Patent number 4 571 262

Kimweri, H.T.H., 1990. Solubility of oxygen in aqueous sulphuric acid-metallic salt solutions under pressure leaching conditions. *Master Thesis*, Department of Chemical Engineering, University of Ottawa, Canada

Kyllo, A.K., Richards, G.G., 1998a. A kinetic model of the Peirce-Smith converter: Part I. model formulation and validation. *Metallurgical and Materials Transactions*, 29B(1):239-249

Kyllo, A.K., Richards, G.G., 1998b. A kinetic model of the Peirce-Smith converter: Part II. model application and discussion. *Metallurgical and Materials Transactions*, 29B(1):251-259

Lampinen, M., Laari, A., and Turunen, I., 2010. Simulation of direct leaching of zinc concentrate in a non-ideally mixed CSTR. *The Canadian Journal of Chemical Engineering*, 88:625-632

Lamya, R.M., and Lorenzen, L., 2005. A study of factors influencing the kinetics of copper cementation during atmospheric leaching of converter matte. *The Journal of The South African Institute of Mining and Metallurgy*, 105(1):21-28

Lamya, R.M., and Lorenzen, L., 2006. Atmospheric acid leaching of nickel-copper matte from Impala Platinum Refineries. *The Journal of The South African Institute of Mining and Metallurgy*, 106(6):385-396

Lamya, R.M., 2007. A fundamental evaluation of the atmospheric pre-leaching section of the nickel-copper matte treatment process. *PhD Dissertation*, Department of Process Engineering, Stellenbosch University, South Africa

Lenahan, W.C., and Murray-Smith, R. De L., 1986. *Assay and analytical practice in the South African mining industry*, The South African Institute of Mining and Metallurgy, Johannesburg, South Africa, pp. 507-517

Levason, W., 1991. Recent developments in the chemistry of the platinum metals in high oxidation states. In: *Chemistry of the Platinum Group Metals: Recent Developments*, Editor: Hartley, F.R., Elsevier Science Publishers B.V., Amsterdam, The Netherlands

Levenspiel, O., 1972. *Chemical reaction engineering*, John Wiley & Sons Inc., New York, United States of America, pp. 359-399

Martin, F.S., 1952. A sexavalent ruthenium sulphate. *Journal of the Chemical Society*, pp. 3055-3059

McGeorge, B., Gaylard, P., and Lewis, A., 2009. Mechanism of rhodium(III) co-precipitation with copper sulphide (at low Rh concentrations) incorporating a new cationic substitution path. *Hydrometallurgy*, 96:235-245

Milbourne, J., Tomlinson, M., and Gormely, L., 2003. Use of hydrometallurgy in direct processing of base metal/PGM concentrates. *Hydrometallurgy 2003 – Proceedings of the Fifth International Symposium: Volume 1*, Vancouver, Canada, Editors: Young, C.A., Alfantazi, A.M., Anderson, C.G., Dreisinger, D.B., Harris, B., and James, A., pp. 617-630

Miller, J.D., Li, J., Davidtz, J.C., and Vos, F., 2005. A review of pyrrhotite flotation chemistry in the processing of PGM ores. *Minerals Engineering*, 18:855-865

Nell, J., 2004. Melting of platinum group metal concentrates in South Africa. *The Journal of The South African Institute of Mining and Metallurgy*, 104(7):423-428

Nikkhah, K., 1998. Autoclave design and scale-up from batch test data: a review of sizing methods and their bases. *Society of Mining Engineers of AIME Preprints*, 149:1-9

Padilla, R., Pavez, P., and Ruiz, M.C., 2008. Kinetics of copper dissolution from sulfidized chalcopyrite at high pressures in $H_2SO_4 – O_2$. *Hydrometallurgy*, 91:113-120

Papangelakis, V.G., Berk, D., and Demopoulus, G.P., 1990. Mathematical modelling of an exothermic leaching reaction system: pressure oxidation of wide size arsenopyrite particulates. *Metallurgical Transactions B*, 21B:827-837

Papangelakis, V.G., and Demopoulos, G.P., 1992a. Reactor models for a series of continuous stirred tank reactors with a gas-liquid-solid leaching system: Part I. Surface reaction control. *Metallurgical Transactions B*, 23A:847-856

Papangelakis, V.G., and Demopoulus, G.P., 1992b. Reactor models for a series of continuous stirred tank reactors with a gas-liquid-solid leaching system: Part II. Gas transfer control. *Metallurgical Transactions B*, 23B:857-864

Prosser, A.P., 1996. Review of uncertainty in the collection and interpretation of leaching data. *Hydrometallurgy*, 41:119-153

Provis, J.L., Van Deventer, J.S.J., Rademan, J.A.M., and Lorenzen, L., 2003. A kinetic model for the acid-oxygen pressure leaching of Ni-Cu matte. *Hydrometallurgy*, 70:83-99

Rademan, J.A.M., 1995. The simulation of a transient leaching circuit. *PhD Dissertation*, Department of Process Engineering, Stellenbosch University, South Africa

Rademan, J.A.M., Lorenzen, L., and Van Deventer, J.S.J., 1999. The leaching characteristics of Ni-Cu matte in the acid-oxygen pressure leach process at Impala Platinum. *Hydrometallurgy*, 52:231-252

Rard, J.A., 1985. Chemistry and thermodynamics of ruthenium and some of its inorganic compounds and aqueous species. *Chemical Reviews*, 85(1):1-39

Renner, H., 1992. Platinum Group Metals and Compounds. In: *Ullmann's Encyclopedia of Industrial Chemistry: Volume A21*, Fifth Completely Revised Edition, Editors: Elvers, B., Hawkins, S., Schulz, G., VCH Verlagsgesellschaft mbH, Weinstein, Germany

Rubisov, D.H., and Papangelakis, V.G., 2000. Sulphuric acid pressure leaching of laterites – a comprehensive model of a continuous autoclave. *Hydrometallurgy*, 58:89-101

Ruiz, M.C., Abarzúa, E., and Padilla, R., 2007. Oxygen pressure leaching of white metal. *Hydrometallurgy*, 86:131-139

Salmi, T., Grénman, H., Bernas, H., Wärnå, J., and Murzin, D.Y., 2010. Mechanistic modelling of kinetics and mass transfer for a solid-liquid system: leaching of zinc with ferric iron. *Chemical Engineering Science*, 65:4460-4471

Sassani, D.C., and Shock, E.L., 1998. Solubility and transport of platinum-group elements in supercritical fluids: summary and estimates of thermodynamic properties for ruthenium, rhodium, palladium, and platinum solids, aqueous ions, and complexes to 1000°C and 5 kbar. *Geochimica et Cosmochimica Acta*, 62(15):2643-2671

Seymour, R.J., and O'Farrelly, J.I., 2006. Platinum-group metals. In: *Kirk-Othmer Encyclopedia of Chemical Technology: Volume 19*, Fifth Edition, Editor: Seidel, A., John Wiley & Sons Inc., New Jersey, United States of America

Shackleton, N.J., Malysiak, V., and O'Connor, C.T., 2007. Surface characteristics and flotation behaviour of platinum and palladium tellurides. *Minerals Engineering*, 20:1232-1245

Steenekamp, N., and Dunn, G.M., 1999. Operations of and Improvements to the Lonrho Platinum Base Metal Refinery. *Proceedings of EPD Congress 1999*, San Diego, California, Editor: Mishra, B., pp. 365-378

Steenekamp, N., 2009a. Process Specialist: Lonmin BMR. *Private communication*, 10 July 2009

Steenekamp, N., 2009b. Draft operating philosophy: autoclaves. *Lonmin Internal Communication*, Accessed: 10 July 2009

Trahar, W.J., 1981. A rational interpretation of the role of particle size in flotation. *International Journal of Mineral Processing*, 8(4):289-327

Tromans, D., 1998a. Temperature and pressure dependent solubility of oxygen in water: a thermodynamic analysis. *Hydrometallurgy*, 48:327-342

Tromans, D., 1998b. Oxygen solubility modelling in inorganic solutions: concentration, temperature and pressure effects. *Hydrometallurgy*, 50:279-296

Venkoba Rao, B., 2007. Extension of particle stratification model to incorporate particle size effects. *International Journal of Mineral Processing*, 85:50-58

Van Schalkwyk, R.F., 2011. Leaching of Ni-Cu-Fe-S Peirce Smith converter matte: effects of the Fe-endpoint and leaching conditions on kinetics and mineralogy. *MScEng Thesis*, Department of Process Engineering, Stellenbosch University, South Africa

Van Schalkwyk, R.F., Eksteen, J.J., Petersen, J., Thyse, E.L., and Akdogan, G., 2011. An experimental evaluation of the leaching kinetics of PGM-containing Ni-Cu-Fe-S Peirce Smith converter matte, under atmospheric leach conditions. *Minerals Engineering*, 24:524-534

Vyazovoy, O.V., Mamonov, S.N., Shulgin, D.R., Ryumin, A.I., and Mironkina, N.V., 2010. Process technology improvement for refining intermediates treatment. *Proceedings of The Second International Congress: Non-Ferrous Metals 2010*, Krasnoyarsk, Russia, Part IV: Precious Metals Production, pp. 201-204

Wiese, J.G., Harris, P.J., and Bradshaw, D.J., 2008. The use of very low molecular weight polysaccharides as depressants in PGM flotation. *Minerals Engineering*, 21:471-482

Wilkins, R.G., 1974. *The study of kinetics and mechanism of reactions of transition metal complexes*, Allyn and Bacon, Inc., Boston, United States of America

Xiao, Z., Laplante, A.R., and Finch, J.A., 2009. Quantifying the content of gravity recoverable platinum group minerals in ore samples. *Minerals Engineering*, 22:304-310

Xiao, Z., and Laplante, A.R., 2004. Characterizing and recovering the platinum group minerals – a review. *Minerals Engineering*, 17:961-979

APPENDIX A: NOMENCLATURE

Symbols		
a	Specific interfacial area	m^2/m^3
A	Area	m^2
A_0	Initial surface area	m^2
C_i	Molar concentration of species *i*	mol/ℓ
C_i'	Molal concentration of solute *i*	mol/kg water
$C_{O_2,Eq}$	Dissolved oxygen concentration at equilibrium	mol/ℓ
$C_{O_2,Liq}$	Dissolved oxygen concentration in the bulk liquid	mol/ℓ
$C'_{O_2,Liq}$	Molal concentration of oxygen in the bulk liquid	mol/kg water
C_P	Heat capacity	J/kg·°C
$C_{P,L,i}$	Heat capacity of the liquid portion of stream *i*	J/kg·°C
$C_{P,S,i}$	Heat capacity of the solid portion of stream *i*	J/kg·°C
D_{AC}	Autoclave diameter	m
$\%D_{i,j}$	Percentage dissolution of species *i* at sample *j*	%
E_a	Activation energy	J/mol
f_{sh}	Shape factor	
g	Gravitational acceleration	m/s^2
ΔG	Gibbs free energy change	J/mol
h	Time step used in the Runge-Kutta method	minutes
$\widehat{H}_i$	Specific enthalpy of stream *i*	J/kg
$\Delta\widehat{H}_{Evap}$	Heat of evaporation	J/kg
$\Delta\widehat{H}^{\circ}_{rxn,j}$	Standard heat of reaction for reaction *j*	J/mol
K_i'	Proportionality constant relating flow from system *i* to mass in system *i*	$kg^{0.5}$/min
K_{SB}	Stefan-Boltzmann constant	$W/m^2{\cdot}K^4$
k	Overall reaction rate constant	
k_c	Rate constant for chemically controlled process	
k_d	Rate constant for diffusion controlled process	
k_L	Oxygen mass transfer coefficient	m/s
k_0	Pre-exponential factor for calculation of *k*	
k_{Air}	Thermal conductivity of air	W/m·K
k_1', k_2', k_3', k_4'	Runge-Kutta method constants	
L	Length	m

m	Mass	kg
m_i	Mass of material in system *i*	kg
$\dot{m}_i$	Mass flow rate of stream *i*	kg/h
$m_{j,L,i}$	Mass of liquid component *j* in system *i*	kg
$m_{j,S,i}$	Mass of solid component *j* in system *i*	kg
$m_{L,i}$	Mass of liquid in system *i*	kg
$m_{S,i}$	Mass of solid material in system *i*	kg
m_0	Mass of particles initially in system	kg
$[M_i]$	Mass concentration of species *i*	g/ℓ
$[M_i^*]_j$	Adjusted mass concentration of species *i* at sample *j*	g/ℓ
M_w	Molecular weight	g/mol
n_i	Molar amount of species *i*	mol
n_0	Molar amount at an initial time instance	mol
Nu	Nusselt number	
$[O_2]_{H_2O}$	Mass concentration of dissolved oxygen in pure water	mg/ℓ
P	Pressure	bar or Pa
$P^*_{H_2O}$	Water vapour pressure	bar or Pa
P_{O_2}	Oxygen partial pressure	bar or Pa
Pr_{Air}	Prandtl number of air	
R	Ideal gas constant	J/mol·K
R^2	Coefficient of determination	
r_j	Rate of reaction *j*	mol/ℓ·min
r_{O_2}	Rate of oxygen transfer	mol/ℓ·s
$\dot{Q}$	Rate of heat transfer	J/min
q	Model parameter used to calculate oxygen solubility	
T	Temperature	°C or K
t	Time	min or hr
V	Volume	m^3
$\dot{W}_{shaft}$	Shaft work	J/min
$x_{j,L,i}$	Mass fraction of component *j* in the solids in stream *i*	kg *j*/kg solids
$x_{j,S,i}$	Mass fraction of component *j* in the liquid in stream *i*	kg *j*/kg liquid
$x_{L,i}$	Mass fraction liquid in stream *i*	kg liquid/kg total
$x_{S,i}$	Mass fraction solids in stream *i*	kg solids/kg total
$\bar{y}$	Mean of experimental values	

y_{H_2O}	Mol fraction water in vapour phase	
y_i	Model parameter used to calculate oxygen solubility	
y_n	n^{th} experimental value	
$\hat{y}_n$	n^{th} model predicted value	

Greek letters		
α_{Air}	Thermal diffusivity of air	m^2/s
α_r	Order of reaction with respect to reagent *r*	
β_{Air}	Volumetric thermal expansion coefficient of air	1/°C
ε_{AC}	Autoclave surface emissivity	
ϕ_{eff}	Overall water fraction available for oxygen interaction	
ϕ_i	Available water fraction calculated for species *i*	
η_i	Model parameter used to calculate oxygen solubility	
κ_i	Model parameter used to calculate oxygen solubility	
μ_{Air}	Kinematic viscosity of air	m^2/s
ρ	Density	kg/ℓ
σ	Specific surface area	m^2/kg
υ_i	Stoichiometric coefficient of species *i*	

APPENDIX B: EXPERIMENTAL SETUP HAZARD IDENTIFICATION

Table B.1. Summary of the hazard identification analysis performed for the experimental setup.

Hazard	Examples of hazard	Examples of activities	Control measure/Preventive action in place
Chemicals			
Sulphuric acid		Leaks during operation	Put container below reactor; do regular leak tests; ensure drain valve closed before operation
		Loading reactor contents, sampling	Handle with care; wear PPE
		Maintenance	Wash and rinse vessel and all components prior to maintenance
Oxygen	Oxygen cylinder leaking	Increased fire hazard in reactor vicinity	Close regulator valve when not in operation; leak-tight fitment of hoses; adequate ventilation; keep flammable substances away from reactor
High temperatures			
Reactor vessel	High temperature of bottom of reactor	Removal of vessel	Allow reactor to cool before handling
	Overheating	Performing exothermic reaction	Check cooling water before operation; set appropriate maximum limit on temperature controller
		Reprogramming of temperature controller	Check temperature control cycle before operation; test programming with non-hazardous content (e.g. water); set appropriate max. limit on temperature controller
		Cooling water line blocked	Check cooling water before operation; rinse cooling water lines with acetic acid once every two months
	Reactor heated while not in use		Disconnect electricity supply when not in operation
	Fire		Keep flammable substances away from reactor
Samples	Reactor content samples	Sampling for analysis	Allow sample to cool down in sampling tube before collecting sample; Handle with care; wear PPE

Hazard	Examples of hazard	Examples of activities	Control measure/Preventive action in place
Cooling water	Cooling water flow rate too low	Cooling of reactor	Cooling water outlet line to be put in safe location; maintain sufficient cooling water flow rate during operation
Purged gas	High temperature outlet gas	Venting/purging of reactor	Purge line outlet to be put in safe location; do not obstruct purge line
Physical hazards			
Moving parts	Fast rotating agitator	Stirring of open reactor	Limit usage of stirrer in open reactor; do not switch on stirrer outside reactor
	Unexpected rotation	Maintenance of stirrer	Disconnect electricity supply prior to performing any maintenance work
Falling objects	Reactor vessel dropped on floor	Removal/mounting of vessel	Be watchful; ensure enough open bench space to place reactor vessel; limit handling of vessel
Loose objects	Agitator not properly fixed to shaft	Stirring of open reactor	Regularly check agitator screws
High pressure			
Reactor vessel	Bursting	Addition of oxygen to reactor	Ensure appropriate bursting disk installed; put all reactor locking mechanisms in place; close protective shield; do not overfill reactor with slurry
	Unexpected pressure release	Discharging of reactor	Vent reactor as part of shut-down procedure
		Opening reactor for maintenance	Ensure reactor is vented prior to releasing any of the locking mechanisms; do not attempt to open reactor during operation
Cooling water lines	Steam explosion	Cooling water line blocked	Check cooling water before operation; rinse cooling water lines with acetic acid once every two months
Oxygen cylinder	Regulator valve failure	Cylinder dislodgment	Securely fasten oxygen cylinder

APPENDIX C: EXPERIMENTAL DATA

C.1: XRD analysis for the converter matte validation tests

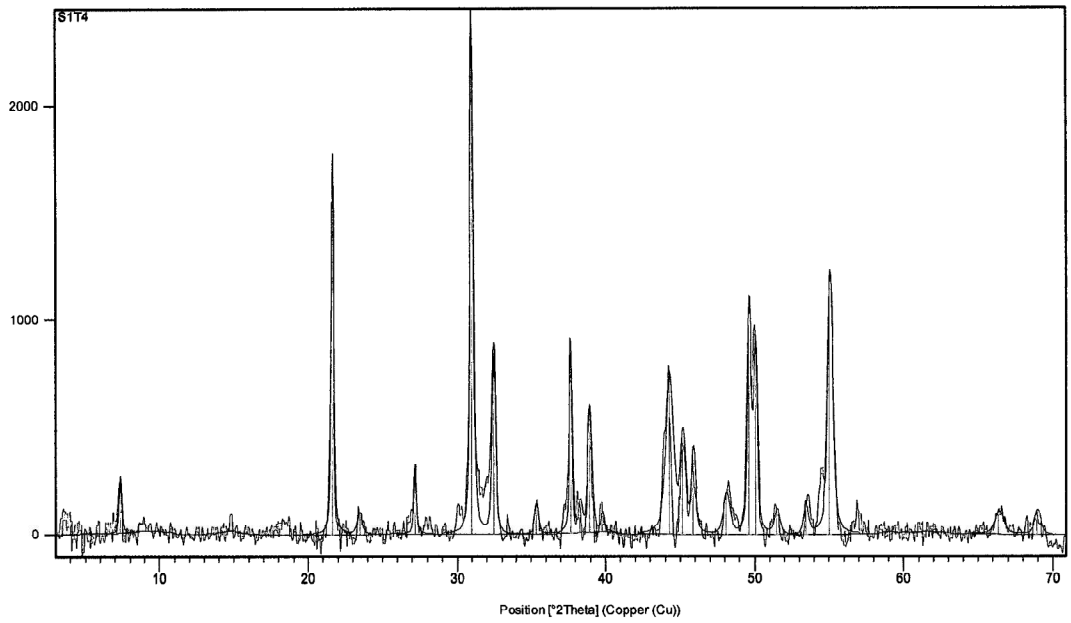

Visible	Ref. Code	Score	Compound Name	Displacement [°2Th.]	Scale Factor	Chemical Formula
*	01-085-1802	78	Heazlewoodite, syn	-0.092	0.858	Ni3 S2
*	01-072-1071	53	copper(I) sulfide	-0.143	0.375	Cu2 S

Figure C.1. XRD analysis of the fresh converter matte.

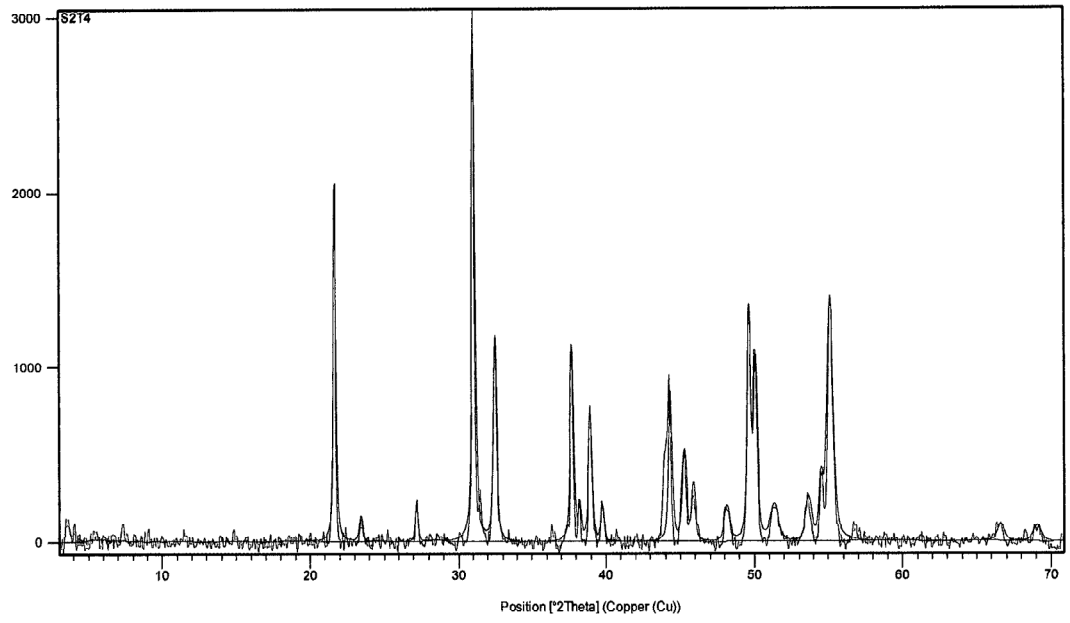

Visible	Ref. Code	Score	Compound Name	Displacement [°2Th.]	Scale Factor	Chemical Formula
*	01-071-1682	83	Heazlewoodite, syn	-0.084	0.885	Ni3 S2
*	01-072-1071	62	copper(I) sulfide	-0.158	0.357	Cu2 S

Figure C.2. XRD analysis of the converter matte after five minutes of leaching.

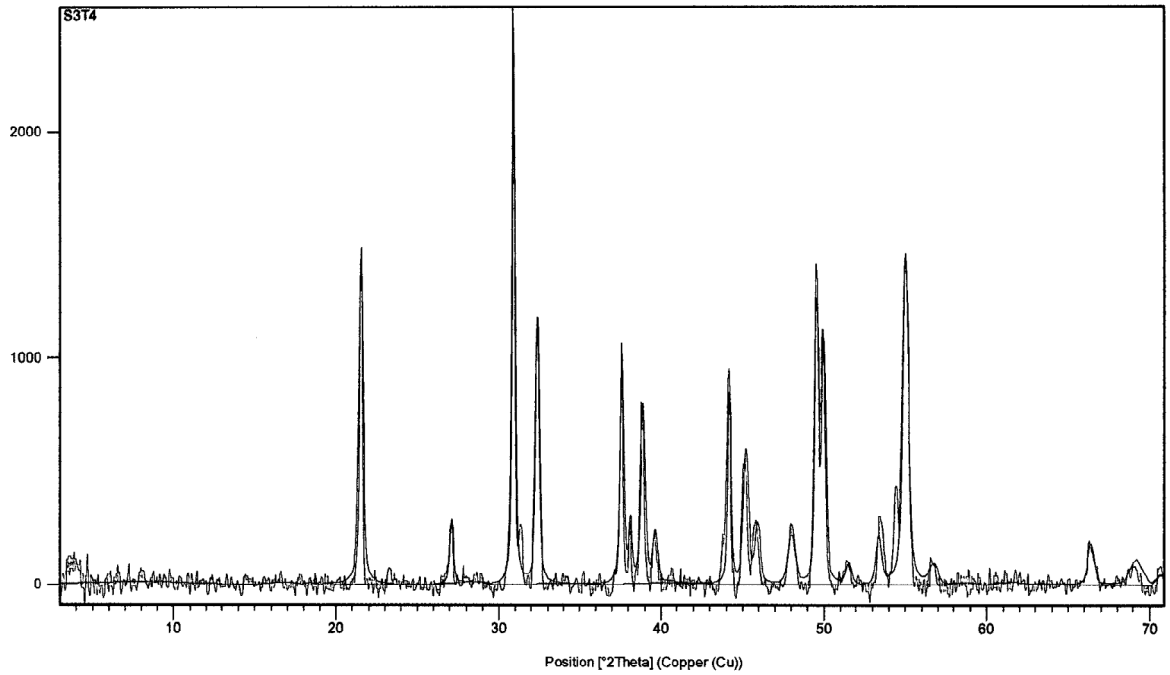

Visible	Ref. Code	Score	Compound Name	Displacement [°2Th.]	Scale Factor	Chemical Formula
*	01-073-0698	60	Heazlewoodite	-0.181	0.832	Ni3 S2
*	01-072-1071	69	copper(I) sulfide	-0.210	0.451	Cu2 S

Figure C.3. XRD analysis of the converter matte after 10 minutes of leaching.

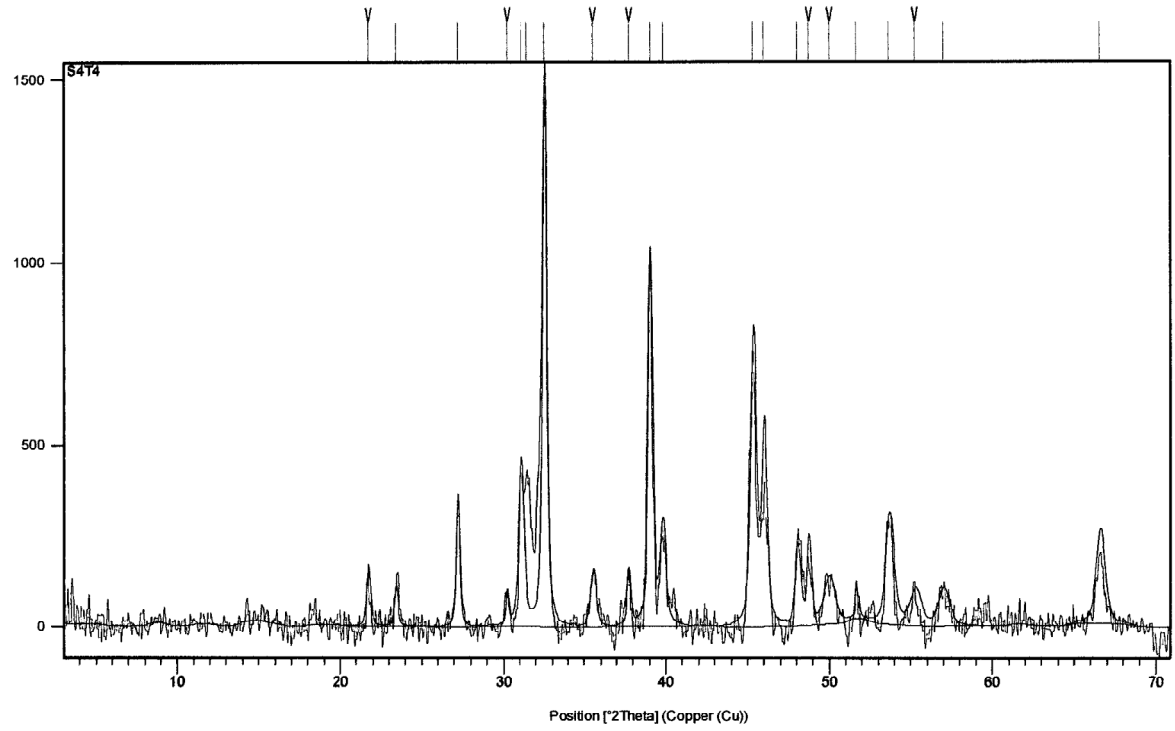

Visible	Ref. Code	Score	Compound Name	Displacement [°2Th.]	Scale Factor	Chemical Formula
*	00-029-0578	74	Chalcocite-Q, syn	-0.072	0.895	Cu1.96 S

Figure C.4. XRD analysis of the converter matte after 20 minutes of leaching.

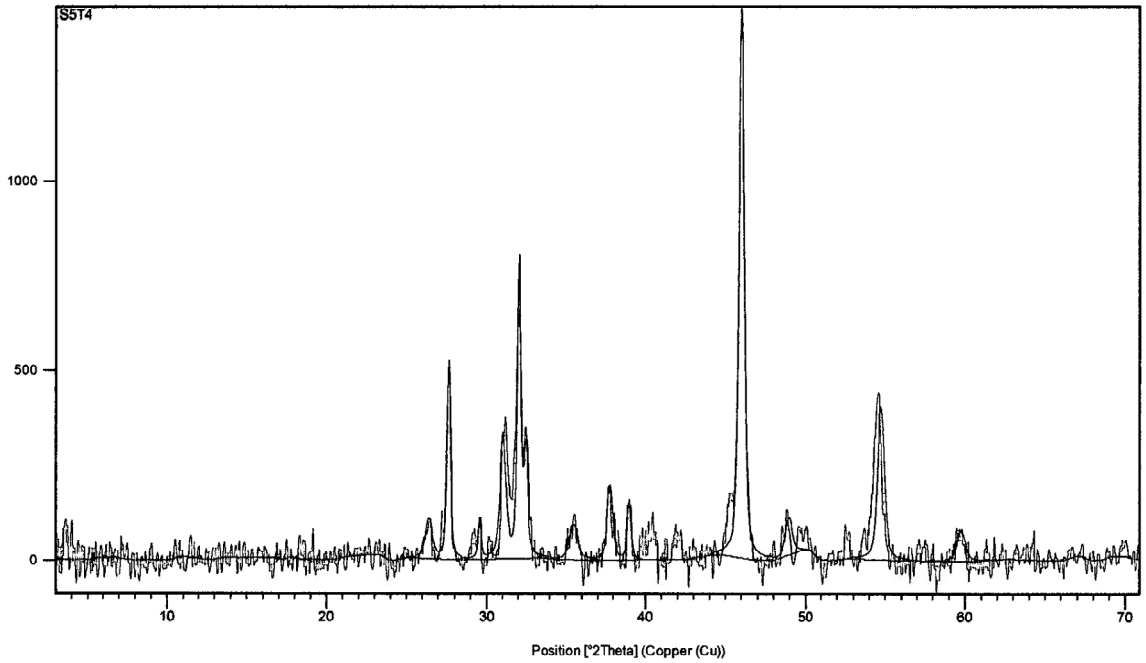

Visible	Ref. Code	Score	Compound Name	Displacement [°2Th.]	Scale Factor	Chemical Formula
*	01-072-1966	68	Digenite high	-0.009	0.966	Cu7.2 S4
*	00-023-0959	20	Djurleite, syn	-0.002	0.446	Cu31 S16

Figure C.5. XRD analysis of the converter matte after 40 minutes of leaching.

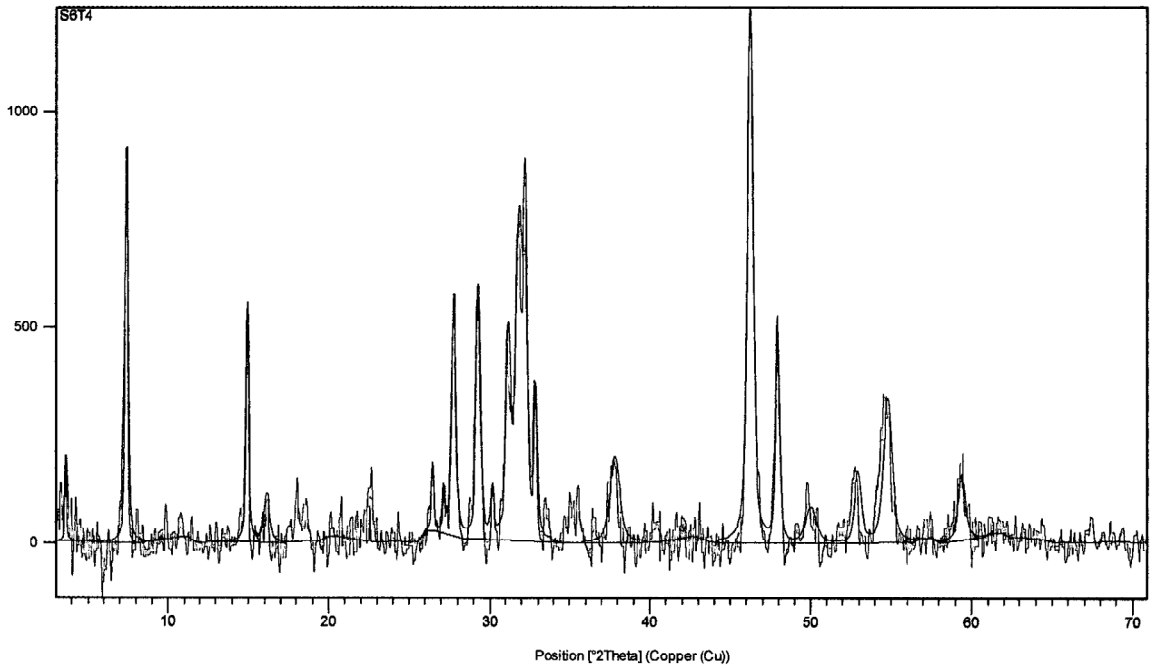

Visible	Ref. Code	Score	Compound Name	Displacement [°2Th.]	Scale Factor	Chemical Formula
*	01-071-4316	62	Digenite high, syn	0.108	0.971	Cu7.2 S4
*	00-043-1469	38	Polydymite	-0.070	0.232	Ni3 S4
*	01-078-2391	54	Covellite, syn	0.056	0.632	Cu S

Figure C.6. XRD analysis of the converter matte after 80 minutes of leaching.

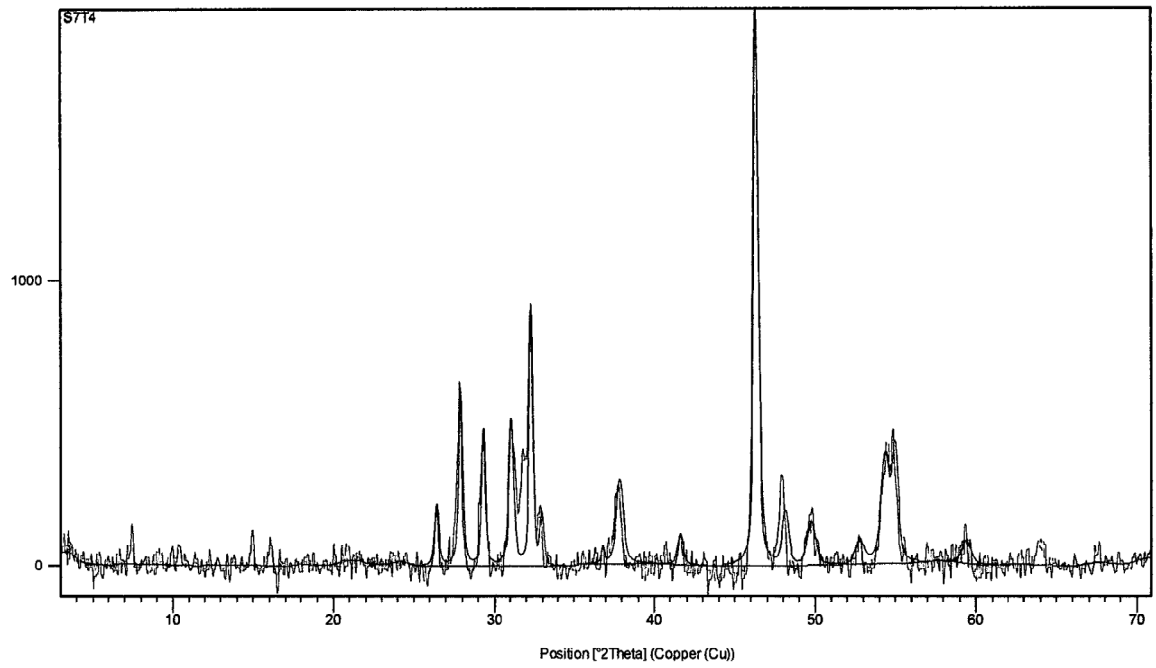

Visible	Ref. Code	Score	Compound Name	Displacement [°2Th.]	Scale Factor	Chemical Formula
*	01-071-4316	67	Digenite high, syn	0.208	0.897	Cu7.2 S4
*	00-047-1739	46	Polydymite	-0.106	0.273	Ni3 S4
*	03-065-3556	30	Copper Sulfide	0.217	0.194	Cu S

Figure C.7. XRD analysis of the converter matte after 120 minutes of leaching.

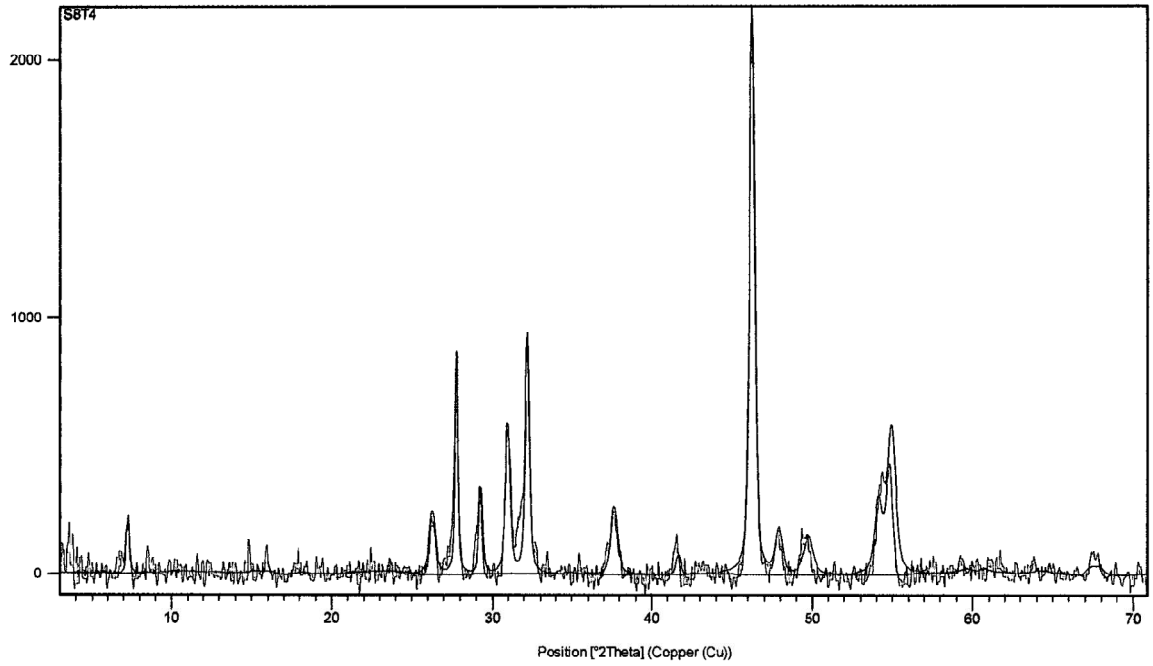

Visible	Ref. Code	Score	Compound Name	Displacement [°2Th.]	Scale Factor	Chemical Formula
*	00-047-1748	67	Digenite	0.025	0.917	Cu9 S5
*	01-071-4247	46	dicobalt(III) copper sulfide	-0.195	0.238	Co2 Cu S4

Figure C.8. XRD analysis of the converter matte after 160 minutes of leaching.

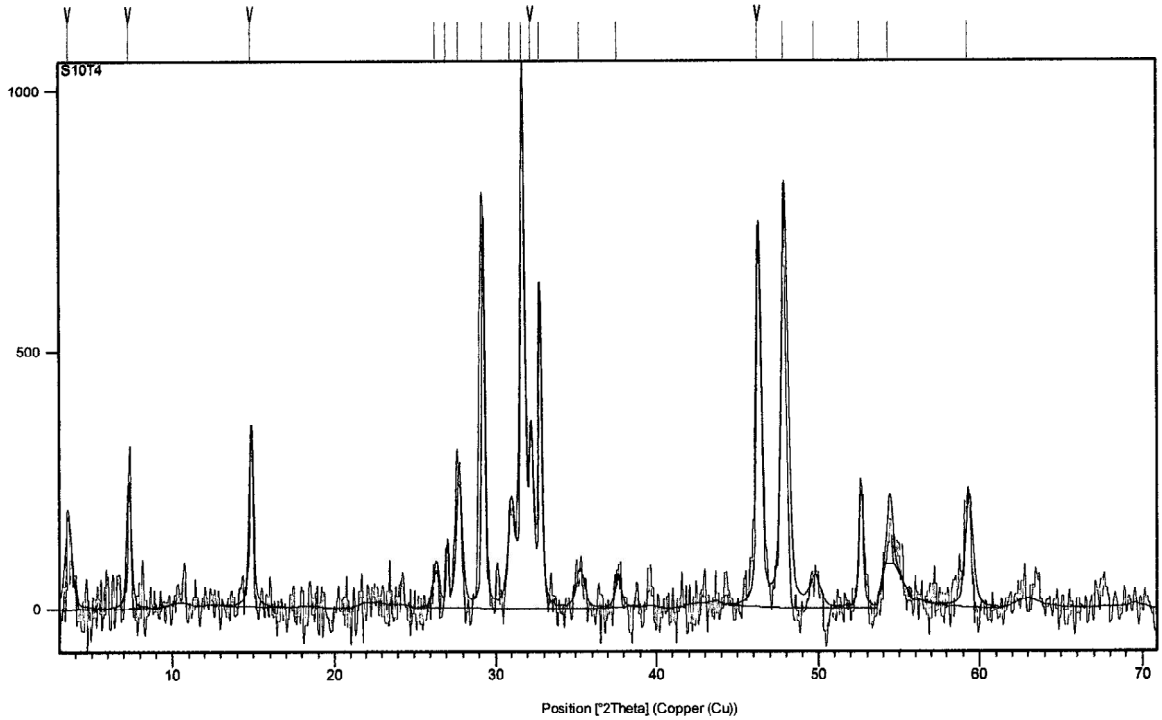

Visible	Ref. Code	Score	Compound Name	Displacement [°2Th.]	Scale Factor	Chemical Formula
	03-065-3556	61	Copper Sulfide	-0.002	1.121	Cu S
*	00-002-0788	Unmatched Strong	Siegenite	-0.160	0.175	(Co , Ni)3 S4

Figure C.9. XRD analysis of the converter matte after 240 minutes of leaching.

C.2: XRD analysis of the first stage leach residue

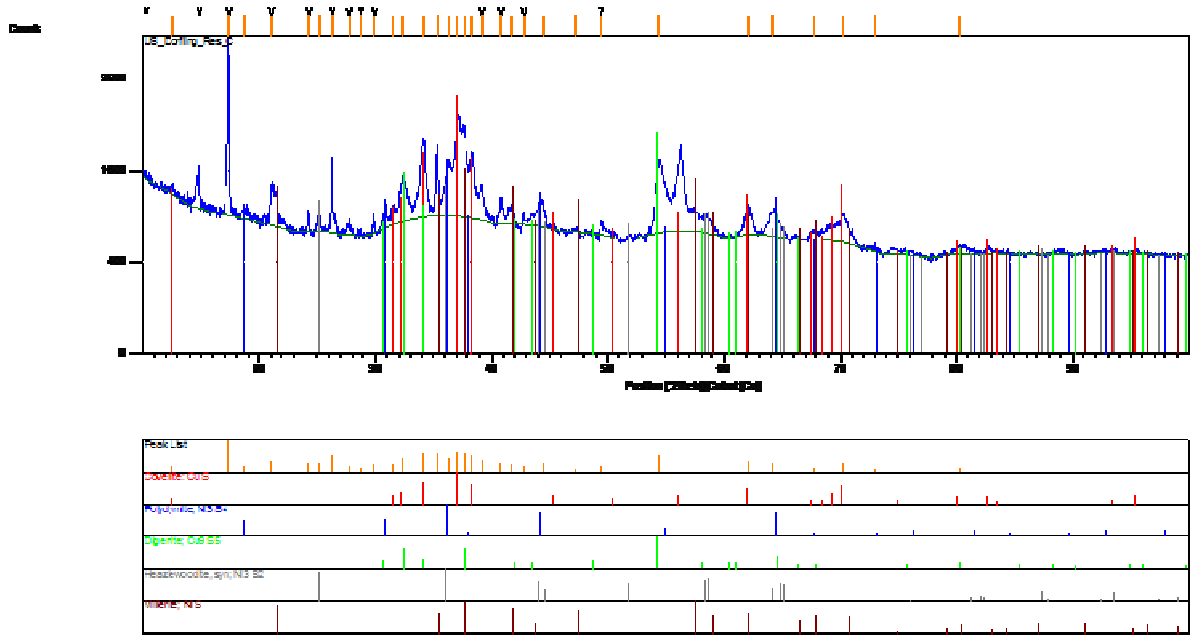

Figure C.10. XRD analysis of the first stage leach residue supplied by Lonmin Plc.

C.3: Experimental conditions for first stage leach residue leaching tests

Table C.1. Experimental conditions for the first set of leaching experiments performed on the first stage leach residue.

	Temperature (°C)	Pressure (bar)	Initial [M_{H2SO4}] (g/ℓ)	Solids content (g/ℓ)
Test 1a	144	7	26	180
Test 1b	116	7	26	180
Test 1c	116	7	36	180
Test 1d	144	5	36	180
Test 1e	116	5	26	180
Test 1f	116	5	36	180
Test 1g	144	7	36	180
Test 1h	144	5	26	180
Test 1i	116	7	36	290
Test 1j	144	7	26	290
Test 1k	144	7	36	290
Test 1l	144	5	26	290
Test 1m	116	5	36	290
Test 1n	116	5	26	290
Test 1o	144	5	36	290
Test 1p	116	7	26	290

Table C.2. Experimental conditions for the second set of leaching experiments performed on the first stage leach residue.

	Temperature (°C)	Pressure (bar)	Initial [M_{H2SO4}] (g/ℓ)	Solids content (g/ℓ)
Test 2a	116	9	165	130
Test 2b	130	9	165	130
Test 2c	116	7	165	130
Test 2d	130	7	140	80
Test 2e	130	7	140	130
Test 2f	130	9	140	130
Test 2g	130	9	165	80
Test 2h	116	7	165	80
Test 2i	116	9	140	130
Test 2j	116	9	165	80
Test 2k	130	7	165	80
Test 2l	130	9	140	80
Test 2m	130	7	165	130
Test 2n	116	9	140	80
Test 2o	116	7	140	130
Test 2p	116	7	140	80

C.4: Experimental results – leaching of converter matte

Table C.3. Results for leaching of converter matte at the conditions specified in Table 3.2.

Time (minutes)	Ni (g/ℓ)	Cu (g/ℓ)	Fe (g/ℓ)	Rh (mg/ℓ)	Ru (mg/ℓ)
0	26.74	23.11	1.74	22.78	140.48
5	32.96	19.98	2.21	18.69	104.69
10	40.61	14.57	2.57	8.00	63.68
20	85.04	0	3.15	0	51.20
40	108.84	8.58	3.59	0	46.17
80	125.49	8.01	1.47	2.96	63.58
120	130.39	11.68	1.80	9.72	77.03
160	136.02	19.23	3.01	26.37	169.83
200	127.81	21.95	3.34	35.67	198.69
240	129.59	26.89	3.11	41.57	200.20
300	127.54	28.03	2.61	28.77	144.90

Table C.4. Results for the leaching of converter matte at the conditions specified in Table 3.2, with the air flow rate changed to 7.5 g/h per litre.

Time (minutes)	Ni (g/ℓ)	Cu (g/ℓ)	Fe (g/ℓ)	Rh (mg/ℓ)	Ru (mg/ℓ)
0	26.77	23.85	1.70	26.05	152.04
5	31.20	21.99	2.07	4.72	129.48
10	47.28	14.43	2.55	3.81	82.15
20	92.39	2.16	3.02	5.64	45.93
40	107.33	6.22	3.41	6.83	44.65
80	121.61	5.55	1.01	2.07	36.18
120	133.92	11.14	2.04	10.73	91.16
160	132.88	12.96	1.89	0	94.20
200	137.24	14.87	2.24	12.93	119.17
240	134.09	22.45	2.69	23.52	163.65
300	123.68	28.96	1.21	9.42	95.71

Table C.5. Results for the leaching of converter matte at the conditions specified in Table 3.2, with the air flow rate changed to 78 g/h per litre.

Time (minutes)	Ni (g/ℓ)	Cu (g/ℓ)	Fe (g/ℓ)	Rh (mg/ℓ)	Ru (mg/ℓ)
0	26.75	23.37	1.89	29.89	163.00
5	34.85	19.86	2.32	13.04	107.17
10	59.75	8.84	3.08	0	94.67
20	96.12	4.39	3.54	2.13	63.90
40	112.78	10.89	3.09	0	60.12
80	133.28	10.72	1.37	8.64	52.59
120	133.58	15.73	2.08	19.85	96.34
160	129.21	18.60	2.63	18.27	130.24
200	131.94	15.84	2.85	13.34	114.63
240	134.67	13.09	3.06	8.42	99.02
300	130.91	9.95	3.26	11.89	77.12

C.5: Experimental results – leaching of first stage leach residue

Table C.6. ICP results for test 1a.

Time (minutes)	Fe (mg/ℓ)	Ni (g/ℓ)	Cu (g/ℓ)	Ru (mg/ℓ)	Rh (mg/ℓ)	Pd (mg/ℓ)	Os (mg/ℓ)	Pt (mg/ℓ)	Ir (mg/ℓ)
0	841	14.0	20.7	54.0	5.2	3.8	5.3	0.19	11.45
5	851	16.3	22.7	48.0	5.6	4.3	6.2	0.37	9.65
10	797	17.9	24.7	45.5	6.3	4.3	6.2	0.51	8.75
20	826	20.2	33.2	76.5	11	7.1	8.4	0.93	13.75
40	651	21.3	43.0	61.5	12	8.7	8.3	0.67	14.75
80	576	26.3	72.2	60.5	19	16	9.3	1.83	19.70
120	469	29.3	92.8	82.5	32	45	10		25.75
160		32.4	109				13	0	34.10
200	600	31.1	116	195	70	137	13	0	
240	619	31.6	113	186	81	137	15		44.45
300	371	43.3	149		74	111	17	161	
360	893	40.7	147	367	161	318	29	444	82.15

Table C.7. ICP results for test 1b.

Time (minutes)	Fe (mg/ℓ)	Ni (g/ℓ)	Cu (g/ℓ)	Ru (mg/ℓ)	Rh (mg/ℓ)	Pd (mg/ℓ)	Os (mg/ℓ)	Pt (mg/ℓ)	Ir (mg/ℓ)
0	746	11.9	21.8	77	11	4.1	4.7	0.15	16.7
5	784	12.7	30.1	70	8.1	5.9	5.0	0.47	15.9
10	555	13.6	37.2	37	8.6	7.6	4.6	1.11	12.9
20	468	15.0	39.8	27	6.7	8.3	5.7	1.06	12.5
40	426	18.9	48.9	21	7.9	11	6.8	0.94	13.4
80	343	25.8	76.4	32	15	19	8.5	4.19	16.2
120	297	34.9	107	64	33	42	12	0	26.8
160	444	37.9	127	120	50	77	14		32.5
200	391	28.3	108	114	42	71	11		63.6
240	439	36.1		138	65	90	16		38.3
300	396	38.4	137	133	68	102	14	193	38.6
360	653	31.3	115	285	123	251	24	336	65.9

Table C.8. ICP results for test 1c.

Time (minutes)	Fe (mg/ℓ)	Ni (g/ℓ)	Cu (g/ℓ)	Ru (mg/ℓ)	Rh (mg/ℓ)	Pd (mg/ℓ)	Os (mg/ℓ)	Pt (mg/ℓ)	Ir (mg/ℓ)
0	829	11.2	21.6	73	8.4	4.2	4.8	<0.1	15.4
5	828	11.6	30.9	65	7.0	6.0	4.8	0.32	14.4
10	786	12.1	36.1	64	7.4	6.7	5.0	0.62	15.2
20	769	13.7	41.0	77	9.6	9.1	6.3	0.82	16.8
40	730	17.5	48.9	88	11	10	7.5	0.34	16.3
80	750	24.9		135	23	14	9.7	0.66	21.8
120		27.7	85.7		0			0.13	34.6
160									
200									
240	829	28.8	108	263	75	86	15	<0.1	43.1
300	863	28.8	101	314	105	197	12	301	0.53
360	864	29.0	111	337	140	268	23	367	74.2

Table C.9. ICP results for test 1d.

Time (minutes)	Fe (mg/ℓ)	Ni (g/ℓ)	Cu (g/ℓ)	Ru (mg/ℓ)	Rh (mg/ℓ)	Pd (mg/ℓ)	Os (mg/ℓ)	Pt (mg/ℓ)	Ir (mg/ℓ)
0	847	12.4	19.9	45	<5	4.0	4.9	0.28	9.42
5	900	14.3	19.9	34	<5	4.4	5.6	0.38	6.28
10	894	16.2	18.4	23	<5	3.2	5.7	0.51	3.94
20	976	17.7	18.6	22	<5	2.9	7.6	0.72	3.64
40	963	19.2	25.2	24	<5	3.8	8.1	0.22	3.89
80	992	22.1	55.4	47	7.7	7.6	8.5	1.3	7.75
120	949	21.9	48.9	76	13	12	9.1	0.94	13.5
160	914	22.5	59.0	119	24	16	9.6	4.9	20.7
200									
240	823	24.2	76.2	138	40	12	13	1.1	22.2
300	815	25.1	80.2	162	40	31	10	12.8	25.6
360	768	24.0	85.4	227	88	122	23	143	47.3

Table C.10. ICP results for test 1e.

Time (minutes)	Fe (mg/ℓ)	Ni (g/ℓ)	Cu (g/ℓ)	Ru (mg/ℓ)	Rh (mg/ℓ)	Pd (mg/ℓ)	Os (mg/ℓ)	Pt (mg/ℓ)	Ir (mg/ℓ)
0	776	12.1	21.9	77	10	4.0	5.0	<0.1	16.8
5	828	12.7	29.3	73	8.1	5.9	5.2	0.59	15.7
10	781	12.9	30.3	62	6.9	5.6	5.1	0.26	14.1
20	609	13.8	34.8	49	7.3	6.3	5.8	0.40	14.2
40	562	15.9	40.4	31	6.0	7.7	6.2	0.13	11.8
80	566	20.9	54.9	57	14	13	7.8	1.55	16.1
120	479	23.5	66.5	35	14	13	8.5	0.14	18.5
160		26.5	79.9	66	26	31	9.5		
200	424	32.5	117	42	30	24	12	0.35	53.9
240	492	35.1	119	59	43	28	14	<0.1	26.9
300	359	29.4	101	54	31	20	9.7	0.59	16.3
360									

Table C.11. ICP results for test 1f.

Time (minutes)	Fe (mg/ℓ)	Ni (g/ℓ)	Cu (g/ℓ)	Ru (mg/ℓ)	Rh (mg/ℓ)	Pd (mg/ℓ)	Os (mg/ℓ)	Pt (mg/ℓ)	Ir (mg/ℓ)
0	789	10.9	20.3	68	8.2	3.8	4.6	0.43	15.3
5	834	11.5	25.3	60	6.0	4.8	4.9		13.2
10	816	11.8	29.3	53	5.5	5.5	4.8	0.24	12.1
20	836	12.4	34.6	68	6.8	6.7	6.1	0.35	14.4
40	768	13.9	39.4	77	8.2	7.8	6.4	0.13	14.5
80	784	20.1	59.7	112	15	14	8.2	1.1	15.5
120	746	22.6	94.3	125	20	12	9.3	0.10	23.5
160									
200	712	25.5	91.4	157	39	19	11	0.20	62.2
240	782	29.0	103	180	57	18	23	0.60	31.9
300									
360									

Table C.12. ICP results for test 1g.

Time (minutes)	Fe (mg/ℓ)	Ni (g/ℓ)	Cu (g/ℓ)	Ru (mg/ℓ)	Rh (mg/ℓ)	Pd (mg/ℓ)	Os (mg/ℓ)	Pt (mg/ℓ)	Ir (mg/ℓ)
0	856	12.1	18.8	44	<5	3.4	4.9	<0.1	9.57
5	886	14.3	22.6	35	<5	4.0	5.3	<0.1	7.36
10	899	15.7	26.1	34	<5	4.5	5.8	0.21	7.03
20	892	16.9	32.2	48	6.4	5.4	7.4	0.29	9.07
40	820	19.2	43.7	75	20	3.4	10	0.35	15.3
80	809	23.3	73.3	148	30	16	9.3	2.27	23.1
120	923	27.7	104	219	52	43	12	1.36	35.6
160	830	29.4	99.0	208	53	29	12		
200	721	26.5	93.7	160		20	12	2.26	83.4
240	681	28.0	100	78	70	26	14	0.95	35.2
300	776	31.2	107	81	83	37	12	<0.1	
360	717	29.4	108	82	92	43	22	34	45.2

Table C.13. ICP results for test 1h.

Time (minutes)	Fe (mg/ℓ)	Ni (g/ℓ)	Cu (g/ℓ)	Ru (mg/ℓ)	Rh (mg/ℓ)	Pd (mg/ℓ)	Os (mg/ℓ)	Pt (mg/ℓ)	Ir (mg/ℓ)
0	835	13.7	19.8	53	<5	3.4	5.2	<0.1	11
5	854	15.1	17.8	42	<5	3.1	5.7	<0.1	8.10
10	889	17.7	16.5	30	<5	2.5	6.0	0.19	4.98
20	966	19.2	25.6	45	6.2	4.2	8.4	0.58	6.48
40	912	20.8	20.3	40	5.0	2.3	8.9	0.12	5.85
80	815	23.3	31.7	71	11	4.8	9.0		10.5
120	874	23.0	44.4	111	27	3.1	12	<0.1	20.3
160	849	29.3	57.3			30	11	<0.1	23.6
200	704	24.2	71.3	108	28	20	11	2.21	48.4
240	712	26.7	79.3	126	33	15	10	0.19	22.4
300	624	32.3	76.7	104	33	15	10	0.52	4.85
360	620	25.8	82.3	95	54	14	22	2.27	0

Table C.14. ICP results for test 2a.

Time (minutes)	Fe (mg/ℓ)	Ni (g/ℓ)	Cu (g/ℓ)	Ru (mg/ℓ)	Rh (mg/ℓ)	Pd (mg/ℓ)	Os (mg/ℓ)	Pt (mg/ℓ)	Ir (mg/ℓ)
0	1190	22.4	40	160	6.9	4.1	31	0.21	31
5	1310	23.5	50.2	127	2.9	7.6	33	0.18	26
10	1330	24.8	42.6	111	1.5	7.0	35	0.15	21
20	1355	26.9	46.4	93.5	1.5	5.3	38	0.15	17
40		24.5	42.6	68	1.5	11	32	0.14	17
80	1380	35.8	41	176	19	1.3	50	0.28	29
120	1400	36.8	37.2	246	33	2.0	51	0.65	35
160	1440	38.1	36	323	50	6.1	53	2.4	43
200	1440	38.6	36.4	358	61	16	53	2.7	44
240	1380	37	29.8	377	73	23	51	3.0	
300	1395	36.7	21.5	398	83	28	49	2.9	
360	1320	35.4	35.2	396	84	72	48	6.0	50
420	1410	36.4	35.4	419	93	99	48	9.0	55

Table C.15. ICP results for test 2b.

Time (minutes)	Fe (mg/ℓ)	Ni (g/ℓ)	Cu (g/ℓ)	Ru (mg/ℓ)	Rh (mg/ℓ)	Pd (mg/ℓ)	Os (mg/ℓ)	Pt (mg/ℓ)	Ir (mg/ℓ)
0	1190	22.4	31.5	137	3.4	4.4	30	0.1	25
5	1270	23.3	41.9	98	0	7.8	32	0.1	20
10	1280	25.7	43.3	74	0	8.5	34	0.1	10
20	1320	27.3	48.9	46	0	8.9	38	0.1	7
40	1325	31.1	51.4	38	0	9.0	42	0.1	7
80	1340	34.1	51.0	114	13	7.5	47	0.3	17
120	1350	34.3	53.6	278	46	17	48	1.6	32
160	1330	35.8	50.5	358	70	31	51	4.0	45
200	1360	36.5	50.3	403	86	46	52	3.9	53
240	1375	35.8	43.6	421	106	125	49	9.3	53
300	1390	36.4	41.3	435	114	152	50	11	64
360	1360	36.0	47.1	427	112	156	49	10	60
420	1370	36.0	46.0	434	118	167	49	25	61

Table C.16. ICP results for test 2c.

Time (minutes)	Fe (mg/ℓ)	Ni (g/ℓ)	Cu (g/ℓ)	Ru (mg/ℓ)	Rh (mg/ℓ)	Pd (mg/ℓ)	Os (mg/ℓ)	Pt (mg/ℓ)	Ir (mg/ℓ)
0	1150	21.8	34.2	164	9.9	5.7	31	0.2	28
5	1200	23.0	48.3	129	3.2	8.8	32	0.1	28
10	1290	25.0	43.4	109	1.7	8.7	32	0.4	22
20	1300	26.9	52.0	89	0.3	10	37	0.2	16
40	1310	30.1	54.2	91	0	9.7	41	0	0
80	1320	33.3	56.3	92	4.4	9.4	44	0.2	17
120	1330	34.6	62.1	168	23	13	47	0.3	26
160	1310	35.5	57.8	224	30	13	48	0.6	31
200	1305	35.4	61.1	287	45	18	49	1.4	35
240	1330	36.1	62.3	319	53	27	48	2.4	41
300	1330	34.2	59.8	353	64	40	48	3.8	44
360	1380	36.9	59.3	383	82	84	49	0	53
420	1350	32.1	58.7	403	85	96	51	45	50

Table C.17. ICP results for test 2d.

Time (minutes)	Fe (mg/ℓ)	Ni (g/ℓ)	Cu (g/ℓ)	Ru (mg/ℓ)	Rh (mg/ℓ)	Pd (mg/ℓ)	Os (mg/ℓ)	Pt (mg/ℓ)	Ir (mg/ℓ)
0	1010	20.5	32.2	143	11	5.5	30	0.2	29
5	1130	21.1	38.7	116	2.4	7.5	32	0.2	25
10	1130	21.6	42.5	86	1.0	8.1	31	0.1	17
20	1100	23.2	45.9	66	0.3	9.5	33	0.1	11
40	1110	24.2	51	63	1.4	11	37	0.1	9.5
80	1130	25.6	63.7	132	16	16	39	0.4	19
120	1120	25.8	66.3	238	39	23	40	1.7	31
160	1140	26.5	63.4	272	51	26	40	0	37
200	1135	26.2	62	287	59	22	39	1.8	38
240	1140	26.4	63.1	299	66	36	39	0	42
300	1150	26.4	58.2	308	74	72	39	0	49
360	1160	26.6	62.9	312	76	75	40	0	48
420	1170	27	62.4	335	82	87	42	0	52

Table C.18. ICP results for test 2e.

Time (minutes)	Fe (mg/ℓ)	Ni (g/ℓ)	Cu (g/ℓ)	Ru (mg/ℓ)	Rh (mg/ℓ)	Pd (mg/ℓ)	Os (mg/ℓ)	Pt (mg/ℓ)	Ir (mg/ℓ)
0	1350	21.3	26.0	145	5.5	8.2	33	0.13	31
5	1290	21.7	37.1	106	2.3	9.6	34	0.13	22
10	1310	22.1	42.2	82	0.8	11	33	0.11	15
20	1330	24	46.7	57	0.2	11	35	0.21	9
40	1330	26.4	47.9	38	0.3	14	39	0.12	8
80	1390	31.7	57.2	74	3.8	19	46	6.0	14
120	1360	32.9	75.3	156	20	17	47	0.5	22
160	1340	32.0	62.6	282	46	28	49	1.6	33
200	1370	32.4	64.1	343	64	35	48	3.9	43
240	1385	33.0	65.6	369	78	26	48	3.1	49
300	1370	32.0	65.7	399	94	60	48	3.5	55
360	1380	31.8	63.2	403	104	124	46	12	57
420	1420	33.3	70.0	417	105	114	49	18	65

Table C19. ICP results for test 2f.

Time (minutes)	Fe (mg/ℓ)	Ni (g/ℓ)	Cu (g/ℓ)	Ru (mg/ℓ)	Rh (mg/ℓ)	Pd (mg/ℓ)	Os (mg/ℓ)	Pt (mg/ℓ)	Ir (mg/ℓ)
0	1240	20.5	32.8	144	4.7	6.4	32	0.12	28
5	1320	21.7	43.2	106	1.7	10	34	0.80	20
10	1370	22.0	51.0	79	0.9	12	34	0.13	15
20	1390	25.5	58.1	57	0.0	13	38	0.10	10
40	1360	28.2	62.0	57	1.6	15	41	0.19	12
80	1420	32.5	63.4	161	20	16	50	0.40	24
120	1420	33.8	60.3	282	44	21	51	1.4	35
160	1420	33.6	62.9	352	66	34	49	4.3	48
200	1395	32.1	61.6	394	84	43	50	3.4	46
240	1420	32.4	66.4	412	99	107	50	6.5	60
300	1410	32.6	68.4	422	110	145	47	9.8	62
360	1460	32.6	54.4	434	115	151	49	14.9	65
420	1510	32.7	40.4	446	120	156	51	20	68

Table C.20. ICP results for test 2g.

Time (minutes)	Fe (mg/ℓ)	Ni (g/ℓ)	Cu (g/ℓ)	Ru (mg/ℓ)	Rh (mg/ℓ)	Pd (mg/ℓ)	Os (mg/ℓ)	Pt (mg/ℓ)	Ir (mg/ℓ)
0	1050	19.9	31.5	147	14.5	5.7	30	0.14	28
5	1090	20.2	36.7	103	6.0	7.8	30	0.80	21
10	1080	21.7	40.6	78	3.0	9.4	32	0.12	13
20	1080	23.3	45.7	62	2.6	11	34	0.12	9
40	1080	25.3	58.3	80	8.1	14	36	0.16	12
80	1100	25.6	57.4	214	35	21	38	1.2	29
120	1090	26.0	57.3	261	48	35	38	3.1	34
160	1110	26.0	54.9	287	59	22	39	3.2	38
200	1105	26.3	60.8	301	68	54	39	5.5	44
240	1095	25.8	57.3	301	72	86	38	15.5	45
300	1120	25.3	56.7	310	76	100	38	23.5	47
360	1120	25.5	55.0	312	78	96	38	25.5	48
420	1140	26.7	58.2	313	78	110	38	31	49

Table C.21. ICP results for test 2h.

Time (minutes)	Fe (mg/ℓ)	Ni (g/ℓ)	Cu (g/ℓ)	Ru (mg/ℓ)	Rh (mg/ℓ)	Pd (mg/ℓ)	Os (mg/ℓ)	Pt (mg/ℓ)	Ir (mg/ℓ)
0	1000	16.1	27.8	163	13	5.6	30	0.13	28
5	1080	20.1	34.7	138	12	8.2	31	0.14	27
10	1080	20.7	39.3	123	8.0	9.3	30	0.12	24
20	1080	21.3	44.2	111	7.2	11	31	0.12	22
40	1070	22.3	50.4	110	8.2	14	32	0.14	20
80	1080	23.8	55.3	146	12	15	34	0.17	26
120	1090	25.4	58.7	187	21	15	38	0.34	30
160	1090	25.5	56.9	233	34	21	38	6.5	33
200	1080	25.8	56.4	247	39	24	38	1.7	33
240	1095	25.9	55.2	258	43	31	37	2.6	35
300	1080	26.5	56.7	272	55	41	39	4.1	37
360	1150	26.4	60.4	300	60	41	40	4.3	41
420	1120	26.4	55.7	300	60	62	39	5.0	39

Table C.22. ICP results for test 2i.

Time (minutes)	Fe (mg/ℓ)	Ni (g/ℓ)	Cu (g/ℓ)	Ru (mg/ℓ)	Rh (mg/ℓ)	Pd (mg/ℓ)	Os (mg/ℓ)	Pt (mg/ℓ)	Ir (mg/ℓ)
0	1220	21.2	31.2	163	12	6.3	31	0.15	31
5	1330	22.3	39.7	136	10	9.4	32	0.14	28
10	1340	23.4	44.8	115	7.6	11	34	0.32	24
20	1340	25.0	50.8	93	6.6	12	36	0.11	19
40	1375	28.3	59.7	94	8.5	16	41	0.15	18
80	1380	31.3	59.5	179	26	15	46	0.33	29
120	1410	33.4	55.2	233	30	12	51	0.35	37
160	1380	35.4	54.3	279	40	15	50	0.80	38
200	1440	35.1	61.3	312	47	17	48	1.5	45
240	1390	33.7	60.7	341	55	29	49	2.5	43
300	1370	34.5	57.6	368	66	48	50	4.5	50
360	1350	33.4	52.3	396	82	74	50	0	50
420	1230	30.3	51.0	383	85	102	45	6.0	49

Table C.23. ICP results for test 2j.

Time (minutes)	Fe (mg/ℓ)	Ni (g/ℓ)	Cu (g/ℓ)	Ru (mg/ℓ)	Rh (mg/ℓ)	Pd (mg/ℓ)	Os (mg/ℓ)	Pt (mg/ℓ)	Ir (mg/ℓ)
0	1010	20.3	30.4	158	17.7	5.3	29	0.14	27
5	1070	21.0	42.4	136	11.9	8.1	30	0.11	28
10	1080	21.7	44.6	128	8.9	10	29	0.12	25
20	1070	21.9	50.5	124	7.7	13	31	0.14	22
40	1080	22.7	60.0	142	9.2	15	31	0.15	25
80	1120	25.2	58.6	178	16	14	38	0.25	28
120	1120	26.0	59.2	218	29	15	39	0.47	32
160	1100	26.1	60.4	242	36	20	38	1.2	34
200		26.0	60.1	243	40	25	35	2.2	36
240	1095	26.4	63.7	269	46	33	38	2.6	35
300	1110	28.3	61.5	286	54	45	39	4.5	39
360	1130	26.3	61.8	300	61	50	40	5.5	39
420	1140	27.1	60.9	309	64	77	39	8.5	41

Table C.24. ICP results for test 2k.

Time (minutes)	Fe (mg/ℓ)	Ni (g/ℓ)	Cu (g/ℓ)	Ru (mg/ℓ)	Rh (mg/ℓ)	Pd (mg/ℓ)	Os (mg/ℓ)	Pt (mg/ℓ)	Ir (mg/ℓ)
0	1020	20.8	33.8	144	8.5	0	13	0.12	27
5	1070	22.0	39.6	109	6.1	8.0	13	0.11	23
10	1100	22.5	40.2	85	2.8	4.7	13	0.11	14
20	1100	23.6	48.8	59	1.4	3.7	13	0.11	8
40	1110	25.1	42.0	46	1.7	3.6	15	0.12	6
80	1110	28.5	54.9	110	9.0	0	17	0.20	14
120	1120	27.5	63.3	231	35	0	16	1.4	29
160	1120	27.6	54.3	275	50	0	16	2.0	31
200	1110	27.4	65.0	288	55	7.0	16	2.2	38
240	1135	28.3	48.6	307	62	21	16	2.3	40
300	1120	27.2	64.8	313	67	58	16	9	45
360	1150	28.7	49.9	318	72	54	16	18	49
420	1150	28.6	49.3	321	72	55	16	16	49

Table C.25. ICP results for test 2l.

Time (minutes)	Fe (mg/ℓ)	Ni (g/ℓ)	Cu (g/ℓ)	Ru (mg/ℓ)	Rh (mg/ℓ)	Pd (mg/ℓ)	Os (mg/ℓ)	Pt (mg/ℓ)	Ir (mg/ℓ)
0	1020	21.5	31.4	143	9.6	2.5	13	0.16	27
5	1080	23.3	43.1	106	7.4	2.4	13	0.31	23
10	1090	23.8	45.2	84	4.5	1.1	14	0.13	16
20	1080	23.7	50.9	69	3.3	8.0	14	0.17	11
40	1100	27.2	62.1	91	11	5.5	15	0.28	15
80	1120	28.4	63.4	218	35	5.5	16	0.70	26
120	1120	27.9	61.6	270	52	0	17	2.6	35
160	1130	28.8	68.1	293	55	10	17	2.7	43
200	1135	28.8	66.9	308	65	47	16	6.0	47
240	1130	28.9	64.1	316	71	67	16	0	46
300	1150	28.7	62.6	320	73	80	16	7.9	49
360	1140	28.7	64.8	320	73	86	16	11	48
420	1140	29.6	68.0	314	73	78	16	11	49

Table C.26. ICP results for test 2m.

Time (minutes)	Fe (mg/ℓ)	Ni (g/ℓ)	Cu (g/ℓ)	Ru (mg/ℓ)	Rh (mg/ℓ)	Pd (mg/ℓ)	Os (mg/ℓ)	Pt (mg/ℓ)	Ir (mg/ℓ)
0	1210	22.2	34.1	137	6	1.3	13	0.18	25
5	1300	22.7	42.5	101	5.3	0.8	14	0.16	20
10	1350	24.0	59.6	77	1.8	1.2	14	0.15	12
20	1400	26.5	60.5	49	1.1	0.7	15	0.14	8
40	1340	27.7	59.5	25	0.9	0.6	15	0.14	5
80	1360	31.8	66.8	41	4.3	1.3	18	0.19	9
120	1390	35.3	64.6	123	11	1.5	20	0.29	18
160	1340	33.6	66.4	291	43	12	21	2.2	36
200	1380	34.0	72.1	360	63	16	21	4.0	47
240	1400	34.9	71.9	385	76	18	21	3.5	48
300	1380	33.4	66.4	416	92	6.9	21	3.1	53
360	1400	33.8	57.4	433	104	100	20	15	62
420	1410	34.4	71.5	419	106	48	19	20	66

Table C.27. ICP results for test 2n.

Time (minutes)	Fe (mg/ℓ)	Ni (g/ℓ)	Cu (g/ℓ)	Ru (mg/ℓ)	Rh (mg/ℓ)	Pd (mg/ℓ)	Os (mg/ℓ)	Pt (mg/ℓ)	Ir (mg/ℓ)
0	996	21.2	32.2	165	14	0.7	13	0.15	29
5	1090	23.0	43.7	146	8	1.1	14	0.14	30
10	1100	22.4	43.5	131	6	1.2	13	0.34	24
20	1090	23.6	58.6	125	5	0.7	14	0.17	24
40	1100	23.3	64.6	148	10	0.7	15	0.18	27
80	1120	27.9	70.1	188	16	0.6	16	0.22	31
120	1120	27.6	62.4	240	30	2.6	17	0.70	32
160	1100	28.6	70.2	262	35	7.0	16	1.7	37
200	1120	29.3	68.3	286	45	24	17	0	41
240	1145	28.0	64.3	292	45	19	17	3.2	38
300	1130	28.1	62.9	301	50	23	17	4.1	40
360	1120	29.4	72.0	310	57	52	17	7.0	44
420	1140	30.0	67.6	323	63	75	17	12	44

Table C.28. ICP results for test 2o.

Time (minutes)	Fe (mg/ℓ)	Ni (g/ℓ)	Cu (g/ℓ)	Ru (mg/ℓ)	Rh (mg/ℓ)	Pd (mg/ℓ)	Os (mg/ℓ)	Pt (mg/ℓ)	Ir (mg/ℓ)
0	1180	22.0	36.8	170	11	0.6	21	0	29
5	1270	22.4	43.0	141	6.0	0.6	22	0	28
10	1290	23.0	48.6	123	8.4	0.9	22	0	25
20	1350	24.6	55.0	100	6.2	0.6	24	0	20
40	1320	28.1	58.8	83	6.0	0.5	26	0	15
80	1290	31.6	62.6	120	8.3	1.2	30	0	19
120	1360	33.6	47.2	200	21	1.0	33	0.3	30
160	1360	33.2	63.7	232	27	1.2	32	0.4	31
200	1360	33.5	60.0	269	34	7.0	33	0.6	33
240	1390	34.3	68.5	313	46	8.5	32	10	41
300	1365	33.8	66.7	347	52	6.7	33	2.5	41
360	1350	32.8	58.6	381	62	28	32	2.9	44
420	1410	35.0	47.6	414	74	58	33	4.7	50

Table C.29. ICP results for test 2p.

Time (minutes)	Fe (mg/ℓ)	Ni (g/ℓ)	Cu (g/ℓ)	Ru (mg/ℓ)	Rh (mg/ℓ)	Pd (mg/ℓ)	Os (mg/ℓ)	Pt (mg/ℓ)	Ir (mg/ℓ)
0	1040	20.9	32.9	173	14	0	20	0.12	28
5	1080	22.2	40.1	149	8.8	0	20	0	27
10	1100	22.8	48.7	132	6.0	0	21	0.13	27
20	1080	23.8	61.9	115	7.3	0	21	0	21
40	1120	22.3	57.6	119	7.8	0	22	0	20
80	1100	26.8	62.6	162	14	0	24	0.10	24
120	1130	27.9	70.4	219	28	0	26	0.48	32
160	1120	28.3	68.8	252	35	0	26	0.85	33
200	1115	27.9	65.2	268	38	6.3	26	1.7	35
240	1125	27.8	63.6	282	44	16	26	2.0	35
300	1110	28.4	68.4	292	48	27	26	3.3	39
360	1130	28.1	66.2	306	54	40	26	4.0	41
420	1130	27.1	62.8	313	61	44	26	4.1	39

APPENDIX D: SAMPLE CALCULATIONS

D.1: Calculation of spent electrolyte acid concentration

The concentrations of Cu, Ni, Fe, and Co in the spent electrolyte listed in Table 3.1 are 25.3 g/ℓ, 22.8 g/ℓ, 0.856 g/ℓ, and 0.261 g/ℓ, respectively, while the SO_4^{2-} concentration was 113.7 g/ℓ. For any species, *i*, the molar concentration, C_i, can be calculated from the mass concentration, $[M_i]$ using Equation D-1:

$$C_i = \frac{[M_i]}{M_{w,i}} \qquad [D\text{-}1]$$

where $M_{w,i}$ is the molecular weight of component *i*. A summary of the molar concentrations of the respective species is given in Table D.1.

Table D.1. Summary of mass and molar concentrations of species required for calculation of the spent electrolyte acid concentration.

	Cu^{2+}	**Ni^{2+}**	**Fe^{3+}**	**Co^{2+}**	**SO_4^{2-}**
Mass concentration (g/ℓ)	25.3	22.8	0.856	0.261	113.7
Molecular weight (g/mol)	63.55	58.71	55.85	58.93	96.06
Molar concentration (mol/ℓ)	0.398	0.388	0.0153	0.00443	1.184

Given the assumptions regarding the oxidation states for the respective metals in solution (i.e., Cu^{2+}, Ni^{2+}, Fe^{3+}, and Co^{2+} are present in solution), the ratio of sulphate ions to metal ions is 1:1 for all the metals except for iron, in which case the ratio of sulphate ions to metal ions is 3:2. The concentration of the sulphate ions not associated with metallic cations, and therefore the H_2SO_4 concentration, can hence be calculated using Equation D-2:

$$C_{H_2SO_4} = C_{SO_4^{2-}} - C_{Cu^{2+}} - C_{Ni^{2+}} - \frac{3}{2} \cdot C_{Fe^{3+}} - C_{Co^{2+}} \qquad [D\text{-}2]$$

$$C_{H_2SO_4} = 1.184 - 0.398 - 0.388 - \frac{3}{2} \cdot 0.0153 - 0.00443 = 0.371 \text{ mol/l}$$

Using Equation D-1, the mass concentration of the sulphuric acid can be calculated:

$$0.371 = \frac{[M_{H_2SO_4}]}{98.08}$$

$$\therefore [M_{H_2SO_4}] = 36.4 \text{ g/l}$$

D.2: Calculation of feed quantities

The properties of the solid-liquid slurry were estimated using the properties of the individual components that were fed into the autoclave, as summarised in Table D-2.

Table D.2. Summary of the properties of the feed components used in the calculation of the relative feed amounts.

Material Properties				
	Acid (wt%)	**Density (kg/ℓ)**	**C_{H2SO4} (mol/ℓ)**	**$[M_{H2SO4}]$ (g/ℓ)**
Fresh Acid	96	1.836	17.966	1762.1
Water	0	1	0	0
Spent electrolyte	3.14	1.16	0.371	36.4
Solids	0	4.453	0	0

It was assumed that the volumes of the individual components, V_i, are additive in calculation of the final solution volume. The density of the slurry could hence be calculated using Equation D-3:

$$\rho_{slurry} = \frac{\sum m_i}{\sum V_i} \qquad [D\text{-}3]$$

where m_i is the mass of each of the respective components (i.e., first stage leach residue, spent electrolyte, sulphuric acid, and demineralised water). The amount of acid in the slurry was assumed to be equal to the sum of the molar amounts of sulphuric acid added as fresh sulphuric acid and as spent electrolyte. In calculating the relative amounts of the different components required for specific operating conditions, a fixed amount of solids was selected for each density setting, and the ratio of demineralised water to sulphuric acid was fixed at value that would allow reasonable additions for the respective components. The Solver-function in Excel® was then used to minimise the sum of the square of the differences between the calculated properties and the desired properties (i.e., the acid concentration and the density of the slurry), as shown in Equation D-4, by varying the amounts of sulphuric acid and spent electrolyte added to the autoclave:

$$f_{feed} = (\rho_{calc} - \rho_{required})^2 + ([M_{H_2SO_4}]_{calc} - [M_{H_2SO_4}]_{required})^2 \qquad [D\text{-}4]$$

where f_{feed} is the objective function to be minimised, ρ_{calc} and $\rho_{required}$ are the calculated density and the desired density, respectively, and $[M_{H2SO4}]_{calc}$ and $[M_{H2SO4}]_{required}$ are the calculated acid concentration and the desired acid concentration, respectively.

Table D.3. Summary of the feed quantities of spent electrolyte, sulphuric acid, demineralised water, and solids added to obtain the different operating conditions.

	Operating conditions		**Relative feed amounts**			
	Density (kg/ℓ)	**Initial [M_{H2SO4}] (g/ℓ)**	**Spent (ml)**	**Water (ml)**	**Acid (ml)**	**Solids (g)**
First stage residue leach (1st experimental design)	1.2	26	335	643	8.3	180
	1.2	36	287	686	15.1	180
	1.34	26	736	224	0.1	290
	1.34	36	694	261	6.8	290
First stage residue leach (2nd experimental design)	1.27	140	945	0	62.1	80
	1.27	165	930	0	76.9	80
	1.31	140	933	0	62.3	130
	1.31	165	918	0	77.2	130

D.3: Adjustment of metal concentrations to compensate for sampling losses

The adjusted concentration of a specific species *i* at sample number *j*, $[M_i^*]_j$, is what the concentration of that species would have been at that particular time instance (sample number 1, j = 1, represents time instance 0 minutes, sample number 2, j = 2, represents time instance 5 minutes, etc.) if no dissolved species was lost due to sampling and if the leach solution volume remained constant. $[M_i^*]_j$ can be calculated using Equation D-5 for $j > 1$ ($[M_i^*]_1 = [M_i]_1$, since no sampling occurred before this time instance):

$$[M_i^*]_j = \frac{\left(V_1 - \sum_{b=1}^{j-1} V_{sample,b}\right) \cdot [M_i]_j + \sum_{b=1}^{j-1}\left(V_{sample,b} \cdot [M_i]_b\right)}{V_1} \qquad [D\text{-}5]$$

where V_i is the leach solution volume prior to sample *i* being taken, $V_{sample,b}$ is the volume of the sample taken at sample number *b*, and $[M_i]_j$ is the mass concentration of species *i* at sample number *j*. The first term in the numerator therefore calculates the amount of dissolved metal present in solution at the time instance associated with sample number *j*, while the second term sums the amount of dissolved species removed from the autoclave during each sampling. The adjusted concentration values, expressed in mol per litre, are illustrated graphically in Appendix E.

D.4: Calculation of percentage dissolution of a specific metal

The percentage dissolution of species *i* at sample number *j*, $\%D_{i,j}$, is defined as the percentage of the particular species that was originally present in the first stage leach residue that have reported to the leach solution by that particular time instance (sample number 1, $j = 1$, represents time instance 0 minutes, sample number 2, $j = 2$, represents time instance 5 minutes, etc.), and can be calculated using Equation D-6 for $j > 1$ ($\%D_{i,1} = 0$):

$$\%D_{i,j} = \frac{\left(V_1 - \sum_{b=1}^{j-1} V_{sample,b}\right) \cdot [M_i]_j + \sum_{b=1}^{j-1}\left(V_{sample,b} \cdot [M_i]_b\right) - V_1 \cdot [M_i]_1}{x_i \cdot m_{solids,initial}} \cdot 100 \quad \text{[D-6]}$$

where V_i is the leach solution volume prior to sample i being taken, $V_{sample,b}$ is the volume of the sample taken at sample number b, and $[M_i]_j$ is the mass concentration of species i at sample number j. x_i is the fraction of component i in the first stage leach residue, and $m_{solids,initial}$ is the initial mass of first stage leach residue added. The first term in the numerator therefore calculates the amount of dissolved metal present in solution at the time instance associated with sample number j, the second term sums the amount of dissolved species removed from the autoclave during each sampling, and the third term indicates the amount of dissolved species initially present in the leach solution. The percentage dissolution values calculated for the respective tests are given in Table D.4 to Table D.27.

Table D.4. Percentage dissolution of the different metals at the respective sampling instances for test 1a.

Time (minutes)	Fe (%)	Ni (%)	Cu (%)	Ru (%)	Rh (%)	Pd (%)	Os (%)	Pt (%)	Ir (%)
0	0.0	0.0	0.0	0.0	0.0	0.0	0.0	0.0	0.0
5	1.3	9.8	2.2	-1.6	0.2	0.1	0.5	0.0	-3.2
10	-5.5	16.1	4.3	-2.2	0.6	0.2	0.5	0.0	-4.8
20	-1.9	25.4	13.2	5.7	3.5	1.0	1.6	0.1	3.9
40	-23.3	30.0	23.4	1.9	4.0	1.4	1.6	0.1	5.7
80	-32.5	49.7	53.2	1.7	7.8	3.5	2.1	0.2	14.1
120	-45.2	61.4	74.0	7.1	15.5	11.4	2.4		24.3
160		73.3	90.1				3.9	0.0	38.2
200	-30.7	68.4	97.0	33.7	36.4	36.4	3.9	0.0	
240	-28.6	70.1	94.1	31.6	42.1	36.4	4.9		54.2
300	-56.6	113.4	128.5		38.6	29.5	5.8	19.8	
360	1.7	103.7	126.6	72.6	85.0	83.2	11.2	53.9	112.6

Table D.5. Percentage dissolution of the different metals at the respective sampling instances for test 1b.

Time (minutes)	Fe (%)	Ni (%)	Cu (%)	Ru (%)	Rh (%)	Pd (%)	Os (%)	Pt (%)	Ir (%)
0	0.0	0.0	0.0	0.0	0.0	0.0	0.0	0.0	0.0
5	4.8	3.3	8.9	-1.8	-1.8	0.5	0.2	0.0	-1.4
10	-24.0	7.0	16.5	-10.4	-1.5	1.0	-0.1	0.1	-6.8
20	-34.8	12.7	19.2	-12.9	-2.6	1.2	0.5	0.1	-7.5
40	-40.0	28.3	28.6	-14.5	-1.9	2.0	1.1	0.1	-5.9
80	-50.0	55.5	56.7	-11.7	2.2	4.3	2.0	0.5	-1.1
120	-55.5	90.9	87.6	-3.8	12.5	10.7	3.7	0.0	16.8
160	-38.2	102.2	107.5	9.7	22.1	20.2	4.5		26.2
200	-44.3	66.0	88.8	8.3	17.6	18.7	3.2		77.3
240	-38.8	95.2		14.0	30.2	23.8	5.6		36.3
300	-43.7	103.7	115.1	12.8	31.8	26.9	4.7	23.8	36.8
360	-15.0	77.9	94.4	47.7	61.1	65.7	9.4	40.9	79.8

Table D.6. Percentage dissolution of the different metals at the respective sampling instances for test 1c.

Time (minutes)	Fe (%)	Ni (%)	Cu (%)	Ru (%)	Rh (%)	Pd (%)	Os (%)	Pt (%)	Ir (%)
0	0.0	0.0	0.0	0.0	0.0	0.0	0.0	0.0	0.0
5	-0.1	1.7	10.0	-2.1	-0.9	0.5	0.0	0.0	-1.8
10	-5.4	3.7	15.5	-2.4	-0.6	0.7	0.1	0.1	-0.4
20	-7.5	10.2	20.7	1.0	0.7	1.4	0.8	0.1	2.4
40	-12.3	25.4	28.8	3.7	1.5	1.7	1.4	0.0	1.6
80	-9.9	54.6		15.5	8.5	2.8	2.5	0.1	11.0
120		65.4	65.3		-4.7			0.0	32.5
160									
200									
240	-4.4	66.7	84.6	44.4	36.4	21.9	4.9	0.0	44.8
300	-0.5	66.7	77.9	56.2	52.6	51.2	3.5	37.1	
360	-0.4	67.4	87.3	61.5	71.3	69.7	8.6	44.6	92.8

Table D.7. Percentage dissolution of the different metals at the respective sampling instances for test 1d.

Time (minutes)	Fe (%)	Ni (%)	Cu (%)	Ru (%)	Rh (%)	Pd (%)	Os (%)	Pt (%)	Ir (%)
0	0.0	0.0	0.0	0.0	0.0	0.0	0.0	0.0	0.0
5	6.8	7.9	0.0	-2.9	0.0	0.1	0.4	0.0	-5.6
10	6.0	15.7	-1.6	-5.7	0.0	-0.2	0.4	0.0	-9.8
20	16.2	21.7	-1.4	-6.0	0.0	-0.3	1.4	0.1	-10.3
40	14.6	27.7	5.5	-5.5	0.0	-0.1	1.7	0.0	-9.9
80	18.1	39.2	36.3	0.2	4.5	1.0	1.9	0.1	-3.3
120	13.0	38.4	29.8	7.4	7.5	2.2	2.2	0.1	6.4
160	8.8	40.7	39.8	17.8	13.7	3.3	2.4	0.6	18.4
200									
240	-3.1	45.9	55.7	21.9	22.3	2.2	4.0	0.1	20.3
300	-4.0	49.0	59.5	27.5	22.0	7.1	2.6	1.5	25.8
360	-9.2	45.2	64.4	42.4	47.8	30.9	8.7	17.4	59.9

Table D.8. Percentage dissolution of the different metals at the respective sampling instances for test 1e.

Time (minutes)	Fe (%)	Ni (%)	Cu (%)	Ru (%)	Rh (%)	Pd (%)	Os (%)	Pt (%)	Ir (%)
0	0.0	0.0	0.0	0.0	0.0	0.0	0.0	0.0	0.0
5	6.6	2.5	8.0	-1.0	-1.2	0.6	0.1	0.1	-2.0
10	0.7	3.3	9.0	-3.9	-1.9	0.5	0.1	0.0	-4.8
20	-20.7	7.0	13.7	-7.2	-1.6	0.7	0.4	0.1	-4.6
40	-26.4	15.3	19.5	-11.8	-2.4	1.1	0.6	0.0	-8.8
80	-26.0	35.1	34.4	-5.3	2.2	2.6	1.4	0.2	-1.5
120	-36.4	45.2	46.1	-10.7	2.2	2.6	1.8	0.0	2.6
160		56.7	59.4	-3.2	9.0	7.5	2.3		
200	-43.5	79.4	95.8	-8.9	11.2	5.6	3.5	0.0	60.3
240	-35.7	89.1	97.8	-4.9	18.3	6.7	4.5	0.0	16.6
300	-50.8	68.1	80.6	-6.1	11.8	4.6	2.4	0.1	-0.4
360									

Table D.9. Percentage dissolution of the different metals at the respective sampling instances for test 1f.

Time (minutes)	Fe (%)	Ni (%)	Cu (%)	Ru (%)	Rh (%)	Pd (%)	Os (%)	Pt (%)	Ir (%)
0	0.0	0.0	0.0	0.0	0.0	0.0	0.0	0.0	0.0
5	5.7	2.5	5.3	-2.1	-1.4	0.3	0.2		-3.9
10	3.5	3.5	9.6	-4.0	-1.7	0.5	0.1	0.0	-5.8
20	6.0	6.1	15.1	-0.1	-0.9	0.8	0.8	0.0	-1.8
40	-2.4	11.9	20.2	2.1	0.0	1.2	0.9	0.0	-1.6
80	-0.5	36.6	40.9	10.9	3.9	2.9	1.9	0.1	0.2
120	-5.0	46.3	75.8	14.1	6.7	2.4	2.4	0.0	13.7
160									
200	-10.1	56.1	71.7	21.4	17.1	4.2	3.2	0.0	76.7
240	-2.2	69.0	82.4	26.8	27.0	3.8	8.7	0.0	27.6
300									
360									

Table D.10. Percentage dissolution of the different metals at the respective sampling instances for test 1g.

Time (minutes)	Fe (%)	Ni (%)	Cu (%)	Ru (%)	Rh (%)	Pd (%)	Os (%)	Pt (%)	Ir (%)
0	0.0	0.0	0.0	0.0	0.0	0.0	0.0	0.0	0.0
5	3.8	9.1	4.1	-2.4	0.0	0.2	0.2	0.0	-4.0
10	5.5	14.9	7.8	-2.6	0.0	0.3	0.5	0.0	-4.6
20	4.6	19.7	14.2	1.0	3.8	0.6	1.3	0.0	-1.0
40	-4.2	28.9	26.1	7.8	11.8	0.0	2.7	0.0	9.8
80	-5.6	45.1	56.4	26.0	17.5	3.6	2.3	0.3	23.1
120	8.1	62.2	87.3	43.4	30.1	11.1	3.7	0.2	44.2
160	-2.9	68.7	82.4	40.8	30.7	7.2	3.7		
200	-15.6	57.8	77.2	29.3		4.8	3.7	0.3	121.9
240	-20.2	63.4	83.3	9.9	39.6	6.4	4.6	0.1	43.8
300	-9.4	75.1	89.9	10.6	46.6	9.3	3.7	0.0	
360	-16.1	68.4	90.4	10.7	51.4	10.9	8.3	4.1	59.0

Table D.11. Percentage dissolution of the different metals at the respective sampling instances for test 1h.

Time (minutes)	Fe (%)	Ni (%)	Cu (%)	Ru (%)	Rh (%)	Pd (%)	Os (%)	Pt (%)	Ir (%)
0	0.0	0.0	0.0	0.0	0.0	0.0	0.0	0.0	0.0
5	2.4	5.8	-2.2	-2.9	0.0	-0.1	0.3	0.0	-5.2
10	6.8	16.5	-3.5	-6.0	0.0	-0.3	0.4	0.0	-10.8
20	16.4	22.5	6.0	-2.2	3.7	0.2	1.7	0.1	-8.1
40	9.8	28.9	0.5	-3.4	3.0	-0.3	1.9	0.0	-9.2
80	-2.0	38.6	12.1	4.2	6.4	0.4	2.0		-1.3
120	5.1	37.6	25.0	14.1	15.6	-0.1	3.5	0.0	15.3
160	2.1	61.8	37.8			7.3	3.0	0.0	20.7
200	-14.7	42.5	51.6	13.1	15.9	4.6	3.0	0.3	61.5
240	-13.8	51.8	59.3	17.3	18.7	3.3	2.5	0.0	19.4
300	-23.8	72.5	56.8	12.2	18.7	3.3	2.5	0.1	-8.7
360	-24.2	48.9	62.1	10.1	29.9	3.0	8.1	0.3	-16.3

Table D.12. Percentage dissolution of the different metals at the respective sampling instances for test 2a.

Time (minutes)	Fe (%)	Ni (%)	Cu (%)	Ru (%)	Rh (%)	Pd (%)	Os (%)	Pt (%)	Ir (%)
0	0.0	0.0	0.0	0.0	0.0	0.0	0.0	0.0	0.0
5	21.4	6.4	15.3	-12.1	-3.4	1.5	1.5	0.0	-12.6
10	24.9	13.8	4.0	-17.9	-4.5	1.2	3.0	0.0	-26.2
20	29.2	25.7	9.6	-24.1	-4.5	0.5	5.2	0.0	-36.0
40		12.3	4.1	-33.1	-4.5	2.8	0.8	0.0	-36.0
80	30.5	74.5	1.8	4.5	9.6	-1.0	13.6	0.0	-6.2
120	33.8	80.0	-3.5	28.5	20.8	-0.8	14.3	0.1	6.8
160	40.4	86.9	-5.2	54.6	34.1	0.8	15.7	0.4	26.6
200	40.4	89.6	-4.6	66.3	42.7	4.6	15.7	0.4	27.7
240	30.8	81.2	-13.6	72.6	51.5	7.2	14.0	0.5	
300	33.1	79.7	-24.7	79.4	59.2	9.1	13.2	0.5	
360	21.5	73.1	-6.6	78.7	60.1	25.3	12.4	1.0	38.2
420	35.4	78.1	-6.4	86.0	66.7	35.0	12.4	1.5	49.1

Table D.13. Percentage dissolution of the different metals at the respective sampling instances for test 2b.

Time (minutes)	Fe (%)	Ni (%)	Cu (%)	Ru (%)	Rh (%)	Pd (%)	Os (%)	Pt (%)	Ir (%)
0	0.0	0.0	0.0	0.0	0.0	0.0	0.0	0.0	0.0
5	14.2	5.2	15.6	-14.3	-2.9	1.4	1.5	0.0	-13.8
10	16.0	19.0	17.7	-23.0	-2.9	1.7	3.0	0.0	-37.4
20	22.9	28.0	25.9	-33.0	-2.9	1.9	5.9	0.0	-45.9
40	23.8	48.9	29.5	-35.8	-2.9	1.9	8.8	0.0	-44.7
80	26.3	65.7	28.9	-9.3	7.6	1.3	12.3	0.0	-20.9
120	28.0	66.8	32.6	47.0	33.9	5.0	13.0	0.3	13.3
160	24.7	74.9	28.3	74.1	52.8	10.4	15.1	0.7	43.5
200	29.6	78.6	28.0	89.2	65.2	16.1	15.8	0.7	61.9
240	32.0	74.9	18.9	95.0	80.1	45.4	13.7	1.6	62.4
300	34.4	78.0	15.9	99.7	86.6	55.6	14.4	1.9	87.5
360	29.7	76.0	23.5	97.1	85.1	57.0	13.8	1.8	77.6
420	31.2	76.0	22.1	99.3	89.5	61.0	13.8	4.3	80.9

Table D.14. Percentage dissolution of the different metals at the respective sampling instances for test 2c.

Time (minutes)	Fe (%)	Ni (%)	Cu (%)	Ru (%)	Rh (%)	Pd (%)	Os (%)	Pt (%)	Ir (%)
0	0.0	0.0	0.0	0.0	0.0	0.0	0.0	0.0	0.0
5	8.9	7.0	21.2	-12.8	-5.7	1.3	0.7	0.0	-1.3
10	24.7	18.4	13.9	-20.0	-6.9	1.2	0.7	0.0	-16.1
20	26.5	29.1	26.5	-27.2	-8.1	1.8	4.4	0.0	-29.6
40	28.2	47.0	29.6	-26.7	-8.4	1.7	6.9	0.0	-68.3
80	29.9	64.6	32.7	-26.1	-4.8	1.5	9.4	0.0	-27.7
120	31.5	71.7	40.9	0.0	10.0	2.9	11.5	0.0	-7.7
160	28.2	76.5	34.9	19.0	15.6	2.9	12.2	0.1	5.1
200	27.4	75.7	39.3	40.0	27.2	4.6	12.9	0.2	14.8
240	31.4	79.4	41.0	50.4	32.9	8.2	11.9	0.4	27.9
300	31.4	69.8	37.7	61.7	41.6	13.0	12.2	0.6	34.6
360	39.2	83.6	37.0	71.3	55.0	29.0	12.8	0.0	54.4
420	34.6	59.5	36.3	77.6	57.2	33.3	14.1	7.6	47.8

Table D.15. Percentage dissolution of the different metals at the respective sampling instances for test 2d.

Time (minutes)	Fe (%)	Ni (%)	Cu (%)	Ru (%)	Rh (%)	Pd (%)	Os (%)	Pt (%)	Ir (%)
0	0.0	0.0	0.0	0.0	0.0	0.0	0.0	0.0	0.0
5	35.1	5.7	16.1	-16.3	-11.9	1.4	2.5	0.0	-16.5
10	35.1	10.4	25.3	-34.1	-13.9	1.8	1.2	0.0	-47.1
20	26.6	25.3	33.5	-45.8	-14.9	2.7	3.6	0.0	-71.3
40	29.4	34.5	45.6	-47.6	-13.5	3.7	8.4	0.0	-77.2
80	34.9	47.2	75.5	-8.1	6.0	6.9	10.7	0.1	-39.9
120	32.2	49.0	81.5	51.9	36.1	11.4	11.9	0.4	6.6
160	37.6	54.7	74.8	70.8	51.0	13.0	11.9	-0.1	29.5
200	36.3	52.1	71.7	79.1	61.9	10.5	10.2	0.5	31.4
240	37.6	54.2	74.2	85.6	70.7	19.4	10.7	0.0	48.2
300	40.2	54.2	63.4	90.4	80.7	41.3	10.7	0.0	72.1
360	42.8	55.9	73.6	92.5	83.1	43.1	11.8	0.0	70.3
420	45.3	59.2	72.5	104.5	90.4	50.2	13.9	0.0	82.8

Table D.16. Percentage dissolution of the different metals at the respective sampling instances for test 2e.

Time (minutes)	Fe (%)	Ni (%)	Cu (%)	Ru (%)	Rh (%)	Pd (%)	Os (%)	Pt (%)	Ir (%)
0	0.0	0.0	0.0	0.0	0.0	0.0	0.0	0.0	0.0
5	-10.7	2.3	16.7	-14.3	-2.8	0.6	0.7	0.0	-21.3
10	-7.2	4.6	24.2	-23.0	-4.0	1.2	0.0	0.0	-39.9
20	-3.7	15.3	30.8	-31.9	-4.5	1.2	1.5	0.0	-53.4
40	-3.7	28.7	32.6	-38.6	-4.5	2.4	4.3	0.0	-57.0
80	6.5	57.9	45.8	-26.1	-1.6	4.3	9.3	1.1	-42.7
120	1.5	64.5	71.3	2.1	11.3	3.5	10.0	0.1	-22.7
160	-1.8	59.6	53.7	44.8	31.8	7.8	11.4	0.3	1.7
200	3.0	61.5	55.7	65.1	45.3	10.4	10.7	0.7	24.7
240	5.4	64.9	57.8	73.6	56.4	7.1	10.4	0.5	38.2
300	3.1	59.7	57.9	83.6	68.5	19.6	10.7	0.6	52.7
360	4.6	58.7	54.6	84.9	76.0	42.9	9.4	2.1	57.1
420	10.8	66.2	63.4	89.3	76.7	39.3	11.3	3.0	73.4

Table D.17. Percentage dissolution of the different metals at the respective sampling instances for test 2f.

Time (minutes)	Fe (%)	Ni (%)	Cu (%)	Ru (%)	Rh (%)	Pd (%)	Os (%)	Pt (%)	Ir (%)
0	0.0	0.0	0.0	0.0	0.0	0.0	0.0	0.0	0.0
5	14.2	7.0	15.6	-13.9	-2.5	1.5	1.5	0.1	-18.8
10	23.0	8.7	27.2	-23.7	-3.3	2.3	1.5	0.0	-31.2
20	26.5	28.5	37.6	-31.5	-4.0	2.7	4.4	0.0	-43.5
40	21.4	43.5	43.2	-31.5	-2.7	3.5	6.6	0.0	-39.8
80	31.5	67.2	45.2	4.7	12.2	3.9	13.0	0.1	-10.0
120	31.5	74.3	40.9	46.2	31.3	5.9	13.7	0.2	14.7
160	31.5	73.2	44.5	70.0	48.6	10.9	12.3	0.7	44.9
200	27.4	65.0	42.7	83.8	62.2	14.3	13.0	0.6	41.5
240	31.5	66.8	49.1	89.8	74.1	38.2	13.0	1.1	72.0
300	29.9	67.6	51.9	93.2	82.4	52.2	11.0	1.7	76.5
360	37.7	68.0	33.4	97.1	86.1	54.2	12.3	2.6	83.1
420	45.4	68.3	15.3	100.9	89.8	56.2	13.6	3.4	89.6

Table D18. Percentage dissolution of the different metals at the respective sampling instances for test 2g.

Time (minutes)	Fe (%)	Ni (%)	Cu (%)	Ru (%)	Rh (%)	Pd (%)	Os (%)	Pt (%)	Ir (%)
0	0.0	0.0	0.0	0.0	0.0	0.0	0.0	0.0	0.0
5	11.7	2.9	12.8	-26.5	-11.8	1.4	0.0	0.2	-28.9
10	8.8	17.0	22.4	-41.4	-16.0	2.5	2.4	0.0	-61.5
20	8.8	31.8	34.6	-50.8	-16.5	3.6	4.8	0.0	-77.6
40	8.8	50.2	64.6	-40.3	-9.1	5.5	7.2	0.0	-63.7
80	14.4	52.9	62.5	36.4	26.7	10.1	9.5	0.3	1.1
120	11.6	56.5	62.3	63.0	43.7	19.1	9.5	0.9	20.5
160	17.1	56.5	56.8	77.5	57.9	10.8	10.7	0.9	35.8
200	15.7	58.7	70.0	85.2	69.4	30.5	10.1	1.6	59.4
240	13.1	54.8	62.2	85.2	73.9	50.5	9.0	4.5	65.0
300	19.6	50.6	61.0	90.0	79.4	59.0	9.5	6.7	71.4
360	19.6	52.2	57.3	91.1	81.9	56.6	9.5	7.3	73.2
420	24.7	62.1	64.1	91.6	81.9	64.9	9.5	8.8	76.8

Table D.19. Percentage dissolution of the different metals at the respective sampling instances for test 2h.

Time (minutes)	Fe (%)	Ni (%)	Cu (%)	Ru (%)	Rh (%)	Pd (%)	Os (%)	Pt (%)	Ir (%)
0	0.0	0.0	0.0	0.0	0.0	0.0	0.0	0.0	0.0
5	23.4	38.1	17.0	-15.1	-1.8	1.8	1.2	0.0	-6.2
10	23.4	43.8	28.3	-24.0	-7.0	2.5	0.0	0.0	-16.4
20	23.4	49.3	40.1	-31.0	-8.0	3.6	1.2	0.0	-24.4
40	20.6	58.5	54.8	-31.6	-6.7	5.6	2.4	0.0	-32.4
80	23.4	72.1	66.3	-11.0	-1.6	6.3	4.7	0.0	-10.8
120	26.1	86.4	74.2	12.2	10.2	6.3	9.3	0.1	4.7
160	26.1	87.3	70.1	37.9	27.0	10.1	9.3	1.9	16.2
200	23.4	89.9	68.8	45.6	33.4	11.9	8.8	0.5	19.0
240	27.4	90.8	66.3	51.3	38.4	16.2	7.7	0.7	26.5
300	23.5	95.9	69.6	59.0	53.4	22.3	10.4	1.2	31.1
360	41.5	95.0	77.6	73.8	59.5	22.3	11.5	1.2	45.6
420	33.9	95.0	67.6	73.8	59.5	34.7	10.4	1.4	38.4

Table D.20. Percentage dissolution of the different metals at the respective sampling instances for test 2i.

Time (minutes)	Fe (%)	Ni (%)	Cu (%)	Ru (%)	Rh (%)	Pd (%)	Os (%)	Pt (%)	Ir (%)
0	0.0	0.0	0.0	0.0	0.0	0.0	0.0	0.0	0.0
5	19.6	6.7	12.8	-9.7	-1.5	1.3	0.7	0.0	-7.5
10	21.3	13.0	20.3	-17.3	-3.7	1.9	2.2	0.0	-17.5
20	21.3	22.0	29.1	-25.2	-4.6	2.3	3.7	0.0	-28.5
40	27.3	40.4	41.9	-24.8	-3.0	3.9	6.9	0.0	-31.5
80	28.2	56.9	41.7	4.8	11.4	3.6	10.8	0.0	-5.8
120	33.2	68.4	35.6	23.3	14.3	2.4	14.3	0.0	13.0
160	28.2	79.1	34.4	38.9	22.2	3.5	13.6	0.1	16.5
200	38.0	77.5	44.0	50.0	27.6	4.3	12.3	0.2	32.6
240	30.0	70.2	43.2	59.5	33.8	8.8	12.9	0.4	28.0
300	26.8	74.3	39.0	68.3	42.1	15.8	13.6	0.8	43.6
360	23.7	68.7	32.1	77.3	53.6	25.2	13.6	0.0	43.6
420	5.2	53.2	30.4	73.2	56.2	35.3	10.4	1.0	40.4

Table D.21. Percentage dissolution of the different metals at the respective sampling instances for test 2j.

Time (minutes)	Fe (%)	Ni (%)	Cu (%)	Ru (%)	Rh (%)	Pd (%)	Os (%)	Pt (%)	Ir (%)
0	0.0	0.0	0.0	0.0	0.0	0.0	0.0	0.0	0.0
5	17.6	6.7	29.6	-13.2	-8.1	1.9	1.2	0.0	4.1
10	20.5	13.3	35.0	-18.0	-12.1	3.2	0.0	0.0	-10.1
20	17.6	15.1	49.2	-20.4	-13.8	5.2	2.4	0.0	-20.2
40	20.4	22.5	71.8	-9.9	-11.8	6.5	2.4	0.0	-10.3
80	31.6	45.1	68.5	10.7	-2.8	5.9	10.6	0.0	3.5
120	31.6	52.3	69.9	33.3	14.3	6.5	11.7	0.1	17.0
160	26.1	53.2	72.7	46.7	23.4	9.7	10.6	0.3	24.7
200		52.3	71.9	47.3	28.5	12.8	7.2	0.6	34.1
240	20.9	55.3	80.0	61.4	36.0	17.4	10.0	0.7	29.5
300	24.8	71.4	75.2	70.2	45.4	25.0	11.1	1.3	45.1
360	29.9	55.1	75.8	77.9	54.5	28.0	12.7	1.5	45.1
420	32.5	61.7	73.9	82.6	58.2	43.9	11.7	2.4	52.2

Table D.22. Percentage dissolution of the different metals at the respective sampling instances for test 2k.

Time (minutes)	Fe (%)	Ni (%)	Cu (%)	Ru (%)	Rh (%)	Pd (%)	Os (%)	Pt (%)	Ir (%)
0	0.0	0.0	0.0	0.0	0.0	0.0	0.0	0.0	0.0
5	14.6	11.4	14.3	-21.1	-3.4	5.5	0.0	0.0	-18.6
10	23.3	16.1	15.8	-35.3	-7.9	3.2	0.0	0.0	-53.2
20	23.3	26.4	36.5	-50.6	-9.8	2.6	0.0	0.0	-77.4
40	26.1	40.1	20.3	-58.2	-9.5	2.5	2.4	0.0	-85.4
80	26.1	70.9	50.6	-21.5	0.3	0.2	4.7	0.0	-53.9
120	28.9	62.0	70.1	46.9	34.4	0.2	3.5	0.4	4.2
160	28.9	62.9	49.5	71.4	53.8	0.2	3.5	0.5	11.9
200	26.2	61.1	73.7	78.3	60.2	4.5	3.5	0.6	36.4
240	32.8	68.9	37.1	88.9	68.4	12.8	3.5	0.7	43.8
300	28.9	59.5	72.7	92.1	75.2	35.6	3.5	2.6	62.2
360	36.6	72.1	40.4	94.8	81.4	33.2	3.5	4.9	76.7
420	36.6	71.3	39.2	96.3	81.4	33.8	3.5	4.5	78.5

Table D.23. Percentage dissolution of the different metals at the respective sampling instances for test 2l.

Time (minutes)	Fe (%)	Ni (%)	Cu (%)	Ru (%)	Rh (%)	Pd (%)	Os (%)	Pt (%)	Ir (%)
0	0.0	0.0	0.0	0.0	0.0	0.0	0.0	0.0	0.0
5	17.6	17.2	28.9	-22.3	-3.1	-0.1	0.0	0.0	-16.5
10	20.5	21.9	34.0	-35.4	-7.0	-0.9	1.2	0.0	-43.0
20	17.6	20.9	47.7	-44.2	-8.7	3.6	1.2	0.0	-63.2
40	23.2	53.1	74.4	-31.4	1.6	2.0	2.4	0.0	-49.2
80	28.8	63.9	77.4	41.3	34.0	2.0	3.6	0.2	-4.1
120	28.8	59.5	73.3	70.7	55.8	-1.5	4.7	0.7	30.8
160	31.5	67.4	88.1	83.5	59.7	4.8	4.7	0.8	59.5
200	32.9	67.0	85.3	91.8	71.9	27.9	3.6	1.7	76.5
240	31.5	67.8	79.2	96.2	79.4	40.2	3.6	0.0	70.9
300	36.7	66.6	75.9	98.3	82.5	48.1	3.6	2.2	81.9
360	34.2	66.6	80.7	98.3	82.5	51.7	3.6	3.1	78.3
420	34.2	74.0	87.5	95.2	82.5	47.0	3.6	3.1	83.7

Table D.24. Percentage dissolution of the different metals at the respective sampling instances for test 2m.

Time (minutes)	Fe (%)	Ni (%)	Cu (%)	Ru (%)	Rh (%)	Pd (%)	Os (%)	Pt (%)	Ir (%)
0	0.0	0.0	0.0	0.0	0.0	0.0	0.0	0.0	0.0
5	16.0	2.9	12.6	-13.2	-0.6	-0.2	0.7	0.0	-12.6
10	24.8	10.3	38.0	-21.9	-3.5	-0.1	0.7	0.0	-32.4
20	33.5	24.5	39.3	-31.9	-4.1	-0.2	1.5	0.0	-43.4
40	23.2	31.2	37.9	-40.3	-4.3	-0.3	1.5	0.0	-49.5
80	26.6	53.7	48.3	-34.8	-1.5	0.0	3.6	0.0	-41.1
120	31.6	72.8	45.2	-6.6	3.8	0.1	5.0	0.0	-19.9
160	23.4	63.7	47.7	50.4	29.0	3.9	5.7	0.4	21.9
200	29.9	65.8	55.5	73.3	44.1	5.4	5.7	0.7	47.2
240	33.1	70.2	55.2	81.5	54.5	6.5	5.4	0.6	50.6
300	29.9	62.7	47.9	91.8	66.5	2.3	5.7	0.5	61.7
360	33.0	64.8	36.0	97.2	75.5	36.1	5.0	2.5	80.4
420	34.6	67.8	54.3	92.8	76.9	17.5	4.4	3.4	89.1

Table D.25. Percentage dissolution of the different metals at the respective sampling instances for test 2n.

Time (minutes)	Fe (%)	Ni (%)	Cu (%)	Ru (%)	Rh (%)	Pd (%)	Os (%)	Pt (%)	Ir (%)
0	0.0	0.0	0.0	0.0	0.0	0.0	0.0	0.0	0.0
5	27.5	17.2	28.4	-11.4	-8.4	0.3	1.2	0.0	4.1
10	30.4	11.5	27.9	-20.4	-11.1	0.3	0.0	0.1	-18.3
20	27.5	22.7	64.3	-23.9	-12.5	0.0	1.2	0.0	-20.3
40	30.4	19.9	78.6	-10.5	-6.3	0.0	2.4	0.0	-6.4
80	35.9	61.6	91.5	12.4	2.2	-0.1	3.6	0.0	9.3
120	35.9	58.9	73.6	41.8	20.6	1.2	4.7	0.2	13.2
160	30.5	67.7	91.5	54.0	27.0	4.0	3.6	0.4	30.4
200	35.9	73.4	87.1	67.0	39.2	14.8	4.7	0.0	48.3
240	42.5	62.2	78.3	70.5	39.2	11.7	4.7	0.9	34.4
300	38.6	63.5	75.2	75.3	46.0	13.7	4.7	1.1	41.7
360	36.0	74.4	94.9	80.1	54.6	31.0	4.7	2.0	58.0
420	41.1	79.3	85.5	86.9	61.8	44.9	4.7	3.3	58.0

Table D.26. Percentage dissolution of the different metals at the respective sampling instances for test 2o.

Time (minutes)	Fe (%)	Ni (%)	Cu (%)	Ru (%)	Rh (%)	Pd (%)	Os (%)	Pt (%)	Ir (%)
0	0.0	0.0	0.0	0.0	0.0	0.0	0.0	0.0	0.0
5	16.0	2.3	9.3	-10.6	-4.2	0.0	0.7	0.0	-2.5
10	19.5	5.8	17.6	-17.1	-2.3	0.1	0.7	0.0	-8.7
20	30.0	14.8	27.0	-25.3	-4.0	0.0	2.2	0.0	-22.2
40	24.8	34.3	32.5	-31.3	-4.2	0.0	3.6	0.0	-34.3
80	19.7	53.6	37.9	-18.5	-2.4	0.2	6.5	0.0	-23.5
120	31.4	64.5	16.2	9.0	7.8	0.2	8.6	0.1	2.4
160	31.4	62.3	39.2	19.9	12.5	0.2	7.9	0.1	4.7
200	31.4	63.9	34.1	32.3	17.9	2.4	8.6	0.1	9.3
240	36.2	68.1	45.6	46.8	26.7	3.0	7.9	1.7	26.8
300	32.3	65.5	43.1	57.7	31.6	2.3	8.2	0.4	27.4
360	29.9	60.4	32.5	68.7	39.1	10.1	7.9	0.5	32.9
420	39.2	71.5	18.2	79.2	47.9	20.8	8.6	0.8	47.0

Table D.27. Percentage dissolution of the different metals at the respective sampling instances for test 2p.

Time (minutes)	Fe (%)	Ni (%)	Cu (%)	Ru (%)	Rh (%)	Pd (%)	Os (%)	Pt (%)	Ir (%)
0	0.0	0.0	0.0	0.0	0.0	0.0	0.0	0.0	0.0
5	11.7	12.3	17.8	-14.5	-7.3	0.0	0.0	0.0	-2.1
10	17.5	17.9	38.8	-24.6	-11.1	0.0	1.2	0.0	-4.1
20	11.8	27.2	70.6	-34.5	-9.4	0.0	1.2	0.0	-26.3
40	23.1	13.5	60.3	-32.2	-8.7	0.0	2.4	0.0	-30.2
80	17.5	54.2	72.1	-7.6	-0.2	0.0	4.7	0.0	-16.5
120	25.7	64.1	90.2	24.6	17.9	0.0	7.0	0.1	16.5
160	23.0	67.6	86.5	43.0	27.0	0.0	7.0	0.2	20.3
200	21.7	64.1	78.4	51.8	30.8	3.9	7.0	0.4	26.0
240	24.3	62.8	74.7	59.2	38.4	9.9	7.0	0.5	26.0
300	20.4	68.3	85.4	64.8	43.4	16.6	7.0	0.9	40.6
360	25.6	65.8	80.6	72.2	50.7	24.4	7.0	1.1	47.9
420	25.6	57.6	73.3	75.9	59.2	26.7	7.0	1.1	42.5

D.5: Fourth order Runge-Kutta method

The Runge-Kutta method was used to numerically solve the ordinary differential equations derived by performing mass balances for the respective species present in the experimental batch system, as given by Equations 5.59 to 5.79. In the general case, the diffential equation is given by equation D-7 for species i, where the initial value of C_i at time zero, $C_{i,0}$, is known:

$$\frac{dC_i}{dt} = f(t, C_i) \qquad [D\text{-}7]$$

The Runge-Kutta solution is given by Equation D-8:

$$C_{i,n+1} = C_{i,n} + \frac{k_1' + 2 \cdot k_2' + 2 \cdot k_3' + k_4'}{6} \qquad [D\text{-}8]$$

where:

$$k_1' = h \cdot f(t_n, C_{i,n}) \qquad [D\text{-}9]$$

$$k_2' = h \cdot f\left(t_n + {}^{h}/_{2}, C_{i,n} + {}^{k_1'}/_{2}\right) \qquad [D\text{-}10]$$

$$k_3' = h \cdot f\left(t_n + {}^{h}/_{2}, C_{i,n} + {}^{k_2'}/_{2}\right) \qquad [D\text{-}11]$$

$$k_4' = h \cdot f(t_n + h, C_{i,n} + k_3') \qquad [D\text{-}12]$$

where h is the time step, which was taken to be 0.2 minutes in this study.

APPENDIX E: REACTION KINETICS RESULTS

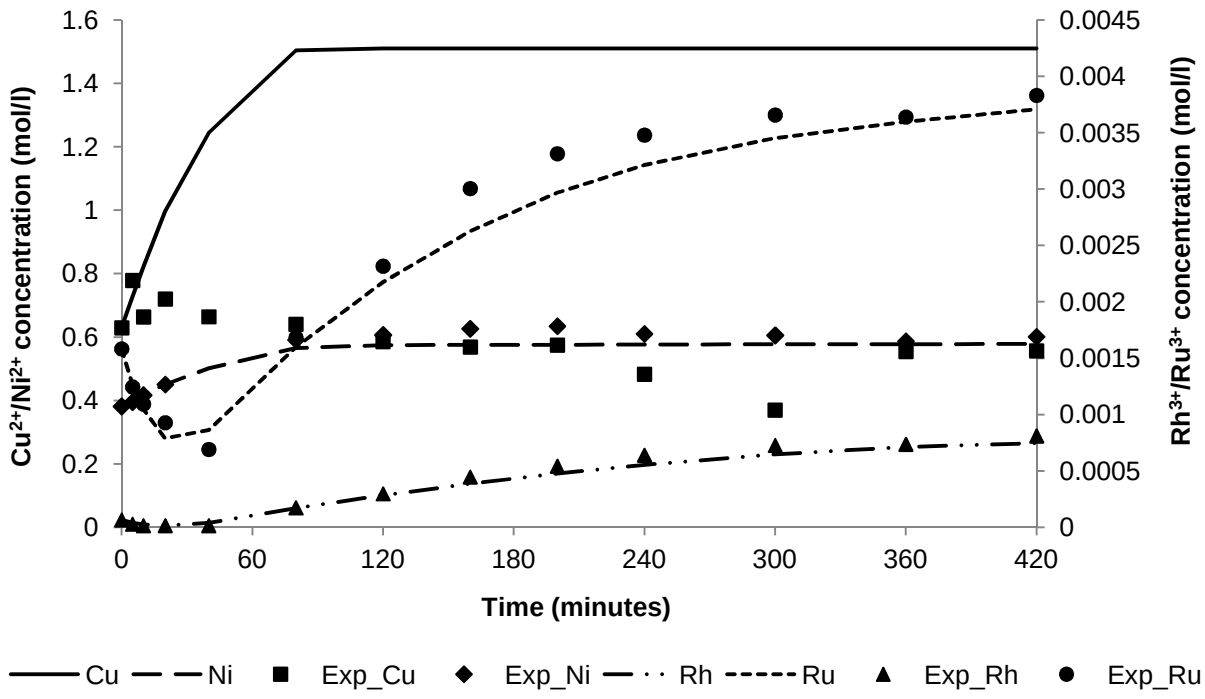

Figure E.1. Comparison of the model predicted metal concentrations as a function of leaching time and the experimental metal concentrations after correction for sampling losses for test 2a (T = 116°C; P = 9 bar; [M_{H2SO4}] = 165 g/ℓ; solids content = 130 g/ℓ).

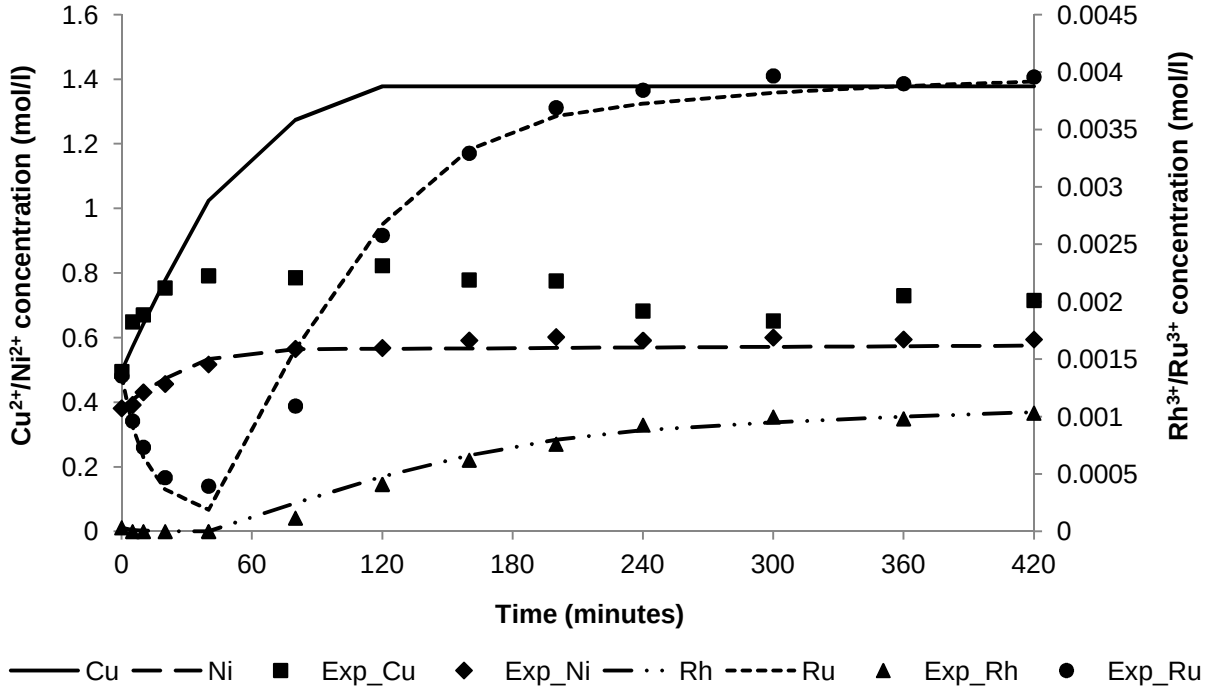

Figure E.2. Comparison of the model predicted metal concentrations as a function of leaching time and the experimental metal concentrations after correction for sampling losses for test 2b (T = 130°C; P = 9 bar; [M_{H2SO4}] = 165 g/ℓ; solids content = 130 g/ℓ).

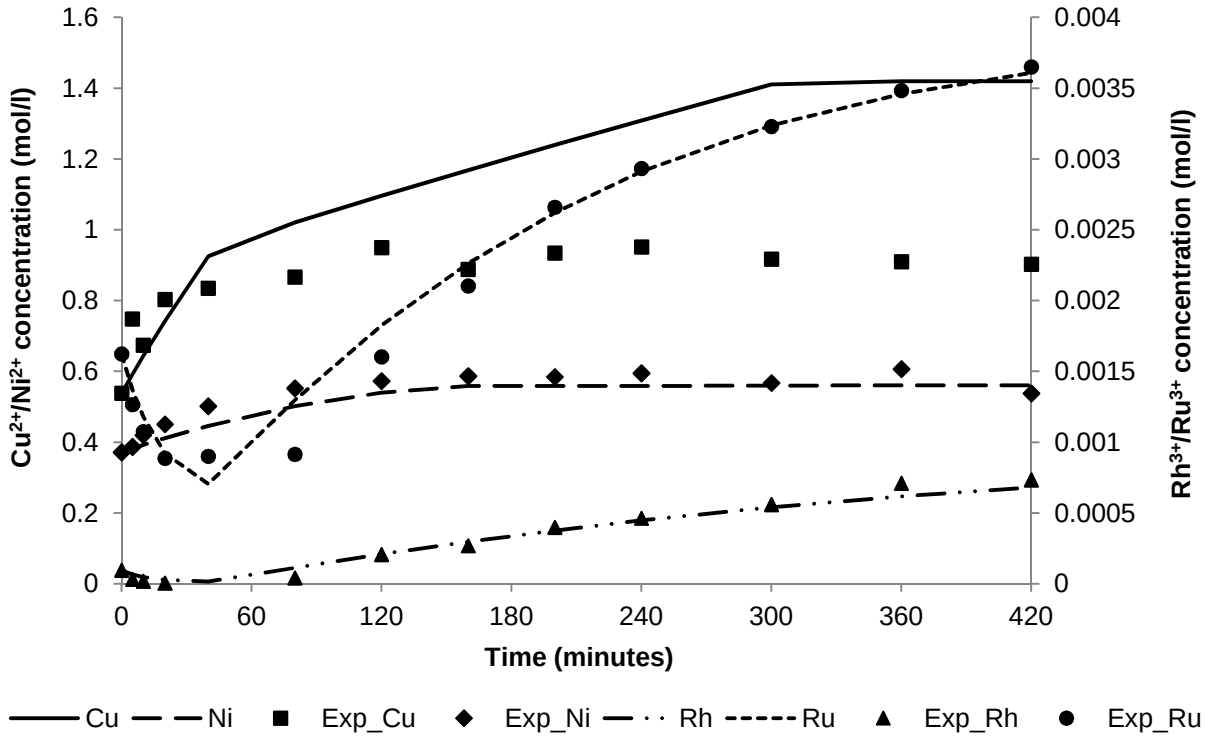

Figure E.3. Comparison of the model predicted metal concentrations as a function of leaching time and the experimental metal concentrations after correction for sampling losses for test 2c (T = 116°C; P = 7 bar; [M_{H2SO4}] = 165 g/ℓ; solids content = 130 g/ℓ).

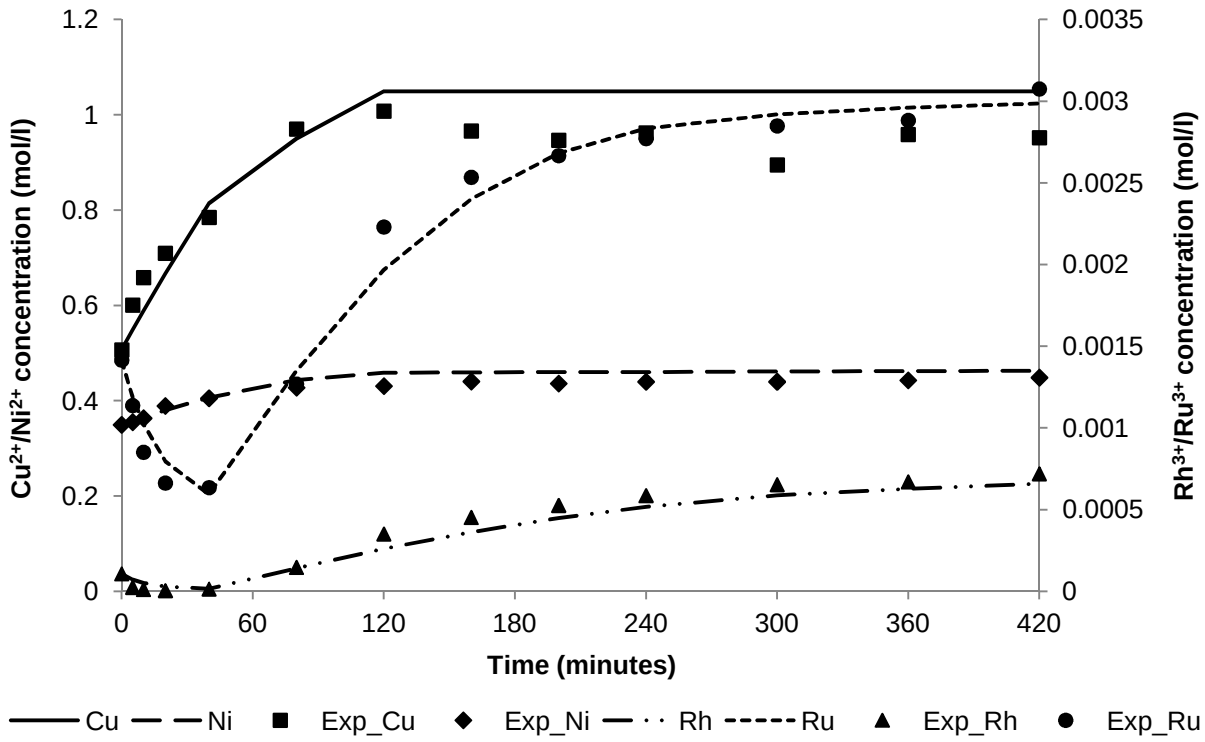

Figure E.4. Comparison of the model predicted metal concentrations as a function of leaching time and the experimental metal concentrations after correction for sampling losses for test 2d (T = 130°C; P = 7 bar; [M_{H2SO4}] = 140 g/ℓ; solids content = 80 g/ℓ).

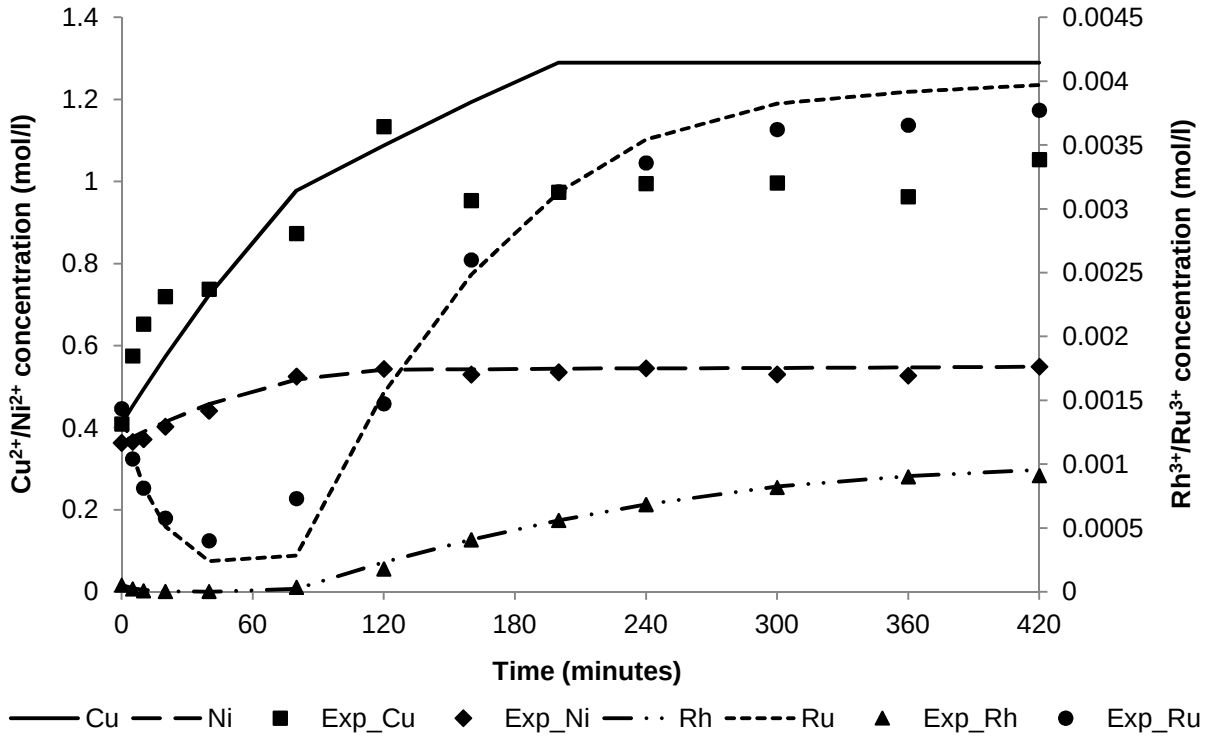

Figure E.5. Comparison of the model predicted metal concentrations as a function of leaching time and the experimental metal concentrations after correction for sampling losses for test 2e (T = 130°C; P = 7 bar; [M_{H2SO4}] = 140 g/ℓ; solids content = 130 g/ℓ).

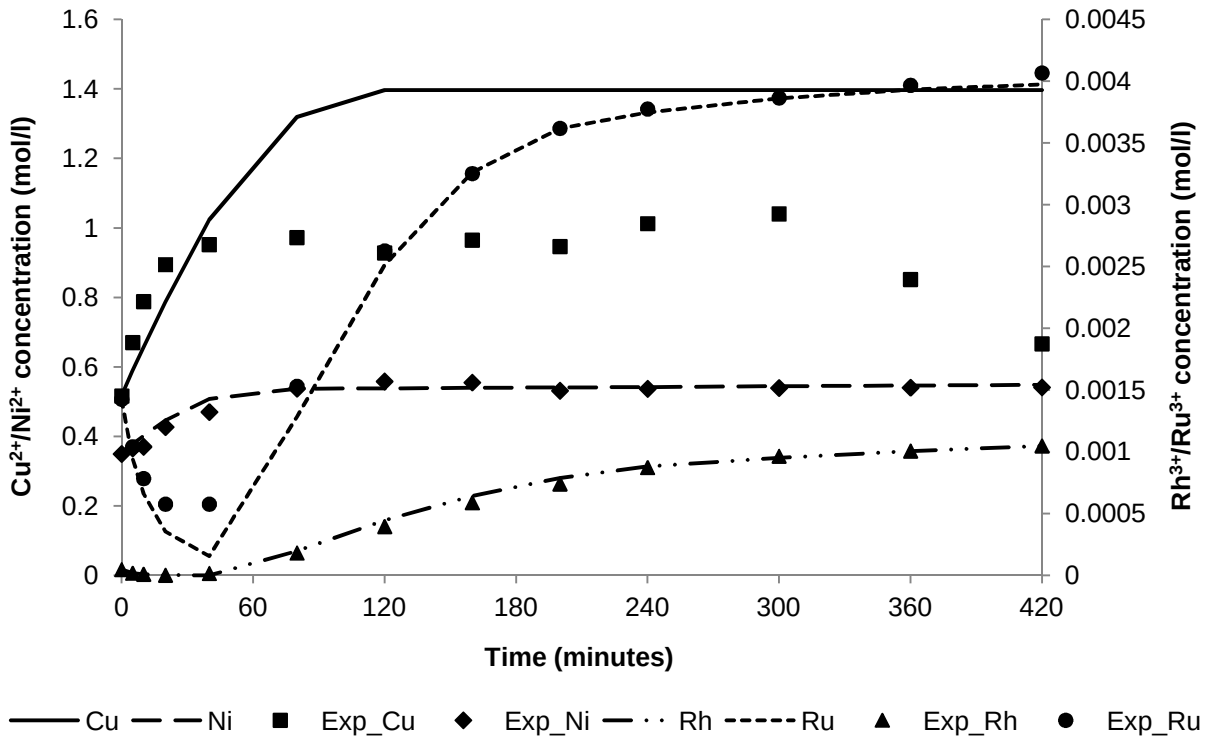

Figure E.6. Comparison of the model predicted metal concentrations as a function of leaching time and the experimental metal concentrations after correction for sampling losses for test 2f (T = 130°C; P = 9 bar; [M_{H2SO4}] = 140 g/ℓ; solids content = 130 g/ℓ).

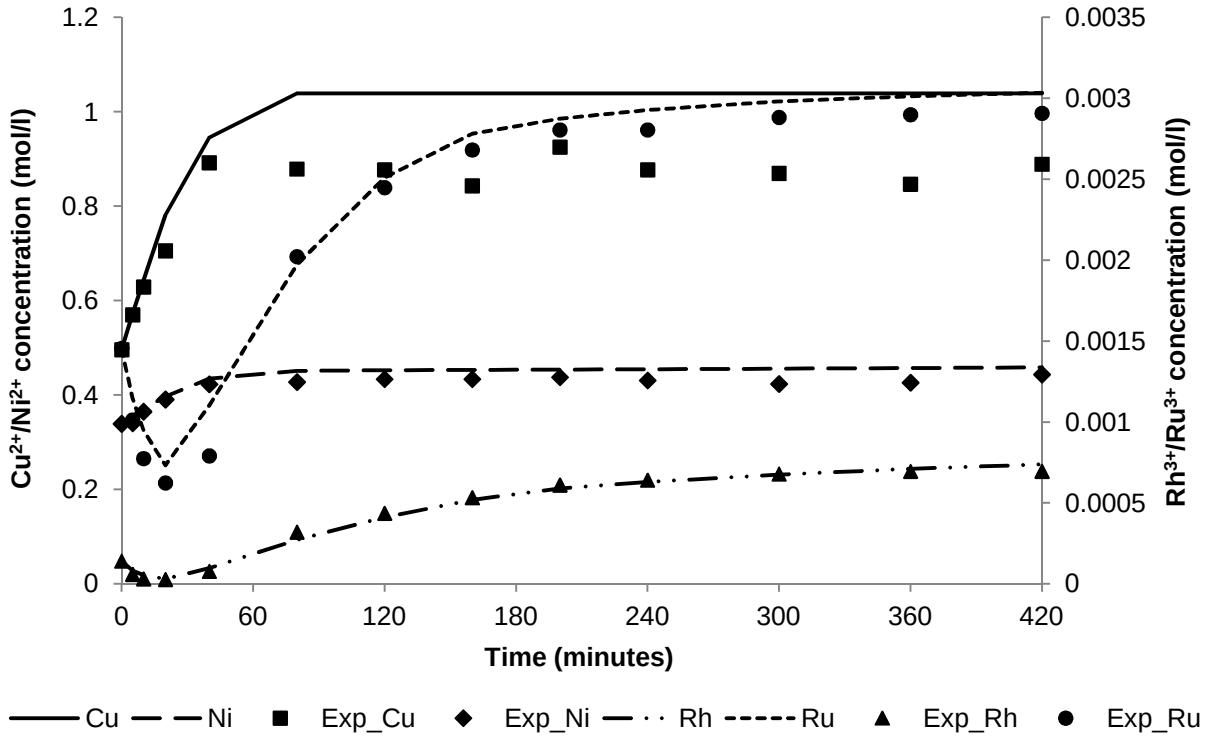

Figure E.7. Comparison of the model predicted metal concentrations as a function of leaching time and the experimental metal concentrations after correction for sampling losses for test 2g (T = 130°C; P = 9 bar; [M_{H2SO4}] = 165 g/ℓ; solids content = 80 g/ℓ).

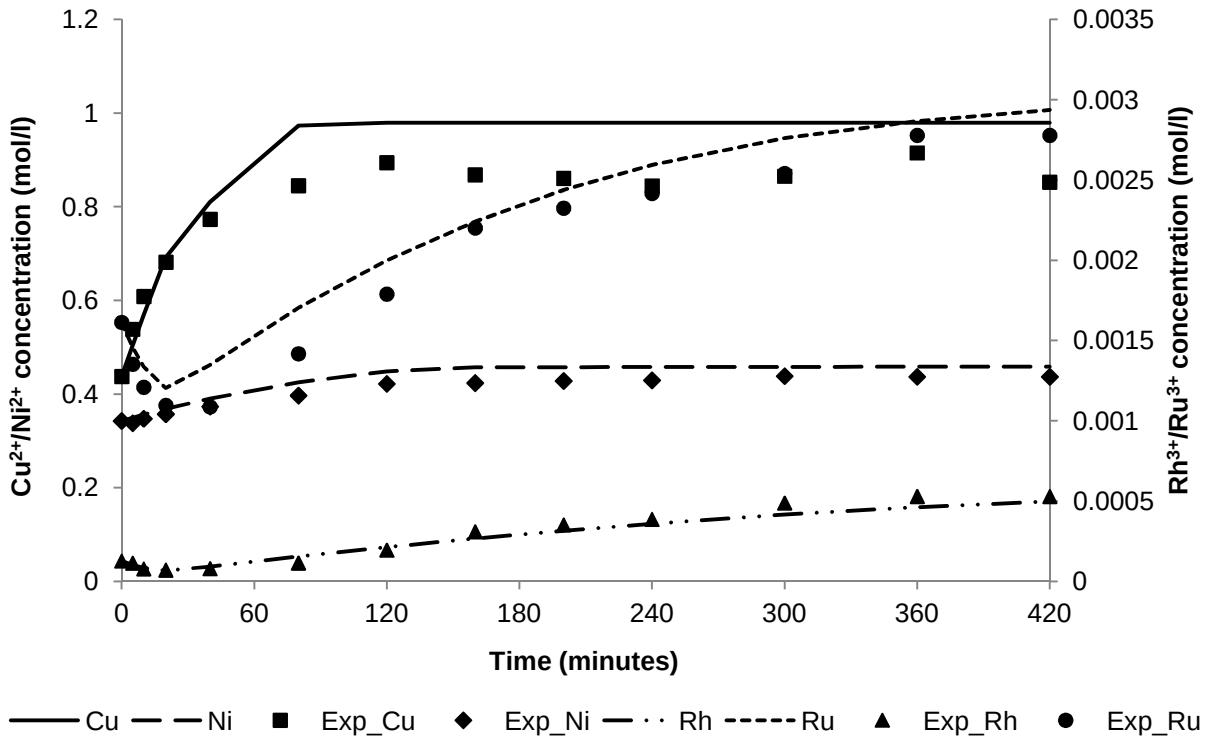

Figure E.8. Comparison of the model predicted metal concentrations as a function of leaching time and the experimental metal concentrations after correction for sampling losses for test 2h (T = 116°C; P = 7 bar; [M_{H2SO4}] = 165 g/ℓ; solids content = 80 g/ℓ).

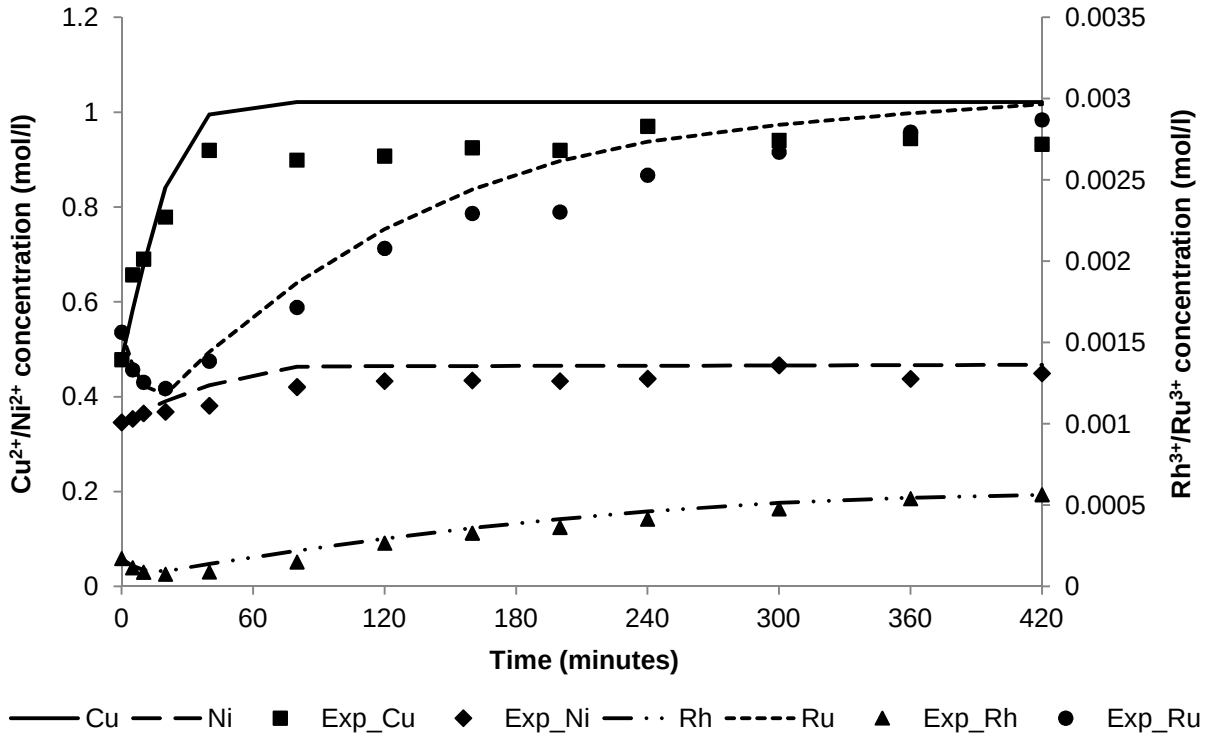

Figure E.9. Comparison of the model predicted metal concentrations as a function of leaching time and the experimental metal concentrations after correction for sampling losses for test 2j (T = 116°C; P = 9 bar; [M_{H2SO4}] = 165 g/ℓ; solids content = 80 g/ℓ).

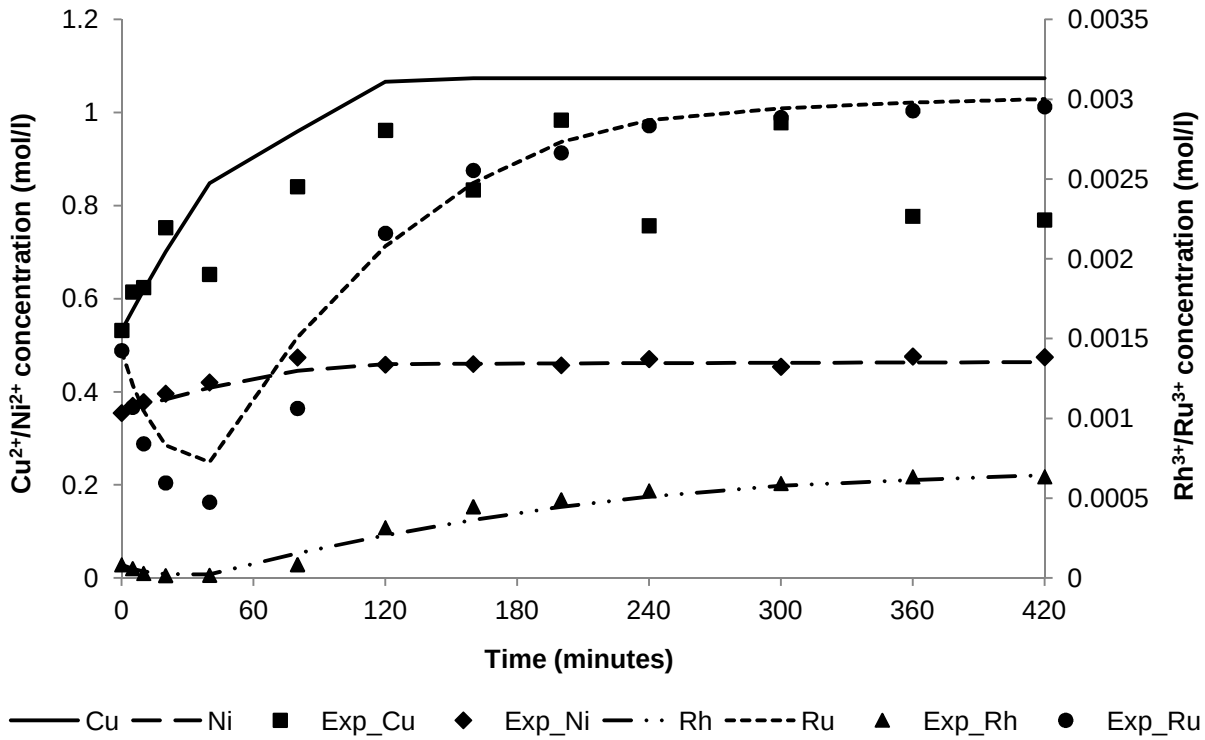

Figure E.10. Comparison of the model predicted metal concentrations as a function of leaching time and the experimental metal concentrations after correction for sampling losses for test 2k (T = 130°C; P = 7 bar; [M_{H2SO4}] = 165 g/ℓ; solids content = 80 g/ℓ).

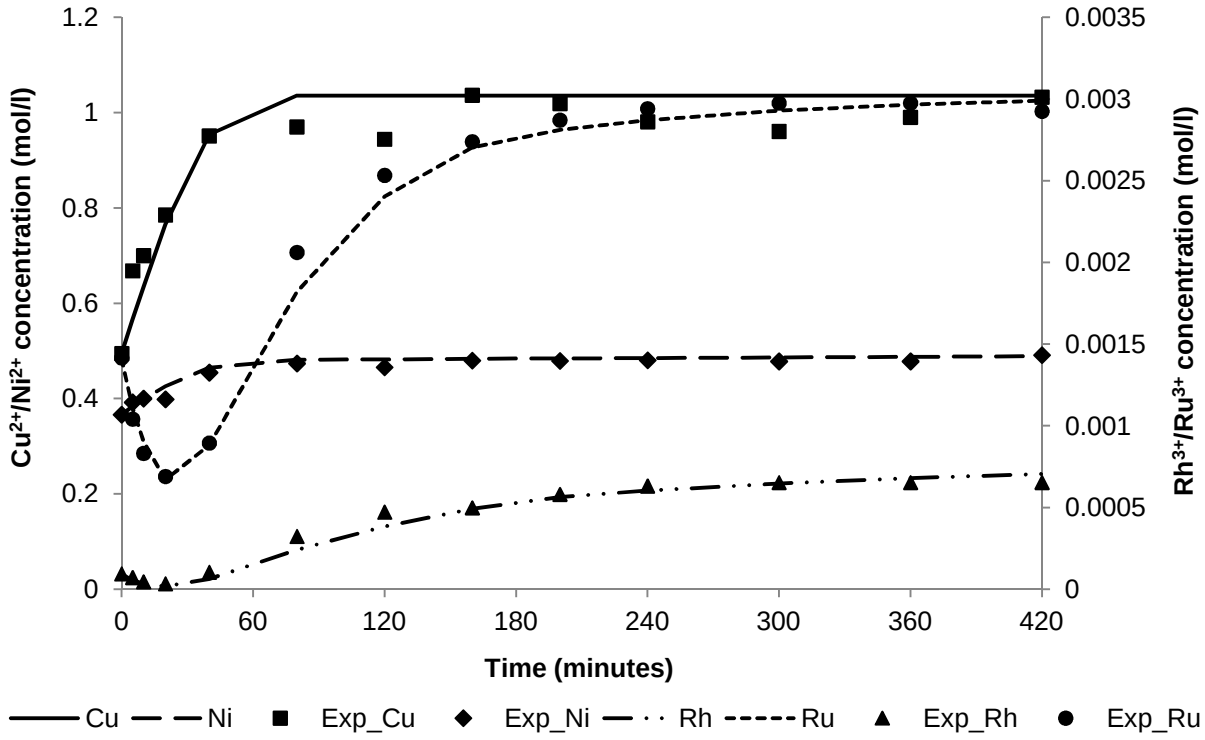

Figure E.11. Comparison of the model predicted metal concentrations as a function of leaching time and the experimental metal concentrations after correction for sampling losses for test 2l (T = 130°C; P = 9 bar; [M_{H2SO4}] = 140 g/ℓ; solids content = 80 g/ℓ).

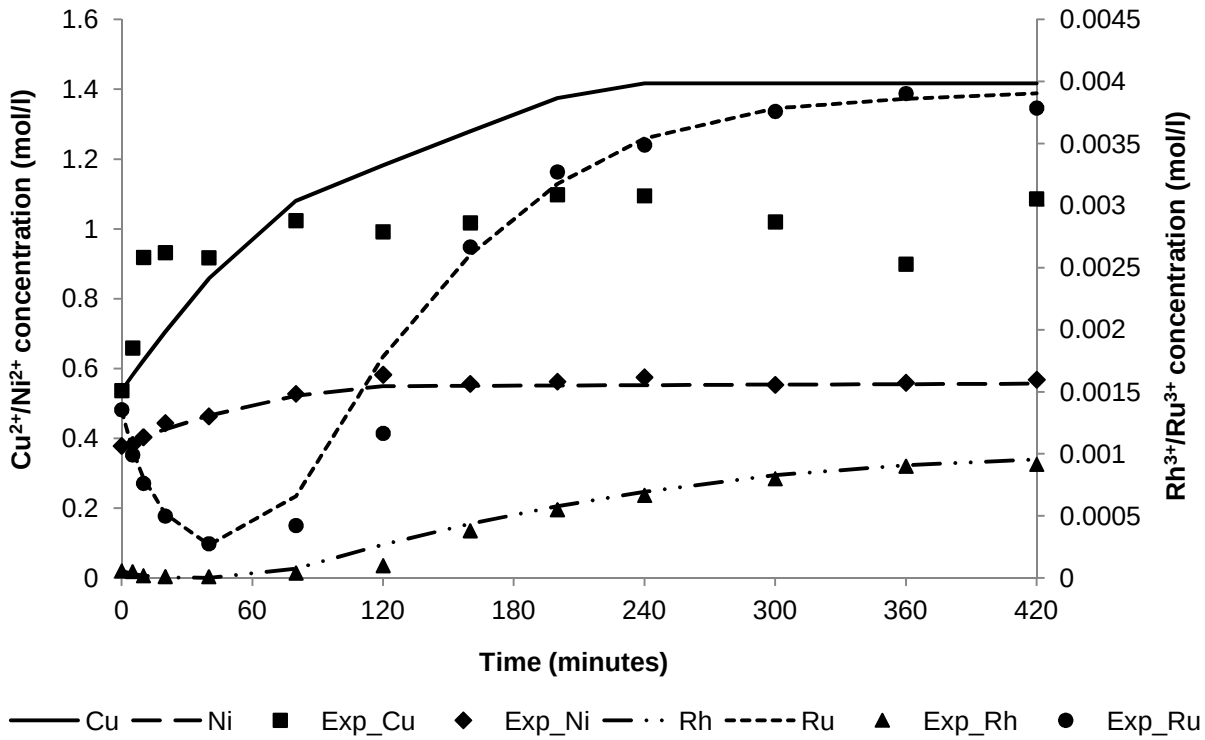

Figure E.12. Comparison of the model predicted metal concentrations as a function of leaching time and the experimental metal concentrations after correction for sampling losses for test 2m (T = 130°C; P = 7 bar; [M_{H2SO4}] = 165 g/ℓ; solids content = 130 g/ℓ).

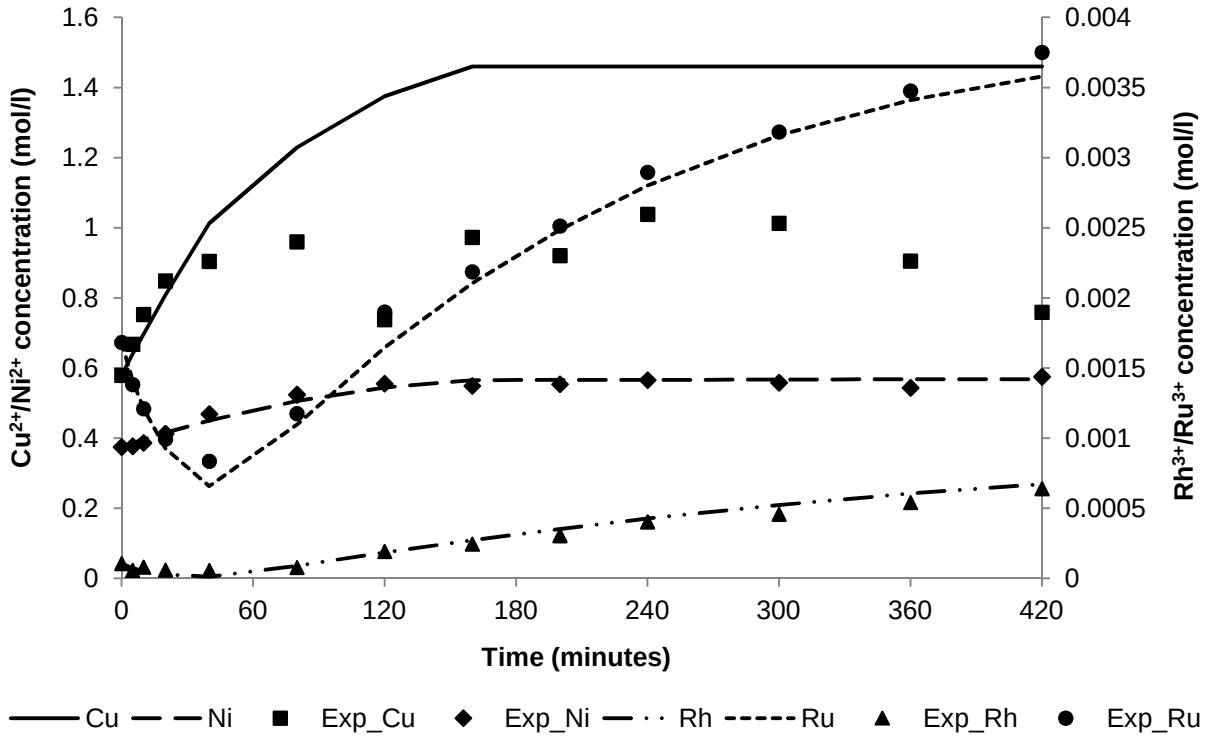

Figure E.13. Comparison of the model predicted metal concentrations as a function of leaching time and the experimental metal concentrations after correction for sampling losses for test 2o (T = 116°C; P = 7 bar; [M_{H2SO4}] = 140 g/ℓ; solids content = 130 g/ℓ).

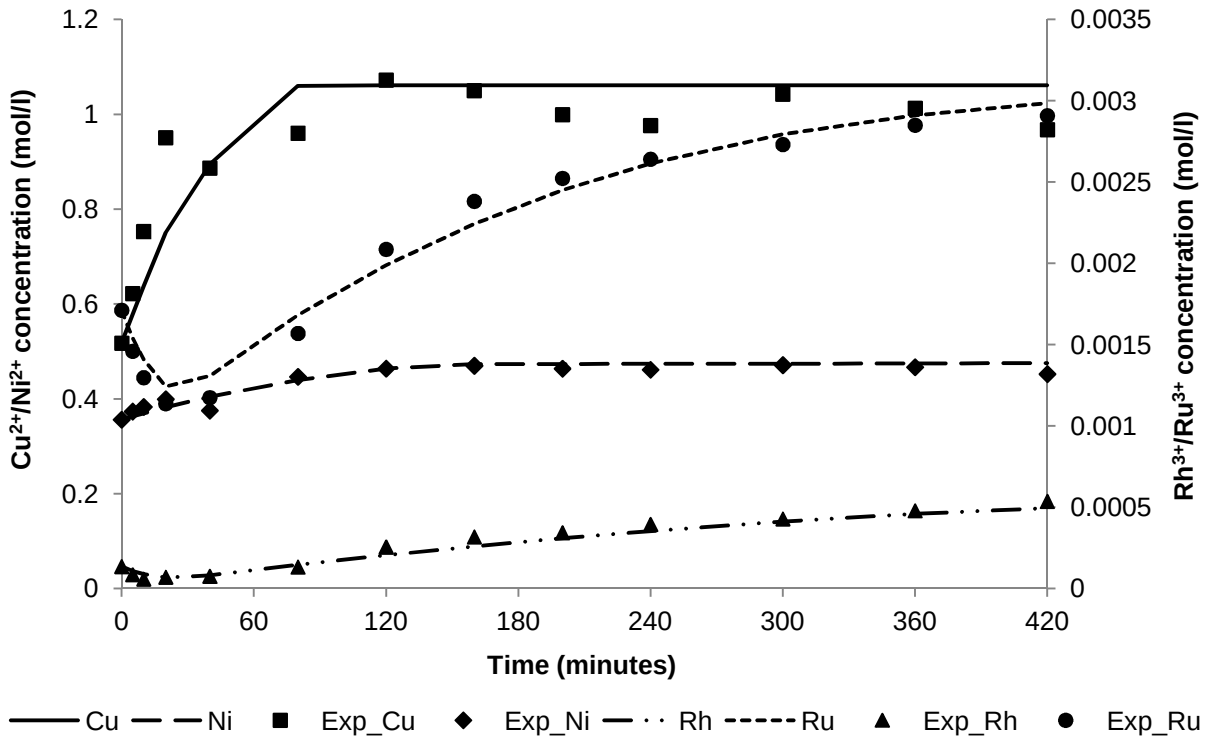

Figure E.14. Comparison of the model predicted metal concentrations as a function of leaching time and the experimental metal concentrations after correction for sampling losses for test 2p (T = 116°C; P = 7 bar; [M_{H2SO4}] = 140 g/ℓ; solids content = 80 g/ℓ).

APPENDIX F: MODEL EQUATIONS

The mass and energy balances for the respective subsystems discussed in Section 6.3 are given in the following sections of this appendix. For each subsystem, the balances were written in accordance with the stream numbers shown in the respective figures. For all energy balances, the reagents and products at 25°C were used as reference state for enthalpy calculations. In any given equation, the symbols are defined as follows (these symbols are included in the nomenclature, but are repeated here for clarity):

- $x_{S,i}$ – mass fraction solids in steam *i*, kg solids/kg total mass
- $x_{L,i}$ – mass fraction liquid in steam *i*, kg liquid/kg total mass
- $x_{j,S,i}$ – mass fraction of component *j* in the solids in stream *i*, kg *j*/kg solids
- $x_{j,L,i}$ – mass fraction of component *j* in the liquid in stream *i*, kg *j*/kg liquid
- m_i – mass of material in system *i*, kg
- $m_{S,i}$ – mass of solid material in system *i*, kg
- $m_{j,S,i}$ – mass of solid component *j* in system *i*, kg
- $m_{L,i}$ – mass of liquid in system *i*, kg
- $m_{j,L,i}$ – mass of liquid component *j* in system *i*, kg
- $\dot{m}_i$ – mass flow rate of stream *i*, kg/h
- T_i – temperature of stream *i*, °C
- $C_{P,L,i}$ – heat capacity of the liquid portion of stream *i*, J/kg·°C
- $C_{P,S,i}$ – heat capacity of the solid portion of stream *i*, J/kg·°C
- $\widehat{H}_i$ – specific enthalpy of stream *i*, J/kg
- $\Delta\widehat{H}_{Evap}$ – heat of evaporation, J/kg

F.1: Second stage slurry preparation tank

Total mass balance:

$$\frac{dm_{TK10}}{dt} = \dot{m}_1 + \dot{m}_2 + \dot{m}_3 + \dot{m}_4 - \dot{m}_5 \quad [F.1]$$

As discussed in Section 6.3, the mass flow rate out of the second stage slurry preparation tank, $\dot{m}_5$, was assumed to be proportional to the square root of the mass of slurry inside the tank:

$$\dot{m}_5 = K'_{TK10} \cdot \sqrt{m_{TK10}} \quad [F.2]$$

where the proportionality factor, K'_{TK10}, was calculated from the initial steady state operating conditions:

$$K'_{TK10} = \frac{\dot{m}_1 + \dot{m}_2 + \dot{m}_3 + \dot{m}_4}{\left(\sqrt{m_{TK10}}\right)_{Steady\ state}} \quad [F.3]$$

Solids mass balance:

Given the assumption that chemical reactions do not occur in the auxiliary process units, the accumulation of solids in the slurry preparation tank could only be attributed to solids flowing into and out of the unit:

$$\frac{dm_{S,TK10}}{dt} = x_{S,1} \cdot \dot{m}_1 - x_{S,5} \cdot \dot{m}_5 \quad [F.4]$$

The slurry preparation tank was assumed to be perfectly mixed, implying that the composition of the tank content and stream 5 had to be the same:

$$\therefore \frac{d\left(x_{S,5} \cdot m_{TK10}\right)}{dt} = x_{S,1} \cdot \dot{m}_1 - x_{S,5} \cdot K'_{TK10} \cdot \sqrt{m_{TK10}} \quad [F.5]$$

$$\therefore \frac{dx_{S,5}}{dt} = \frac{x_{S,1} \cdot \dot{m}_1 - x_{S,5} \cdot K'_{TK10} \cdot \sqrt{m_{TK10}} - x_{S,5} \cdot \frac{dm_{TK10}}{dt}}{m_{TK10}} \quad [F.6]$$

Solid species mass balance (for any mineralogical phase):

$$\frac{dm_{j,S,TK10}}{dt} = x_{j,S,1} \cdot x_{S,1} \cdot \dot{m}_1 - x_{j,S,5} \cdot x_{S,5} \cdot \dot{m}_5 \quad [F.7]$$

$$\therefore \frac{d\left(x_{j,S,5} \cdot x_{S,5} \cdot m_{TK10}\right)}{dt} = x_{j,S,1} \cdot x_{S,1} \cdot \dot{m}_1 - x_{j,S,5} \cdot x_{S,5} \cdot K'_{TK10} \cdot \sqrt{m_{TK10}} \quad [F.8]$$

$$\therefore \frac{dx_{j,S,5}}{dt} = \frac{x_{j,S,1} \cdot x_{S,1} \cdot \dot{m}_1 - x_{j,S,5} \cdot x_{S,5} \cdot K'_{TK10} \cdot \sqrt{m_{TK10}} - x_{j,S,5} \cdot \frac{d\left(x_{S,5} \cdot m_{TK10}\right)}{dt}}{x_{S,5} \cdot m_{TK10}} \quad [F.9]$$

Liquid mass balance:

The sum of the fraction of liquid in the slurry in the system and the fraction of solids in the slurry in the system had to be equal to one; as a result, the mass fraction liquid in stream 5 could be written in terms of the mass fraction solids in stream 5:

$$\frac{dx_{L,5}}{dt} = \frac{d\left(1 - x_{S,5}\right)}{dt} = -\frac{dx_{S,5}}{dt} \quad [F.10]$$

Liquid species mass balance (for solutes):

$$\frac{dm_{j,L,TK10}}{dt} = x_{j,L,1} \cdot x_{L,1} \cdot \dot{m}_1 + x_{j,L,2} \cdot \dot{m}_2 + x_{j,L,4} \cdot \dot{m}_4 - x_{j,L,5} \cdot x_{L,5} \cdot \dot{m}_5 \quad [F.11]$$

Following an approach similar to the derivation of Equation F.9, Equation F.12 could be derived to calculate the mass fraction of the dissolved species in the liquid portion of stream 5:

$$\therefore \frac{dx_{j,L,5}}{dt} = \frac{x_{j,L,1} \cdot x_{L,1} \cdot \dot{m}_1 + x_{j,L,2} \cdot \dot{m}_2 + x_{j,L,4} \cdot \dot{m}_4 - x_{j,L,5} \cdot x_{L,5} \cdot K'_{TK10} \cdot \sqrt{m_{TK10}} - x_{j,L,5} \cdot \frac{d\left(x_{L,5} \cdot m_{TK10}\right)}{dt}}{x_{L,5} \cdot m_{TK10}} \quad [F.12]$$

where:

$$\frac{d\left(x_{L,5} \cdot m_{TK10}\right)}{dt} = m_{TK10} \cdot \frac{dx_{L,5}}{dt} + x_{L,5} \cdot \frac{dm_{TK10}}{dt} \quad [F.13]$$

Energy balance:

Since the temperature of stream 5 was treated as a user specified variable, no energy balance had to be performed for this subsystem.

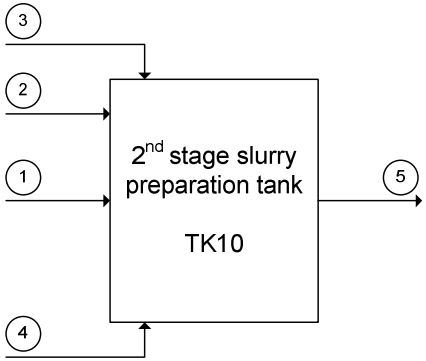

Figure F.1. Defined subsystem and corresponding stream numbers for the second stage slurry preparation tank.

F.2: Flash recycle tank

Unless stated otherwise, the derivation of mass and energy balance equations for the flash recycle tank was done in a fashion similar to the derivations done for the second stage slurry preparation tank. The final equations are given to present a complete set of equations.

Total mass balance:

Since it was assumed that the autoclave vent stream passes through the flash recycle stream unaffected, this stream could be omitted from the mass balance on the slurry content of the flash recycle tank, resulting in Equation F.14:

$$\frac{dm_{TK20}}{dt} = \dot{m}_5 + \dot{m}_9 - \dot{m}_7 - \dot{m}_{Water,Flash\ evap} \quad [F.14]$$

where $\dot{m}_5$ is given by Equation F.2 and $\dot{m}_9$ is a user specified process variable. The rate at which water is flash evaporated from the recycle stream, $\dot{m}_{Water,Flash\ evap}$, was calculated assuming that the energy removed to cool the recycle stream from the first autoclave compartment temperature to the boiling point temperature of the slurry at 1 atm lead to the evaporation of water from the recycle stream. The boiling point temperature of the recycle stream at 1 atm was assumed to be equal to that of pure water, namely 100°C. Given the additional assumption that water is the only component evaporating during the flashing process (as discussed in Section 6.2), the energy balance for the flash process could be written as:

$$\dot{m}_{Water,Flash\ evap} = \frac{\dot{m}_9 \cdot \left(x_{L,9} \cdot C_{P,L,9} + x_{S,9} \cdot C_{P,S,9}\right) \cdot (T_9 - 100)}{\Delta \widehat{H}_{Evap}} \quad [F.15]$$

As was the case for stream 5, the flow rate of stream 7 was calculated in terms of its proportionality to the square root of the mass of the slurry inside the tank from which it is flowing:

$$\dot{m}_7 = K'_{TK20} \cdot \sqrt{m_{TK20}} \quad [F.16]$$

where:

$$K'_{TK20} = \frac{\dot{m}_5 + \dot{m}_9 - \dot{m}_{Water,Flash\ evap}}{\left(\sqrt{m_{TK20}}\right)_{Steady\ state}} \quad [F.17]$$

Solids mass balance:

$$\frac{dx_{S,7}}{dt} = \frac{x_{S,5} \cdot \dot{m}_5 + x_{S,9} \cdot \dot{m}_9 - x_{S,7} \cdot K'_{TK20} \cdot \sqrt{m_{TK20}} - x_{S,7} \cdot \frac{dm_{TK20}}{dt}}{m_{TK20}} \quad [F.18]$$

Solid species mass balance (for any mineralogical phase):

$$\therefore \frac{dx_{j,S,7}}{dt} = \frac{x_{j,S,5} \cdot x_{S,5} \cdot \dot{m}_5 + x_{j,S,9} \cdot x_{S,9} \cdot \dot{m}_9 - x_{j,S,7} \cdot x_{S,7} \cdot K'_{TK20} \cdot \sqrt{m_{TK20}} - x_{j,S,7} \cdot \frac{d\left(x_{S,7} \cdot m_{TK20}\right)}{dt}}{x_{S,7} \cdot m_{TK20}} \quad [F.19]$$

Liquid mass balance:

$$\frac{dx_{L,7}}{dt} = -\frac{dx_{S,7}}{dt} \qquad [F.20]$$

Liquid species mass balance (for solutes):

$$\therefore \frac{dx_{j,L,7}}{dt} = \frac{x_{j,L,5} \cdot x_{L,5} \cdot \dot{m}_5 + x_{j,L,9} \cdot x_{L,9} \cdot \dot{m}_9 - x_{j,L,7} \cdot x_{L,7} \cdot K'_{TK20} \cdot \sqrt{m_{TK20}} - x_{j,L,7} \cdot \frac{d(x_{L,7} \cdot m_{TK20})}{dt}}{x_{L,7} \cdot m_{TK20}} \qquad [F.21]$$

Energy balance:

The energy balance considered the slurry phase in the flash recycle tank as the system for which the balance had to be performed. The streams entering the system were thus stream 5 at the user specified temperature and the remainder of stream 9 (after water had been flash evaporated) at the normal boiling point temperature of water. Stream 7 was hence considered to be the only stream leaving the system at a temperature equal to that of the tank contents. The assumption was thus that there is no significant heat transfer between the vapour phase and the slurry phase in the flash recycle tank. Heat loss to the environment was furthermore neglected. The resulting energy balance is given by Equation F.22:

$$\frac{dT_{TK20}}{dt} = \frac{\dot{m}_5 \cdot \widehat{H}_5 + \left(\dot{m}_9 - \dot{m}_{Water,Flash\ evap}\right) \cdot \widehat{H}_{9,after\ flash} - \dot{m}_7 \cdot \widehat{H}_7}{m_{TK20} \cdot C_{p,TK20}} \qquad [F.22]$$

where the specific enthalpy of any stream *i*, $\widehat{H}_i$, was calculated relative to the selected reference state of 25°C:

$$\widehat{H}_i = \left(x_{L,i} \cdot C_{P,L,i} + x_{S,i} \cdot C_{P,S,i}\right) \cdot (T_i - 25) \qquad [F.23]$$

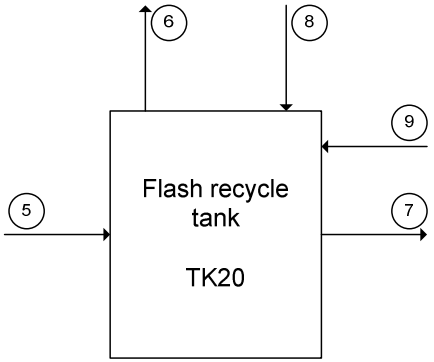

Figure F.2. Defined subsystem and corresponding stream numbers for the flash recycle tank.

F.3: Autoclave compartment 1

Total mass balance:

$$\frac{dm_{Comp1}}{dt} = \dot{m}_7 + \dot{m}_{AC3} - \dot{m}_8 - \dot{m}_9 - \dot{m}_{AC1} \quad [F.24]$$

Given the assumption that there is no mass accumulation in the autoclave compartments (as discussed in Section 6.2), the time derivative of the mass in the first compartment could be set equal to zero:

$$\dot{m}_{AC1} = \dot{m}_7 + \left(\dot{m}_{O_2,AC3} + \dot{m}_{H_2O,AC3}\right) - \left(\dot{m}_{O_2,8} + \dot{m}_{H_2O,8}\right) - \dot{m}_9 \quad [F.25]$$

$\dot{m}_{O_2,i}$ and $\dot{m}_{H_2O,i}$ are the flow rate of oxygen and water vapour, respectively, in stream i. By rearranging Equation F.25, Equation F.26 could be derived:

$$\dot{m}_{AC1} = \dot{m}_7 + \dot{m}_{O_2,Consumed\_Comp1} + \dot{m}_{H_2O,AC3} - \dot{m}_{H_2O,8} - \dot{m}_9 \quad [F.26]$$

Further consider that the vapour phase was assumed to consist of water vapour and oxygen only, that the vapour phase was assumed to be saturated with water vapour, and that the vapour phases in all the compartments are at the same temperature and equal to the temperature of the first autoclave compartment. The mol fraction of water in the vapour phase, y_{H_2O}, could hence be estimated using Equation F.27:

$$y_{H_2O} = \frac{P^*_{H_2O}}{P_{Tot}} \quad [F.27]$$

where $P^*_{H_2O}$ and P_{Tot} are the water vapour pressure at T_9 and the total autoclave pressure, respectively. Equation E.26 could subsequently be rewritten as Equation F.28:

$$\dot{m}_{AC1} = \dot{m}_7 + \dot{m}_{O_2,Consumed\_Comp1} \cdot \left(1 + \frac{M_{w,H_2O} \cdot y_{H_2O}}{\left(1 - y_{H_2O}\right) \cdot M_{w,O_2}}\right) - \dot{m}_9 \quad [F.28]$$

Solids mass balance:

$$\frac{dm_{S,Comp1}}{dt} = \dot{m}_{S,7} - \dot{m}_{S,AC1} - \dot{m}_{S,9} + V_{Comp1} \cdot \sum_{Solids} v_{i,j} \cdot r_j \cdot M_{w,i} \quad [F.29]$$

Again, assuming that the contents of the autoclave compartments are perfectly mixed, Equation F.29 could be rewritten as Equation F.30:

$$\frac{dx_{S,AC1} \cdot m_{Comp1}}{dt} = x_{S,7} \cdot \dot{m}_7 - x_{S,AC1} \cdot \dot{m}_{AC1} - x_{S,9} \cdot \dot{m}_9 + V_{Comp1} \cdot \sum_{Solids} v_{j,k} \cdot r_k \cdot M_{w,j} \quad [F.30]$$

$$\therefore \frac{dx_{S,AC1}}{dt} = \frac{x_{S,7} \cdot \dot{m}_7 - x_{S,AC1} \cdot \dot{m}_{AC1} - x_{S,9} \cdot \dot{m}_9 + V_{Comp1} \cdot \sum_{Solids} v_{j,k} \cdot r_k \cdot M_{w,j}}{m_{Comp1}} \quad [F.31]$$

Solid species mass balance (for any mineralogical phase):

$$\frac{dm_{j,S,Comp1}}{dt} = \dot{m}_{j,S,7} - \dot{m}_{j,S,AC1} - \dot{m}_{j,S,9} + V_{Comp1} \cdot \sum \upsilon_{j,k} \cdot r_k \cdot M_{w,j} \quad \text{[F.32]}$$

$$\therefore \frac{dx_{j,S,AC1} \cdot x_{S,AC1} \cdot m_{Comp1}}{dt} = x_{j,S,7} \cdot x_{S,7} \cdot \dot{m}_7 - x_{j,S,AC1} \cdot x_{S,AC1} \cdot \dot{m}_{AC1} - x_{j,S,9} \cdot x_{S,9} \cdot \dot{m}_9 + V_{Comp1} \cdot \sum \upsilon_{j,k} \cdot r_k \cdot M_{w,j} \quad \text{[F.33]}$$

$$\therefore \frac{dx_{j,S,AC1}}{dt} = \frac{x_{j,S,7} \cdot x_{S,7} \cdot \dot{m}_7 - x_{j,S,AC1} \cdot x_{S,AC1} \cdot \dot{m}_{AC1} - x_{j,S,9} \cdot x_{S,9} \cdot \dot{m}_9 + V_{Comp1} \cdot \sum \upsilon_{j,k} \cdot r_k \cdot M_{w,j} - x_{j,S,AC1} \cdot \frac{dx_{S,AC1} \cdot m_{Comp1}}{dt}}{x_{S,AC1} \cdot m_{Comp1}} \quad \text{[F.34]}$$

Liquid mass balance:

$$\frac{dx_{L,AC1}}{dt} = -\frac{dx_{S,AC1}}{dt} \quad \text{[F.35]}$$

Liquid species mass balance (for solutes):

$$\therefore \frac{dx_{j,L,AC1}}{dt} = \frac{x_{j,L,7} \cdot x_{L,7} \cdot \dot{m}_7 - x_{j,L,AC1} \cdot x_{L,AC1} \cdot \dot{m}_{AC1} - x_{j,L,9} \cdot x_{L,9} \cdot \dot{m}_9 + V_{Comp1} \cdot \sum \upsilon_{j,k} \cdot r_k \cdot M_{w,j} - x_{j,L,AC1} \cdot \frac{dx_{L,AC1} \cdot m_{Comp1}}{dt}}{x_{L,AC1} \cdot m_{Comp1}} \quad \text{[F.36]}$$

Energy balance:

$$\frac{dT_{Comp1}}{dt} = \frac{\dot{Q} - \dot{W}_{shaft} + \dot{m}_7 \cdot \hat{H}_7 + \dot{m}_{O_2,AC3} \cdot \hat{H}_{O_2,AC3} + \dot{m}_{H_2O,AC3} \cdot \hat{H}_{H_2O,AC3} - \dot{m}_{AC1} \cdot \hat{H}_{AC1} - \dot{m}_9 \cdot \hat{H}_9 - \dot{m}_{O_2,8} \cdot \hat{H}_{O_2,8} + \dot{m}_{H_2O,8} \cdot \hat{H}_{H_2O,8} - V_{Comp1} \cdot \sum_{Comp1} r_j \cdot \Delta \hat{H}^{\circ}_{rxn,j}}{m_{Comp1} \cdot C_{p,Comp1}} \quad \text{[F.37]}$$

For any slurry stream *i*, the value of the specific enthalpy, $\widehat{H}_i$, is given by Equation F.23. Given the assumption that the vapour phases in the different compartments are at the same temperature, the specific enthalpy of the vapour stream entering (stream AC3) and leaving (stream 8) had to be the same. Equation F.37 could thus be rewritten as:

$$\frac{dT_{Comp1}}{dt} = \frac{\dot{Q} - \dot{W}_{shaft} + \dot{m}_7 \cdot \widehat{H}_7 + \dot{m}_{O_2,Consumed\_Comp1} \cdot \left(\widehat{H}_{O_2,AC3} + \frac{M_{w,H_2O} \cdot y_{H_2O} \cdot \widehat{H}_{H_2O,AC3}}{(1 - y_{H_2O}) \cdot M_{w,O_2}} \right) - \dot{m}_{AC1} \cdot \widehat{H}_{AC1} - \dot{m}_9 \cdot \widehat{H}_9 - V_{Comp1} \cdot \sum_{Comp1} r_j \cdot \Delta \widehat{H}^{\circ}_{rxn,j}}{m_{Comp1} \cdot C_{p,Comp1}} \quad [F.38]$$

where:

$$\widehat{H}_{O_2,AC3} = C_{P,O_2} \cdot (T_{AC3} - 25) \quad [F.39]$$

and:

$$\widehat{H}_{H_2O,AC3} = C_{P,H_2O_{(v)}} \cdot (T_{AC3} - 100) + \widehat{H}_{Evap} + C_{P,H_2O_{(l)}} \cdot (100 - 25) \quad [F.40]$$

The external heat transfer from the first compartment was assumed to be only as a result of convection and radiation losses, which were estimated using correlations described by Incropera and De Witt (1996):

$$-\dot{Q} = Nu \cdot k_{Air} \cdot \pi \cdot (T_{AC,Out} - T_\infty) + \varepsilon_{AC} \cdot \pi \cdot D_{AC} \cdot K_{SB} \cdot (T^4_{AC,Out} - T^4_{Sur}) \quad [F.41]$$

where $T_{AC,Out}$, ε_{AC}, and D_{AC} refer to the outside surface temperature, surface emissivity, and outer diameter of the autoclave, respectively. T_∞ and T_{Sur} are the ambient temperature and the temperature of the surroundings, respectively, with k_{Air} being the thermal conductivity of air and K_{SB} the Stefan-Boltzmann constant. The Nusselt number, Nu, is given by the following correlation:

$$Nu = \left(0.6 + \frac{0.387 \cdot \left(\frac{g \cdot \beta_{Air} \cdot \left(T_{AC,Out} - T_{\infty} \right) \cdot D_{AC}^{3}}{\mu_{Air} \cdot \alpha_{Air}} \right)^{1/6}}{\left(1 + \left(0.559 / Pr_{Air} \right)^{9/16} \right)^{8/27}} \right)^{2} \quad [F.42]$$

where g is the gravitational acceleration, β_{Air}, μ_{Air}, α_{Air}, and Pr_{Air} are the volumetric thermal expansion coefficient, kinematic viscosity, thermal diffusivity, and Prandtl number of air, respectively.

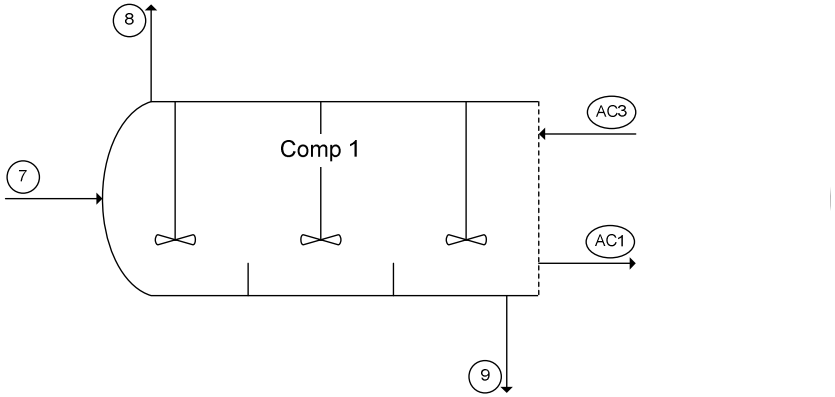

Figure F.3. Defined subsystem and corresponding stream numbers for the first autoclave compartment.

F.4: Autoclave compartment 2

Unless stated otherwise, the derivation of mass and energy balance equations for the second autoclave compartment was done in a fashion similar to the derivations done for the first autoclave compartment. The final equations are given to present a complete set of equations.

Total mass balance:

$$\dot{m}_{AC2} = \dot{m}_{AC1} + \dot{m}_{O_2,Consumed\_Comp2} + \left(\dot{m}_{O_2,Consumed\_Comp2} - \dot{m}_{10} \right) \cdot \left(\frac{M_{w,H_2O} \cdot y_{H_2O}}{\left(1 - y_{H_2O} \right) \cdot M_{w,O_2}} \right) \quad [F.43]$$

Solids mass balance:

$$\therefore \frac{dx_{S,AC2}}{dt} = \frac{x_{S,AC1} \cdot \dot{m}_{AC1} - x_{S,AC2} \cdot \dot{m}_{AC2} + V_{Comp2} \cdot \sum_{Solids} \upsilon_{j,k} \cdot r_k \cdot M_{w,j}}{m_{Comp2}} \quad [F.44]$$

Solid species mass balance (for any mineralogical phase):

$$\therefore \frac{dx_{j,S,AC2}}{dt} = \frac{x_{j,S,AC1} \cdot x_{S,AC1} \cdot \dot{m}_{AC1} - x_{j,S,AC2} \cdot x_{S,AC2} \cdot \dot{m}_{AC2} + V_{Comp2} \cdot \sum \upsilon_{j,k} \cdot r_k \cdot M_{w,j} - x_{j,S,AC2} \cdot \frac{dx_{S,AC2} \cdot m_{Comp2}}{dt}}{x_{S,AC2} \cdot m_{Comp2}} \quad [F.45]$$

Liquid mass balance:

$$\frac{dx_{L,AC2}}{dt} = -\frac{dx_{S,AC2}}{dt} \quad [F.46]$$

Liquid species mass balance (for solutes):

$$\therefore \frac{dx_{j,L,AC2}}{dt} = \frac{x_{j,L,AC1} \cdot x_{L,AC1} \cdot \dot{m}_{AC1} - x_{j,L,AC2} \cdot x_{L,AC2} \cdot \dot{m}_{AC2} + V_{Comp2} \cdot \sum \upsilon_{j,k} \cdot r_k \cdot M_{w,j} - x_{j,L,AC2} \cdot \frac{dx_{L,AC2} \cdot m_{Comp2}}{dt}}{x_{L,AC2} \cdot m_{Comp2}} \quad [F.47]$$

Energy balance:

$$\frac{dT_{Comp2}}{dt} = \frac{\dot{Q} - \dot{W}_{shaft} + \dot{m}_{AC1} \cdot \widehat{H}_{AC1} + \dot{m}_{10} \cdot \widehat{H}_{10} + \left(\dot{m}_{O_2,Consumed\_Comp2} - \dot{m}_{10}\right) \cdot \left(\widehat{H}_{O_2,AC4} + \frac{M_{w,H_2O} \cdot y_{H_2O} \cdot \widehat{H}_{H_2O,AC4}}{\left(1 - y_{H_2O}\right) \cdot M_{w,O_2}}\right) - \dot{m}_{AC2} \cdot \widehat{H}_{AC2} - V_{Comp2} \cdot \sum_{Comp2} r_j \cdot \Delta \widehat{H}^{\circ}_{rxn,j}}{m_{Comp2} \cdot C_{p,Comp2}} \quad [F.48]$$

where $\dot{Q}$ includes the radiation and convection losses given by Equation F.41 as well as external heat transfer achieved by means of a cooling coil.

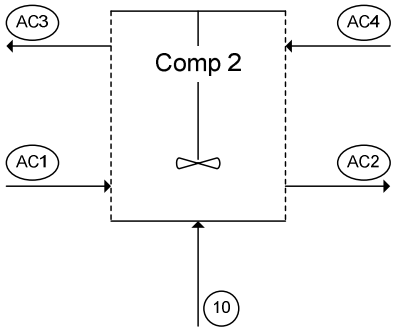

Figure F.4. Defined subsystem and corresponding stream numbers for the second autoclave compartment.

F.5: Autoclave compartment 3

Unless stated otherwise, the derivation of mass and energy balance equations for the third autoclave compartment was done in a fashion similar to the derivations done for the second autoclave compartment. The final equations are given to present a complete set of equations.

Total mass balance:

$$\dot{m}_{14} = \dot{m}_{AC2} + \dot{m}_{O_2,Consumed\_Comp3} + \left(\dot{m}_{O_2,Consumed\_Comp3} - \dot{m}_{11}\right) \cdot \left(\frac{M_{w,H_2O} \cdot y_{H_2O}}{\left(1 - y_{H_2O}\right) \cdot M_{w,O_2}}\right) \quad [F.49]$$

Solids mass balance:

$$\therefore \frac{dx_{S,14}}{dt} = \frac{x_{S,AC2} \cdot \dot{m}_{AC2} - x_{S,14} \cdot \dot{m}_{14} + V_{Comp3} \cdot \sum_{Solids} \upsilon_{j,k} \cdot r_k \cdot M_{w,j}}{m_{Comp3}} \quad [F.50]$$

Solid species mass balance (for any mineralogical phase):

$$\therefore \frac{dx_{j,S,14}}{dt} = \frac{x_{j,S,AC2} \cdot x_{S,AC2} \cdot \dot{m}_{AC2} - x_{j,S,14} \cdot x_{S,14} \cdot \dot{m}_{14} + V_{Comp3} \cdot \sum \upsilon_{j,k} \cdot r_k \cdot M_{w,j} - x_{j,S,14} \cdot \frac{dx_{S,14} \cdot m_{Comp3}}{dt}}{x_{S,14} \cdot m_{Comp3}} \quad [F.51]$$

Liquid mass balance:

$$\frac{dx_{L,14}}{dt} = -\frac{dx_{S,14}}{dt} \quad [F.52]$$

Liquid species mass balance (for solutes):

$$\therefore \frac{dx_{j,L,14}}{dt} = \frac{x_{j,L,AC2} \cdot x_{L,AC2} \cdot \dot{m}_{AC2} - x_{j,L,14} \cdot x_{L,14} \cdot \dot{m}_{14} + V_{Comp3} \cdot \sum \upsilon_{j,k} \cdot r_k \cdot M_{w,j} - x_{j,L,14} \cdot \frac{dx_{L,14} \cdot m_{Comp3}}{dt}}{x_{L,14} \cdot m_{Comp3}} \quad [F.53]$$

Energy balance:

$$\frac{dT_{Comp3}}{dt} = \frac{\dot{Q} - \dot{W}_{shaft} + \dot{m}_{AC2} \cdot \widehat{H}_{AC2} + \dot{m}_{11} \cdot \widehat{H}_{11} + \left(\dot{m}_{O_2,Consumed\_Comp3} - \dot{m}_{11}\right) \cdot \left(\widehat{H}_{O_2,AC5} + \frac{M_{w,H_2O} \cdot y_{H_2O} \cdot \widehat{H}_{H_2O,AC5}}{\left(1 - y_{H_2O}\right) \cdot M_{w,O_2}}\right) - \dot{m}_{14} \cdot \widehat{H}_{14} - V_{Comp3} \cdot \sum_{Comp3} r_j \cdot \Delta \widehat{H}^{\circ}_{rxn,j}}{m_{Comp3} \cdot C_{p,Comp3}} \quad [F.54]$$

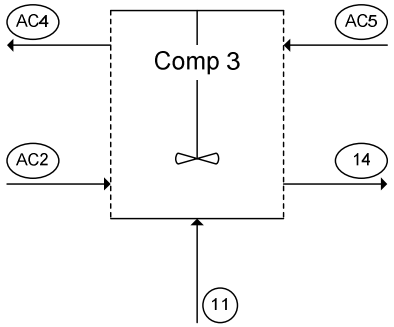

Figure F.5. Defined subsystem and corresponding stream numbers for the third autoclave compartment.

F.6: Second stage leach discharge tank

Unless stated otherwise, the derivation of mass and energy balance equations for the second stage leach discharge tank was done in a fashion similar to the derivations done for the second stage slurry preparation tank. The final equations are given to present a complete set of equations.

Total mass balance:

$$\frac{dm_{TK40}}{dt} = \dot{m}_{14} - \dot{m}_{15} \quad [F.55]$$

where:

$$\dot{m}_{15} = K'_{TK40} \cdot \sqrt{m_{TK40}} \quad [F.56]$$

and:

$$K'_{TK40} = \frac{\dot{m}_{14}}{\left(\sqrt{m_{TK40}}\right)_{Steady\ state}} \quad [F.57]$$

Solids mass balance:

$$\therefore \frac{dx_{S,15}}{dt} = \frac{x_{S,14} \cdot \dot{m}_{14} - x_{S,15} \cdot K'_{TK40} \cdot \sqrt{m_{TK40}} - x_{S,15} \cdot \frac{dm_{TK40}}{dt}}{m_{TK40}} \quad [F.58]$$

Solid species mass balance (for any mineralogical phase):

$$\therefore \frac{dx_{j,S,15}}{dt} = \frac{x_{j,S,14} \cdot x_{S,14} \cdot \dot{m}_{14} - x_{j,S,15} \cdot x_{S,15} \cdot K'_{TK40} \cdot \sqrt{m_{TK40}} - x_{j,S,15} \cdot \frac{d\left(x_{S,15} \cdot m_{TK40}\right)}{dt}}{x_{S,15} \cdot m_{TK40}} \quad [F.59]$$

Liquid mass balance:

$$\frac{dx_{L,15}}{dt} = -\frac{dx_{S,15}}{dt} \qquad [F.60]$$

Liquid species mass balance (for solutes):

$$\therefore \frac{dx_{j,L,15}}{dt} = \frac{x_{j,L,14} \cdot x_{L,14} \cdot \dot{m}_{14} - x_{j,L,15} \cdot x_{L,15} \cdot K'_{TK40} \cdot \sqrt{m_{TK40}} - x_{j,L,15} \cdot \frac{d(x_{L,15} \cdot m_{TK40})}{dt}}{x_{L,15} \cdot m_{TK40}} \qquad [F.61]$$

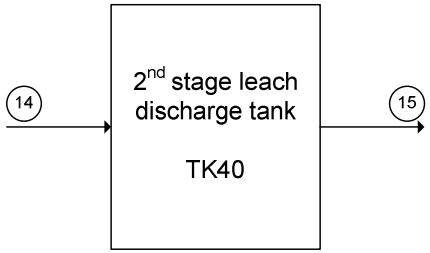

Figure F.6. Defined subsystem and corresponding stream numbers for the second stage leach discharge tank.

F.7: Second stage leach discharge thickener

Unless stated otherwise, the derivation of mass and energy balance equations for the second stage leach discharge thickener was done in a fashion similar to the derivations done for the second stage slurry preparation tank. The final equations are given to present a complete set of equations.

Total mass balance:

$$\frac{dm_{TH700}}{dt} = \dot{m}_{15} - \dot{m}_{16} - \dot{m}_{17} \qquad [F.62]$$

For perfect solid/ℓiquid separation:

$$\dot{m}_{16} = x_{L,TH700} \cdot K'_{TH700} \cdot \sqrt{m_{TH700}} \qquad [F.63]$$

$$\dot{m}_{17} = x_{S,TH700} \cdot K'_{TH700} \cdot \sqrt{m_{TH700}} \quad [F.64]$$

where

$$K'_{TH700} = \frac{\dot{m}_{15}}{\left(\sqrt{m_{TH700}}\right)_{Steady\ state}} \quad [F.65]$$

Solids mass balance:

$$\therefore \frac{dx_{S,TH700}}{dt} = \frac{x_{S,15} \cdot \dot{m}_{15} - x_{S,TH700} \cdot K'_{TH700} \cdot \sqrt{m_{TH700}} - x_{S,TH700} \cdot \frac{dm_{TH700}}{dt}}{m_{TH700}} \quad [F.66]$$

Solid species mass balance (for any mineralogical phase):

$$\therefore \frac{dx_{j,S,TH700}}{dt} = \frac{x_{j,S,15} \cdot x_{S,15} \cdot \dot{m}_{15} - x_{j,S,TH700} \cdot x_{S,TH700} \cdot K'_{TH700} \cdot \sqrt{m_{TH700}} - x_{j,S,TH700} \cdot \frac{d\left(x_{S,TH700} \cdot m_{TH700}\right)}{dt}}{x_{S,TH700} \cdot m_{TH700}} \quad [F.67]$$

Liquid mass balance:

$$\frac{dx_{L,TH700}}{dt} = -\frac{dx_{S,TH700}}{dt} \quad [F.68]$$

Liquid species mass balance (for solutes):

$$\therefore \frac{dx_{j,L,TH700}}{dt} = \frac{x_{j,L,15} \cdot x_{L,15} \cdot \dot{m}_{15} - x_{j,L,TH700} \cdot x_{L,TH700} \cdot K'_{TH700} \cdot \sqrt{m_{TH700}} - x_{j,L,TH700} \cdot \frac{d\left(x_{L,TH700} \cdot m_{TH700}\right)}{dt}}{x_{L,TH700} \cdot m_{TH700}} \quad [F.69]$$

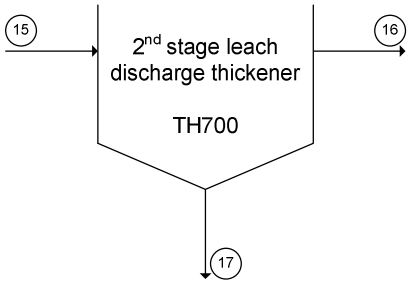

Figure F.7. Defined subsystem and corresponding stream numbers for the second stage leach discharge thickener.

F.8: Third stage slurry preparation tank

Unless stated otherwise, the derivation of mass and energy balance equations for the third stage slurry preparation tank was done in a fashion similar to the derivations done for the second stage slurry preparation tank. The final equations are given to present a complete set of equations.

Total mass balance:

$$\frac{dm_{TK50}}{dt} = \dot{m}_{17} + \dot{m}_{18} + \dot{m}_{19} + \dot{m}_{20} - \dot{m}_{21} \quad [F.70]$$

where:

$$\dot{m}_{21} = K'_{TK50} \cdot \sqrt{m_{TK50}} \quad [F.71]$$

and:

$$K'_{TK50} = \frac{\dot{m}_{17} + \dot{m}_{18} + \dot{m}_{19} + \dot{m}_{20}}{\left(\sqrt{m_{TK50}}\right)_{Steady\ state}} \quad [F.72]$$

Solids mass balance:

$$\therefore \frac{dx_{S,21}}{dt} = \frac{\dot{m}_{17} - x_{S,21} \cdot K'_{TK50} \cdot \sqrt{m_{TK50}} - x_{S,21} \cdot \frac{dm_{TK50}}{dt}}{m_{TK50}} \quad [F.73]$$

Solid species mass balance (for any mineralogical phase):

$$\therefore \frac{dx_{j,S,21}}{dt} = \frac{x_{j,S,17} \cdot \dot{m}_{17} - x_{j,S,21} \cdot x_{S,21} \cdot K'_{TK50} \cdot \sqrt{m_{TK50}} - x_{j,S,21} \cdot \frac{d\left(x_{S,21} \cdot m_{TK50}\right)}{dt}}{x_{S,21} \cdot m_{TK50}} \quad [F.74]$$

Liquid mass balance:

$$\frac{dx_{L,21}}{dt} = -\frac{dx_{S,21}}{dt} \quad [F.75]$$

Liquid species mass balance (for solutes):

$$\therefore \frac{dx_{j,L,21}}{dt} = \frac{x_{j,L,18} \cdot \dot{m}_{18} + x_{j,L,20} \cdot \dot{m}_{20} - x_{j,L,21} \cdot x_{L,21} \cdot K'_{TK50} \cdot \sqrt{m_{TK50}} - x_{j,L,21} \cdot \frac{d\left(x_{L,21} \cdot m_{TK50}\right)}{dt}}{x_{L,21} \cdot m_{TK50}} \quad [F.76]$$

Energy balance:

Since the temperature of stream 21 was treated as a user specified variable, no energy balance had to be performed for this subsystem.

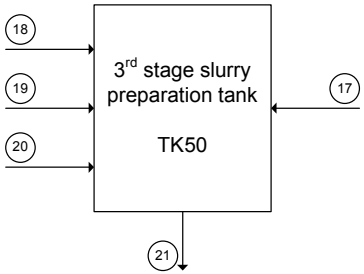

Figure F.8. Defined subsystem and corresponding stream numbers for the third stage slurry preparation tank.

F.9 Autoclave compartment 4 (third stage leach)

Unless stated otherwise, the derivation of mass and energy balance equations for the fourth autoclave compartment was done in a fashion similar to the derivations done for the third autoclave compartment. The final equations are given to present a complete set of equations.

Total mass balance:

$$\dot{m}_{22} = \dot{m}_{21} + \dot{m}_{13} + \dot{m}_{O_2,Consumed\_Comp4} + \left(\dot{m}_{O_2,Consumed\_Comp4} - \dot{m}_{12}\right) \cdot \left(\frac{M_{w,H_2O} \cdot y_{H_2O}}{\left(1 - y_{H_2O}\right) \cdot M_{w,O_2}}\right) \quad [F.77]$$

Solids mass balance:

$$\therefore \frac{dx_{S,22}}{dt} = \frac{x_{S,21} \cdot \dot{m}_{21} - x_{S,22} \cdot \dot{m}_{22} + V_{Comp4} \cdot \sum_{Solids} \upsilon_{j,k} \cdot r_k \cdot M_{w,j}}{m_{Comp4}} \quad [F.78]$$

Solid species mass balance (for any mineralogical phase):

$$\therefore \frac{dx_{j,S,22}}{dt} = \frac{x_{j,S,21} \cdot x_{S,21} \cdot \dot{m}_{21} - x_{j,S,22} \cdot x_{S,22} \cdot \dot{m}_{22} + V_{Comp4} \cdot \sum \upsilon_{j,k} \cdot r_k \cdot M_{w,j} - x_{j,S,22} \cdot \frac{dx_{S,22} \cdot m_{Comp4}}{dt}}{x_{S,22} \cdot m_{Comp4}} \quad [F.79]$$

Liquid mass balance:

$$\frac{dx_{L,22}}{dt} = -\frac{dx_{S,22}}{dt} \quad [F.80]$$

Liquid species mass balance (for solutes):

$$\therefore \frac{dx_{j,L,22}}{dt} = \frac{x_{j,L,21} \cdot x_{L,21} \cdot \dot{m}_{21} - x_{j,L,22} \cdot x_{L,22} \cdot \dot{m}_{22} + V_{Comp4} \cdot \sum \upsilon_{j,k} \cdot r_k \cdot M_{w,j} - x_{j,L,22} \cdot \frac{dx_{L,22} \cdot m_{Comp4}}{dt}}{x_{L,22} \cdot m_{Comp4}} \quad [F.81]$$

Energy balance:

$$\frac{dT_{Comp4}}{dt} = \frac{\dot{Q} - \dot{W}_{shaft} + \dot{m}_{21} \cdot \widehat{H}_{21} + \dot{m}_{12} \cdot \widehat{H}_{12} + \dot{m}_{13} \cdot \widehat{H}_{13} + \left(\dot{m}_{O_2,Consumed\_Comp3} - \dot{m}_{12}\right) \cdot \left(\widehat{H}_{O_2,AC5} + \frac{M_{w,H_2O} \cdot y_{H_2O} \cdot \widehat{H}_{H_2O,AC5}}{\left(1 - y_{H_2O}\right) \cdot M_{w,O_2}}\right) - \dot{m}_{22} \cdot \widehat{H}_{22} - V_{Comp4} \cdot \sum_{Comp4} r_j \cdot \Delta \widehat{H}^{\circ}_{rxn,j}}{m_{Comp4} \cdot C_{p,Comp4}} \quad [F.82]$$

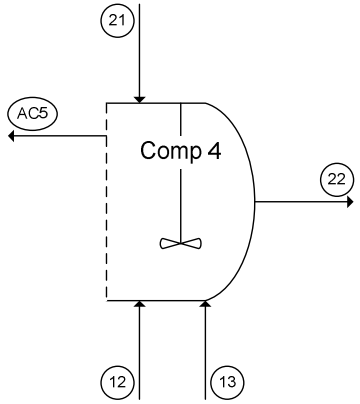

Figure F.9. Defined subsystem and corresponding stream numbers for the fourth autoclave compartment.

APPENDIX G: PUBLICATIONS BASED ON THIS DISSERTATION

Papers in refereed journals

- Dorfling, C., Akdogan, G., Bradshaw, S.M., and Eksteen, J.J., 2011. Determination of the relative leaching kinetics of Cu, Rh, Ru and Ir during the sulphuric acid pressure leaching of leach residue derived from Ni-Cu converter matte enriched in platinum group metals. *Minerals Engineering*, 24(6):583-589

Refereed full length papers in the proceedings of international symposia

- Dorfling, C., Akdogan, G., Bradshaw, S.M., and Eksteen, J.J., 2010. High pressure sulphuric acid/oxygen leaching of PGM bearing Ni-Cu mattes. *Proceedings of XXV International Mineral Processing Congress*, Brisbane, Australia, pp. 299-308
- Dorfling, C., Akdogan, G., Bradshaw, S.M., and Eksteen, J.J., 2012. Kinetics of Rh, Ru, and Ir dissolution during the sulfuric acid pressure leaching of first stage leach residue. *Proceedings of XXVI International Mineral Processing Congress*, New Delhi, India, pp. 1196-1210

Non-refereed papers presented at international symposia and workshops

- Dorfling, C., Akdogan, G., Bradshaw, S.M., and Eksteen, J.J., 2010. Experimental determination of the kinetics of pressure leaching of first stage leach residue and the solubilisation of Rh, Ru, and Ir. *Precious Metals '10*, Falmouth, UK, 15-16 June 2010
- Dorfling, C., Akdogan, G., Bradshaw, S.M., and Eksteen, J.J., 2012. Modelling of an autoclave used for high pressure sulphuric acid/oxygen leaching of first stage leach residue. *Precious Metals '12*, Cape Town, South Africa, 12-13 November 2012

Presentations at national symposia and workshops

- Dorfling, C., Akdogan, G., Bradshaw, S.M., and Eksteen, J.J., 2010. Investigating the dissolution behaviour of PGMs during the pressure leaching of first stage leach residue. *Mineral Processing 2010*, Western Cape Branch of SAIMM, Cape Town, South Africa, 5-6 August 2010
- Dorfling, C., Akdogan, G., Bradshaw, S.M., and Eksteen, J.J., 2011. Reaction mechanism and leaching kinetics of Rh and Ru dissolution during the pressure leaching of first stage leach residue. *Mineral Processing 2011*, Western Cape Branch of SAIMM, Cape Town, South Africa, 4-5 August 2011

APPENDIX H: MATLAB CODE